

UNDERSTANDING THE ROLE OF RAGE IN CELL ADHESION

A Dissertation
Submitted to the Graduate Faculty
of the
North Dakota State University
of Agriculture and Applied Science

By

Swetha Thiyagarajan

In Partial Fulfillment of the Requirements
for the Degree of
DOCTOR OF PHILOSOPHY

Major Department:
Pharmaceutical Sciences

January 2022

Fargo, North Dakota

North Dakota State University
Graduate School

Title

UNDERSTANDING THE ROLE OF RAGE IN CELL ADHESION

By

Swetha Thiyagarajan

The Supervisory Committee certifies that this *disquisition* complies with North Dakota State University's regulations and meets the accepted standards for the degree of

DOCTOR OF PHILOSOPHY

SUPERVISORY COMMITTEE:

Dr. Stefan W. Vetter

Chair

Dr. Yagna PR. Jarajapu

Dr. Sathish Venkatachalem

Dr. John C. Wilkinson

Approved:

July 11, 2022

Date

Dr. Jagdish Singh

Department Chair

ABSTRACT

The Receptor for Advanced Glycation Endproducts (RAGE) is a mammalian specific cell surface receptor. RAGE consists of three extracellular domains (V, C1, and C2), a transmembrane domain, and an intracellular cytoplasmic tail. RAGE has a significant role in human pathogenesis, including neurodegenerative diseases, diabetic complications, and certain cancers. Deregulation of cell adhesion is one of the contributing cellular events common in many of the above listed human pathologies and might be mediated via RAGE signaling. In our study, we aimed to understand the role of RAGE in cell adhesion and to define the importance of the different domains of RAGE in mediating this phenomenon.

For this study, a protein engineering approach was used to express full-length RAGE (FL-RAGE) and a panel of domain deletion constructs (ΔV -, $\Delta C1$ -, $\Delta C2$ -, DN-, TmCyto- RAGE) of the receptor. The necessary expression constructs were assembled in the pcDNA3 vector, and the RAGE variants were expressed in HEK293 cells. The expression and cellular localization of RAGE in HEK 293 cells were analyzed using Western blot, immunofluorescence microscopy, and flow cytometry techniques. Our results show that the cytoplasmic domain of RAGE was sufficient to contribute to cell adhesion to the extracellular matrix to a level comparable to that of the FL-RAGE expressing cells.

The current mechanistic model suggests that RAGE signaling is initiated by ligand binding to the extracellular region, followed by conformational changes in the intracellular domain. Subsequently, this conformation change leads to the recruitment of RAGE-interacting proteins on the intracellular side of the plasma membrane. However, in this thesis, we present evidence of an alternative mechanism of RAGE signaling possibly involving the translocation of RAGE into the nucleus. The results from our study suggest an alternative model for RAGE signaling and will help

to better understand RAGE signaling in pathophysiological conditions. Our results could contribute to the development of new small molecule drugs targeting intracellular RAGE or the intracellular RAGE domain as a novel approach for inhibiting RAGE signaling.¹

¹ Note: The engineered RAGE mutants in this thesis are referred as RAGE domain deletion variants or RAGE variants

ACKNOWLEDGMENTS

I would like to start by thanking my advisor, Dr. Vetter, for his mentorship and research guidance. I am grateful to him for being a huge support and for giving me the freedom to volunteer and serve in many leadership roles. I would like to convey my sincere gratitude to Dr. Leclerc for her insights and help with my research. She was my go-to person in the department and always there to guide me with work and career-related circumstances. I am glad I also got the opportunity to collaborate and contribute to her research. I am immensely thankful to my committee members, Dr. Jarajapu, Dr. Venkatachalem, and Dr. Wilkinson, for their valuable suggestions and timely feedback on my research. My committee members and Dr. Vetter were also of enormous support with my job search by providing beneficial career guidance and writing recommendation letters. I want to convey my deepest gratitude to the Department chair Dr. Jagdish Singh who genuinely cared for the department and his people. I also truly admire his leadership skills and his commitment to work.

My sincere thanks to Mrs. Janet Krom for always being there to encourage and motivate me during tough times at school. She always reminded me of my worth and to keep my head high. I am grateful to Mrs. Diana Kowalski and Tiffany Olson for all their help and for being a great support system to the department. I want to acknowledge my lab members, Dr. Swami, Dr. Kadasah, Dr. Taneja, and Yousuf, for all their support in the lab. My special thanks to Dr. Joshi, Dr. Ambhore, and Dr. Bhallamudi for all their help with my experiments. I am obligated to all the students and the faculty in our department for their immense support and help. I want to thank Dr. Pawel (Director, NDSU Advanced Imaging and Microscopy (AIM) Core Lab) for his help with confocal imaging and Dr. Mikhail Golovko (Director of Mass Spectrometry Core Facility, UND) and Mrs. Svetlana Golovko (Senior research associate, UND) for their collaboration and help with

proteomics work. Finally, I also want to thank Mr. Danjel Nygard (Dissertation and Thesis Coordinator, NDSU) for helping me format my thesis.

My Ph.D. would not have been possible without my parents. Though miles apart, they stood with me in all those times and sacrificed everything to have their daughter pursue her goals. Thank you, Ammu, Appu, for always being there to cheer me up, for being my besties, and for having taught me to learn from failures and to keep moving forward. I am extremely grateful to both my paternal and maternal grandparents, who stood as great role models and taught me courage, strength, and to be empowered. I am thankful to my brother, my sister-in-law, and all my relatives for their prayers and warm wishes. My besties back home, Bavitra and Krithika, always took the time to check up and motivate me all along the way.

My journey to Fargo started with knowing no one but just a belief that I was going to make good friends. In the end, it turned out that I did not just make friends; they were my Fargo family. My people from Fargo Sai bhajan family (Dr. Padmanabhan & family, Dr. Leelaruban & family), my friends, and roommates (Jagdeep, Neeshma, Bibi, Mena, Tina, Ram, Dipankar, and Eshita) for their moral support and for taking good care of me when I was sick. I have also made great friends at school who turned out to be my cheer squad. Thank you, Ana, Seseer, Muhabbat, and Raquib, for showering me with positivity whenever I was feeling down in the dumps.

I feel so lucky to have known Monika, Satish, and Mathew through my internship at Biogen in Boston. They stood as my well wishers, and I am forever grateful to them. I cannot thank enough Dr. Claudia Tomany, who was my inspiration and a great mentor outside my department. I came to know Dr. Tomany during my association with the Graduate Student Council, NDSU. Dr. Tomany was instrumental in enabling my full potential as a leader and nurtured me with

positivism. I truly admire how she connects with students and guides them toward a path to success.

Finally, I would like to thank the funding agencies NDSU College of Health Professions, the NDSU Department of Pharmaceutical Sciences, NIH Grant GM103332, and the XCELLigence Research grant for supporting my research.

DEDICATION

Dedicated to

my loving parents, Rajalakshmi Govindarajan (Ammu) and Thiyagarajan Venkataraman (Appu)

my grandparents, Mr. and Mrs. Venkataraman (late) & Mr. and Mrs. Govindarajan

all of my mentors, my relatives, my friends, & everyone who supported me in this journey

Almighty God

TABLE OF CONTENTS

ABSTRACT.....	iii
ACKNOWLEDGMENTS	v
DEDICATION.....	viii
LIST OF TABLES	xv
LIST OF FIGURES	xvi
LIST OF ABBREVIATIONS.....	xx
LIST OF APPENDIX FIGURES.....	xxiii
CHAPTER 1. GENERAL INTRODUCTION	1
Extracellular matrix, cell adhesion, and cell adhesion molecules.....	1
Classification and role of cell adhesion molecules in physiology.....	5
Cadherins.....	5
Selectins.....	5
Immunoglobulin (Ig)-superfamily.....	6
Mucin-like family	7
Integrins.....	7
RAGE (receptor for advanced glycation endproducts).....	10
RAGE structure and expression	11
Ligand binding properties of RAGE	14
RAGE signaling.....	16
Involvement of RAGE in pathologies	19
RAGE as a therapeutic target and its inhibitors	20
RAGE as an adhesion relevant molecule	22
RAGE subcellular localization and its functions.....	24
Research goals, approach, and objectives	25

CHAPTER 2. GENERAL MATERIALS AND METHODS	28
Molecular biology and reagents	28
Cell culture	28
Cloning of RAGE variants and plasmid production	29
Transient transfection	29
SDS-PAGE and Western blotting	29
Immunofluorescence	30
Flow cytometry	31
Cell adhesion assay	32
Cell spreading assay	33
RNA extraction and cDNA synthesis.....	33
Quantitative PCR (qPCR)	34
Cell surface proteomics	35
Cell surface protein labeling and enrichment.....	35
Sample processing for mass spectrometry (MS).....	36
Nano LC-MS acquisition.....	36
MS-data processing	37
Statistical analysis	38
CHAPTER 3. RAGE DOMAIN DELETION VARIANTS TO PROBE THE ROLE OF RAGE DOMAINS IN CELL ADHESION	39
Introduction	39
Design and expression of the RAGE domain deletion variants	40
Experimental design	40
Generation of RAGE variants.....	40
Transient transfection optimization using reporter plasmids pcDNA3GFP and pcDNA3SEAP in HEK 293 cells.....	41

Transient expression of RAGE variants	42
Western blot	42
Immunofluorescence and confocal image analysis.....	43
Flow cytometry	44
Results	44
Lipofectamine 3000 showed good transfection efficiency with two tested reporter plasmids	44
Expression of the RAGE variants and Western blot analysis.....	47
Localization of the RAGE variants using immunofluorescence analysis.....	50
Quantitative cellular localization of domain deletion RAGE variants by flow cytometry	52
Discussion.....	54
Effect of RAGE expression in mediating cell-cell contacts on collagen IV coated surface	57
Experimental design	57
Determining RAGE-RAGE or RAGE-nonRAGE contacts on mixed cell population	57
Results	58
RAGE expressing cells preferentially formed RAGE-RAGE contacts during cell- cell adhesion in the presence of collagen IV	58
Discussion.....	61
Effect of RAGE domain deletion variants on cell adhesion and cell spreading on ECM proteins	62
Experimental design	62
Cell-matrix adhesion assay	62
Cell spreading assay.....	65
Results	65

The presence of only the cytoplasmic domain of RAGE enhanced cell adhesion to ECM proteins	65
Enhanced cell adhesion by the cytoplasmic domain is followed by increased cell spreading to ECM proteins	70
Discussion.....	73
Conclusions	75
CHAPTER 4. RAGE EXPRESSION IN HEK 293 CELLS SHOWS EVIDENCE FOR INTRAMEMBRANE PROTEOLYSIS OCCURRENCE FOLLOWED BY NUCLEAR TRANSLOCATION	80
Introduction	80
Ectodomain shedding and regulated intramembrane proteolysis (RIP)	80
Ectodomain shedding and RAGE.....	83
RAGE subcellular localization.....	85
Experimental design	85
Fluorescent tagged FL-RAGE and RAGE-ICD plasmids	85
Results	87
Treatment with ribose glycosylated BSA induced internalization and decreased membrane bound FL-RAGE-YFP in HEK 293 cells	87
Expression of RAGE-ICD showed nuclear translocation without ribose glycosylated BSA treatment in HEK 293 and CHO cells	89
FL-RAGE undergoes intramembrane proteolysis upon treatment with ribose glycosylated BSA and leads to the nuclear translocation of its ICD	92
Characterizing the intranuclear localization of RAGE-ICD revealed localization in the nucleolus.....	96
Discussion	102
Conclusion.....	103
CHAPTER 5. IDENTIFYING DIFFERENTIALLY EXPRESSED GENES AND PROTEINS INVOLVED IN RAGE MEDIATED REGULATION OF CELL ADHESION PROPERTIES.....	105
Introduction	105

Screening of RAGE regulated transcription of adhesion relevant genes	106
Experimental design	106
Gene expression analysis using qPCR.....	106
Results	107
Validation using the linear regression model identified 7 housekeeping genes as stable candidate reference genes	107
qPCR analysis showed selective regulation of cell adhesion molecule (CAM) gene expression in RAGE HEK 293 cells	109
Discussion.....	115
A proteomics approach to identify adhesion relevant cell surface protein regulated by RAGE	116
Experimental design	116
Cell surface proteomics.....	116
Results	118
Validation of cell surface protein labeling, enrichment, and digestion	118
RAGE HEK 293 cells showed altered expression of adhesion relevant proteins.....	121
Discussion.....	125
Effect of RAGE knockdown in cell adhesion and ITGA8 expression.....	126
Experimental design	126
Knockdown of RAGE using shRNA	126
Results	127
RAGE knockdown reduced cell adhesion, cell spreading to ECM, and downregulation of ITGA8.....	127
Discussion.....	133
Conclusion.....	134
CHAPTER 6. SUMMARY AND CONCLUSIONS; CLINICAL RELEVANCE; LIMITATIONS; AND FUTURE DIRECTIONS.....	137

Summary and conclusion	137
Clinical relevance	140
Limitations	141
Future directions.....	142
REFERENCES	143
APPENDIX A. SUPPLEMENTAL FIGURES	165
APPENDIX B. NUCLEOTIDE AND PROTEIN SEQUENCE OF RAGE MUTANTS (CHAPTER 3 AND 4).....	176
APPENDIX C. LIST OF HOUSEKEEPING GENES USED FOR INITIAL SCREENING IN THE STUDY (CHAPTER 5).....	180
APPENDIX D. LIST OF 67 POTENTIAL GENES CANDIDATES RESPONSIBLE FOR MEDIATING CELL ADHESION TESTED IN THE STUDY (CHAPTER 5).....	181

LIST OF TABLES

<u>Table</u>	<u>Page</u>
1.1: RAGE ligands and their binding regions in RAGE domains.	15
1.2: RAGE inhibitors along with their targeted RAGE domains and their effects.....	22
2.1: Details of the antibodies used in this study along with dilution specification for Western blotting (WB), immunofluorescence (IF), and flow cytometry (FC) experiments.	32
3.1: Percentage of cell surface localized RAGE in FL-, DN-, Δ C1-, and Δ C2-RAGE variant transfected HEK 293 cells.	54
3.2: Quantitative analysis of the identified cell-cell contacts between RAGE HEK 293 (RFP expressing) and WT HEK 293 (GFP expressing) cells.	61
5.1: Ct values of housekeeping genes (HKGs) in WT HEK 293 and RAGE HEK 293 cells expressed as mean \pm SEM (n=3).	108
5.2: C _t values of genes mediating cell adhesion in WT HEK 293 and RAGE HEK 293 cells expressed as mean \pm SEM (n=3).	110

LIST OF FIGURES

<u>Figure</u>	<u>Page</u>
1.1: Cartoon representation showing cell-matrix interactions.	3
1.2: Schematic representation of five major families of cell adhesion molecules involved in cell-cell and cell-matrix interactions.....	4
1.3: Classification of integrin receptor family.	9
1.4: Schematic representation of full-length RAGE.	12
1.5: Schematic representation of RAGE splice variants.	14
1.6: Different models illustrating RAGE signaling.	18
1.7: Model illustrating (A) structural comparison of RAGE V and C1 domains to a family of cell adhesion molecules and (B) RAGE-RAGE homophilic interaction in mediating cell adhesion.	24
3.1: Domain organization of full-length RAGE (FL-RAGE) and the domain deletion variants used in this study.	40
3.2: Hydrolysis of pNPP catalyzed by alkaline phosphatase.	42
3.3: Binding regions of the antiRAGE antibodies 9A11 and D1A12 used in this study.	43
3.4: Epifluorescence images of HEK 293 cells transfected with pcDNA3 GFP using different ratios of PEI at 24 and 48 hours.	45
3.5: (A) Epifluorescence images of HEK 293 cells transfected with pcDNA3 GFP using Lipofectamine 3000 with optimized conditions after 24 hours. (B) Plot showing the integrated intensity of the fluorescence from the GFP-positive cells.....	46
3.6: Plot showing absorbance at 405 nm from SEAP assay in HEK 293 cells transfected with pcDNA3 SEAP for 24 hours.	47
3.7: Protein expression of FL-RAGE and other RAGE variants at different transfection time points.....	49
3.8: Confocal microscopy images of HEK 293 cells expressing the FL-RAGE and different domain deletion variants.	51
3.9: Flow cytometry dot blots of HEK 293 cells transiently transfected with mock, FL-RAGE, DN-RAGE, Δ C1-RAGE, and Δ C2-RAGE.	53

3.10:	Flow cytometry dot blot of HEK 293 cells transiently transfected with ΔV -RAGE and TmCyto-RAGE under permeabilized conditions using antiRAGE D1A12 antibody.....	54
3.11:	Schematic representation of the RAGE-RAGE and RAGE-nonRAGE association study.....	58
3.12:	Confocal microscopy image of RAGE HEK 293 cells stained with c-terminus antiRAGE D1A12 antibody on collagen IV coated surface.	59
3.13:	Confocal microscopy images showing cell-cell adhesion in RAGE HEK 293 and HEK 293 cells.	60
3.14:	Percentage of different cell-cell contacts; RAGE-RAGE, RAGE-nonRAGE, nonRAGE-nonRAGE, and nonfluorescent cells.....	61
3.15:	Schematic workflow of the Xcelligence RTCA dp system, Agilent.	63
3.16:	Plot of cell index/cell impedance value (Z) at 30 min time point between glass and plastic surface type E-16 well plates with different cell densities.	64
3.17:	Plot of Xcelligence RTCA data showing cell adhesion of HEK 293 cell transiently transfected with RAGE variants to collagen IV at 30 min and 6 hours.....	66
3.18:	Plot of Xcelligence RTCA data showing cell adhesion of HEK 293 cell transiently transfected with RAGE variants (FL-, DN-, TmCyto-) and mock to matrigel for 5 hours.....	68
3.19:	Plots of cell adhesion plate assay data in HEK 293 cell transiently transfected with RAGE variants (FL-, DN-, TmCyto-) and mock to different ECM proteins.	69
3.20:	Microscopy images from cell spreading assay in HEK 293 cell transiently transfected with RAGE variants (FL-, DN-, TmCyto-) and mock to different ECM proteins.....	72
3.21:	Quantitative analysis of circularity of cells transfected with RAGE variants (FL-, DN-, TmCyto- RAGE) and mock transfected cells.	73
3.22:	Schematic illustration of results of cell-cell contacts formed from wild type and RAGE expressing HEK 293 cells on collagen IV coated surface.	77
3.23:	Overall findings from chapter 3 on the effect of RAGE variant expression on cell adhesion and cell spreading to ECM in HEK 293 cells.....	78
4.1:	Cartoon representation of the different plasmids constructed to monitor ligand induced changes in the subcellular localization in RAGE.....	86

4.2:	Confocal images of WT HEK 293 cells transfected with (A) control, YFP, and FL-RAGE-YFP plasmids. (B) Images of cells transfected with FL-RAGE-YFP and treated with ribose glycated BSA at different time points (1, 6, and 24 hours). (C) 3D image of cells transfected with FL-RAGE and treated with ribose glycated BSA for 24 hours.	88
4.3:	Confocal microscopy images of cells transfected with control plasmid containing only cyan fluorescent protein (CFP) tagging and RAGE-ICD CFP in HEK 293 (left) and CHO cells (right).....	91
4.4:	Data from the SeqNLS software.	92
4.5:	Confocal images (2D and 3D view) of WT HEK 293 cells transfected with EGFP-FL- RAGE-RFP in non-treated and ribose glycated BSA treated conditions.	94
4.6:	Confocal microscopy images of WT HEK 293 cells co-transfected with RAGE-ICD-CFP and mTagRFP-T-Fibrillarin-7.	97
4.7:	Confocal microscopy images of HEK 293 cells co-transfected with FL-RAGE-YFP and mTagRFP-T-Fibrillarin-7, treated with ribose glycated BSA.	99
4.8:	Colocalization analysis of RAGE-ICD-EGFP and mTagRFP-T-Fibrillarin-7 using Image Pro Premier software.....	100
4.9:	Screenshot of the output window from the Nucleolar localization sequence Detector (NoD) online software.....	101
4.10:	Proposed mechanism for nucleolar localization of RAGE through intramembrane proteolysis.	104
5.1:	Expression correlation plot with the mean Ct values of the 15 housekeeping genes from WT HEK 293 and RAGE HEK 293 cells.	108
5.2:	Gene expression of integrin alpha 8 (ITGA8) and contactin 1 (CNTN 1) in WT HEK 293 and RAGE HEK 293 cells.	112
5.3:	Change in the gene expression of melanoma cell adhesion molecules – (MCAM & MUC18) (left), fibronectin 1 (FN1), and thrombospondin-1 (THBS1) between WT HEK 293 and RAGE HEK 293 cells.	113
5.4:	Western blot against ITGA8 and CNTN1 in WT HEK 293 and RAGE HEK 293 cells.	114
5.5:	Schematic illustration of sample preparation and processing for cell surface proteomics.....	118
5.6:	Results from optimization of cell surface protein labeling for proteomics experiment.....	120

5.7:	Differentially expressed adhesion relevant proteins in WT and RAGE HEK 293 cells identified by LC-MS-MS proteomics.....	122
5.8:	Differentially expressed adhesion proteins upon RAGE expression in HEK 293 cells by cell surface proteomics (top). Pathway analysis using the Panther classification system on the genes identified in RAGE HEK 293 cells (bottom).	124
5.9:	qPCR and Western blot data showing relative fold change in RAGE expression after shRNA knockdown in RAGE HEK 293 cells.....	127
5.10:	Plots from cell adhesion plate assay with RAGE HEK 293 cells transfected with control and RAGE shRNA to collagen IV (top center), fibronectin (bottom left), and collagen I (bottom right) coated surfaces.....	129
5.11:	Images from cell spreading assay in RAGE HEK 293 cells transfected with control and RAGE shRNA.....	130
5.12:	Western blot against ITGA8 in RAGE HEK 293 cells transfected with control/scrambled and RAGE shRNA.....	131
5.13:	Validation of endogenous expression of RAGE and ITGA8 in MIA PaCa-2 cells.....	132
5.14:	Western blot showing expression of RAGE and ITGA8 in MIA PaCa-2 cells after RAGE knockdown.....	133
5.15:	Overall findings from Chapter 5 show RAGE expression increases cell adhesion and cell spreading to ECM by regulating ITGA8 expression.....	136
6.1:	Overall findings and proposed model of RAGE signaling to cell adhesion by intramembrane proteolysis.....	140

LIST OF ABBREVIATIONS

AA.....	Amino Acid Residues
AGEs.....	Advanced Glycation Endproducts
AKT	Protein Kinase B
ALCAM	Activated Leukocyte Cell Adhesion Molecule
BCAM.....	Basal Cell Adhesion Molecule
BSA.....	Bovine Serum Album
CAMs.....	Cell Adhesion Molecules
CFP	Cyan Fluorescent Protein
CNTN1.....	Contactin1
C _t	Cycle Threshold
DAMPs	Damaged Associated Molecular Patterns
DMEM	Dulbecco's Modified Eagle Medium
DNA.....	Deoxyribonucleic Acid
DN-RAGE.....	Dominant Negative Variant Receptor for Advanced Glycation End Products
DTT.....	Dithiothreitol
ECM.....	Extracellular Matrix
EGFP.....	Emerald Green Fluorescent Protein
EMT	Epithelial-Mesenchymal Transition
ERK.....	Extracellular Signal-Regulated Kinases
FBS	Fetal Bovine Serum
FITC.....	Fluorescein Isothiocyanate
FL-RAGE.....	Full-Length Receptor for Advanced Glycation Endproducts
FN1	Fibronectin1

HEK 293	Human Embryonic Kidney 293 Cells
HKG	Housekeeping Genes
HMGB1.....	High Mobility Group Box1
HRP.....	Horseradish Peroxidase
ICAM	Intercellular Adhesion Molecule
ICD.....	Intracellular Cytoplasmic Domain
ITGA8.....	Integrin Alpha 8
LC-MS	Liquid Chromatography- Mass Spectrometry
MAPK.....	Mitogen Activated Protein Kinase
MCAM.....	Melanoma Cell Adhesion Molecule
MMPs.....	Matrix Metalloproteinases
NF- κ B	Nuclear Factor kappa-Light-Chain-Enhancer of Activated B Cells
NLS	Nuclear Localization Signal
NoD.....	Nucleolar Localization Sequence Detector
NP-40	Nonyl Phenoxypolyethoxyethanol
PEI.....	Polyethylenimine
PI3K	Phosphatidylinositol-3-Kinase
pNPP	pNitrophenyl Phosphate
QPCR	Quantitative Polymerase Chain Reaction
RAGE.....	Receptor for Advanced Glycation Endproducts
RFP	Red Fluorescent Protein
RIP	Regulated Intramembrane Proteolysis
RIPA	Radioimmunoprecipitation Assay Buffer
RNA	Ribonucleic Acid
ROI.....	Region of Interest

SEAP.....	Secreted Alkaline Phosphatase
THBS1	Thrombospondin-1
TLRs	Toll-Like Receptors
TmCyto-RAGE.....	Transmembrane and Cytoplasmic Domain of the Receptor for Advanced Glycation Endproducts
VCAM.....	Vascular Cell Adhesion Molecule
WT	Wild Type
YFP	Yellow Fluorescent Protein
Δ C1-RAGE	Receptor for Advanced Glycation Endproducts in Which the C1 Domain Is Deleted
Δ C2-RAGE	Receptor for Advanced Glycation Endproducts in Which the C2 Domain Is Deleted
Δ V-RAGE.....	Receptor for Advanced Glycation Endproducts in Which the V Domain Is Deleted

LIST OF APPENDIX FIGURES

<u>Figure</u>	<u>Page</u>
A1: Agarose gel (1.5%) with the PCR products amplified from mycoplasma primers.	165
A2: UV spectra of the pcDNA3 FL-RAGE plasmid (left). Extracted plasmids pcDNA3 empty vector (MOCK) and pcDNA3 full length (FL)-RAGE ran on a agarose gel (0.8%) with 10Kbp DNA ladder (New England Biolabs) (right).....	165
A3: Extracted total RNA sample ran on a agarose gel.	166
A4: Additional western blot data from different experiments representing figure 3.7 of chapter 3. Protein expression in WT HEK 293 cells transfected with FL-RAGE and other RAGE variants at time points (A) 24, 48, and 72 hours and (B) at 24 hours in WT HEK 293 cells.....	167
A5: Additional images from different experiments representing figure 3.8 of chapter 3. Confocal microscopy images of cells expressing the FL-RAGE and different domain deletion variants.	168
A6: Microscopy images from all four individual experiments (A, B, C, and D) n=4, showing cell-cell adhesion in RAGE HEK 293 and WT HEK 293 cells (additional images for figure 3.13 of chapter 3).....	169
A7: Additional images representing figure 4.2 of chapter 4. Confocal images of HEK 293 cells transfected with FL-RAGE-YFP plasmids and treated with ribose glycosylated BSA at different time points (1, 6 and 24 hours).	170
A8: Additional images representing figure 4.3 of chapter 4. Confocal microscopy images of cells transfected with control plasmid containing only cyan fluorescent protein (CFP) tagging and RAGE-ICD CFP in HEK 293 (left) and CHO cells (right).	171
A9: Additional images representing figure 4.5 of chapter 4. Confocal images (2D and 3D view) of WT HEK 293 cells transfected with EGFP-FL- RAGE-RFP plasmid in ribose glycosylated BSA treated conditions.....	172
A10: Detection of GAPDH in enriched biotinylated samples labeled with aminooxy biotin and EZ-Link Sulfo-NHS-LC-Biotin.....	173
A11: Venn diagram of adhesion relevant proteins identified from cell surface proteomics.....	174
A12: Relative changes in RAGE expression at mRNA and protein levels upon RAGE shRNA transfection in RAGE HEK 293 cells.	175

CHAPTER 1. GENERAL INTRODUCTION

Extracellular matrix, cell adhesion, and cell adhesion molecules

Extracellular matrix (ECM) is the non-cellular component that is present within all tissues and organs and provides essential physical scaffolding for the cellular constituents. ECM is crucial for initiating various biochemical and biomechanical cues for tissue morphogenesis (1). The composition and the topology of the ECM exhibit variability depending on the tissue type and the protein microenvironment. The fundamental ECM composition includes water, polysaccharides, and two main classes of macromolecules: proteoglycans and fibrous proteins with distant physical and biochemical properties. Proteoglycans are composed of glycosaminoglycans which are linear anionic polysaccharides. There are three main families: small leucine-rich proteoglycans, modular proteoglycans, and cell-surface proteoglycans which are widely expressed in all tissue types. The extreme hydrophilic nature and highly extended conformation of proteoglycans are essential for hydrogel and matrix formation (2).

The major fibrous ECM proteins are the collagens, fibronectins, elastin, and laminins, with collagen being the main occupant contributing over 30% of ECM proteins (3). The collagens represent the triple helical structure protein family of repeating peptide triplets of glycine and proline or hydroxyproline, which contributes to 46 distinct collagen chains. In vertebrates, these collagen chains assemble to form 28 different collagen types and are majorly categorized as fibril and network forming collagens (4). The fibril form collagen forms the backbone of the interstitial tissue stroma. These collagen types include I, II, III, V, and IX. The network forming collagens, also known as basement membrane collagens, are nonfibrillar in nature. Type IV collagen is the major collagen component of the basement membrane underlining epithelial and endothelial cells (5).

The fibronectins are ubiquitous, abundant ECM proteins secreted as soluble dimers. The soluble dimeric fibronectin forms into a fibrillar matrix network due to extracellular and intracellular promoting fibrillar formation. The secreted dimers also contribute to fibronectin fibrils formation by binding to other fibronectin dimers, collagens, and cell surface receptors (6,7). Like collagen, elastins are a major constituent of the ECM of connective tissue with greater flexibility. The monomeric soluble precursor tropoelastin is the main component of elastin, contributing to its elastic and recoiling nature. The characteristic domain arrangement in tropoelastin consists of hydrophobic sequences alternating with lysine containing cross-linking motifs. These cross-linking motifs aid in the direct interaction of microfibrillar proteins required for the assembly of the elastin (8). The laminins are heterotrimeric ECM proteins with α -, β - and γ -subunits. The laminins can self-assemble or associate with type IV collagens to form a matrix network in the basement membrane (9).

ECM plays a regulatory role in controlling key cellular mechanisms, including cell adhesion. Cell adhesion is referred to as the process where a cell forms contact with other cells, substratum in their surroundings, or ECM (10-12). It involves stimulating signals required for tissue/organ development, growth, and anchorage. Cell adhesion also plays a vital role in cell communication and regulation, which is of fundamental importance in maintaining the structural integrity of multicellular organs and their physiological functions (13). Adhesion occurs via controlled cell-cell or cell-ECM interactions and is performed by a group of specialized proteins called cell adhesion molecules (CAMs) (14,15).

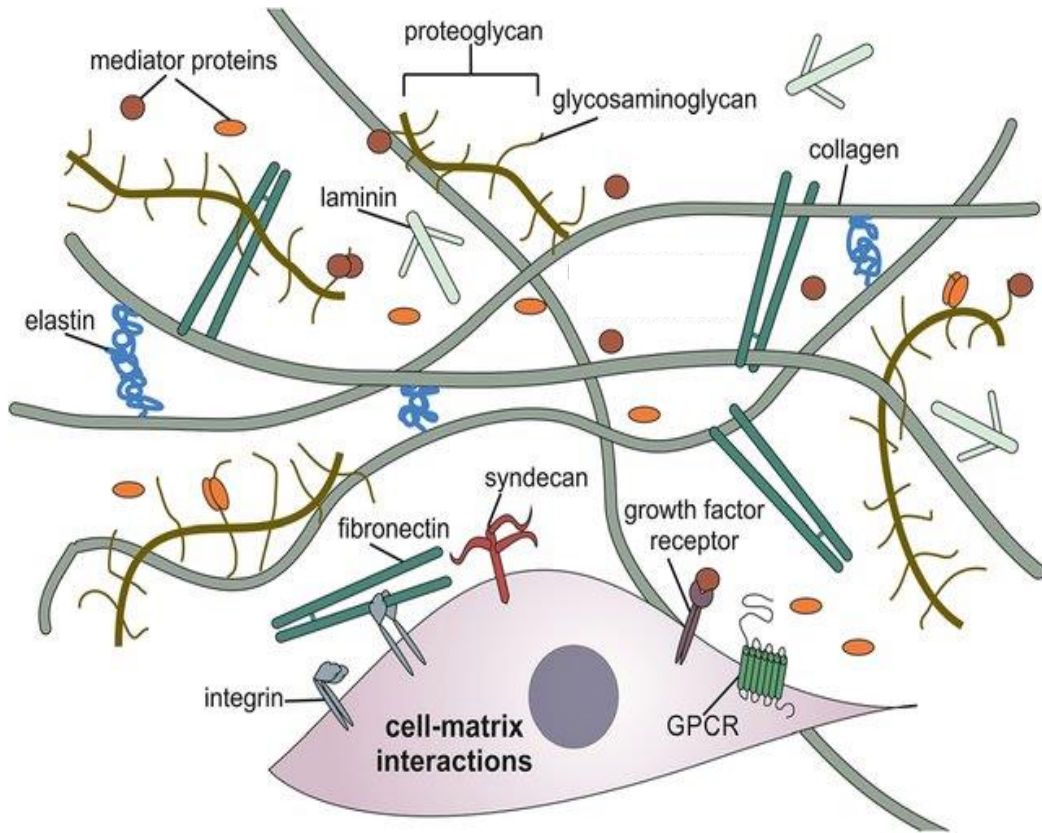


Figure 1.1: Cartoon representation showing cell-matrix interactions.

Major ECM proteins such as proteoglycan, collagen, elastin, laminin, and fibronectin forms association with the cell surface and adhesion receptors such as syndecans, growth factor receptors, G-protein coupled receptors (GPCR), and integrins to mediate cell adhesion. Taken from (16).

CAMs are glycoproteins expressed on the surface of cells that mediate adhesion to ECM and with other cells. They are typically transmembrane receptors composed of an extracellular domain, a transmembrane domain, and a cytoplasmic tail. CAMs link extracellular signals to intracellular responses through their cytoplasmic domain, which associates with cytoskeletal and cytoplasmic proteins to activate downstream cellular signaling (17,18). Cell-cell adhesion requires the association of one or more CAMs, which are then reinforced by clustering of specific adhesion molecules in cell junctions involving homophilic, heterophilic, or mixed interactions (19-21). The probability and degree of strength in forming these interactions depend on the expression of specific cell adhesion receptors, their localization, and relative binding affinities (22). In cell-ECM

interaction, CAMs serve as contact sites between them and activate multiprotein adhesion signaling complexes (1,3,23). The matricellular proteins, including CAMs and cytoskeletal proteins, constitute the multiprotein adhesion signaling complex capable of transducing bidirectional signals between extracellular and intracellular compartments (24). Cell-cell and cell-ECM adhesion is regulated by CAMs surface density, receptor clustering, and receptor activation state. Based on CAMs structure, protein sequence, and mode of interaction, the CAMs are classified into five families: cadherins, selectins, Ig-superfamily receptors, mucins, and integrins (Figure 1.2) (19,25).

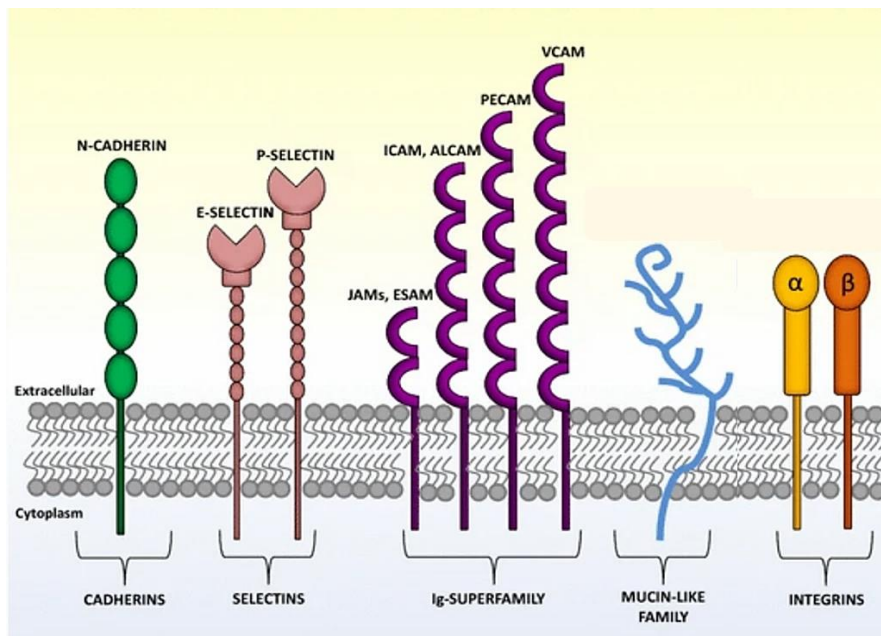


Figure 1.2: Schematic representation of five major families of cell adhesion molecules involved in cell-cell and cell-matrix interactions.

From left: cadherins, selectins, immunoglobulin (Ig)-superfamily, mucin-like family, and integrins, taken from (26). The tentacles like structure in the extracellular region of mucins represent the O-linked glycans. Integrins are heterodimeric type 1 transmembrane proteins containing α and β subunits linked together by a disulfide bond.

Classification and role of cell adhesion molecules in physiology

Cadherins

Cadherins are generally reported to mediate cell-cell adhesion and tend to be concentrated at cellular junctions. The typical structure of cadherins comprises five tandem repeated extracellular domains, a single membrane-spanning segment, and a cytoplasmic tail (27,28). The major cadherin family includes: epithelial (E)-cadherin, placental (P)-cadherin, and neural (N)-cadherin, and there are at least 20 different subtypes that were reported (29). Cadherins function depends on the levels of calcium ions, and their depletion makes cadherins more prone to proteolysis, decreasing adhesion (30). The five extracellular domains of cadherin mediate calcium dependent adhesion by forming either homophilic or heterophilic interaction (31). Extracellular domain interactions trigger the cytoplasmic tail of cadherins to bind with cytoplasmic binding partners such as α -catenin and β -catenin (28). Catenin bridges the adherent junctions to the actin filaments activating a range of signaling networks, including Rho GTPases, mitogen activated protein kinase (MAPK), Wnt, and Hedgehog pathways (32,33). Loss of cadherin expression or any disruption in cadherin-catenin binding is reported to alter cell adhesion behavior and promote tumorigenesis, renal injury, and autoimmune diseases such as rheumatoid arthritis and systemic sclerosis by signaling to inflammation (34-36).

Selectins

Selectins belong to the C-type mammalian lectins that bind carbohydrate ligands in a calcium dependent manner. They mediate transient cell-cell adhesion in the bloodstream by recognizing carbohydrates on the cell surface (37-39). Selectins consist of an N-terminal calcium dependent lectin domain (CRD), an epidermal growth factor like domain, a series of consensus repeat domains, a transmembrane domain, and a short cytoplasmic tail (40). There are three

members of the selectin family: leukocyte (L)-selectin, platelet (P)-selectin, and endothelial (E)-selectin. The members of the selectin family have high sequence similarities between each other and across different species. Selectins were reported to have an essential role in leukocyte recruitment to the inflammatory site. They mediate leukocyte rolling to sites of inflammation by enabling chemokine or platelet activating factor triggered activation of $\beta 2$ integrins. Several signaling events are activated during this process, such as Src family kinases and phosphatidylinositol-3-kinase, and protein kinase B (PI3K-AKT) (41,42). Abnormal functioning of selectins is associated with various pathologies, including cancer and diabetes (42-45).

Immunoglobulin (Ig)-superfamily

Proteins that have a structure similar to immunoglobulins (Ig) are classified into the Ig-superfamily. The Ig-superfamily is defined by the Ig-domains in the protein structure. There are three types of Ig-like domains: V-like domains, C1-like domains, and C2 like domains. Most of the Ig super family members belong to the type 1 transmembrane protein family and are broadly classified into three general classes based on the presence of (i) only Ig domains, (ii) Ig domains with additional domains resembling ECM component fibronectin (FN-like domains), and (iii) Ig domains with additional domains other than FN-like domains (46,47). The functioning of the Ig superfamily is independent of the presence of calcium ions. The Ig protein family members can form homophilic or heterophilic interactions to mediate cell adhesion (48). Members of the Ig superfamily adhesion molecules include intercellular adhesion molecule (ICAM), vascular cell adhesion molecule (VCAM), activated leukocyte cell adhesion molecule (ALCAM), and junctional adhesion molecule (JCAM). The Ig superfamily adhesion molecules are reported to play a key role in various adhesion events, including leukocyte trafficking involving nuclear factor kappa-light-chain-enhancer of activated B cells (NF- κ B) pathway (49-51). Increased expression

of Ig type CAMs are reported in cancer (52-57), vascular disease (58-60), and renal disease (61,62).

Mucin-like family

Mucins consist of serine and threonine rich proteins and are heavily glycosylated. Their structural organization usually contains proline/threonine/serine (PTS)-rich O-glycosylated domains, EGF-like, and sea urchin sperm protein, enterokinase and agrin (SEA) domains in the extracellular region, a transmembrane domain, and a cytoplasmic tail (63). There are 21 different mucin genes designated as MUC1- MUC21, and they are classified as secreted or membrane-associated (64). Secreted mucins are small soluble mucins or gel-forming mucins which are stored in secretory granules and released upon stimulus (65). Membrane associated mucins are involved in cell adhesion and have the ability to function as a cell's barrier and in cell adhesion by controlling the interactions mediated by integrins and E-cadherins (66,67). The signaling of membrane associated mucin proteins is initiated with the cleavage of the extracellular domain by metalloproteases and by regulated intramembrane proteolysis (RIP). Phosphorylation of the cytoplasmic domain activates Wnt- β -catenin, p53, and NF- κ B pathways, (63). Evidence suggests that membrane associated mucins contribute to carcinogenesis both via their glycosylated extracellular domain which may protect cancer cells by forming a cellular barrier and via their intracellular domain that links to pathways which regulate cell differentiation, apoptosis, and inflammation (68,69).

Integrins

Integrins are large heterodimeric type 1 transmembrane proteins containing α and β subunits linked together by a disulfide bond (70). The integrin family comprises 18 α and 8 β subunits that can assemble into 24 different integrins in vertebrates. The sizes of the α and β

subunits vary but typically contain around 750 to 1000 amino acids. The α subunit consists of four or five extracellular domains: a seven-bladed β -propeller, a thigh, two calf domains (calf1 and calf2), a transmembrane domain, and a short cytoplasmic domain. Nine of the 18 integrin α subunits have an α -I domain (~200 amino acids) inserted between blades 2 and 3. The α -I domain undergoes numerous conformational changes, which are important for regulating the binding affinity with the β subunit. The β subunit contains seven domains: β -I domain, plexin-semaphorin-integrin (PSI) domain, four cysteine-rich epidermal growth factor (EGF) modules, and a β -tail domain (71,72). The $\alpha\beta$ pairings occur via the β -propeller surface on the α subunit and the β -I and PSI domain in the β subunit. Integrins are the principal receptors linking ECM to cytoskeletal proteins (73). They bind to the ECM proteins with their large ectodomain and engage with the cytoskeleton through their short cytoplasmic tails. The α subunit, primarily the α -I domain of the integrin, determines the specificity of ligand binding. Depending on their ligand specificity, integrins are broadly grouped into four categories; arginine-lysine-aspartic acid (RGD) receptors, laminin receptors, leukocyte-specific receptors, and collagen receptors (Figure 1.3) (74).

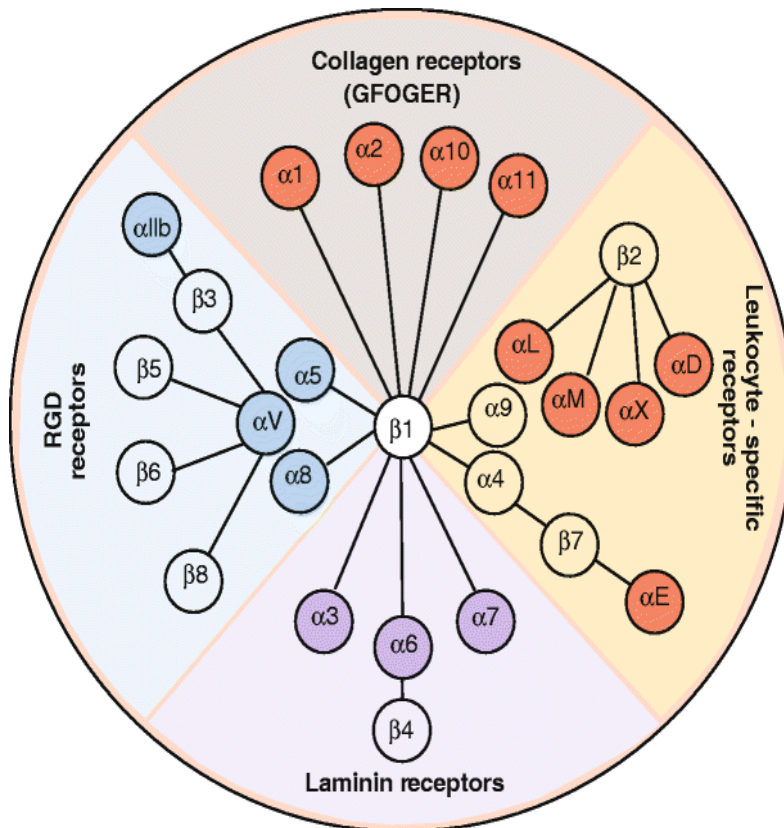


Figure 1.3: Classification of integrin receptor family.

The integrin heterodimers in vertebrates are classified into four major families; RGD, collagen, leukocyte, and laminin binding integrin receptors (taken from (74)). The RGD type integrins recognize the RGD sequence, and the collagen binding integrin receptors recognize the triple helical GFOGER sequence. Laminin integrin receptors bind to laminin and leukocyte specific receptors to mediate leukocyte activation and extravasation.

The RGD type integrins recognize the RGD sequence in their ligands and bind to from cell attachment. Nearly half of the integrin family are categorized as RGD type integrins. The four collagen binding αI domain integrins ($\alpha 1$, $\alpha 2$, $\alpha 10$, and $\alpha 11$) along with $\beta 1$ integrin serves as collagen binding integrin receptors with the ability to recognize the triple-helical GFOGER sequence (Glycine-Phenylalanine-Hydroxyproline-Glycine-Glutamic acid-Arginine). Similarly, several members of the integrin family, including $\alpha 3\beta 1$, $\alpha 6\beta 1$, and $\alpha 7\beta 1$, serve as laminin receptors. Leukocyte integrins consist of several α subunits coupled to either $\beta 1$ or $\beta 2$ integrin.

They mediate leukocyte adhesion by regulating their expression depending on the stage of leukocyte activation and extravasation (72,74).

Integrin activation occurs either through ligand binding or conformational changes in the cytoplasmic tail resulting in “outside – in” or “inside – out” signaling. Integrin clustering on the cell surface also modulates the receptor signaling by shifting from a low affinity folded conformation to a high affinity state. Clustered integrins are also capable of recruiting cytoskeletal proteins such as talin, kindlin, focal adhesion kinase (FAK), scaffold molecules, and Src family kinases, leading to conformational changes in the cytoplasmic region and receptor activation (75). Such processes link integrins to downstream signalings, such as the PI3K/AKT pathways, Rac1 GTPases, and MAPK pathways. The cytoskeletal proteins such as talin, kindlin, and FAK also regulate integrin signaling by modulating the association of the cytoplasmic domain with its respective downstream effectors of integrins (76,77). Integrins are involved in many pathological conditions by signaling to inflammation and angiogenesis (78). In cancers, integrins' expression is deregulated and is a key player in epithelial and mesenchymal transition (EMT) transition. Integrins crosstalk with other receptors and growth factors and regulate cancer cell adhesion and migration, ultimately contributing to cancer cell invasion and metastasis (79-81). Integrins also mediate other pathological conditions, including fibrosis (82-84), vascular pathologies (85-87), and neurological disorders (88-90). Because of their involvement in various pathologies, integrins are evaluated as potential therapeutic targets (91-93).

RAGE (receptor for advanced glycation endproducts)

The receptor for advanced glycation endproducts (RAGE) belongs to the type 1 transmembrane protein family and is a member of the immunoglobulin Ig superfamily of receptors (94). RAGE was initially identified as the receptor for advanced glycation end products (AGE),

produced by non-enzymatic glycation of proteins (95). RAGE is a pattern recognition receptor and is capable of binding to multiple ligands such as advanced glycation end products (AGEs), S100 proteins, and high mobility group box 1 (HMGB1), collectively called damaged associated molecular patterns (DAMPs). DAMPs are endogenous molecules released by stressed or damaged cells which signal to initiate proinflammatory responses (96). RAGE binding to DAMPs is capable of activating NF- κ B via various downstream signaling pathways such as the mitogen-activated protein kinase (MAPK) pathway, Janus kinase (JAK)/signal transducer, and activator of transcription (STAT) pathway, extracellular signal-regulated kinase (ERK1/2) pathway. RAGE signaling regulates the transcription of adhesion molecules, chemokines, chemokine receptors, and cellular processes, including proliferation, cell survival, differentiation, migration, and autophagy (97-100). RAGE overexpression is associated with the progression of disease states like diabetes, cancer, Alzheimer's, and cardiovascular diseases (101).

RAGE structure and expression

The RAGE gene is localized in the class III MHC region of chromosome 6. The RAGE gene is comprised of a short 3' UTR, 11 exons, and a 5' flanking region that regulates transcription (102). Protein sequence analysis revealed that the mature form of RAGE is comprised of 1. The extracellular region (23-342 amino acid residues (aa)), 2. a transmembrane domain (TM) (343-363 aa), and 3. an intracellular cytoplasmic tail (Cyto) (364-404 aa). The extracellular structure of RAGE is composed of an N-terminal variable type Ig domain (V) (23-116 aa) and two constant type Ig domains (C1 and C2) domains (124-221 & 227-317 aa) (103,104) (Figure 1.4). The secondary structures of the RAGE V, C1, and C2 domains show typical immunoglobulin fold consisting of β -strands connected via loops. The VC1C2 domains are followed by a helical transmembrane domain (TM), and the intracellular cytoplasmic domain of the RAGE (Cyto). The

C1 and C2 domains are linked via an unstructured flexible linker (105,106). The RAGE VC1 ectodomain forms an integral structural unit where the V domain contains two glycosylation sites (Asn²⁵ and Asn⁸¹) required for the plasma membrane localization of the receptor (104). Studies have also identified that the RAGE V domain is crucial for RAGE dimer formation (107). Mutation or deletion of the V domain of RAGE decreased the stability of the C1 domain highlighting the dependence of the two domains (108). The cytoplasmic tail of RAGE is unstructured, short, and positively charged and is essential for signal transduction (97,109).

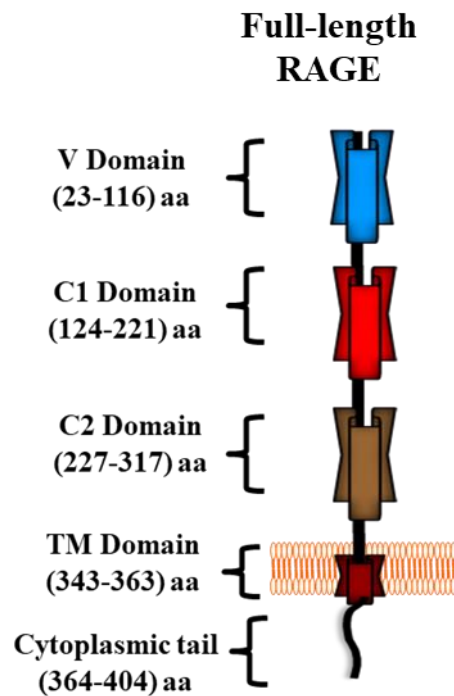


Figure 1.4: Schematic representation of full-length RAGE.

RAGE is comprised of 1) the extracellular region containing the V domain (23-116 aa), C1 domain (124-221 aa), and the C2 domain (227-317 aa), 2) a transmembrane domain (TM) (343-363 aa), and 3) an intracellular cytoplasmic tail (Cyto) (364-404 aa).

The signal peptide (1-22 aa) in RAGE directs its translocation to the cell surface and is removed by a signal peptidase located within the endoplasmic reticulum lumen. The native RAGE protein lacks the signal peptide and has a molecular weight of about 45-55 kDa, depending on the

level of glycosylation. During embryonic development, RAGE is constitutively expressed in various tissues, including the brain, kidney, smooth muscle cells, and vasculature, and is downregulated in adulthood (110-112). The only exception is type I alveolar epithelial cells, where RAGE is expressed in greater abundance throughout life, and deletion/absence of RAGE in these cells has been reported to affect the epithelial and matrix interactions (113-116).

RAGE undergoes proteolytic cleavage and splicing events to yield different isoforms, and it has been reported that there are over 20 isoforms found in mammals at mRNA levels (102,117). The predominant isoforms of RAGE present at the protein level include full-length RAGE (FL-RAGE) and the splice variants dominant-negative RAGE (DN-RAGE, residues 23–363 aa), N-truncated RAGE (N-RAGE, 124–404 aa), and secretory RAGE. The secretory RAGE is the circulating soluble form of RAGE, which lacks the transmembrane and the cytoplasmic domains. The secretory RAGE isoform comprises endogenous secretory RAGE (es-RAGE) produced from alternative splicing, and the proteolytically generated C-terminal truncated RAGE known as soluble RAGE (sRAGE, 23–342 aa) (Figure 1.5) (112,118,119). The secreted RAGE isoforms in the plasma act as decoy receptors by actively binding to RAGE ligands (120). Different levels of truncations at the N- and C-terminal of RAGE were found to have a significant effect on the RAGE-mediated disease states. In particular, the DN-RAGE isoform was observed to abolish the downstream RAGE signaling events and decrease the associated pathological effects *in vitro* and *in vivo* (98,102,121).

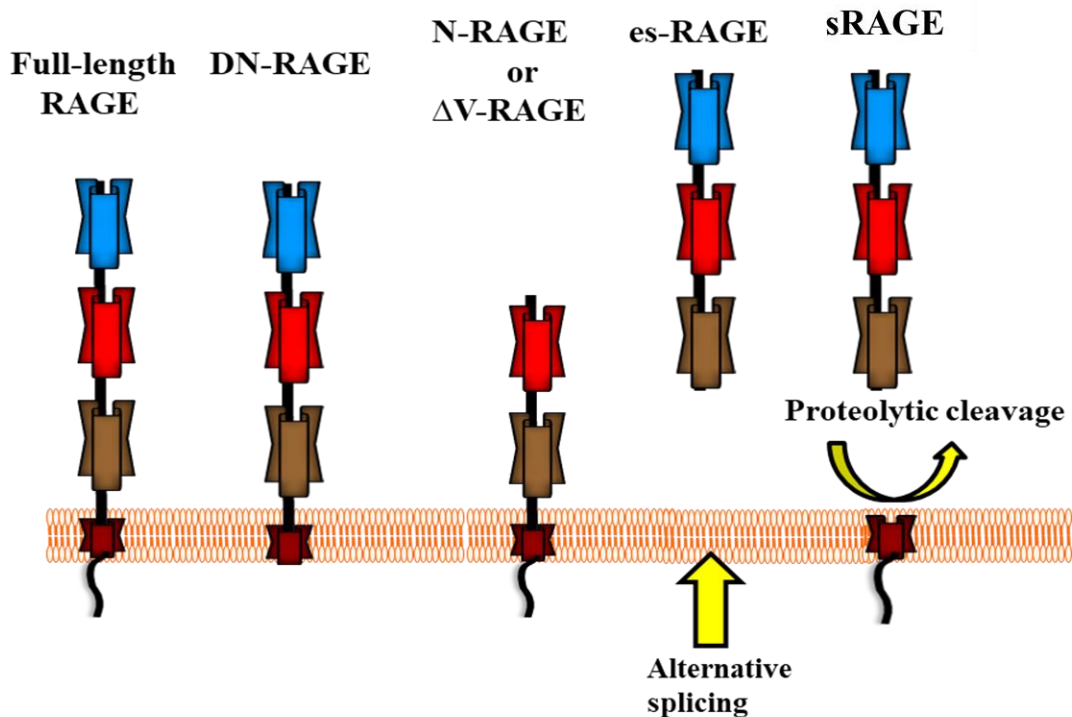


Figure 1.5: Schematic representation of RAGE splice variants.

From left: native/full-length RAGE, dominant-negative RAGE (DN-RAGE), N-truncated RAGE (N-RAGE), endogenous secretory (es-RAGE), and soluble form RAGE (sRAGE). DN-RAGE lacks the cytoplasmic domain and acts cell bound decoy receptor, and is not involved in signal transduction. The N-truncated or ΔV -RAGE lacks the ligand binding V domain. sRAGE consists of the complete extracellular domain which is produced as a result of proteolytic cleavage. es-RAGE another soluble form of RAGE, is produced from alternative splicing.

Ligand binding properties of RAGE

RAGE forms constitutive homodimers via cysteine mediated disulfide linkages in the extracellular region. Ligands binding to RAGE affect the structure and stoichiometry of the receptor complex and shift the equilibrium distribution in favor of higher order RAGE oligomers (122-124). The oligomerization interface in RAGE was reported to occur in the V-C1 and C1-C2 domains, and recent studies using mass spectroscopy analysis revealed a major role of the C2 and TM domains in oligomerization by contributing to their stability (125,126). Furthermore, *in vitro* studies showed that RAGE oligomerization is a major step of receptor-ligand interaction as it also

increases the number of binding sites (104,127). N- Glycosylation of RAGE has been shown to help with AGE recognition but does not affect the binding capacity with AGE (128,129). However, another study reported that deglycosylation of RAGE reduced binding affinity for the ligand amphoterin (107,128).

Being a multiligand receptor, RAGE can also interact with other molecules apart from DAMPs, such as Mac1, RNA/DNA, and β -amyloid fibrils. Ligand binding occurs in the extracellular V, C1, or VC1 domains (Table 1.1). This is because most of the ligands of RAGE display a net negative charge at neutral pH and will be attracted by the complementary positive surface charge of the VC1 domain (96,130). The uniqueness of the RAGE receptor lies in the fact that its intracellular domain lacks intrinsic kinase activity. RAGE-ligand complex formation drives the orientation of the cytoplasmic tail of RAGE in specific proximity to binding to adaptor proteins to initiate signaling. Studies performed *in vitro* and *in vivo* showed that the DN-RAGE variant or the deletion of the RAGE intracellular cytoplasmic domain prevented its ligands from activating signaling cascades (121,131).

Table 1.1: RAGE ligands and their binding regions in RAGE domains. Adapted from (132).

RAGE Ligands	RAGE Binding Domain
AGEs	V
β amyloid	V
S100/calgranulins	V or VC1 or C2
HMGB1	VC1C2
β -sheet fibrils	V
Mac1	V or VC1 or C2
RNA or DNA	VC1

RAGE signaling

The classical signaling of RAGE (Figure 1.6 A) involves ligand binding to the extracellular domains V, C1, and C2, whereas the transmembrane and the intracellular cytoplasmic domains are involved in the signal transmission (104,105). Oligomerization of RAGE was also reported to initiate receptor activation via homodimerization of the V or the C1 domains (124,133). The classical signaling suggests that RAGE signaling requires the involvement of adaptor proteins like diaphanous-1 (DIAPH1), Toll-Interleukin 1 Receptor Domain-Containing Adapter Protein (TIRAP), myeloid differentiation primary response gene 88 (MYD88), and Dedicator of cytokinesis protein 7 (DOCK7) (reviewed in (134)). In microglial cells, following RAGE binding with its ligand S100B led to the recruitment of the adaptor protein DIAPH1, a member of the formin family that mediates the effects of small GTPase of the Rho family near the C-terminus of RAGE. DIAPH1 recruits Rac1/Cdc42 with subsequent activation of the RhoA/ RhoA associated kinase (ROCK) pathway that governs the microglial motility (135). Affinity purification with mass spectroscopy analysis discovered another intracellular effector, DOCK7, which functions as a guanine nucleotide exchange factor. DOCK7 binds to the intracellular C-terminal region in RAGE, activating the Cdc42 pathway. siRNA knockdown of DOCK7 was reported to downregulate RAGE activated Cdc42 signaling in HEK 293T cells (132).

The phosphorylation of the cytoplasmic domain of RAGE at its residue Serine 391 by protein kinase C promotes recruitment of TIRAP and MyD88, other adaptor proteins in RAGE signaling (136). The signaling cascade is followed by the activation of inflammatory pathways through kinases (JAK; ERK1/2, mitogen-activated kinase (MAPK); phosphoinositide 3-kinase (PI3K)), and GTPases (cell division cycle 42 (cdc42)), which signals through transcription factors such as NF- κ B, activator protein 1 (AP-1), and signal transducer and activator of transcription 3

(STAT3) (137,138). The signaling pathways and the functional consequences of RAGE engagement strongly depend on the cell type, the specific ligand bound, and their local concentration. The hallmarks of RAGE signaling contributed to increased inflammation, cell proliferation, migration, cell adhesion, and a positive feedback loop mechanism inducing increased expression of the receptor through sustained receptor expression and activation, thus contributing to the severity of pathological conditions (Figure 1.5 A) (139,140).

Apart from the existing classical signaling of RAGE, there were studies that had reported other modes of RAGE signaling involving a change in the geometrical distance of its cytoplasmic domain. Xue et al. showed that ligand induced association of RAGE homodimers on the cell surface increased the molecular dimension of the receptor, recruiting DIAPH1 and activating signaling pathways (141). In this model, the Ca^{2+} bound S100B dimer binds to two V domains from different sRAGE homodimers. The induced oligomerization of RAGE by Ca^{2+} -S100B causes the C-termini of the C2 domains of the RAGE homodimer to move a distance of 100 Å from each other, which is twice the distance of C2 domains from a sRAGE homodimer. This change in the distance to 100 Å corresponded to the distance of the dimers of the Formin homology 1 (FH 1) domains of the adaptor protein, DIAPH1, and residues R366/Q367 of the cytoplasmic domain of RAGE was reported to be involved. Upon binding to the intracellular cytoplasmic tail of RAGE, the dimer of the domain FH 1 activates the autoregulatory/catalytic domain of the Diaphanous 1 to carry out subsequent signaling (Figure 1.6 B). Results from *in vitro* and *in vivo* studies also support this model as deleted mutant diaphanous 1 that lacks the FH 1 domain failed to undergo ERK1/2 phosphorylation (109,142-144).

Yatime et al. demonstrated that in addition to oligomerization, ligand binding could induce substantial conformational changes in the receptor ectodomain and bring into proximity the

intracellular domains from two RAGE molecules bound to the same dimeric S100 ligand (145). The crystal structures of two sRAGE (VC1C2) molecules formed dimers in the V domain region, leading to a spacing distance of 190Å in the C-terminus of the two C2 domains in a ligand unbound state. In comparison, the binding of S100A6 dimer with two C2 domains from different sRAGE dimers caused oligomerization and conformational changes, which decreased the spacing between the two C2 domains to 60Å. This distance coincides with the distance between the two receptor binding loops from the Toll-Interleukin 1 Receptor Domain-Containing Adapter Protein (TIRAP), an adaptor protein in RAGE signaling (145).

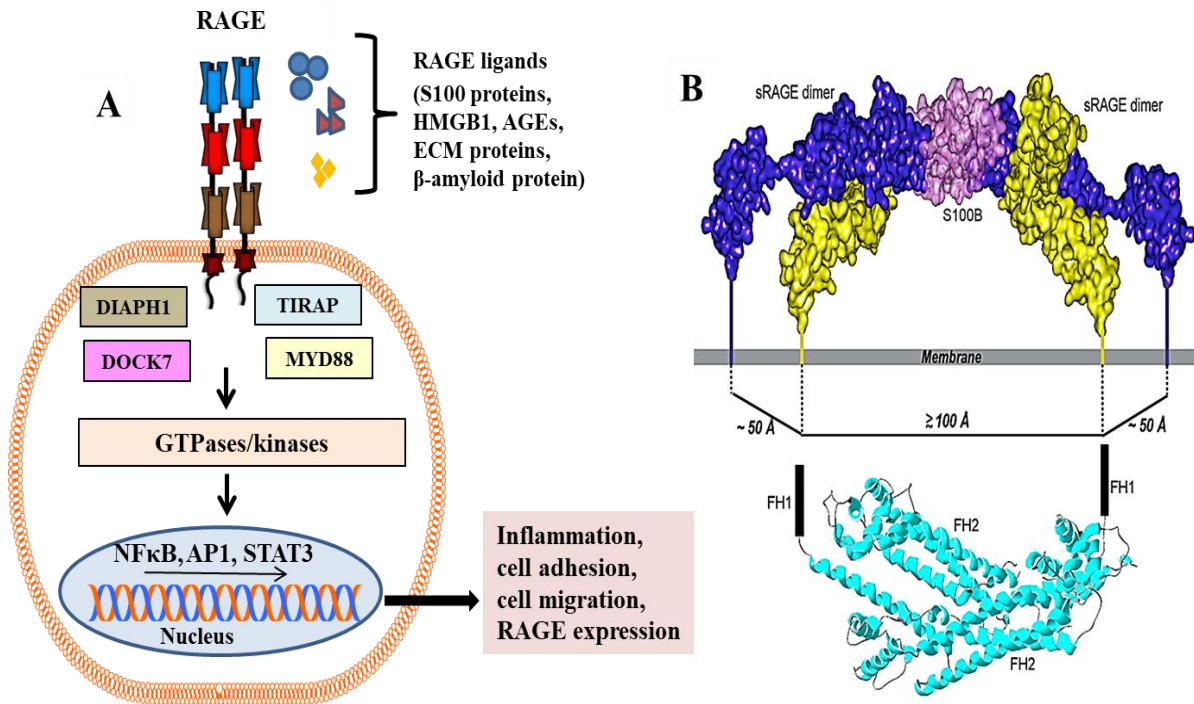


Figure 1.6: Different models illustrating RAGE signaling.

(A) Representation of classical signaling in RAGE (left): Ligand binding to the extracellular region in RAGE recruits adaptor proteins like DIAPH1, TIRAP, MYD88, and DOCK7. This is followed by activation of GTPases/kinases via the NF- κ B/STAT3/AP1 pathway, contributing to increased inflammation, cell adhesion, and RAGE expression. (B) Model illustrating signal transduction in sRAGE - S100B complex (right); taken from (141). The oligomerization of sRAGE induced by the Ca²⁺-S100B causes the C-terminal of the C2 domain from the two sRAGE homodimers to move a distance of 100 Å from each other, which corresponds to the distance between 2 FH1 domains of the DIAPH1. Recruitment of DIAPH1 is followed by activation of GTPases/kinases and NF- κ B pathway.

Involvement of RAGE in pathologies

RAGE signaling links to several pathways, including NF κ B, MAPK, and PI3K, that mediate inflammatory responses. Overexpression of RAGE is associated with both acute and chronic inflammation and has significant roles in human pathogenesis, including diabetic complications (146,147), neurodegenerative diseases (148,149), and certain cancers (150-152). Uncontrolled hyperglycemia in diabetes leads to the accumulation of AGE compounds. Oxidative stress evoked by the AGE-RAGE axis in renal cells contributes to diabetic nephropathy by eliciting inflammatory responses through ERK1/2, p38MAPK, PKC, and NF- κ B pathways (153). RAGE has been linked to atherosclerosis development via several ligands, including AGEs, HMGB1, and S100 proteins (154,155). The activation of chronic inflammatory signaling pathways stimulates the clotting cascade causing cardio-vascular damage (156). In addition, the interaction of RAGE with S100 proteins and AGE enhances the expression of CAM, including E-selectin, VCAM, and ICAM, and contributes to transendothelial migration (157,158).

RAGE expression is elevated in neuroinflammation and neurodegenerative conditions (159-162). Immunohistochemical studies have demonstrated that RAGE ligands, such as AGEs, S100, and A β , lead to RAGE overexpression in neurons, microglia, astrocytes, and blood brain barrier (BBB) vasculature in Alzheimer's disease (163). RAGE has been implicated in the pathogenesis of a variety of cancer types, including pancreatic (164,165), breast (166,167), melanoma (168,169), and liver (170,171). RAGE binding to S100 proteins sustains signaling to proinflammatory cytokines and autophagy, which directly links to cancer cell survival, proliferation, invasion, and migration (172). RAGE signaling in cancer is also linked to KRAS oncogenic mutations by increasing NF- κ B activity in pancreatic ductal adenocarcinomas (152,164). AGE/RAGE signals to oxidative stress by ROS generation and hypoxia induced

activation of oncogenes such as KRAS (Kirsten rat sarcoma virus), contributing to cancer cell survival, progression, and metastasis (164,173-175). RAGE was also found to enhance growth, metastasis, and EMT (epithelial-mesenchymal transition) by activating the P13K/AKT and RAS/ERK/Rac pathways (176). AGE-RAGE signaling has also been implicated as a key mechanism in the development of other pathologies, including fibrosis by promoting ECM deposition (116,177,178), obesity by inducing insulin resistance in adipocyte tissue (179,180), and psoriasis by activating several inflammatory pathways (181,182).

RAGE as a therapeutic target and its inhibitors

RAGE overexpression is linked to sustained inflammation contributing to disease progression. All preclinical studies focused on blocking the extracellular region of RAGE to prevent ligand mediated activation of the receptor. RAGE ligands bind to the extracellular region, and studies used antiRAGE antibodies and sRAGE to block RAGE from signaling in cancer cell migration and invasion (183,184). In murine models, treatment with sRAGE significantly reduced atherosclerotic lesions and other vascular complications through RAGE signaling, such as impaired renal injury, nephropathy, and retinopathy (185-187). Furthermore, ligand-derived RAGE inhibitors have been shown to be effective in decreasing RAGE mediated inflammation, β amyloid aggregation in *in vivo* models of Alzheimer's disease, and metastasis of cancer (Table 1.2) (188-190). TP488, a small molecule inhibitor of RAGE, blocked the binding of RAGE ligands to the V domain and inhibited inflammatory signaling and neuronal A β accumulation in mouse models of Alzheimer's disease (191,192). A 4,6-disubstituted 2-amino pyrimidine 4-fluorophenoxy analog, a disubstituted pyrimidine derivative is reported to bind to the V domain of RAGE and significantly reduced A β entry into the brain (193,194). FPS-ZM1, a high affinity small

molecule inhibitor, blocks RAGE-mediated inflammatory signaling inhibiting nuclear NF- κ B levels in a mouse model of Alzheimer's disease (195).

In cancer cell models, treatment with FPS-ZM1 impaired primary tumor growth, angiogenesis, inflammatory cell recruitment, and most importantly, inhibited cancer cell migration (165,196). GM-111, a low molecular weight semi-synthetic glycosaminoglycan ether, inhibited interactions between RAGE and its ligands in the extracellular region and reduced inflammatory responses (190). In addition, S100P-derived peptides and HMGB1-derived peptides block RAGE interaction with S100 proteins and HMGB1, respectively, which reduced metastasis and invasion of tumor cells (197,198).

A group of 13 compounds was identified from a high throughput screening assay using a small molecule library of 58,000 compounds. The chemical structures of these small molecule RAGE inhibitors comprise a central heteroaromatic core capable of hydrogen bonding with one or two hydrophobic regions and a protonable nitrogen atom connected to the central core by an alkyl linker. This group of molecules showed a strong affinity for the cytoplasmic domain of RAGE and inhibited the RAGE-diaphanous 1 signal transduction in *in vitro* and *in vivo* (199). Disrupting the RAGE-diaphanous 1 interaction is valued as an important therapeutic approach to target RAGE-mediated inflammatory disease (200,201). Aptamer based antagonist blocks the ligand-binding sites on the extracellular region and is reported to suppress downstream signaling of RAGE (202). Apart from targeting RAGE ligand binding sites, studies demonstrated varied approaches to inhibit the availability of RAGE ligands which inhibited RAGE activation. Treatment with an AGE cross-link breaker, algaebrium (ALT7-11), reduced AGE accumulation, and atherosclerotic plaque formation and lesions (203).

Table 1.2: RAGE inhibitors along with their targeted RAGE domains and their effects. Taken from (132).

Inhibitors	Targeted RAGE Domain	Effects
TTP488 (191,192)	V	AGEs, HMGB1, CML, S100B, and A β -RAGE binding inhibition
4,6-disubstituted 2-amino pyrimidines (193)	V	A β -RAGE binding inhibition
4-fluorophenoxy analog (194)	V	Inhibition of amyloid plaques inside the brain
FPS-ZM1 (204)	V	A β -RAGE binding inhibition and low cytotoxicity <i>in vitro</i> and <i>in vivo</i>
GM-1111 (188)	VC1C2	CML, GMGB1, and S100B-RAGE binding inhibition
S100-derived peptide (197)	VC1C2	Reduced RAGE-mediated activation of NF- κ B, inflammation, tumor growth, and metastasis in various cancer cells
HMGB1-derived Peptide (198)	VC1C2	Suppressed the formation of pulmonary metastasis and invasion in tumor cells
Aptamer-based antagonist (202)	V	inhibit interaction between RAGE and S100B
Group of 13 compounds (199)	cytoplasmic	Inhibition of ctRAGE interaction with mDia1

RAGE as an adhesion relevant molecule

Studies have shown that RAGE expressing cells have increased adherence and spreading in the presence of extracellular matrix (ECM) proteins (196,205-207). The extracellular domain of RAGE (VC1C2) adopts a secondary structure similar to that of cell adhesion molecules. Furthermore, RAGE shares significant homology with MUC18 (melanoma cell adhesion molecule), a glycoprotein that also belongs to the immunoglobulin superfamily, and with activated leukocyte cell adhesion molecule (ALCAM) (54,94). A recent study on the evolutionary origin showed that RAGE shared common ancestors with a family of CAMS; ALCAM, melanoma cell adhesion molecule (MCAM), and basal cell adhesion molecule (BCAM) (207). Also, comparing the gene sequences of RAGE and these CAMS showed evolutionarily similarities in genomic

organization in the cytoplasmic domain with highly conserved sequences in the exon-intron boundaries as an indication of gene duplication. The best structural alignment of the RAGE V-C1 domain matched 194 residues of the two N-terminal domains of human BCAM. It was also proposed that RAGE could have CAMs like properties wherein the expression of full-length RAGE in alveolar type cells showed increased cell adhesion and cell spreading in the presence of extracellular matrix proteins. Within different ECM proteins, RAGE expressing alveolar type cells were reported to adhere much faster to collagens forming an extremely flat phenotype with dense spreading (205). Results from crystal studies suggest that membrane bound RAGE mediates cell adhesion and cell spreading through homophilic interaction on the extracellular V domain (Figure 1.7). The homophilic interaction in RAGE is stabilized by the disulfide bonds formed between cysteine residues and is also stabilized by receptor-ligand binding in the extracellular region (207).

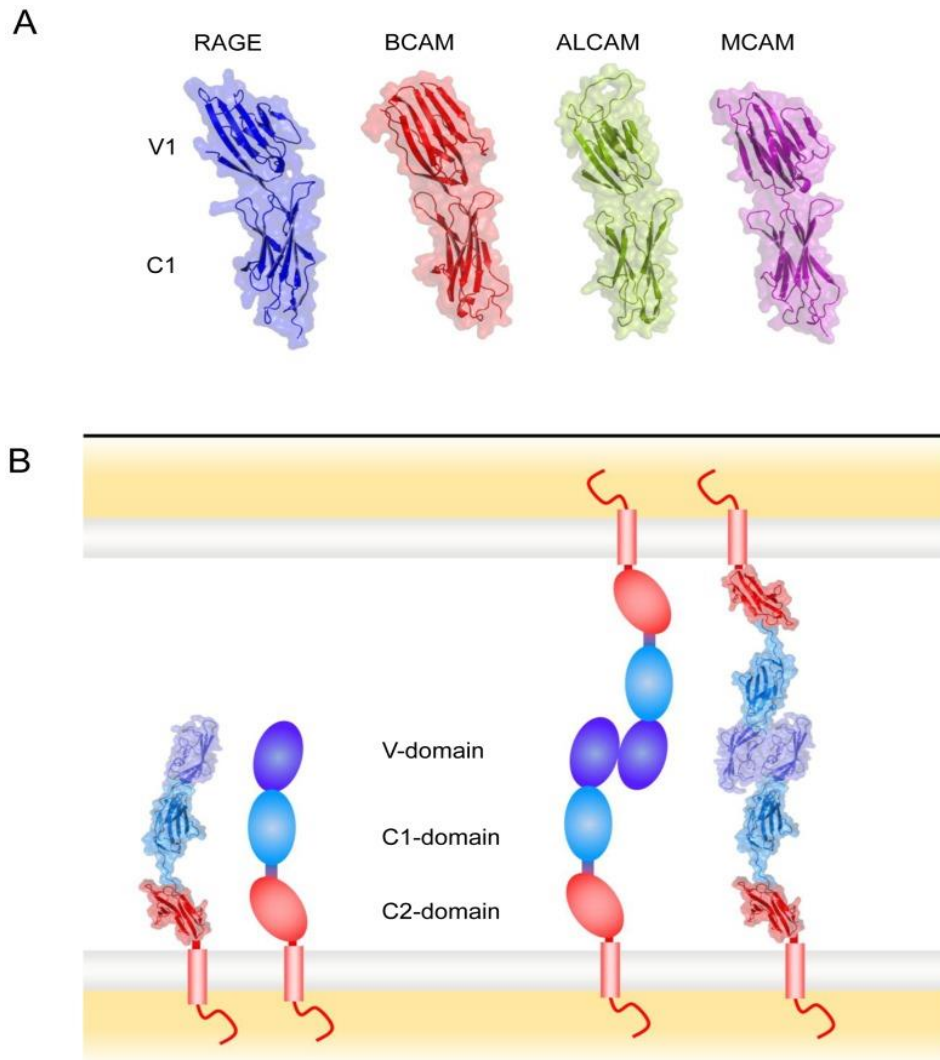


Figure 1.7: Model illustrating (A) structural comparison of RAGE V and C1 domains to a family of cell adhesion molecules and (B) RAGE-RAGE homophilic interaction in mediating cell adhesion.

The well conserved spatial arrangement of V and C1 Ig domains of RAGE closely resembles BCAM (basal cell adhesion molecule), ALCAM (activated leukocyte cell adhesion molecule), and MCAM (melanoma cell adhesion molecule). Based on the crystal structure, sRAGE was the V domains in trans orientation modeled to adopt homophilic interaction in mediating cell adhesion. Taken from (207)

RAGE subcellular localization and its functions

RAGE functioning in physiology is affected by the existence of different isoforms (119), the presence of N-glycans (107), and the level of inflammation (208). The glycosylation sites on the V domain of RAGE were reported to have an important role in increased ligand binding and

cell surface localization of the receptor (209,210). Studies suggest that different subcellular localization of RAGE contributes to the severity of the pathogenesis. In primary melanoma cells, RAGE localization was found to be clustered on the membrane more at the sites of cell-cell contact, whereas in the malignant type, RAGE expression is more distributed in the cytoplasm (168,211). Evidence also shows that in peripheral blood mononuclear cells of obese patients with insulin resistance, there is an increased expression of RAGE on the cell membrane contributing to subsequent damage in specific tissues (212). Overexpression of cell surface RAGE in endothelial cells was reported to be involved in impaired plasma membrane sealing causing endothelial cell death and promoting blood-brain barrier leakage and vascular angiopathy (213). The authors reported RAGE signaling in these cells leads to increased β -catenin clustering at cell-cell junctions and inhibition of F-actin remodeling.

Research goals, approach, and objectives

The overall goal of this study was to investigate the role of the different domains of RAGE towards RAGE mediated cell adhesion and cell spreading. As cell adhesion is an essential biological process that controls cell behavior, defective cell-cell and cell-matrix adhesion mechanisms constitute a significant cause of fatal diseases, including coronary heart disease (214-216), polycystic liver disease (217,218), and cancer (219-221). RAGE expression increased cell adhesion and spreading (205,207), but it is not well understood which part of the extracellular domain is most important if different domains modulate different aspects of cell adhesion, i.e., cell-cell, cell-matrix to different ECM proteins, and if RAGE mediates these effects through homophilic or heterophilic interactions in the presence of ECM proteins.

- **Hypothesis (I): Deletion of individual extracellular domains of RAGE should result in decreased cell adhesion to ECM, should change cell spreading behavior, and could influence cell-cell contacts.**

We investigated this using a panel of different RAGE domain deletion variants. RAGE variants were constructed into pcDNA3 vector and transiently expressed in HEK 293 cells. We then assessed the expression and localization of the RAGE domain deletion variants in HEK 293 cells using Western blotting, immunofluorescence, and flow cytometry. Finally, we evaluated the adhesion and spreading properties of these variants expressing HEK 293 cells to different ECM coated surfaces. These studies revealed that cell adhesion in RAGE expressing cells was increased but surprisingly seemed not to depend on the presence of the extracellular domains on the cell surface. The data from our study also suggested that RAGE expression enhances cell adhesion not only through RAGE itself (homophilic interactions) but also through the increased surface expression of other unidentified adhesion relevant proteins. During the studies, it was also observed that the cytoplasmic domain entered the nucleus.

To further investigate this interesting observation, we formulated,

- **Hypothesis (II): Translocation of the cytoplasmic domain of RAGE is preceded by proteolytic cleavage, and only the cytoplasmic domain, but not full-length RAGE, gets translocated into the nucleus. In addition, RAGE ligand stimulation, such as AGE, can promote RAGE shedding and enhance nuclear localization of the cytoplasmic domain.**

This was investigated using the fluorescently labeled RAGE construct. HEK 293 cells were transfected using the RAGE fluorescent tagged plasmid, and ribose glycosylated BSA was to induce RAGE activation. Subcellular localization changes in RAGE were monitored in ligand induced

and non-induced conditions. Interestingly, we obtained data that suggest that in addition to nuclear localization, the cytoplasmic domain is concentrated in the nucleolar compartment in ligand induced conditions.

To further investigate the impact of nuclear and nucleolar localization of RAGE-ICD, we formulated,

- **Hypothesis (III): RAGE expression leads to the increased surface expression of cell adhesion molecules and thus results in increased cell adhesion and spreading.**

This was investigated using transcript analysis of adhesion relevant genes between wild type HEK 293 (WT HEK 293) and RAGE stably expressing HEK 293 cells (RAGE HEK 293). We also used proteomics to identify CAMs that may show altered surface expression without corresponding changes in transcription. A set of candidate proteins was identified with each method, and gene ITGA8 was found to be regulated at both transcript and translational levels. To further strengthen the evidence that RAGE was driving the expression of one of the candidate CAMs proteins identified (ITGA8), we used shRNA knock-down of RAGE. It was predicted that RAGE knock-down should result in a decrease in ITGA8 expression.

CHAPTER 2. GENERAL MATERIALS AND METHODS

Molecular biology and reagents

Reagents were of molecular biology or ACS purity grade and purchased through VWR or Fischer Scientific. Molecular biology reagents and enzymes were purchased from New England Biolabs. The primers for the qPCR reactions were purchased from Thermo Fischer, and DNA - polymerase was purchased from Solis BioDyne. Media for cell culture were purchased from ATCC.

Cell culture

Human embryonic kidney (HEK293) and chinese hamster ovary (CHO) cells (ATCC) were cultured in Dulbecco's Modified Eagle Medium (DMEM) complete media (ATCC® 30-2002™, Manassas, VA) containing 10% Fetal Bovine Serum (FBS) (PEAK SERUM PS-FB1) and 1% penicillin/streptomycin (Corning, Cat#30-002-CI) in an atmosphere with 5% CO₂ and >90% humidity at 37 °C. HEK 293 cells stably expressing full-length RAGE (RAGE HEK 293) were a generous gift from Dr. Heizmann (University of Zürich, Zürich , Switzerland) and were cultured in DMEM complete media with 0.5% vol/vol of G418 sulfate (Corning, Cat# 30-234-CI) as the selection agent. MiaPaCa2 cells were kindly provided by Dr. Leclerc (North Dakota State University) and cultured in DMEM complete media containing 2.5% horse serum (ATCC, 30-2040).

Cells were routinely tested for mycoplasma using a two stage PCR method with a combination of primers specific to mycoplasma species [(stage 1 PCR primers: # Mycopl_M89: TCACGCTTAGATGCTTTCAGCG; # Mycopl_M78: AAAGTGGGCAATACCCAACGC; # Mycopl_R1: CTTCWTCGACTTYCAGACCCAAGGCAT Y=C/T; # Mycopl_F1: ACACCATGGGAGYTGGTAAT Y=C/T) (stage 2 PCR primers: #Mycopl_R34:

CCACTGTGTGCCCTTTGTTTCCT; # Mycopl_R2: GCATCCACCAWAWACYCTT W= A/T Y=C/T; #Mycopl_F2: GTGSGGMTGGATCACCTCCT S=C/G, M= A/C] as described in (222). The presence of mycoplasma contamination resulted in a PCR product ranging from 236-365 base pairs (bp) depending on the mycoplasma species (Figure A1).

Cloning of RAGE variants and plasmid production

The pcDNA3 vector backbone was used for the constitutive expression of the engineered RAGE domain deletion variants in HEK293 cells. The plasmids were provided by Dr. Vetter (North Dakota State University). Appendix B contains the nucleotide sequences of the expression cassettes and the corresponding protein sequences of the domain variants. The plasmids were amplified in *E. coli* DH5alpha and purified using a plasmid miniprep kit (Omega, #D694). The purity and size of the isolated plasmids were confirmed by UV-VIS spectrometry (Agilent) and by agarose gel electrophoresis (Figure A2).

Transient transfection

Lipofectamine 3000 (Invitrogen, Carlsbad, CA, USA) was used for transfection in HEK 293 cells. In brief, cells of density 5×10^5 per 2 ml were seeded in a 6 well plate and were allowed to grow until 80-90% confluency. Before performing transfection, the media in the wells were replaced with fresh DMEM media without FBS. For each well, 3.0 μ g of DNA diluted in 250 μ l of Opti-MEM reduced serum media (Gibco, ThermoFisher Scientific) was used to transfect the cells. The DNA-lipofectamine mixture in the wells was left for 8 hours and then replaced with fresh complete DMEM media.

SDS-PAGE and Western blotting

Cell lysates for SDS-polyacrylamide gel electrophoresis were prepared as follows: Transfected cells were harvested by scraping them in ice-cold PBS and centrifuging at 200g at

4°C. The pellet was resuspended in 150µl of RIPA lysis buffer (1%NP-40, 0.5% W/V sodium deoxycholate, 0.1% SDS, and 1mM protease inhibitor cocktail Calbiochem set IV) and incubated on ice for 45 min and centrifuged at 13,400g at 4°C. Protein concentration in the supernatant was determined using the Pierce BCA protein assay kit (ThermoFischer). In general, 50-100 µg of total protein was resolved on a 10 or 15% SDS PAGE gel and transferred onto a nitrocellulose membrane by wet-electroblotting for 1hr at 160 mAmps. The blot was blocked using 5% milk in TBS containing 0.1% tween-20 (TBS-T) for one hour at room temperature. Incubation with antibodies was performed at the recommended dilutions overnight in the cold room with gentle rocking. Blots were washed with TBS containing 0.1% tween and incubated with HRP conjugated secondary antibodies (Jackson ImmunoResearch) raised against the primary antibodies at 1:50,000 ratio for 1hr at room temperature. An ECL luminescence substrate (BioRad ECL Western Blotting substrate, Cat# 170-5061) was used for the visualization of the protein on the membrane. Antibody against actin (Santa Cruz Biotechnology sc-1616, and Cell Signaling Technologies #4970) was used on the same membrane after stripping and served as the loading control.

Immunofluorescence

µ-Dish 35 mm from ibidi USA, Inc or the cover glass 18x18 mm (Zeiss) was coated with collagen I (50µg/ml) diluted in 0.02 M acetic acid and incubated for 2 hrs at room temperature. The cells were then seeded onto the collagen I coated cover glass and was allowed to reach a confluency of 70%. The µ- slide 8 well was treated the same way, and 20,000 cells were seeded per well. After 24 hrs of transfection, cells were fixed for 10 min using 4% paraformaldehyde at RT and washed twice in ice-cold PBS. The permeabilization was carried out in 0.1% triton X-100 for 15 min on ice. Blocking was performed using 5% bovine serum albumin (BSA) containing 0.1% tween in PBS for 30 min at room temperature. The incubation with primary antibodies was

performed at recommended dilutions in blocking buffer overnight in the cold room. The cells were washed three times with PBS containing 0.1% tween for 5 min, followed by incubation with FITC conjugated secondary antibodies (Jackson Immuno-Research) diluted in blocking buffer (1:100) for 1hr at room temperature. The Hoechst 33342 stain (Invitrogen) was used to stain the nucleus. Images were taken using a Zeiss confocal microscope LSM700 and a Olympus FV3000 confocal laser scanning microscope.

Flow cytometry

Cells were detached using Cell Stripper (Corning #25-056-CI) solution and were washed three times in ice-cold PBS and centrifuged at 200g at 4°C. After resuspending the cells in ice-cold PBS containing 2% FBS, cell counting was performed, and for each sample, 1×10^6 cells were used. Cells were maintained at 4°C throughout the labeling procedure. In brief, cells were fixed in 4% paraformaldehyde for 10 min; fixed cells were processed to be either permeabilized with 0.1% triton X-100 (15 min) or non-permeabilized. Blocking with 5% FBS in PBS for 30 min was found to be more efficient compared to 5% BSA. Cells were incubated with primary antibody at a dilution recommended by the manufacturer, followed by three washes with ice-cold PBS for 5 min and centrifuging at 200g at 4°C. As the final step, cells were labeled with a fluorescent conjugated secondary antibody (Jackson Immuno Research. Cell Signaling Technologies #4412, #4413) at a dilution of 1:200 in blocking buffer, followed by three washes. The non-transfected and the mock-transfected cells containing only the empty vector were used as controls for the flow cytometry experiments. All experiments were performed using a BD Accuri C6 plus system flow cytometer. The threshold was set to default in the Accuri software, and the program was set to run with 25,000 counts for each sample. The data were analyzed using a gating strategy where singlet cells were

considered. The percentage of fluorescent cells in the gated cell samples was determined based on a fluorescence intensity cut-off derived from the mock and the non transfected cells.

Table 2.1: Details of the antibodies used in this study along with dilution specification for Western blotting (WB), immunofluorescence (IF), and flow cytometry (FC) experiments.

Antibody	Company	Catalog No.	Species	Dilution
RAGE (9A11)	Santa Cruz Biotechnology	Sc-80653	Mouse	1:1000 – WB 1:100 – IF and FC
RAGE (D1A12)	Cell Signaling Technology	6996	Rabbit	1:1000 – WB 1:100 – IF and FC
Human Integrin alpha 8 Antibody	R&D Systems	MAB6194	Mouse	1:2000 – WB 1:200 – FC
Human/Mouse/Rat Contactin-1 Antibody	R&D Systems	AF904	Goat	1:500 – WB
B-Actin	Cell Signaling Technology	4970	Rabbit	1:1000 – WB
GAPDH	Cell Signaling Technology	5174	Rabbit	1:1000 – WB
HRP conjugated	Jackson Immuno Research	715-035-150	Anti-Mouse	1:500000 – WB
HRP conjugated	Jackson Immuno Research	711-035-152	Anti-Rabbit	1:500000 – WB
HRP conjugated	Jackson Immuno Research	705-035-147	Anti-Goat	1:500000 – WB
FITC conjugated	Jackson Immuno Research	115-095-062	Anti-Mouse	1:200 – IF and FC
FITC conjugated	Jackson Immuno Research	711-545-152	Anti-Rabbit	1:200 – IF and FC
Alexa Fluor® 488 Conjugate	Cell Signaling Technologies	4412	Anti-Rabbit	1:200 –FC
Alexa Fluor® 555 Conjugate	Cell Signaling Technologies	4413	Anti-Rabbit	1:200 –FC
Streptavidin, Peroxidase, ELISA Grade	Vector Laboratories	SA-5014		1:500 – WB

Cell adhesion assay

The assay was performed as described in (207). Tissue culture plates were coated with different ECM proteins; Matrigel (10 µg/ml; R&D Systems #343300101), collagen IV (5µg/ml; R&D Systems # 3410-010-01), collagen I (50µg/ml; R&D Systems #344702001), and fibronectin (5µg/ml; R&D Systems #3420-001-01) in nuclease-free water for 2 hrs at room temperature. The ECM coated wells were seeded with 50,000 RAGE variant transfected and mock transfected cells

in 100 ul of DMEM complete media. The cells were incubated for these respective time points, 5, 10, and 20 min, and were washed twice with ice-cold PBS. The wells were filled with 100 ul of DMEM complete media, and 10% V/V of resazurin (1mg/ml) was added and incubated for 3 hours. The resazurin fluorescence was measured at 540/590 nm (excitation/emission) using a SpectraMax multi-plate reader, and percentage adhered cells were calculated using the formula below

$$\% \text{ cells adhered} = \left(\text{Fluorescence from} \frac{\text{washed well}}{\text{non washed well}} \right) \times 100$$

Cell spreading assay

12 well-chambered microscopy slides (Ibidi, # 81201) were coated with ECM proteins as indicated in the cell-matrix adhesion assay. The cells of density 3×10^4 in 250 μ l of media were seeded, and after 3 hrs of incubation at 37°C, the slide was imaged on a Leica DM2000 microscope using 20X magnification. ImageJ software was used for the analysis wherein the original image was converted to a binary image. The region of interest (ROI) was selected using the free hand tool for each cell in the image. The spread area and perimeter for the individual cells were obtained from Image J. The circularity of the cells was determined by using the formula below,

$$\text{Circularity} = 4\pi(\text{area}/\text{perimeter}^2)$$

A circularity value of 1 indicates a perfect circular shape of the cells. BSA coated surface was used as the control.

RNA extraction and cDNA synthesis

Whole-cell RNA was extracted from the cells using the PureLink™ RNA Mini Kit, Invitrogen (Thermo Fisher Scientific #12183020). Briefly, 200,000 cells were seeded in each well of a 6 well plate, and cells were allowed to reach a confluency of 70-80%. Cells were harvested manually using a cell scraper, and RNA extraction was carried out according to the manufacturer's protocol. The concentration of the RNA was measured using the absorbance from UV at 260 nm

(A260). The ratio of the UV absorbance of 260 nm/280 nm (A260/A280) was calculated to estimate the purity of the RNA. Extracted RNAs with 260/280 nm ratio ≥ 2 , which corresponds to good quality RNA, were used for further analysis. The purity of the extracted RNA was further confirmed using agarose gel electrophoresis, which showed intact and no degradation of the 18s and 28s ribosomal RNA (rRNA) (Figure A3). 1 μ g of total RNA was immediately reverse transcribed using the Moloney Murine Leukemia Virus (M-MuLV) Reverse Transcriptase (NEB #M0253) by following the standard cDNA Synthesis protocol on the manufacturer's website using an oligo(dT) primer.

Quantitative PCR (qPCR)

20 ng of cDNA and 250 nM of forward and reverse primers were used in each PCR reaction contained in HOT FIREPol EvaGreen qPCR master mix (ROX) (Solis BioDyne) in a total volume of 20 μ l. The RT-PCR thermal cycle program comprised an initial denaturation step at 95°C for 30sec, followed by 40 cycles of denaturation at 95°C for 30sec, then annealing at 58°C for 30sec, and extension at 72°C for 60 sec. An increase in fluorescence of EvaGreen was measured at every PCR cycle using ROX fluorescence as the reference in each well, and the corresponding cycle threshold (C_t) was determined by the Agilent Stratagene Mx3000P® Multiplex Quantitative PCR (QPCR) System. For calculating the fold change in the gene of interest (GOI), a double delta C_t ($\Delta\Delta C_t$) method was applied using the following equation (223).

$$Fold\ change = 2^{-\Delta\Delta C_t}$$

Where,

$$\Delta\Delta C_t = [(C_t\ of\ GOI) - (C_t\ of\ HKG)]_{RAGE\ HEK\ 293} - [(C_t\ of\ GOI) - (C_t\ of\ HKG)]_{WT\ HEK\ 293}$$

Cell surface proteomics

Cell surface protein labeling and enrichment

Cell surface protein capture from live cells was performed as described in (224,225) with some modifications. Wild type (WT) HEK 293 and RAGE HEK 293 cells were dissociated using CellStripper (Corning Cat# 25-056-CI) and washed twice with ice-cold 1XPBS and centrifuged at 100g for 2 min at 4°C. Cells (1.5×10^7) were subjected to a mild oxidation reaction using 1.25 mM sodium meta periodate (Biosciences) in PBS (pH 6.7) for 30 min. The reaction was quenched using 1mM ethylene glycol for 30 min, followed by washing the cells thrice with ice-cold PBS. The labeling reaction was carried out at 4°C using 250 μ M aminooxy biotin (Biotium 90113) and 10 mM aniline (Sigma) as a catalyst for 90 min. The cells were then washed four times with ice-cold PBS and four times with PBS containing 1mM EDTA. The cells were then lysed in lysis buffer (10 mM Tris, 150 mM NaCl, 1% triton X- 100, and 1 mM Calbiochem cocktail set VII protease inhibitor) followed by 5 cycles of 5 burst of sonication for 25 sec and incubation at 4°C with gentle rocking for 3 hrs. The lysates were centrifuged at 20,000g for 20 min at 4°C. This step was repeated twice by adding half the volume of lysis buffer used in the first lysis step to the pellet in order to extract the remaining proteins from the debris. The supernatant from the lysate was collected and centrifuged again at 20,000g to remove any debris from the process and immediately processed for cell surface protein isolation and enrichment using NeutrAvidin Gel (Prod # 1859388, Pierce). The beads were washed with PBS, and 3 mg of total biotinylated protein was added to the beads and incubated overnight with gentle rocking in the cold room. The next day the beads were washed using a series of buffers with 1 mM Calbiochem cocktail set VII protease inhibitor at 4°C. The first four washes were performed with lysis buffer, followed by PBS with 0.1% tween, PBS, and 50 mM ammonium bicarbonate. A total of 16 washes were performed, with

the last two washes containing 50 mM ammonium bicarbonate without protease inhibitors. The flow-through from the bead incubation and wash steps were stored and used for BCA assay to determine the amount of protein bound to the beads by comparing the total amount of protein used and protein amount found in the flowthroughs.

Sample processing for mass spectrometry (MS)

The washed beads were incubated with 20 mM DTT in 50 mM ammonium bicarbonate containing 0.1% RapiGest SF (Cat # 186001860, Waters) for 1hr at 37 °C. RapiGest is an anionic surfactant used to accelerate the in-solution production of peptides generated by proteases. The beads were alkylated using 50 mM iodoacetamide for 1hr at room temperature, followed by quenching of the alkylation reaction using 20 mM DTT for 15 min. On-bead digestion was performed using a 1:50 (W/W) ratio of protein to trypsin (Pierce Trypsin Protease, MS Grade 90057) for 24 hrs at 37°C. The supernatant from the bead digestion was collected, and 0.1% RapiGest from the peptide mix was precipitated using treatment with 0.5% V/V trifluoroacetic acid. The samples were lyophilized (Labconco Freezone 2.5 Plus Freeze Dryer) overnight and stored at -80°C. The C18 purification was performed in the UND lab on the samples using the manufacturer's protocol before running them on the mass spectrometry instrument (Cat # 87784, Pierce™ C18 Tips, 100 µL bed).

Nano LC-MS acquisition

A Waters Acquity nanoUPLC system equipped with an autosampler (Waters, Milford, MA) was used for peptide chromatographic separation. Peptides were loaded on a trapping column (Waters Acquity UPLC M-class Symmetry, C₁₈, 5 µm, 180µm x 20mm) at a flow rate of 15 µL/min for 3 min with 99.5 % solvent A (0.5% formic acid in water) and 0.5% solvent B (0.5% formic acid in acetonitrile). After trapping, peptides were resolved on a Waters analytical column

(Acquity UPLC M-class HSS T3, 1.8 μm , 100 μm x 100mm) at a flow rate of 0.4 $\mu\text{L}/\text{min}$ using a linear gradient of solvents A and B. Initial %B was increased from 2% to 5% over 1 min, held at 5% for 4 min, then increased to 25% over 120 min, to 32% over 20 min, and further to 95% over 1 min. After holding at 95% for 5 min, %B was returned back to 2% over 1 min and held at this value for 18 min for re-equilibration.

For mass spectrometry, a hybrid quadrupole-Orbitrap Q Exactive mass spectrometer (ThermoFisher Scientific) was used. LC eluent was ionized using a nanoelectrospray ion source in a positive ionization mode with an electrospray voltage set at 1.8 kV. MS/MS data were collected in a data-dependent acquisition mode with dynamic exclusion (30 s). Profile full MS scans were collected at 70,000 resolution (m/z 400–1600), and a maximum of 10 centroid product ion scans at 17,500 resolution per cycle. Fragmentation was performed using collision-induced dissociation (CID) set at 30%. Automatic gain control (AGC) targets were $1 \times e^6$ ions for full scans and $1 \times e^5$ for MS/MS scans.

MS-data processing

For protein identification, Protein Discoverer (version 2.2, ThermoFisher Scientific) was used to search MS/MS spectra, and parent proteins against the *Homo Sapiens* reference proteome database (UniProtKB/Swiss-Prot) downloaded on September 10, 2021. Minora Feature Detector was used for unlabeled quantification. Initial mass deviation of precursor ion and fragment ions were up to 10 ppm and 0.5 Da, respectively. Enzyme specificity was set to trypsin with a maximum of two miscleavages allowed. The minimum peptide length was set to 6, and the maximum to 150 amino acids. Carbamidomethyl-Cys was set as a static modification. Met oxidation, protein N-terminal acetylation, and biotin- Lys were set as dynamic modifications. The expression of identified surface proteins was normalized using Na,K-ATPase alpha 1 subunit

(ATP1A1) (Uniport entry: P05023), a prominent cell surface protein marker (226) which showed equal protein abundance from MS experiments in WT HEK 293 and RAGE HEK 293 samples. The fold change was represented as relative gene expression between WT and RAGE HEK 293 samples.

Statistical analysis

All experiments generating quantitative data were performed at least three times. Data from 3 replicates of each experiment are shown either as Mean \pm SEM or Mean \pm SD. Comparative analysis between two groups was performed by one tail two sample (unpaired). Student's t-test and $p < 0.05$ was considered significant.

CHAPTER 3. RAGE DOMAIN DELETION VARIANTS TO PROBE THE ROLE OF RAGE DOMAINS IN CELL ADHESION

Introduction

Studies have reported that RAGE expression increased cell adherence and spreading in the presence of extracellular matrix (ECM) proteins, and phylogenetic analysis showed RAGE belongs to a family of cell adhesion molecules (CAMs) (196,205-207). Other studies demonstrated that sRAGE binds to different ECM proteins with different affinities suggesting that RAGE-ECM binding primarily occurs in the extracellular region (227). The current model suggests that RAGE mediates the cell-cell and cell-matrix adhesion through homophilic interaction of its V domain at the cell surface (140). This model seems to fit well this is based on the 3D structural model comparison of CAMs to the crystal structure of RAGE. However, it also fails to acknowledge the existence of other possible models involved in RAGE mediated cell adhesion. We aimed to fill this knowledge gap by addressing

- (i) the role of the different domains of RAGE in mediating cell-cell and cell-ECM adhesion
- (ii) if membrane bound RAGE is required to mediate the adhesion phenomenon
- (iii) if the absence of certain domains affects the membrane localization of RAGE

In this chapter, we conducted studies to answer the above questions by investigating the role and contribution of different domains of RAGE towards its expression, localization and mediating cell adhesion to various ECM proteins.

Design and expression of the RAGE domain deletion variants

Experimental design

Generation of RAGE variants

Plasmids encoding full-length (FL) -RAGE (1– 404 residues, NM_001136) and other RAGE variants with deleted V domain, C1 domain, and C2 domain (ΔV -, $\Delta C1$ -, $\Delta C2$ -) was a generous gift from Dr. Heizmann (University of Zurich). The dominant negative or the DN—RAGE and the TmCyto variant, were generated by Dr. Vetter (Department of Pharmaceutical Sciences, NDSU). The ΔV -domain variant lacks residues 23-101; the $\Delta C1$ variant lacks residues 117-221; the $\Delta C2$ variant lacks residues 221-318; the dominant negative (DN-) lacks residues from 364-404; the TmCyto- variant lacks residues 23-318 and has an additional N-terminal Flag tag (Figure 3.1). The plasmid stocks were prepared in batches and stored at -80°C .

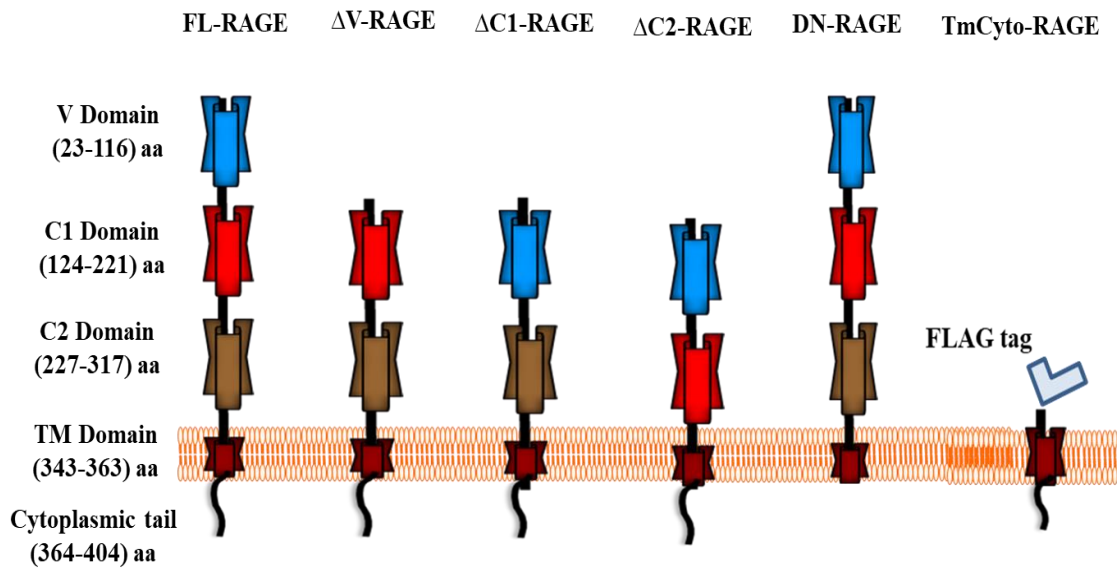


Figure 3.1: Domain organization of full-length RAGE (FL-RAGE) and the domain deletion variants used in this study.

The extracellular portion of RAGE is composed of the V-, C1, and C2-domains. A single helical transmembrane spans the plasma membrane, leading to a 40 residues long, C-terminal, cytoplasmic domain. The DN-RAGE variant lacks the cytoplasmic domain of RAGE. The ΔV , $\Delta C1$, and $\Delta C2$ lack the V-, C1-, and C2-domains, respectively. The TmCyto variant lacks the entire extracellular portion of RAGE.

Transient transfection optimization using reporter plasmids pcDNA3GFP and pcDNA3SEAP in HEK 293 cells

Transient transfection conditions in HEK 293 cells were optimized by estimating the transfection efficiency of two reporter plasmids pcDNA3GFP and pcDNA3SEAP. Two different transfecting reagents, polyethyleneimine PEI and Lipofectamine 3000, were compared and evaluated by varying ratios of the DNA amount (μg) to the transfecting reagent (μg or μl). In brief, cells of density 50×10^3 cells/well in 500 μl DMEM media were seeded onto a 24-well plate, and transfection was performed once the cells in the wells reached 70% confluency. For a well, 0.75 μg of DNA diluted in 50 μl of optiMEM media was used. For transfections using PEI (Cat# 23966, Polysciences Inc), fresh stock solutions of 1mg/ml PEI in DNase-free water were prepared and sterile-filtered. The cells were transfected using different ratios of DNA to PEI (1:2, 1:3, 1:4, and 1:5) as described in (228).

For Lipofectamine 3000 (Invitrogen, Carlsbad, CA, USA), cells were transfected according to the manufacturer's protocol using different volumes of 1.5, 2, and 2.5 μl to recommended DNA amount of 0.75 μg . The transfection efficiency in cells was assessed quantitatively and qualitatively after 24 and 48 hours. The transfection efficiency of cells transfected with pcDNA3GFP plasmid was determined by taking epifluorescence images in blue spectral regions (478-495 nm) to evaluate the green fluorescent protein (GFP) positive cells. A phosphatase activity assay was performed to measure the amount of secreted embryonic alkaline phosphatase (SEAP) after transfection with pcDNA3SEAP. The SEAP assay is a colorimetric assay in which the alkaline phosphatase secreted from the cells can be assessed using p-nitrophenyl phosphate as a substrate. Secreted alkaline phosphatase catalyzes the hydrolysis of p-nitrophenyl phosphate (pNPP), to p-nitrophenolate, which is a yellow product under alkaline conditions and can be

quantified at 405 nm in a spectrophotometer (Figure 3.2). This assay provides a measure of the average transfection efficiency across the entire cell population. In brief, after 24 and 48 hours of transfection, supernatants from the pcDNA3SEAP transfected cells were collected, and the endogenous alkaline phosphatase was heat-inactivated by incubating at 65°C for 10 min. To 90µl of the heat-inactivated sample, 10µl of pNPP (1mg/ml) in nuclease-free water was added, and readings were at different time points 0, 15, 30, and 60 min.

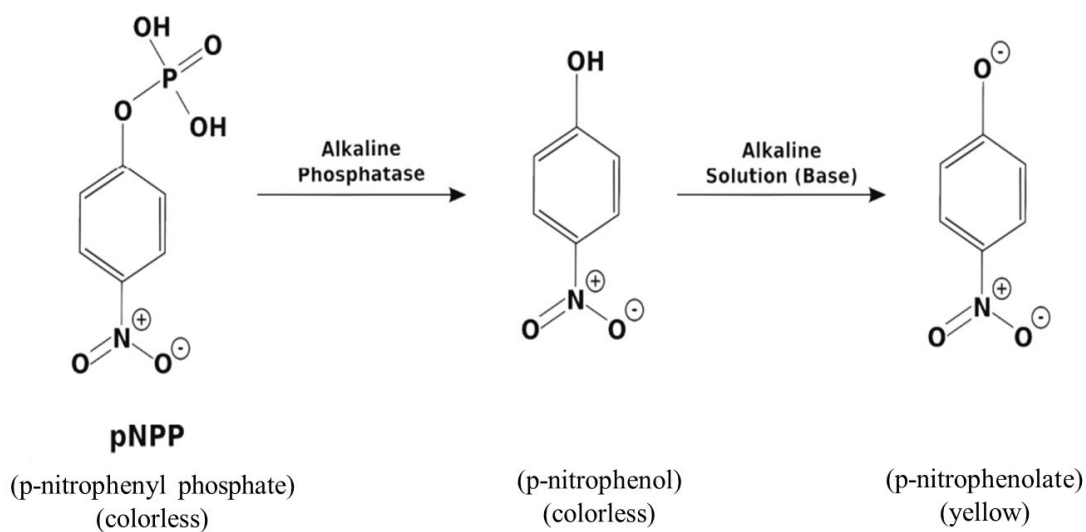


Figure 3.2: Hydrolysis of pNPP catalyzed by alkaline phosphatase.

Transient expression of RAGE variants

Transient transfection of the RAGE variants in wild type (WT) HEK 293 cells was performed with the conditions optimized with the control plasmids and the volumes scaled up proportionally for a 6-well plate. After 24hrs of transfection, cells were processed for Western blotting, confocal imaging, and flow cytometry experiments as described in (Chapter 2).

Western blot

Western blotting experiments were performed as described in general methods (Chapter 2), and 50 µg of total protein was resolved on a 12% SDS PAGE gel. For this experiment,

antiRAGE antibodies targeting two different epitopes were used due to different domain deletion RAGE proteins. AntiRAGE 9A11; (#sc-80653 mouse monoclonal antibody, Santa Cruz Biotechnologies) targets the N-terminus of RAGE in the V domain region, and antiRAGE D1A12; (#6996 rabbit monoclonal antibody, Cell Signaling Technologies) recognizes the epitope in the C-terminal cytoplasmic tail of RAGE (Figure 3.3). For the construct DN-RAGE, which lacks the cytoplasmic tail, antiRAGE 9A11 antibody was used to access the protein expression in Western blot. As there were no commercial antibodies available that specifically recognized the other two domains of RAGE of the extracellular region (C1 and C2). AntiRAGE D1A12 was used for the variant lacking the V domain (Δ V-RAGE).

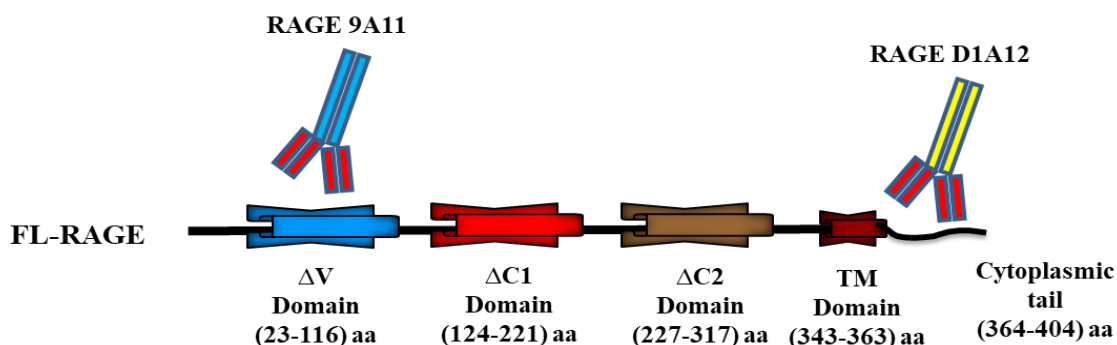


Figure 3.3: Binding regions of the antiRAGE antibodies 9A11 and D1A12 used in this study.

Immunofluorescence and confocal image analysis

For immunofluorescence microscopy experiments, cells were grown on a coverslip and transfected as described. The primary antibody staining was performed at a dilution of 1:50 for RAGE 9A11 and 1:100 for RAGE D1A12. The primary antibody was counter stained using species appropriate FITC conjugated secondary antibody, and images were taken using a Olympus FV3000 confocal laser scanning microscope. The magnification was set to 40X, and we used the default laser setting to measure FITC and DAPI (480 and 360 nm) signals in the samples.

Flow cytometry

AntiRAGE antibody 9A11 was used to assess the membrane bound proteins in (FL, DN, $\Delta C1$, and $\Delta C2$)-RAGE transfected cells at 1:100 dilution. Cells were processed and treated as described in Chapter 2. In non-permeabilized conditions, only the cell surface RAGE will be recognized, but in permeabilized conditions, the antibody has access to both cell surface and intracellular RAGE. Gating was performed using the fluorescence intensity from the mock-transfected cells as the control threshold in both permeabilized and non-permeabilized conditions. The percentage of membrane-bound RAGE was calculated using fluorescence intensities from both the permeabilized (FP) and non-permeabilized (NFP) samples using the formula below.

$$\% \text{ Protein localized to the cell surface} = \left(\frac{FNP}{FP} \right) * 100 \quad (2.1)$$

Results

Lipofectamine 3000 showed good transfection efficiency with two tested reporter plasmids

For the initial set of experiments, the transfection efficiency was compared between PEI and Lipofectamine 3000 using pcDNA3 GFP. The results of transfection efficiency with PEI were observed to be low ($\leq 20\%$) for all the different ratios used. Higher use of PEI in DNA:PEI ratio 1:4 and 1:5 induced cytotoxicity as more necrotic cells ($\geq 30\%$) were observed after 48 hours of transfection. It was also observed that the transfection efficiency did not show any difference at both 24- and 48-hour time points when compared to all the DNA:PEI ratios used (Figure 3.4).

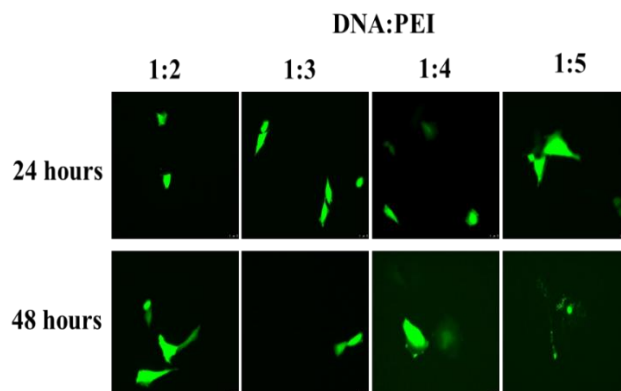


Figure 3.4: Epifluorescence images of HEK 293 cells transfected with pcDNA3 GFP using different ratios of PEI at 24 and 48 hours.

In contrast, Lipofectamine 3000 showed better transfection with low cytotoxicity ($\leq 5\%$). Using 750ng of DNA to 2 μ l of Lipofectamine 3000 gave the best results and had the maximum transfection efficiency of 80-90%, which was determined using GFP expression in the cells (Figure 2.5 (A)). Furthermore, integrated intensity for the individual transfected cells in these images was calculated using ImageJ software. Plotting the integrated intensity vs. the mean integrated intensity/area showed about 80% of the transfected cell population lay within a certain range of intensity. This inferred that the majority of the individual transfected cells had similar protein expression levels but with some heterogeneity (Figure 3.5 (B)).

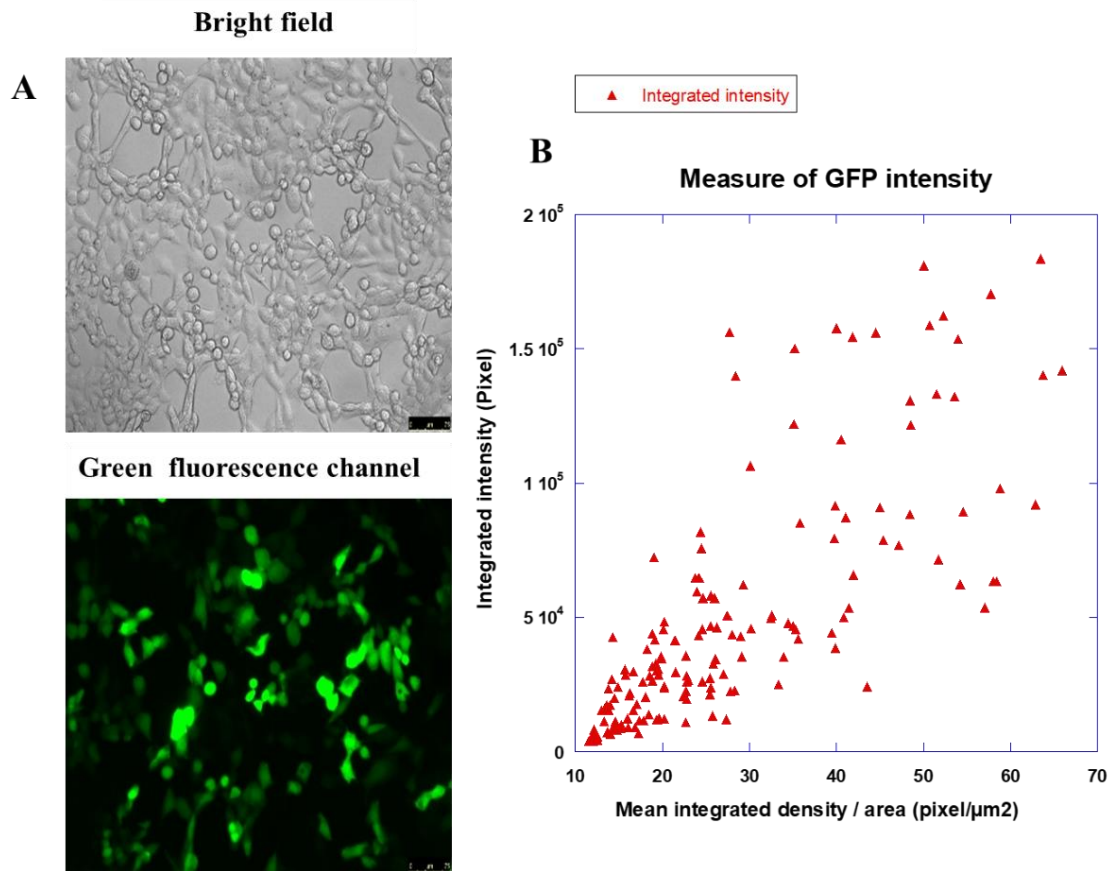


Figure 3.5: (A) Epifluorescence images of HEK 293 cells transfected with pcDNA3 GFP using Lipofectamine 3000 with optimized conditions after 24 hours. (B) Plot showing the integrated intensity of the fluorescence from the GFP-positive cells.

Data from the SEAP assay also showed comparable results using the same transfection conditions. Using 750ng of DNA to 2 μl , Lipofectamine 3000 had the maximum absorbance at 405 nm after 60 min and corresponded to the maximum alkaline phosphate activity of 1.95 mU/ml compared to the other two transfection conditions of transfecting reagent volume 1.5 μl and 2.5 μl . used in the experimental setup (Figure 2.6).

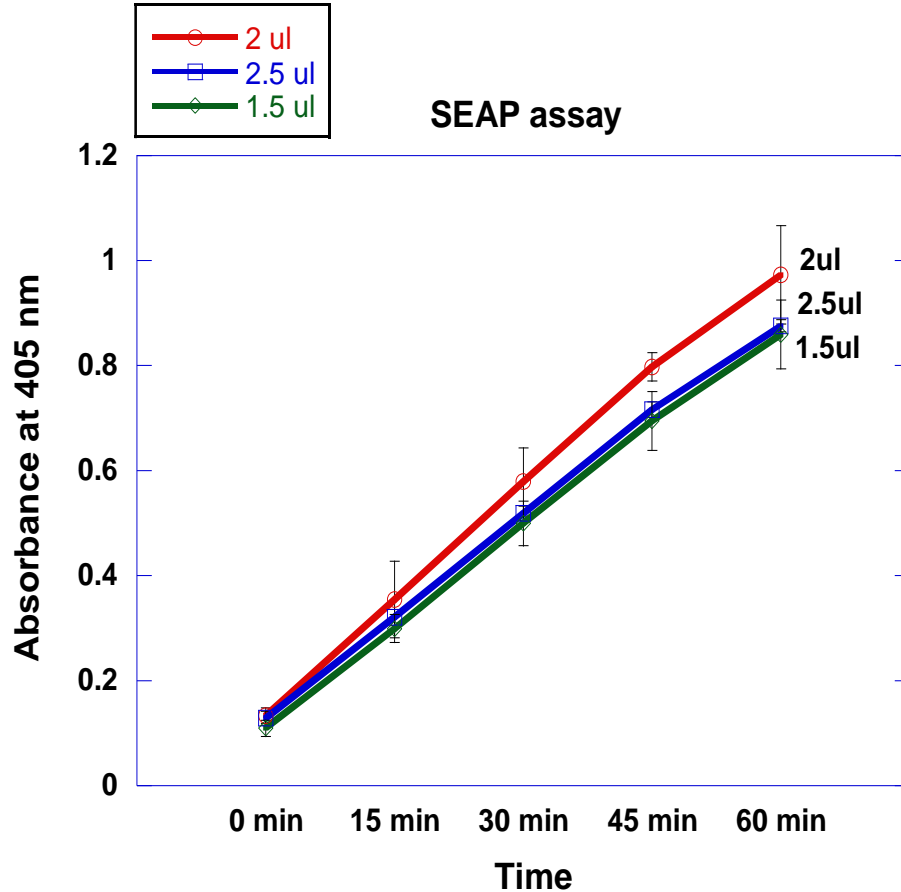


Figure 3.6: Plot showing absorbance at 405 nm from SEAP assay in HEK 293 cells transfected with pcDNA3 SEAP for 24 hours.

Expression of the RAGE variants and Western blot analysis

Western blots of HEK293 cells transfected with the six RAGE constructs are shown in figure 3.7. HEK293 cells do not express endogenous RAGE, and none was detected on Western blots of nontransfected cells or cells transfected with pcDNA3 without a RAGE insert (mock transfected cells). Transfection with full-length RAGE (FL-RAGE) resulted in a single clear band of approximately 55kDa size. This molecular weight is approximately 10 kDa higher than theoretically expected but is typical for RAGE due to post-translational modification (glycosylation). In order to assess the expression and stability of the domain deletion variants (ΔV ,

$\Delta C1$, $\Delta C2$, DN, and TmCyto)- RAGE over time, protein expression for these variants was evaluated at 24, 48, and 72 hours. The three single domain deletion variants (ΔV , $\Delta C1$, $\Delta C2$) show molecular weights close to the calculated size of the domain deletion forms (40, 42, and 39 KDa). The DN-RAGE variant shows a lower apparent molecular weight (~ 50 kDa) compared to the FL-RAGE, which matches the expected molecular weight of the variant. It was also observed that the expression of DN-RAGE reduced after 24-hour transfection time. The TmCyto-variant, which lacks all three extracellular domains, shows the lowest molecular weight of approximately 15 kDa and had comparable expression pattern changes over time with that of the DN-RAGE variant. The possible reason behind the loss of expression in DN-RAGE and TmCyto after 24 hours of transfection could be due to occurrences of proteolytic cleavage near the transmembrane region. This could lead to the formation of sRAGE in the case of DN-RAGE variant that is secreted and a small cytoplasmic fragment in the case of TmCyto, which can be difficult to see by Western blotting. It was also observed that at 24-hour time points, a strong higher molecular weight band in TmCyto-RAGE was detected.

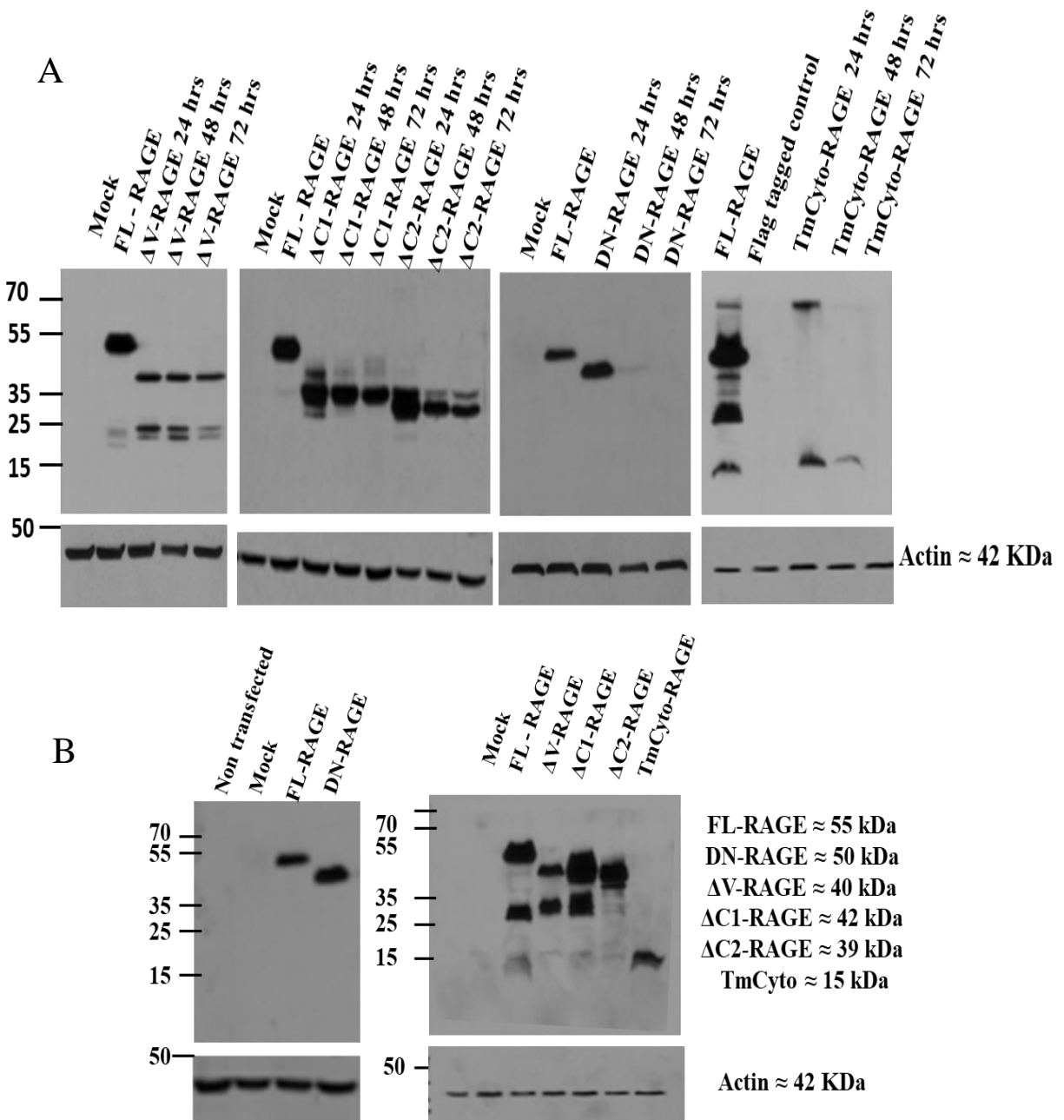


Figure 3.7: Protein expression of FL-RAGE and other RAGE variants at different transfection time points.

(A) 24, 48, and 72 hours and (B) at 24 hours in HEK 293 cells, n=2. Actin was used as the loading control. The N-terminus antiRAGE 9A11 antibody was used to determine expression in FL-RAGE and DN-RAGE. For all other RAGE domain deletion variants, including FL-RAGE, expression was detected using the C-terminal antiRAGE D1A12 antibody.

Using the D1A12 antiRAGE antibody, which recognizes the C-terminal cytoplasmic domain of RAGE, some proteolytic processing of the extracellular domain of FL-RAGE, ΔV -RAGE, and $\Delta C1$ -RAGE was detectable. The detected fragments were observed to have molecular weights ranging from 2515 kDa. The result from other experiments performed is provided in appendix figure A4.

Data from the Western blot analysis showed that at the 24-hour time point, cells had the maximum expression of these variants.

Localization of the RAGE variants using immunofluorescence analysis

Immunofluorescence was used to visualize the localization of the different RAGE variants. Representative microscopic images are shown in figure 3.8. FL-, DN-, $\Delta C1$ -, and $\Delta C2$ - RAGE localized exclusively to the plasma membrane. Images for (ΔV and TmCyto)- RAGE showed intracellular localization as intense fluorescence was observed in the cytoplasmic regions of the cell. Also, the TmCyto-RAGE variant shows some plasma membrane localization, as well as some nuclear localization. Additional images from different experiments representing the localization of the RAGE variants are provided in appendix figure A5.

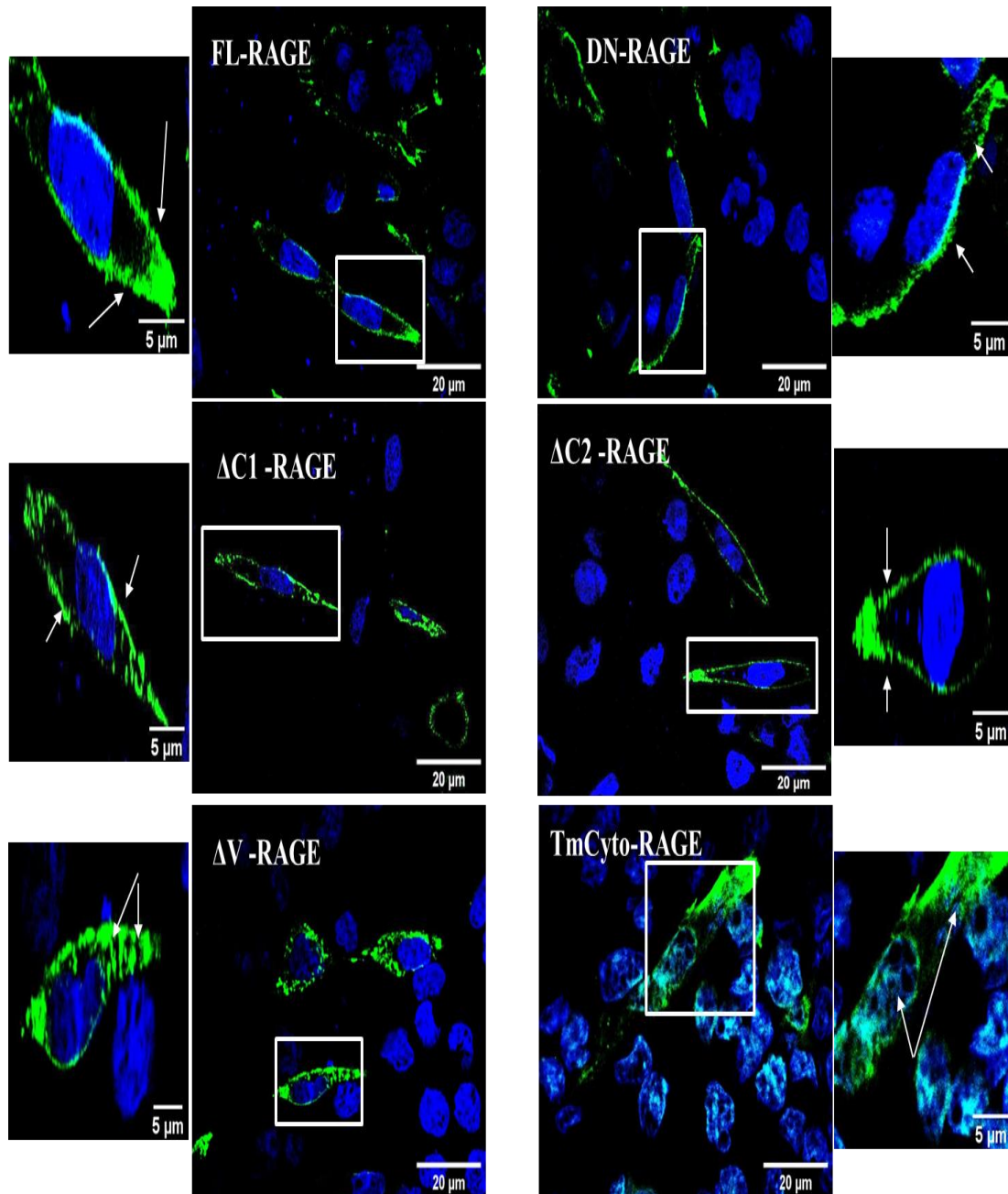


Figure 3.8: Confocal microscopy images of HEK 293 cells expressing the FL-RAGE and different domain deletion variants.

For the DN-RAGE construct antiRAGE 9A11 antibody was used, and for all other constructs, antiRAGE D1A12 antibody was used. The images are taken at 40X objective using Olympus FV3000 at the same exposure time. Images adjacent are enlarged images indicated with arrows to highlight the different localization of these variants in the cells.

Quantitative cellular localization of domain deletion RAGE variants by flow cytometry

Flow cytometry was used to quantitatively measure the distribution of plasma membrane versus intracellularly localized RAGE variants. The cells were analyzed either with their plasma membrane intact to quantify the amount of cell surface localized RAGE or after membrane permeabilization, which allows antibody binding to both intracellular and cell surface exposed RAGE. Results are shown in figure 3.9 and table 3.1. The data shows that FL-RAGE and Δ C2-RAGE are almost exclusively expressed on the cell surface, 85% and 80% of cell surface expression, respectively. DN-RAGE and Δ C1-RAGE showed slightly lower cell surface expression, 78%, and 75%, respectively. The analysis of the Δ V-RAGE variant was hampered by the fact that we could not identify an antibody that would bind to the RAGE C1- or C2- domain. The engineered flag tag on the TmCyto domain was not recognized by two commercial anti-flag antibodies for unknown reasons and could not be used for flow cytometric analysis. Also, the antiRAGE antibody D1A12 recognizes the epitope at the C terminal; we, therefore, could not measure the cell surface presence of either Δ V- or TmCyto-RAGE, and whether a fraction of the protein is localized to the cell surface remains unclear. However, we were able to determine the percentage of increased FL1-A signal in Δ V- and TmCyto-RAGE compared to mock using antiRAGE D1A12 antibody in permeabilized conditions. The signal was observed to be about $80\pm 5\%$ and was comparable to the signal from FL-RAGE under the same conditions (Figure 3.10).

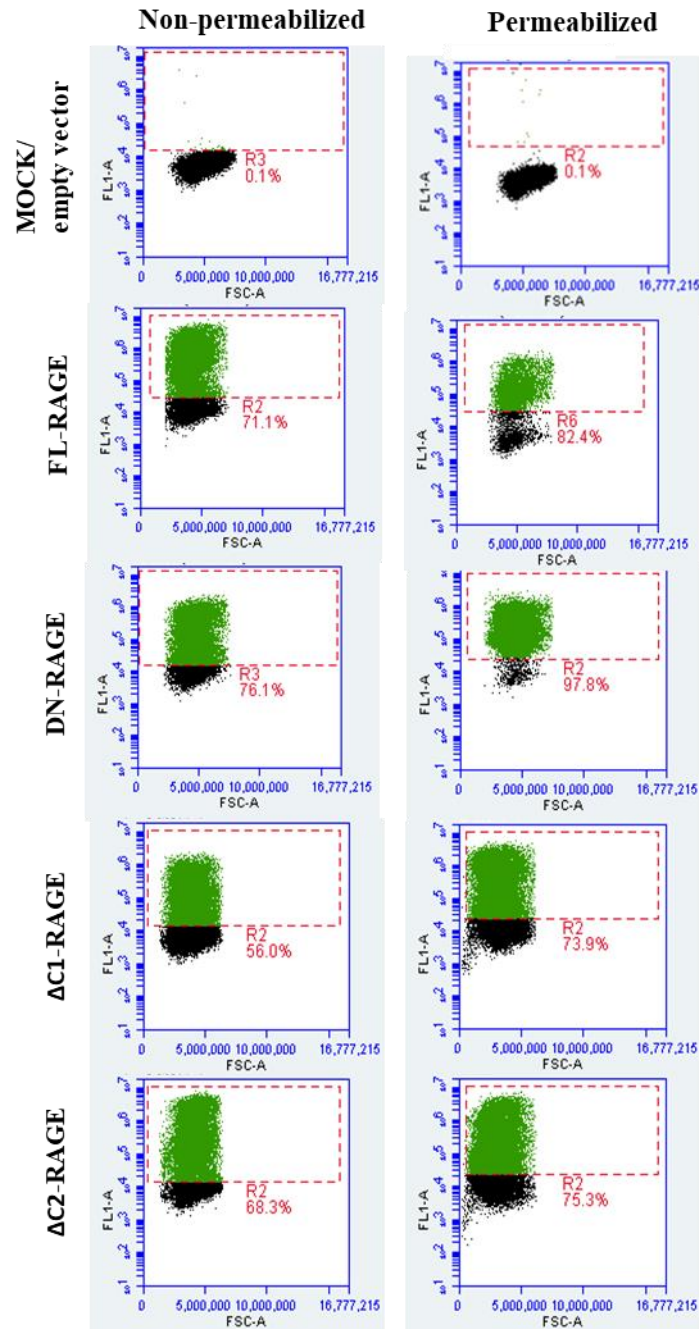


Figure 3.9: Flow cytometry dot blots of HEK 293 cells transiently transfected with mock, FL-RAGE, DN-RAGE, Δ C1-RAGE, and Δ C2-RAGE.

The left column shows flow cytometry dot plots in non-permeabilized conditions and the right column in permeabilized conditions. The gating was performed using mock in both non-permeabilized and permeabilized conditions. The percentage cell population with increased FL1-A signal is compared to mock and as considered the qualitative representation of the transfected cells. One representative example of three experiments (n=3) performed is shown.

Table 3.1: Percentage of cell surface localized RAGE in FL-, DN-, Δ C1-, and Δ C2-RAGE variant transfected HEK 293 cells.

RAGE variants	% Cells with increased FL1-A signal compared to mock in Non-permeabilized condition (FNP)	% Cells with increased FL1-A signal compared to mock in permeabilized condition (FP)	% Localized to the cell surface (FNP/FP)*100
FL-RAGE	70±5	80±6	≈ 85
DN-RAGE	68±7	95±3	≈ 78
Δ C1-RAGE	54±8	68±4	≈ 75
Δ C2-RAGE	62±4	70±7	≈ 80

The percentage of protein localized to the cell surface was estimated by dividing the gated FL1-A signal in non-permeabilized to the permeabilized condition. Results from three individual experiments are displayed as mean and SEM.

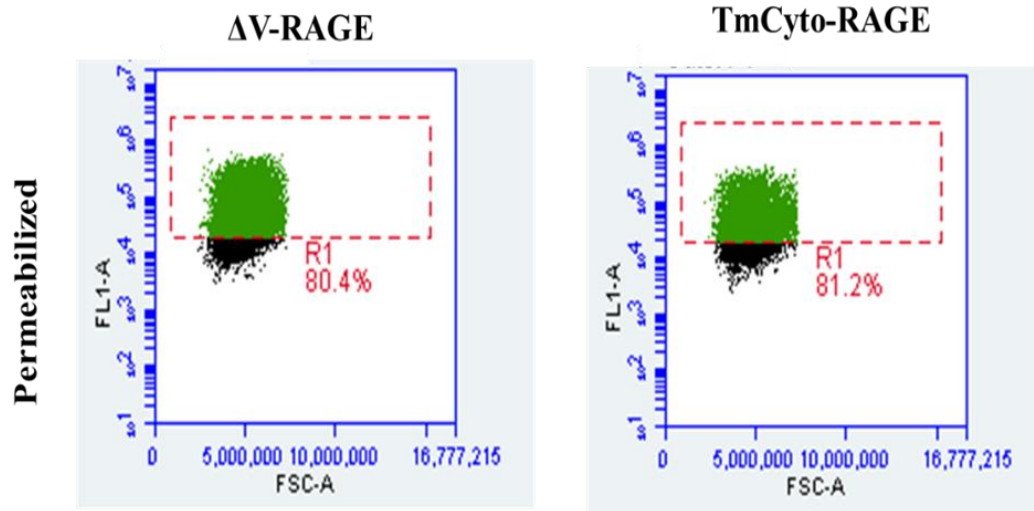


Figure 3.10: Flow cytometry dot blot of HEK 293 cells transiently transfected with Δ V-RAGE and TmCyto-RAGE under permeabilized conditions using antiRAGE D1A12 antibody.

The gating was performed using mock in both non-permeabilized and permeabilized conditions. The percentage cell population with increased FL1-A signal is compared to mock and considered as the qualitative representation of the transfected cells. One representative example of three experiments (n=3) performed is shown.

Discussion

Our study demonstrates the successful expression of FL-RAGE and five domain deletion variants in HEK293 cells. We chose HEK 293 cells as our study model due to their ability to

express various recombinant proteins, including RAGE. Hence, HEK 293 cells serve as a reliable platform to look at the contribution of recombinantly expressed RAGE, as HEK 293 cells also do not express endogenous RAGE (207,229). Western blot analysis using RAGE D1A12 antibody indicates partial proteolytic processing of about 30% in (FL, ΔV , and $\Delta C1$)-RAGE variants at a 24-hour time point. Although we see different degradation rates in these variants, it could be due to variations in the proteolytic processing between samples. Based on the molecular weights of the detected RAGE fragments, cleavage could occur between the C1- and C2-domain. This site of cleavage appears to be distinct from the proteolytic cleavage of RAGE associated with membrane shedding mediated by MMP9 and ADAM 10 (230,231). The expression of the variants DN-RAGE and TmCyto-RAGE was found to be completely abolished at 48-hour and 72-hour time points. This could be possibly due to proteolytic processing of the variants producing sRAGE from DN-RAGE and the intracellular cytoplasmic domain from TmCyto-RAGE (232,233). The C2 and the transmembrane region were also reported to be important in maintaining the structure and functioning of the receptor (125,234). Proteolytic processing or misfolding in this region might have impacted the expression of DN- and TmCyto-RAGE after 24 hours. This also explains why the FLAG tag could not be recognized in the TmCyto variant by two different commercial antibodies, as it might have been cleaved after being expressed.

Confocal immunofluorescence microscopy also confirmed the successful expression of all the RAGE variants. Surprisingly, not all variants were translocated to the plasma membrane. While the (FL, DN, $\Delta C1$, and $\Delta C2$)-RAGE shows clear localization at the plasma membrane, two variants appear to have intracellular localization. The ΔV domain variant was located in the cellular space between the plasma membrane and the nucleus, with a granular distribution. Since no further investigation was performed on the sub-cellular localization of ΔV -RAGE, it could be

possible that the protein is associated with the endoplasmic reticulum or Golgi apparatus rather than homogeneously distributed in the cytoplasm. Further studies will be necessary to pinpoint the localization of the ΔV domain variant and to understand why it is not successfully translocated to the cell surface. It also opens up a possible hypothesis that the V domain of RAGE might be required for trafficking the receptor to the plasma membrane. Studies also reported that the V domain containing 2 glycosylation sites and cysteine disulfide linkage is involved in the dimerization of the receptor, which is critical for cell surface localization (107,122,141). The TmCyto-RAGE variant showed a cellular localization different from ΔV -RAGE and the membrane-localized RAGE variants. In addition to intracellular localization, there was also evidence that the protein was partially translocated to the nucleus.

Flow cytometry analysis was performed to estimate the amount of RAGE on the cell surface of FL-, DN-, $\Delta C1$ -, and $\Delta C2$ -RAGE. The comparison of the fluorescence intensities of non-permeabilized and permeabilized cells revealed slightly higher fluorescence intensity for the permeabilized cells. The result demonstrates that these RAGE variants were predominantly expressed at the cell surface. Since there were no other commercial antibodies targeting the C1 or the C2 domain of RAGE, we could not report on the percentage of membrane-bound protein for the ΔV -RAGE variant. Knowledge of the expression and localization of different domain deletion variants of RAGE is important for subsequent studies which explore the role of individual domains of RAGE in mediating cell adhesion and cell spreading.

Effect of RAGE expression in mediating cell-cell contacts on collagen IV coated surface

Experimental design

Determining RAGE-RAGE or RAGE-nonRAGE contacts on mixed cell population

HEK 293 cells stably expressing full-length (FL-) RAGE was transiently transfected with a plasmid encoding the red-fluorescent protein (RFP), pcDNA3_RFP (RAGE HEK 293-RFP). The wild type (WT) HEK 293 cells were transiently transfected with a plasmid encoding the green fluorescent protein (GFP), pcDNA3_GFP (WT HEK 293-GFP) with transfection conditions as described under general methods chapter 2 (Figure 3.11). After 24 hours of transfection, cells from these two populations were mixed at equal cell densities and were seeded onto collagen IV (5 μ g/ml; R&D Systems # 3410-010-01) coated μ -dish (Ibidi, 35mm). The cells were allowed to attach for 48 hours, and the nucleus was stained using Hoechst 33342 (Invitrogen). Five different fields were selected and imaged from a single μ -dish using a Zeiss confocal microscope LSM700 using default laser settings with appropriate wavelengths. The pinhole for the laser was set to 0.2 μ m, and the exposure was kept constant for each fluorophore ranging from 550 – 600 mV for this study. The exported images from the Zen software were analyzed for RAGE-RAGE and RAGE-nonRAGE contacts. The cells were identified as RAGE HEK 293 or WT HEK 293 based on the type of fluorescence, and cells that had no fluorescence with just nuclei stained were considered nontransfected. The cell contacts formed from these cells with other cells, i.e., RFP (RAGE HEK 293 cells), GFP (WT HEK 293 cells), or nontransfected cells, were determined using Image J software. The percentage of RAGE-RAGE and RAGE-nonRAGE were calculated by dividing the sum of RFP-RFP/ RFP-GFP/ GFP-GFP/ RFP or GFP with nonfluorescent contacts by the total number of contacts made from RAGE HEK 293 for the RFP expressing cells or WT HEK 293 cell for the GFP expressing cells.

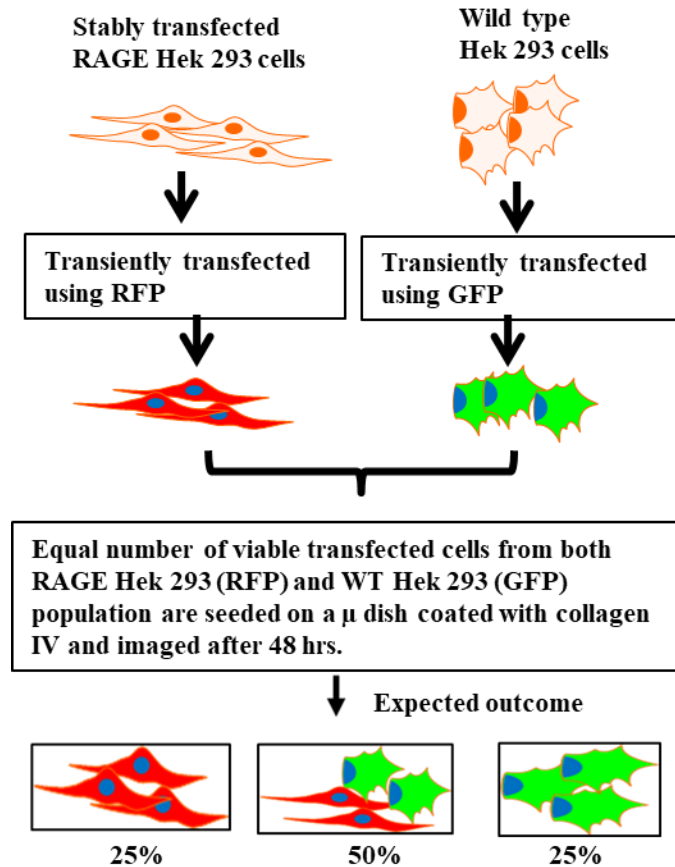


Figure 3.11: Schematic representation of the RAGE-RAGE and RAGE-nonRAGE association study.

Results

RAGE expressing cells preferentially formed RAGE-RAGE contacts during cell-cell adhesion in the presence of collagen IV

Before determining the type of cell-cell contact RAGE expressing cells form when placed in contact with nonRAGE expressing cells, the surface localization of RAGE was assessed in RAGE HEK 293 cells using immunofluorescence imaging. Staining these cells with C-terminal antiRAGE D1A12 antibody demonstrated that RAGE is mostly membrane bound although the cytoplasmic region in the cells showed a faint and diffused fluorescence signal (Figure 3.12).

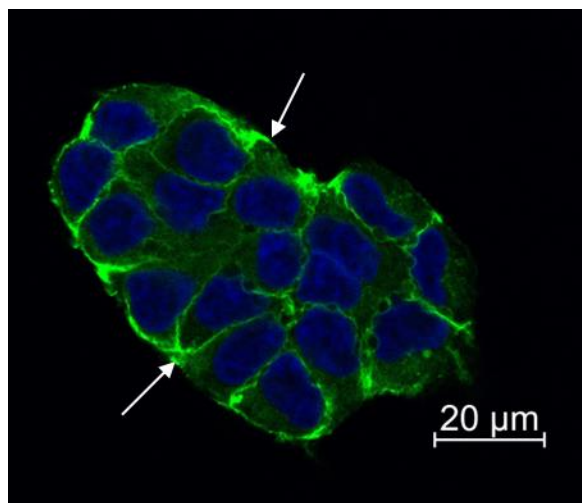


Figure 3.12: Confocal microscopy image of RAGE HEK 293 cells stained with c-terminus antiRAGE D1A12 antibody on collagen IV coated surface. RAGE was detected mainly on the cell surface upon FITC counterstaining the RAGE HEK 293 cells (HEK 293 cells stably transfected with full-length RAGE) with intense staining between cell clusters pointed by arrows.

From the image analysis, most of the cell clusters were formed by RAGE HEK 293-RFP cells (Figure 3.13). The total number of contacts made from RAGE HEK 293 and HEK 293 cells accounted for 876 (Table 3.2), out of which 359 (~ 41%) were from RAGE-RAGE contacts, i.e., RFP-RFP. The contacts made from WT HEK 293 cells, i.e., GFP-GFP, accounted for 157 (~18%) of the total cell contacts. It suggests that RAGE HEK 293 cells mediate cell-cell adhesion by preferentially forming RAGE-RAGE contacts and not through RAGE-nonRAGE association. It was also observed that the total number of cell contacts formed from RAGE HEK 293 cells was twice more than WT HEK 293. From this data, we could infer that RAGE expression leads to increased formation of cell-cell contacts (235). The non-transfected cells were identified by their stained nucleus, which is referred to as nonfluorescent cells. The total cell contacts made from RAGE HEK 293-non fluorescent and WT HEK 293- nonfluorescent constituted 25% of the total cell contacts (Figure 3.14).

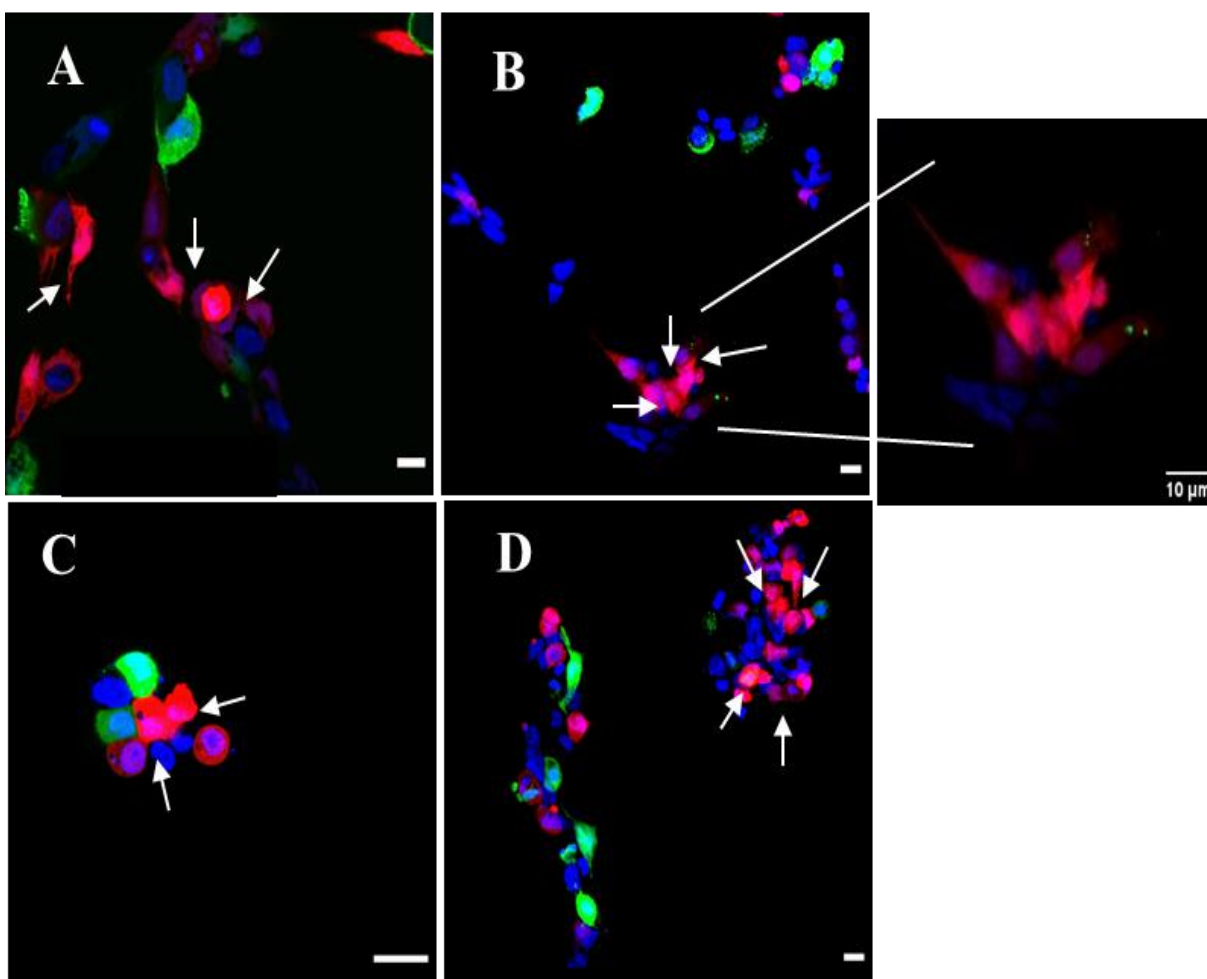


Figure 3.13: Confocal microscopy images showing cell-cell adhesion in RAGE HEK 293 and HEK 293 cells.

The cells were transiently transfected with plasmids encoding the red fluorescent protein (RFP) for RAGE HEK 293 and green fluorescent protein (GFP) for HEK 293. Cells were seeded in equal numbers from the two populations and imaged after 48hrs. RAGE expressing cells formed cell clusters indicated by arrows in the following images. Scale bar 20 μ m. For a single experiment, five images were taken from different fields, and a total of 4 independent experiments (n=4) were performed, which are represented as A, B, C, and D (Refer to appendix Figure A5).

Table 3.2: Quantitative analysis of the identified cell-cell contacts between RAGE HEK 293 (RFP expressing) and WT HEK 293 (GFP expressing) cells.

Fluorescence type	only RFP	Only GFP	RFP-GFP	nuclear stained	Total Contacts
Contacts	RAGE HEK 293 cells	WT HEK 293 cells	RAGE/ WT HEK 293 cells	RAGE/WT HEK 293 with Nonfluorescent cells	
RAGE HEK 293	359	157	140	217	876
HEK 293	(~41%)	(~18%)	(~16%)	(~25%)	

Cells were counted for all 20 images from four different experiments.

PERCENTAGE ESTABLISHED CELL CONTACTS

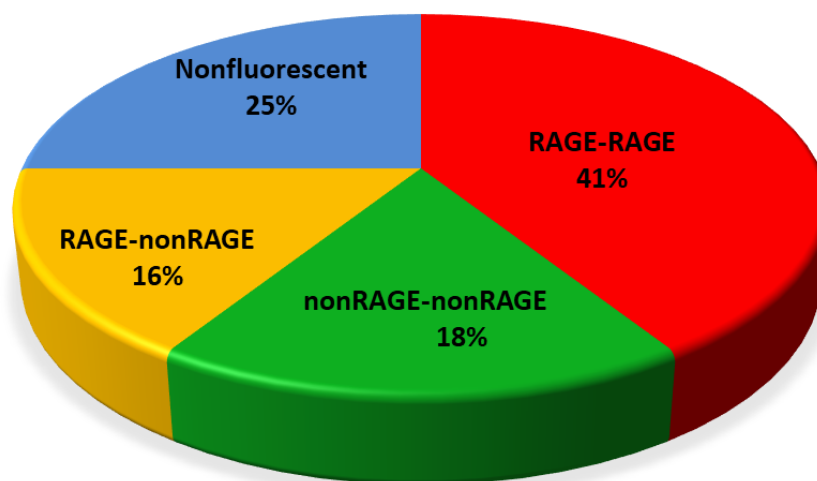


Figure 3.14: Percentage of different cell-cell contacts; RAGE-RAGE, RAGE-nonRAGE, nonRAGE-nonRAGE, and nonfluorescent cells.

RAGE-RAGE association accounted for the maximum percentage of contacts made (~41%); RAGE-nonRAGE and nonRAGE-nonRAGE accounted for approximately 16% and 18%.

Discussion

Immunofluorescence imaging in RAGE HEK 293 cells showed that RAGE was highly clustered at cell-cell contact sites, which agrees with previous studies (200,207). The results from investigating the type of cell contacts associated with RAGE-mediated cell adhesion showed cells preferentially formed homophilic or RAGE-RAGE interaction. The primary reason behind

choosing collagen IV is that it is the primary collagen found in the extracellular basement membranes separating a variety of epithelial and endothelial cells (205,207,236) and RAGE contributes to inflammatory signaling in these cells. Indeed when combined in a mixed cell population, RAGE expressing cells preferentially interact with other RAGE expressing cells and not with nonRAGE cells on collagen IV coated surface. From our study, we estimated that 41% of the total established cell contacts came from RAGE expressing cells. From the image analysis, we expected that the contacts made from RAGE-nonRAGE could account for the maximum percentage of the total cell contacts. However, the observed data showed that $\leq 18\%$ of the total cell contacts were made between RAGE HEK 293 and HEK 293 cells.

Effect of RAGE domain deletion variants on cell adhesion and cell spreading on ECM proteins

Experimental design

Cell-matrix adhesion assay

The cell-matrix adhesion experiments with the RAGE domain deletion variants were performed using the Xcelligence real-time cell analyzer dual plate (RTCA DP, Agilent), as well as the traditional multi-well plate assay using the ECM proteins indicated under methods in Chapter 2. The RTCA-DP Instrument consists of two components: the RTCA Control Unit (a computer that runs the instrumental software) and the RTCA DP Analyzer, which holds three integrated stations for measuring cell responses in parallel or independently (Figure 3.15). The instrument is operated in a standard cell culture incubator, and the control unit is housed outside. It records the signal as cell impedance or cell index (Ω), which is the measure of resistance to the electrical current flow. The change in cell impedance is proportional to the change in cell adhesion.

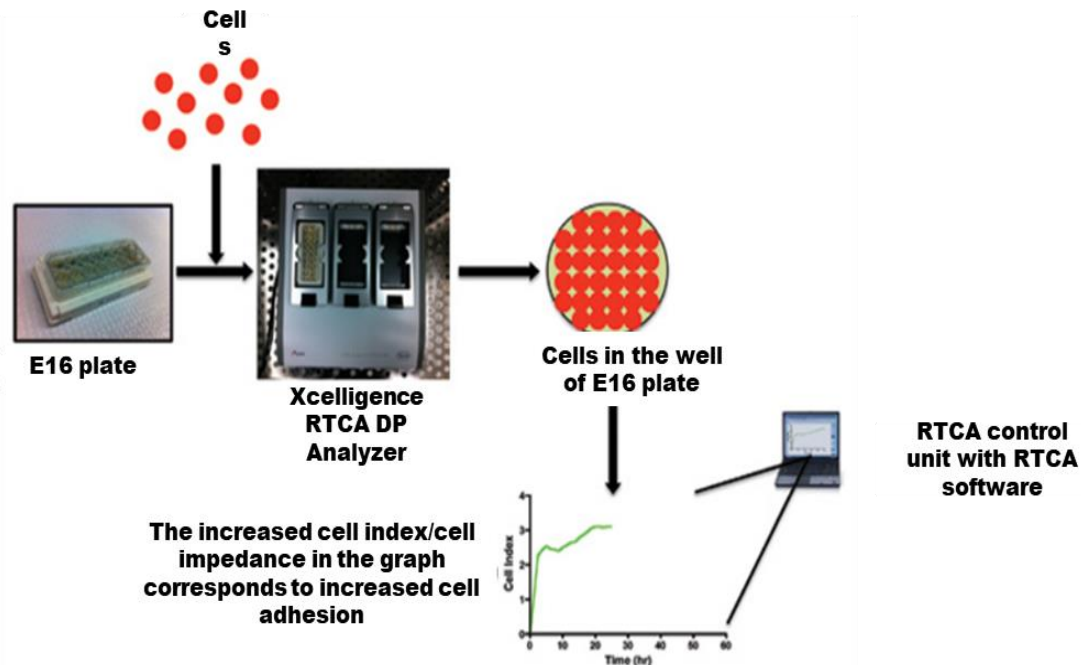


Figure 3.15: Schematic workflow of the Xcelligence RTCA dp system, Agilent. Modified from (237).

The Xcelligence RTCA E16 well plate comes with either a glass or polystyrene (PET) surface. A control experiment was performed to determine the (1) appropriate type of E-16 well plate to be used, (2) if coating the plate surface with ECM proteins interferes with the measurement of the cell impedance value, and (3) to determine the appropriate number of cells to be seeded. The readings from PET E16 well plate showed less background compared to the glass surface with ECM coatings. The PET E16 well plate also had cell index/cell impedance Z that gradually increased relative to the number of cells seeded compared to the glass surface (Figure 3.16). Based on our control experiment, the PET surfaced E-16 well plate with 5000 cells/well in 200 μ l showed the expected outcome with less variation between replicates.

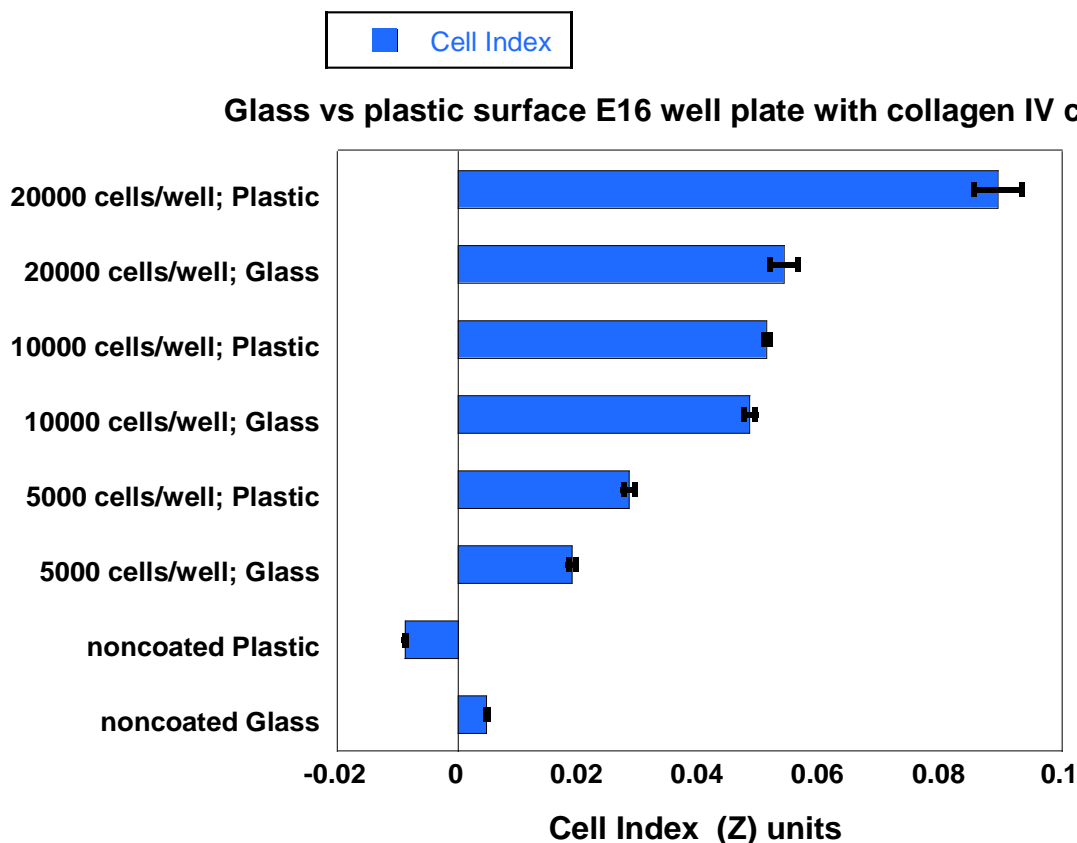


Figure 3.16: Plot of cell index/cell impedance value (Z) at 30 min time point between glass and plastic surface type E-16 well plates with different cell densities.

For the cell-matrix adhesion assay, the wells of the E-16 well polystyrene plate (#300600890) containing sensor gold electrodes were coated with collagen IV (5 μ g/ml; R&D Systems # 3410-010-01) and incubated for 2 hours at RT. After washing the wells with FBS free DMEM media, a background reading was recorded with the instrument with 50 μ l of complete DMEM media with FBS, and cells at a density of 5000 in 150 μ l of media were seeded. The measure of cell adhesion was recorded as the change in cell impedance value (Z) for a time period of 6 hours. The plate assay was performed as described under cell adhesion assay in chapter 2, and for statistical analysis, the student t-test method was used.

Cell spreading assay

The cell spreading assay was performed as described in chapter 2. The cell spread pattern was compared between the mock and RAGE variants using ImageJ software. A total of 3 independent experiments were performed, and statistical significance was determined using the student t-test.

Results

The presence of only the cytoplasmic domain of RAGE enhanced cell adhesion to ECM proteins

Data from the RTCA on the collagen IV coated surface (Figure 3.17) showed that FL-RAGE transfected HEK 293 cells had a steady increase in the cell impedance value with time. The changes were prominent within the first 30 min of the experiment, 0.05 Ω compared to the mock transfected cells, which showed an impedance of about -0.05 Ω . At 6 hours (300 min) time point, the FL-RAGE expressing cells reached an impedance value (Z) of 0.5 Ω and was significant compared to the mock. It was noticed that deleting individual domains on the extracellular region of RAGE lowered the cell impedance compared to the FL-RAGE variant. In particular, deleting the C1 or the C2 domain ($\Delta C1$ & $\Delta C2$) of the RAGE showed a lower impedance value of 0.1 and 0.15 Ω compared to deleting the V domain (ΔV), which had slightly higher impedance $Z = 0.2$ Ω at 6 hours. Surprisingly, removal of the cytoplasmic domain, in the case of the DN-RAGE construct, seems to have no effects on cell adhesion, and the cell impedance over time followed a pattern that was identical to the mock transfected cells, which had an impedance value of 0.1 Ω . This demonstrates that the extracellular domains of RAGE have very little role in modulating cell adhesion to collagen IV. The above observation was further supported by the fact that the TmCyto variant, which lacks the entire ectodomain of RAGE, had an impedance value that was comparable

to that of the FL-RAGE. The impedance value from TmCyto HEK 293 cells exceeded that of the FL-RAGE HEK 293 cells within the first 25 min and, after 6 hours, showed a value of $Z = 0.6 \Omega$.

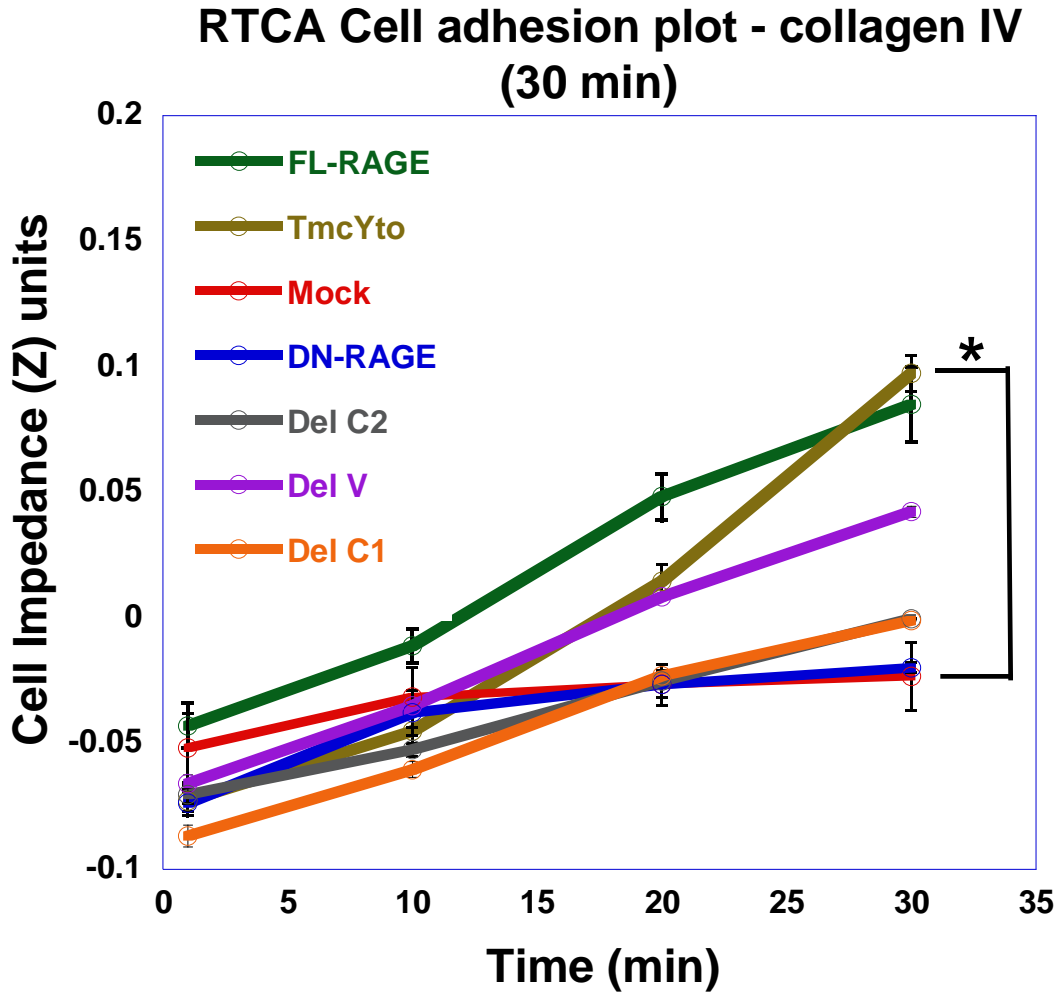


Figure 3.17: Plot of Xcelligence RTCA data showing cell adhesion of HEK 293 cell transiently transfected with RAGE variants to collagen IV at 30 min and 6 hours.

The cell impedance (Z) is directly proportional to the change in cell adhesion. This graph represents the averaged Z values from three independent experiments ($n=3$). Statistical analysis was performed using the Student t-test; $*p<0.05$.

RTCA cell adhesion plot - collagen IV (6 hours)

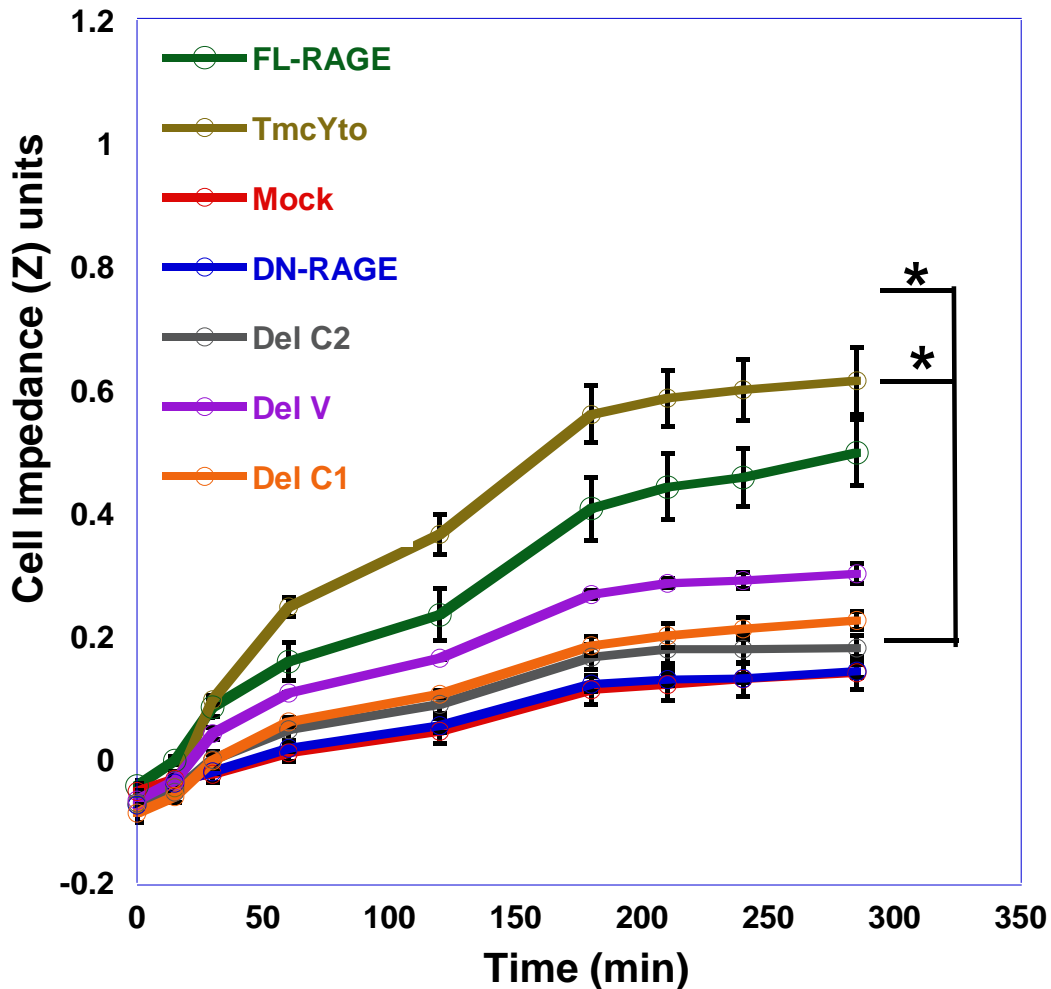


Figure 3.17: Plot of Xcelligence RTCA data showing cell adhesion of HEK 293 cell transiently transfected with RAGE variants to collagen IV at 30 min and 6 hours (continued). The cell impedance (Z) is directly proportional to the change in cell adhesion. This graph represents the averaged Z values from three independent experiments (n=3). Statistical analysis was performed using the Student t-test; *p<0.05.

Interestingly, repeating the same experiment with matrigel coated surface showed no significant change in impedance over time between (FL-, DN-, TmCyto-) RAGE variants and the mock transfected cells (Figure 3.18). It was also noticed that Z values after 5 hours in FL- and TmCyto- RAGE variants were 10 times lower in matrigel ($Z = 0.03 \Omega$) coated surface compared

to collagen IV. Also, from the plots, it was observed that the impedance after 3 hours did not show a steady increase and resembled a stationary adhesion phase. The data implies that these RAGE variants do not contribute to cell adhesion in the presence of matrigel or have the same rate of adherence.

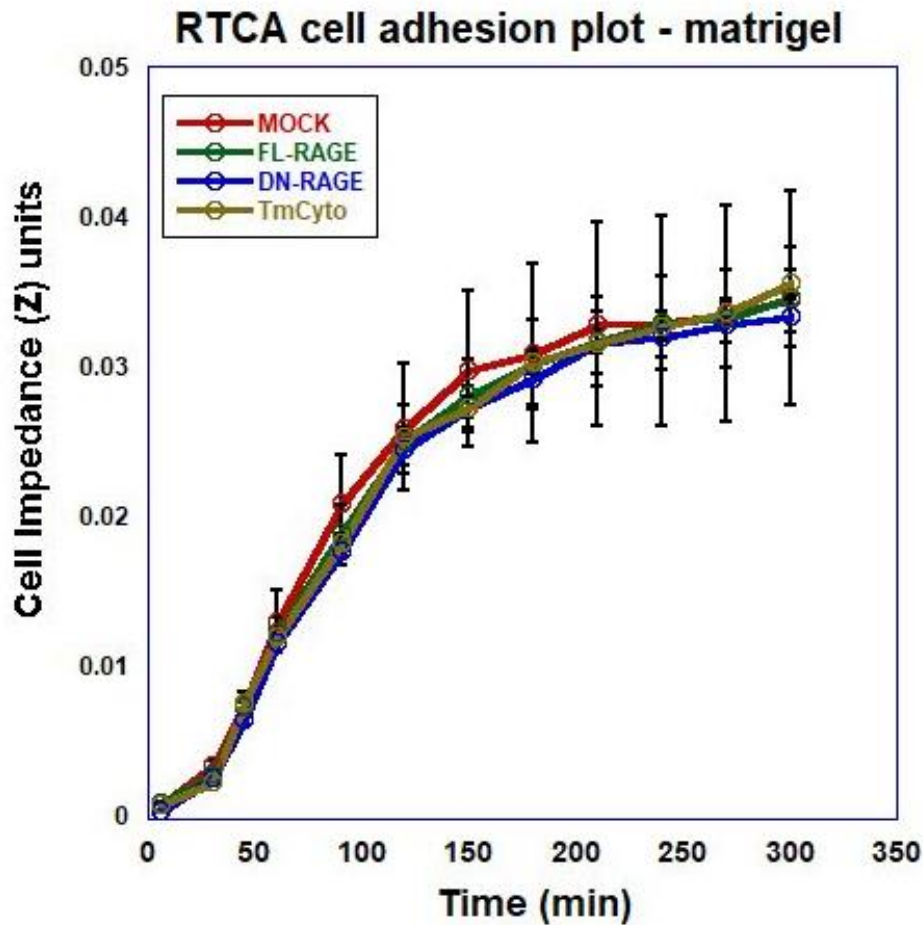


Figure 3.18: Plot of Xcelligence RTCA data showing cell adhesion of HEK 293 cell transiently transfected with RAGE variants (FL-, DN-, TmCyto-) and mock to matrigel for 5 hours. Matrigel is a commercially available matrix derived from a mouse tumor rich in laminin, collagen, and other ECM proteins. This graph represents the averaged Z values from three independent experiments (n=3). Statistical analysis was performed using the Student t-test; *p<0.05.

Plate assay cell adhesion plot - collagen IV

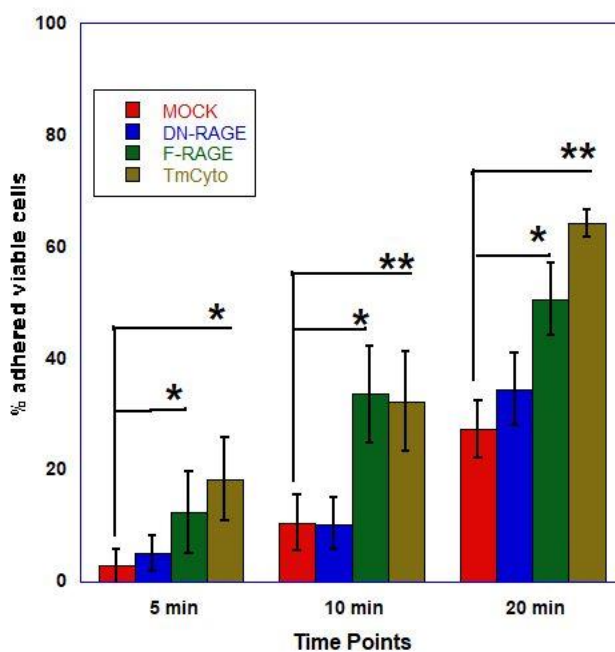


Plate assay cell adhesion plot - fibronectin

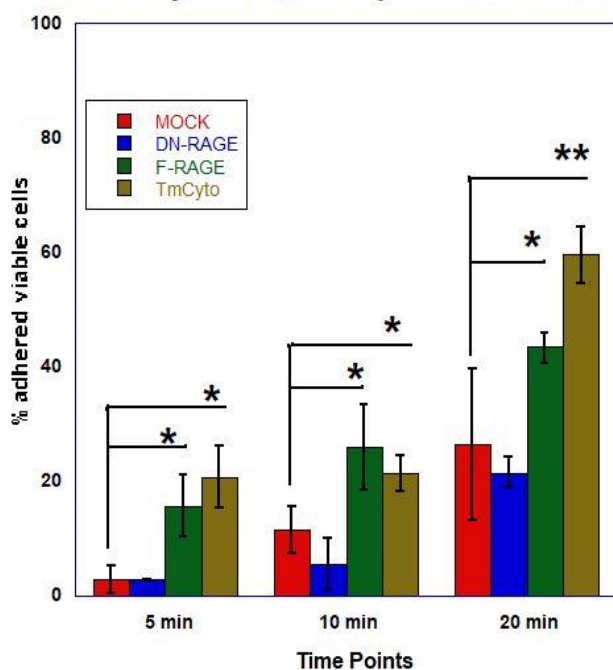


Plate assay cell adhesion plot - collagen I

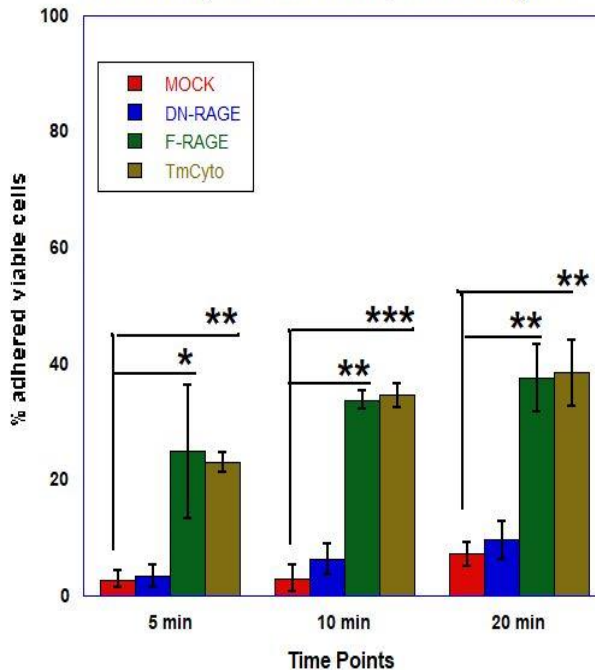


Figure 3.19: Plots of cell adhesion plate assay data in HEK 293 cell transiently transfected with RAGE variants (FL-, DN-, TmCyto-) and mock to different ECM proteins.

Cell adhesion of FL-RAGE, DN-RAGE, TmCyto-RAGE, and mock transfected WT HEK 293 cells to collagen IV (top center), fibronectin (bottom left), and collagen I (bottom right) coated surface. This plot represents the average of three independent experiments (n=3). Statistical analysis was performed using Student t-test; *p<0.05, **p<0.01, ***p<0.001.

A cell adhesion plate assay was performed on the collagen IV coated surface and compared to adhesion data from the RTCA DP system for (FL-, DN-, TmCyto-)RAGE variants and mock transfected cells (Figure 3.19). The data showed a similar change in adhesion pattern with FL- and TmCyto variants showed the highest adherence (57% and 65%) corresponding to the 20 min time point. The adherence of DN-RAGE was observed to increase with time, reaching a maximum adherence of 35%, slightly higher than mock (30%) but was not found to be statistically significant. Comparing the adhesion of these 3 RAGE variants (FL-, DN-, & TmCyto-) to other important ECM proteins in physiology, collagen I and fibronectin showed similar adherence patterns as for collagen IV. With fibronectin coated surface, the TmCyto and FL-RAGE variants reached a maximum adherence of 60% and 45% after 20 min compared to collagen I, which showed 40 % adhered cells. Overall, the results suggest that only the cytoplasmic domain is critical in RAGE-mediated cell adhesion to ECM proteins. It also suggests that RAGE contributes preferential binding to different ECM proteins, which follows the order of collagen IV > fibronectin > collagen I.

Enhanced cell adhesion by the cytoplasmic domain is followed by increased cell spreading to ECM proteins

The cell adhesion phenomenon between cell-cell and cell-ECM is often accompanied by cell spreading. We investigated if the effect on adhesion from FL- and TmCyto-RAGE variant construct to different ECM proteins was linked to cell spreading. Here, we compared the spreading pattern of FL-RAGE, TmCyto, and DN-RAGE to that of the mock-transfected cells on collagen IV, fibronectin, collagen I, and Matrigel coated surfaces (Figure 3.20). Images from cell spreading assays showed that the FL-RAGE and TmCyto RAGE variants showed polarized cell morphology and covered maximum surface area in collagen IV, fibronectin, and collagen I. Although there

were few cells in the images that resembled circular morphology, most of the cells had a dense, almost neuronal-like, spread pattern. Mock and DN-RAGE transfected cells showed circular spread patterns, with most of the cells sparsely attached to the surface and covering a smaller area. Images from the matrigel coated surface showed no change between the RAGE variants FL-, DN-, and TmCyto to the mock. Cells appeared circular in morphology and were observed to be spaced apart from one another.

The images from the cell spreading assay were represented quantitatively by calculating the circularity of the cells using ImageJ software (Figure 3.21). The circularity value for TmCyto- and FL-RAGE variants ranged between 0.5-0.55 for all the tested ECM proteins except for matrigel (0.9). Mock and DN-RAGE, which appeared to be round in morphology, were observed with circularity values > 0.8 . BSA coated surface was used as the control surface where the RAGE variants and mock had equal circularity value ~ 0.9 .

The cell spreading image analysis data demonstrates that adhesion and spreading patterns are linked and follow one another. In the case of FL- and TmCyto-RAGE enhanced cell adhesion is followed by increased cell spreading in all the ECM proteins used in the study except for matrigel. Mock and DN-RAGE resulted in no significant changes in adhesion and spreading behavior to all tested ECM proteins

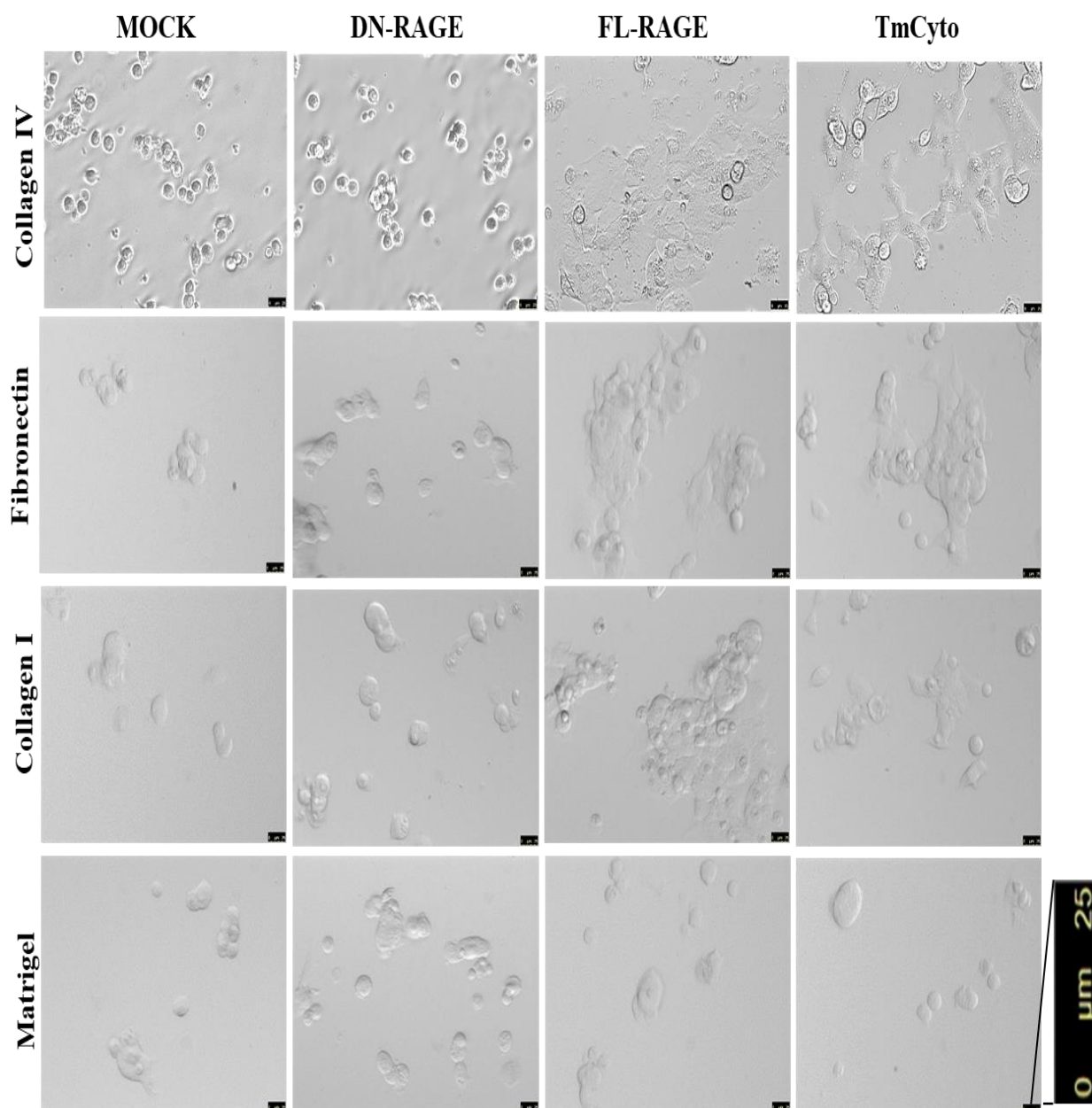


Figure 3.20: Microscopy images from cell spreading assay in HEK 293 cell transiently transfected with RAGE variants (FL-, DN-, TmCyto-) and mock to different ECM proteins. WT HEK 293 cells transfected with mock and (FL-, DN-, and TmCyto-) RAGE variants seeded onto different ECM protein coatings and imaged after 3 hrs. Results from the image analysis demonstrated that FL- and TmCyto-RAGE variant transfected cells had enhanced spreading compared to DN-RAGE variant and mock to all tested ECM coated surfaces except for matrigel. The DN-RAGE variant showed behavior similar to the mock with circular-shaped cells with no spread pattern, (n=2) scale bar 25 μ m.

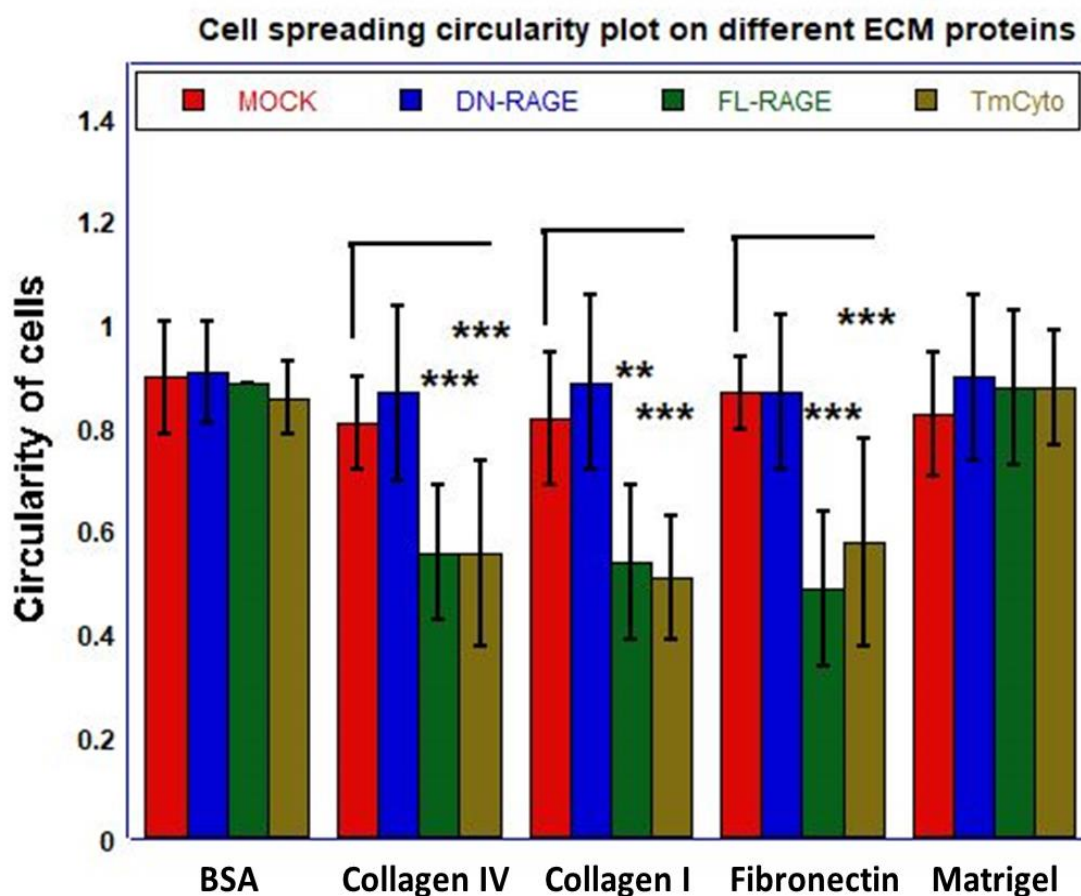


Figure 3.21: Quantitative analysis of circularity of cells transfected with RAGE variants (FL-, DN-, TmCyto- RAGE) and mock transfected cells. The bar graph represents the average cell circularity values from two independent experiments (n=2) using Image J software. A circularity value of 1 denotes the perfect circular shape of a cell. Statistical analysis was performed using the student t-test; *p<0.05, **p<0.01, ***p<0.001.

Discussion

Based on our data from cell adhesion and cell spreading assays, RAGE was found to mediate cell adhesion that is independent of its extracellular domain. Past studies on RAGE have suggested that its extracellular domains mediate cell-cell and cell-matrix adhesion (104,145,207,227,238). Our data demonstrated that the DN-RAGE variant, which contained all the extracellular domains of RAGE (V, C1, and C2), behaved similarly to mock transfected cells in adhesion on collagen IV, collagen I, and fibronectin coated surfaces. The results of the cell

adhesion assay correlated with the cell spreading assays where DN-RAGE variant transfected cells adapted circular in morphology with no apparent spreading onto these ECM coated surfaces (collagen IV, collagen I, and fibronectin). However, the deletion of individual extracellular domains ΔV , $\Delta C1$, and $\Delta C2$ resulted in differences in cell adhesion. Particularly, deleting C1 and C2 domains affected cell adhesion more than deletion of the V domain. Interestingly, the presence of the cytoplasmic domain was found to be important for RAGE mediated cell adhesion and cell spreading to ECM. The FL-RAGE and TmCyto variant showed comparable rates of adherence, suggesting that the transmembrane and the cytoplasmic domains of RAGE could function independently without the extracellular domains. The surface localization in the RAGE variants; DN-, $\Delta C1$ -, and $\Delta C2$ did not correlate with cell adhesion or cell spreading to ECM. The ΔV and the TmCyto variants both showed predominant intracellular cytoplasmic localization.

The cytoplasmic domain of RAGE was reported to share no considerable homology with other receptors and possesses no endogenous receptor tyrosine kinase activity. Previous studies reported that the cytoplasmic domain is needed for effector proteins like Diaphanous 1, DOCK7, and ERK1/2 to carry out downstream signaling (141,239-241). The binding of these effector proteins was mapped to residues R366/Q367 of the RAGE cytoplasmic domain. Truncation of the RAGE cytoplasmic domain via alternative splicing (DN-RAGE) prevented RAGE ligands from activating signaling cascades. DN-RAGE was reported to act as the decoy receptor of RAGE. Expression of FL-RAGE in glioblastoma cells induced the formation of dendritic pseudopodia and increased cell adhesion, whereas DN-RAGE expression was devoid of these changes (119,134,240,242). Pseudopodia are protrusive structures formed at the leading edge of cells that can drive cancer cell migration and adhesion. Recent studies also suggest that RAGE can modulate the expression of various cell adhesion molecules and collagen genes to signal cell migration and

adhesion (165,243). Interestingly from our data, we also observed a preferential binding of FL- and TmCyto- RAGE variants to different ECM proteins, collagen IV was the most preferred ligand. Studies reported that conditional overexpression of RAGE in alveolar epithelial cells decreases collagen IV, and this gives a possible explanation behind increased cell adherence (244). Our study also found significant adhesion to collagen I and fibronectin coated surfaces in FL- and TmCyto-RAGE variants.

The results from our cell spreading data for FL- and TmCyto-RAGE variants showed polarized cell morphology on all tested ECM proteins except for matrigel. Matrigel does not seem to affect the changes in cell adhesion or spreading of these RAGE variants. Matrigel is an ECM mixture containing many factors, including nidogen, collagen IV, and laminin. From our data, it was observed that matrigel does not appear to function as a ligand for RAGE. This observation is similar to other studies on RAGE, where authors have shown that cells expressing FL-RAGE showed no observable change in the adhesion to matrigel (207,242). Overall, our data demonstrate that the RAGE cytoplasmic domain is critical for sustained cell adhesion and increased spreading to ECM proteins.

Conclusions

The goal of this chapter was to elucidate the role of different domains of RAGE in cell-matrix adhesion and spreading. In the first part of the chapter, we constructed domain deletion variants of RAGE (FL, ΔV , $\Delta C1$, $\Delta C2$, DN, and TmCyto). We then investigated these variants expression and localization in HEK 293 cells.

We utilized Western blotting to monitor the expression of those variants using two different epitopes targeting antibodies (N-terminus RAGE9A11 and C-terminus RAGE D1A12) at different time points. Variants FL- ΔV -and $\Delta C2$ - RAGE showed signs of proteolytic cleaved products.

Ectodomain shedding has been reported on RAGE from metalloproteinases, and it has been proposed to play a significant role in RAGE mediated adhesion and migration (131,196,231). Imaging of the variants (FL, Δ C1, Δ C2, and DN)- RAGE showed membrane localization as expected, and the total proteins expressed from these variants localized on the cell membrane. However, deleting the V domain from RAGE appeared to affect the membrane localization of the receptor with variants (Δ V and TmCyto)- RAGE showing intracellular localization. Interestingly, deletion of all the extracellular domains from RAGE in the TmCyto variant showed partial nuclear localization. It highlights the importance of the V domain towards membrane localization of RAGE (122). As reported in other studies, we found that deletion of the C2 domain did not seem to affect the surface localization of RAGE. It shows that the formation of intermolecular disulfide bonds in the C2 domain is not essential for RAGE surface localization in HEK 293 cells (123). This could be possible because RAGE expression and function are altered in different cells (119)

Next, we investigated if RAGE mediates homophilic interactions in collagen IV coated surfaces. For this, we used HEK 293 wild type cells that do not express endogenous RAGE (Figure 3.7) as well as HEK 293 cells that over express RAGE. Based on the clustering pattern, RAGE was observed to increase cell-cell contacts between RAGE-RAGE expressing cells (summarized in Figure 3.22). This emphasizes the involvement of selective interactions between the RAGE expressing cells, and we suspect that this might be the reason behind increased RAGE clustering in cell-cell contacts.

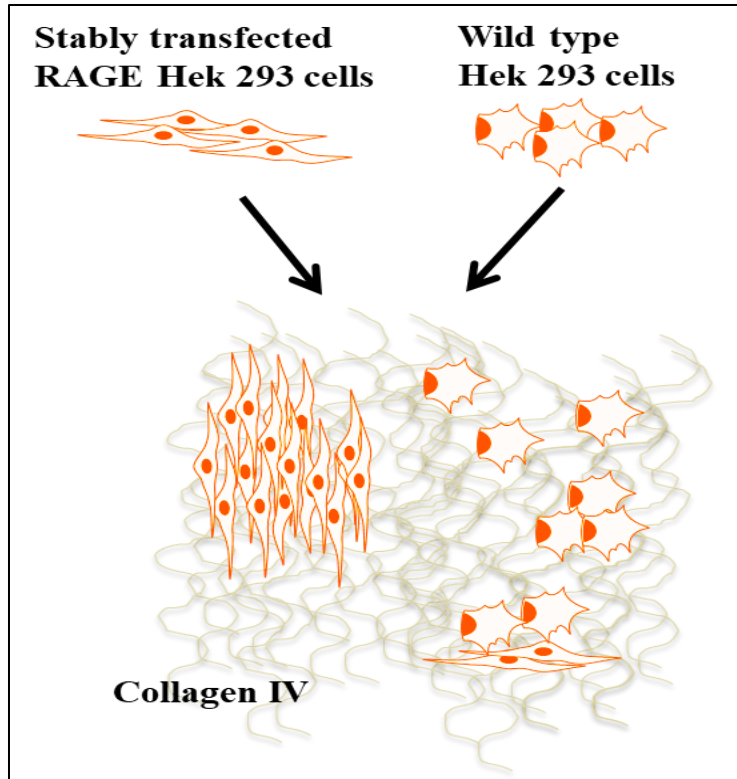


Figure 3.22: Schematic illustration of results of cell-cell contacts formed from wild type and RAGE expressing HEK 293 cells on collagen IV coated surface. Cell clusters/aggregates were mostly formed by RAGE HEK 293 cells and formed preferential homophilic interaction. Wild type HEK 293 formed fewer cell clusters, and analysis showed fewer heterophilic interactions between the cells.

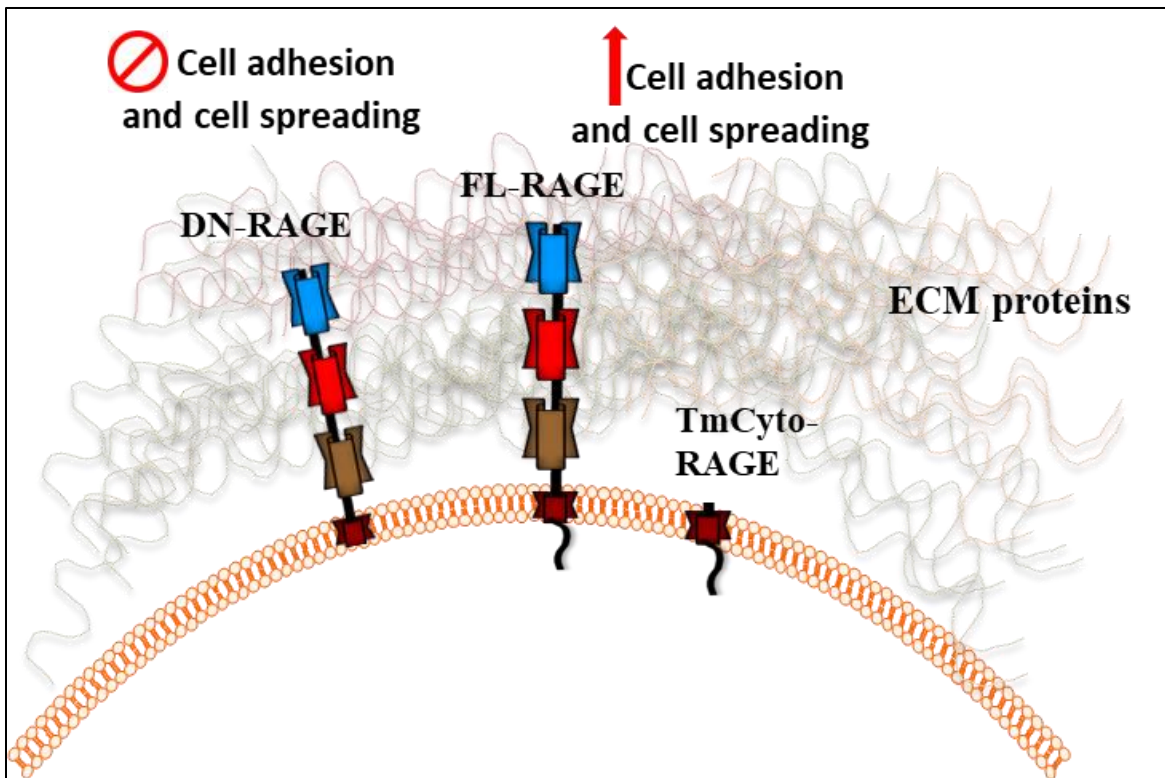


Figure 3.23: Overall findings from chapter 3 on the effect of RAGE variant expression on cell adhesion and cell spreading to ECM in HEK 293 cells. Expression of FL-RAGE and TmCyto-RAGE increased cell adhesion and cell spreading to ECM proteins in comparison to DN-RAGE variant, which completely abolished cell adhesion and spreading effect. These results indicate RAGE mediates signaling to cell adhesion and cell spreading that is independent of the presence of its extracellular domains.

The effect on adherence from these RAGE variants to different extracellular matrix proteins was also determined. We found that of all variants, the DN-RAGE was found to have the lowest adhesion and was comparable to the mock. Deleting individual extracellular domains showed decreased cell adhesion compared to FL-RAGE. Interestingly the TmCyto variant showed adhesion that was comparable to that of the FL-RAGE variant. The pattern in adhesion was similar in the presence of all tested ECM proteins collagen IV, collagen I, and fibronectin but was different in the presence of matrigel. The RAGE variants showed no adhesion changes on matrigel coated surface and showed adhesion behavior similar to the mock. The natural outcome that follows cell and ECM interaction is cell spreading. We observed that the cell spreading effects in FL-, DN-,

TmCyto- RAGE variants mirrored cell adhesion effects. The results of our study do not refute the published work but guide us to the possibility that there exist other mechanisms of RAGE which can signal independently of extracellular domains (summarized in Figure 3.23). Based on our data, membrane bound RAGE was not required to modulate cell-ECM interactions. Our data suggest that RAGE signaling results in enhanced cell adhesion through regulating the expression of other cell adhesion relevant proteins.

CHAPTER 4. RAGE EXPRESSION IN HEK 293 CELLS SHOWS EVIDENCE FOR INTRAMEMBRANE PROTEOLYSIS OCCURRENCE FOLLOWED BY NUCLEAR TRANSLOCATION

Introduction

In chapter 3, we concluded that the presence of the cytoplasmic domain of RAGE is important for enhanced cell adherence and cell spreading on different ECM proteins. Furthermore, data from the Western blot analysis on the expression of RAGE variants demonstrated occurrences of proteolytic cleavage in RAGE. Based on previous studies on RAGE shedding and from our data, we suggest that intramembrane proteolysis of RAGE might be responsible for mediating adhesion, independent of its extracellular domain.

Ectodomain shedding and regulated intramembrane proteolysis (RIP)

Cell adhesion proteins activate various signaling cascades and play an important role in pathophysiology. Recent studies also suggest that these proteins interact with the microenvironment through several mechanisms. One such regulatory mechanism is the proteolytic release of the extracellular domain or ectodomain shedding. Ectodomain shedding is an irreversible posttranslational mechanism that liberates the extracellular domain region of a transmembrane receptor (245-247). During ectodomain shedding, a protease, also called sheddase, cleaves a membrane receptor close to or within its transmembrane domain. This results in 2 fragments of the protein (1) a soluble extracellular form and (2) a membrane bound form consisting of a transmembrane and a cytoplasmic domain (248). Proteases that are reported to have a sheddase-like function are grouped into two major classes; ADAMs (a disintegrin and metalloproteinase) and matrix metalloproteinases (MMPs) (249).

The first sheddase characterized was the transmembrane enzyme responsible for cleaving tumor necrosis factor α (TNF α) and is known as the TNF α -converting enzyme or ADAM17. More than half of the ADAM family members possess zinc-dependent protease activity, including ADAM8, 9, 10, 12, 15, 17, 19, 20, 21, 28, 30, and 33. These proteases share a typical consensus sequence (HEXGHXXGXXHD) present in zinc-binding proteases (250). Other members of the ADAM family including ADAM10 were reported to cleave cell surface proteins that are integral key components of adherent junctions like E-cadherin (251) and N-cadherin (252). The proteolytic cleavage was reported to be crucial for regulating cell-cell adhesion and β -catenin signaling. The matrix associated MMPs such as MMP7 and MMP9 cleave E-cadherin and influence receptor mediated cell-cell adhesion and cell migration (253,254). The membrane type MMPs were also reported to associate with surface proteins via lipid anchors directly or to reside at the cell surface by binding to other transmembrane proteins. MMP 14 transmembrane metalloproteinase mediates the shedding of CAMs, including CD44 and syndecan-1. The ectodomain shedding process is tightly controlled in a spatial and temporal manner by allowing interactions of specific substrates and sheddases (248).

The remaining membrane-embedded protein fragment resulting from the ectodomain shedding is cleaved within its transmembrane domain by a family of proteins known as intramembrane-cleaving proteases (iCliPs), leaving soluble cytoplasmic protein fragment. This sequential proteolytic cleavage event is named the regulated intramembrane proteolysis (RIP) (255). The ectodomain shedding of the transmembrane receptor contributes to the initial half of the RIP process. The second half involves the iCliPs that cleave inside the TM region. There are four main families of iCliPs; the zinc metalloproteases (of which S2P is the only known member), aspartyl proteases that include the presenilin [Presenilin 1 (PS1) or Presenilin 2 (PS2)]-contained

gamma (γ)-secretase protease complex, serine or rhomboid proteases and the recently identified glutamate protease (256). Of these proteases, γ -secretase is the best studied and characterized protease. The γ -secretase proteases form high molecular weight tetrameric protein complexes consisting of PS1 or PS2, nicastrin, anterior pharynx defective-1 (Aph-1) and presenilin enhancer-2 (Pen-2). Studies have demonstrated that these four components of γ -secretase cross-regulate each other, and deregulation of any of the components destabilizes the other and interferes with protease maturation (256).

The best studied and characterized RIP substrates include amyloid precursor protein (APP) (257), Notch (258), CD44 (259), and epithelial cell adhesion molecule (EpCAM) (260). γ -secretase was also reported to act on substrates that lack prior ectodomain shedding. This phenomenon was first discovered in the B cell maturation antigen (BCMA), in which γ -secretase activity was reported within its TM domain when its short 54 amino acids ectodomain was still intact (261). The generation of γ -secretase cleaved protein fragments from various RIP substrates is believed to be a mechanism that contributes to important biological functions like (1) translocating the liberated intracellular cytoplasmic domain (ICD) of the receptor in the nucleus, which signals to regulate gene transcription; (2) enabling the removal and degradation of protein fragments from biological membranes; (3) guiding the spatial segregation of biologically distinct signaling pathways initiated by a RIP substrate (262). The ICD of several RIP substrates contains nuclear localization signals (NLS) which mediate the translocation of cleaved ICD into the nucleus of cells. Ectodomain shedding and RIP are reported to play a major role in pathogenesis by controlling the surface expression and signaling pathways of numerous transmembrane receptors. Constitutive or induced ectodomain shedding was reported to play important roles in cell-cell and cell-matrix adhesion in various organs and is linked to chronic inflammation and tumorigenesis

(263-266). Nuclear translocated ICD upon RIP of transmembrane receptors like EpCAM, CD44 was also reported to activate oncogenic and stress induced signaling responses through selective regulation of genes (260,267).

Ectodomain shedding and RAGE

The existence of sRAGE is an indication that ectodomain shedding of RAGE can occur. sRAGE, as discussed earlier in the introduction section, contains only the extracellular domain of RAGE while lacking the transmembrane and the cytoplasmic domains. The generation of sRAGE was initially assumed to be the result of alternative splicing until it was discovered that 80% of RAGE mRNAs encode for the FL-RAGE protein and only 7% encode the esRAGE variant in human lung samples (117). Results from multiple studies identified that both ADAM 10 and MMP 9 were involved in RAGE shedding between amino acid glycine 331 and serine 332 (230,233). Furthermore, a study reported that ectodomain shedding in RAGE could also be induced following the activation of the Pituitary Adenylate Cyclase-Activating Polypeptide (PACAP) receptor, which belongs to the family of G protein-coupled receptors. This study further demonstrated that apart from knocking down genes of ADAM10 and MMP 9, blocking the PACAP receptor also reduced ectodomain shedding of RAGE (233). The RAGE ligands AGE and HMGB1, as well as the chemical activators of shedding such as ionomycin, phorbol 12-myristate 13-acetate, and 4-aminophenylmercuric acetate were also reported to induce RAGE shedding (196,232,268).

Ectodomain shedding was identified to modulate membrane bound RAGE expression in pathological conditions such as Alzheimer's disease (269), hypertension (270), and coronary artery disease (271). Stress-induced RAGE signaling also contributed to proteolysis and shedding of the receptor and suggested that it might play an important role in neurodegeneration (272,273). Although ectodomain shedding was suggested to be important in influencing RAGE-mediated

processes in cell biology and pathophysiology, no studies have conclusively shown the therapeutic importance of this mechanism. Interestingly, RAGE was reported to share a similar topology as RIP substrates such as notch, amyloid precursor protein, and ErbB4 which undergo constitutive or induced RIP. Three studies have reported that ectodomain shedding of RAGE is followed by γ -secretase cleavage and nuclear translocation of its C-terminal fragment. These studies also suggested that RIP in RAGE is critical to mediate signaling and cell functions including apoptosis and RAGE activated cell migration (196,230,232). Altogether, the result from these studies demand further investigation on the role of ectodomain shedding and RIP of RAGE towards its functioning and regulation.

Therefore in this chapter, we investigated the occurrence of ectodomain shedding in FL-RAGE by monitoring changes in its membrane localization upon AGE stimulation at different time points in HEK 293 cells. For this, we used RAGE which is tagged to a fluorescent protein (FP) at its C-terminus. Since our results from immunofluorescence analysis (chapter 3) with the TmCyto variant demonstrated signs of nuclear localization after 24 hours, and studies suggested γ -secretase cleavage in RAGE, we hypothesized that the RAGE-ICD when expressed individually, could localize to the nucleus. To test this hypothesis, we used a plasmid encoding for RAGE with two distinct fluorescent tags, one at its N-terminus and the other at its C-terminus. We transiently transfected this plasmid in HEK 293 cells. The fluorescence signals were monitored at 12 and 24 hours following ligand stimulation and were analyzed to determine the intracellular and nuclear localization of RAGE.

RAGE subcellular localization

Experimental design

Fluorescent tagged FL-RAGE and RAGE-ICD plasmids

The plasmids mentioned below (Figure 4.1) were constructed by Dr. Vetter. The amino acid sequence of the fluorescent protein is provided in appendix B.

(1) FL-RAGE-YFP

pcDNA3 containing FL-RAGE with m-citrine, a yellow fluorescent protein (YFP) at its C-terminus.

(2) RAGE-ICD-CFP

pcDNA3 containing the RAGE ICD fused to the cyan fluorescent protein (CFP) at its C-terminus.

(3) RAGE-ICD-EGFP

pcDNA3 containing the RAGE ICD fused to the emerald, green fluorescent protein (EGFP) at its C-terminus.

(4) EGFP-FL- RAGE-RFP

pcDNA3 containing FL-RAGE fused with EGFP at the N-terminus and m-Apple, a red fluorescent protein (RFP) at the C-terminus using glycine and serine (GGGSGGG) linkers.

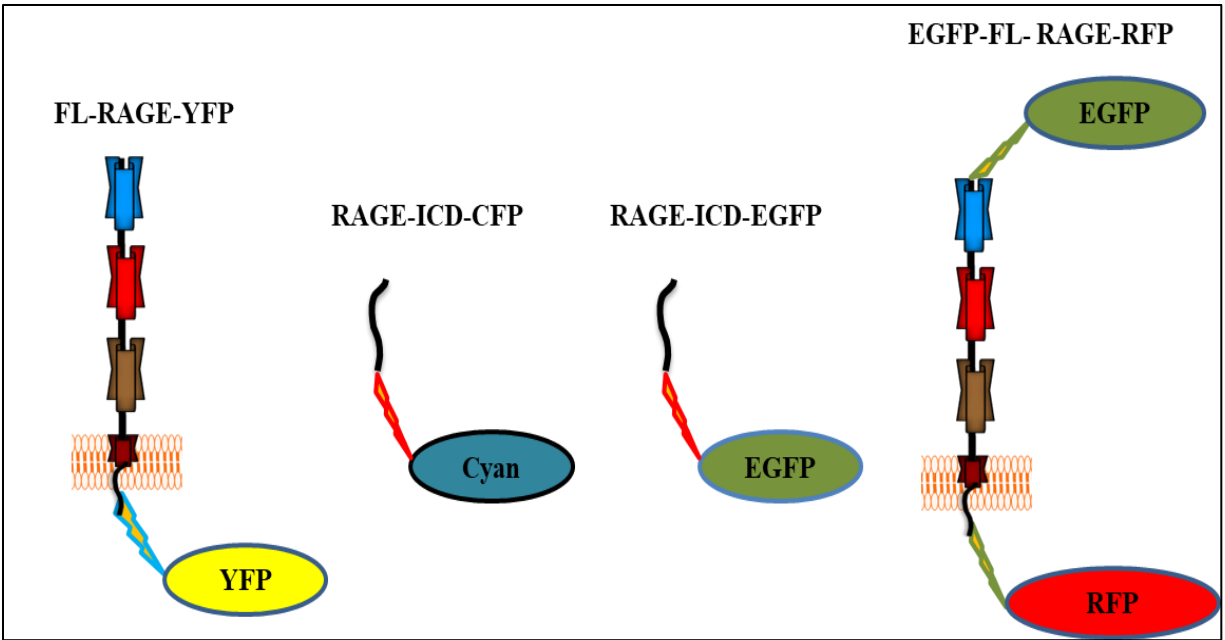


Figure 4.1: Cartoon representation of the different plasmids constructed to monitor ligand induced changes in the subcellular localization in RAGE.

From left; FL-RAGE is tagged with citrine (yellow fluorescent protein) at its C-terminus (FL-RAGE-YFP); RAGE ICD is tagged with cyan fluorescent protein at its C-terminus (RAGE-ICD-CFP); RAGE ICD is tagged with emerald green fluorescent protein at its C-terminus (RAGE-ICD-EGFP); FL-RAGE tagged with EGFP at its N-terminus and m-apple (red fluorescent protein) in its C-terminus (EGFP-FL-RAGE-RFP).

As the control, a pcDNA3 vector containing only the fluorescence protein YFP or Cyan not tagged to the RAGE fragment was used. HEK 293 cells and CHO cells were transfected with the plasmids indicated above using the optimized condition as described earlier in chapter 2 under transient transfection in a μ -dish (Ibidi, 35mm) coated with collagen IV. Cells were transfected with FL-RAGE FP tagged plasmids was stimulated using one of its ligands, ribose glycated BSA (prepared by Dr. Vetter) simultaneously, at 500 μ g/ml concentration for different time points (1, 6, and 24 hours). In this case, the media was not replaced with fresh DMEM after 8 hours of transfection. The cells were then fixed using 4% paraformaldehyde in PBS, and the nuclei of the cells were stained using Hoechst 33342 (Invitrogen #H3570). A prominent subnuclear compartment nucleolus was stained to characterize the intranuclear localization. It involved

cotransfecting the cells with a mTagRFP-T-Fibrillarin-7 plasmid (Addgene #58016) to highlight the fibrillarin region in the nucleolus. Images were taken using the ZEISS LSM 900 Airyscan confocal system. The microscope was set to confocal line switch airyscan mode, and the laser wavelengths were selected from the preprogrammed setting from the Zen software under smart set up. The optimum wavelength option was used to get the maximum signal and to avoid any overlapping signals from different fluorophores. The pinhole for the laser was set to 0.2 μ m and the exposure was kept constant for each fluorophore ranging from 550 – 600 mV for this study. Colocalization analysis was performed using Image Pro Premier software (Media Cybernetics) by selecting the region of interest and by comparing the threshold between the different fluorescence. The Pearson overall colocalization value was used to quantify the degree of colocalization.

Results

Treatment with ribose glycated BSA induced internalization and decreased membrane bound FL-RAGE-YFP in HEK 293 cells

Upon expression of FL-RAGE-YFP in HEK 293 cells, the fluorescence was mainly localized to the cell surface. This agrees with our immunofluorescence data on the FL-RAGE localization using antiRAGE antibodies. Hence, FP tagging of FL-RAGE did not alter its surface localization. HEK 293 cells transfected only with the YFP control plasmid showed localization only in the cytoplasmic (figure 4.2 A).

Treatment with ribose glycated BSA induced no change in the membrane bound expression of FL-RAGE in the first hour of treatment (Figure 4.2 B). However, after 6 hours of treatment, a substantial increase in the intracellular localization of FL-RAGE was observed, and this was accompanied by reduced surface expression. It was also noted that after 24 hours of AGE treatment, the RAGE localization RAGE was observed to have partial nuclear localization. This

result suggests that AGE-RAGE binding initiates internalization of the receptor, which results in decreased membrane bound RAGE.

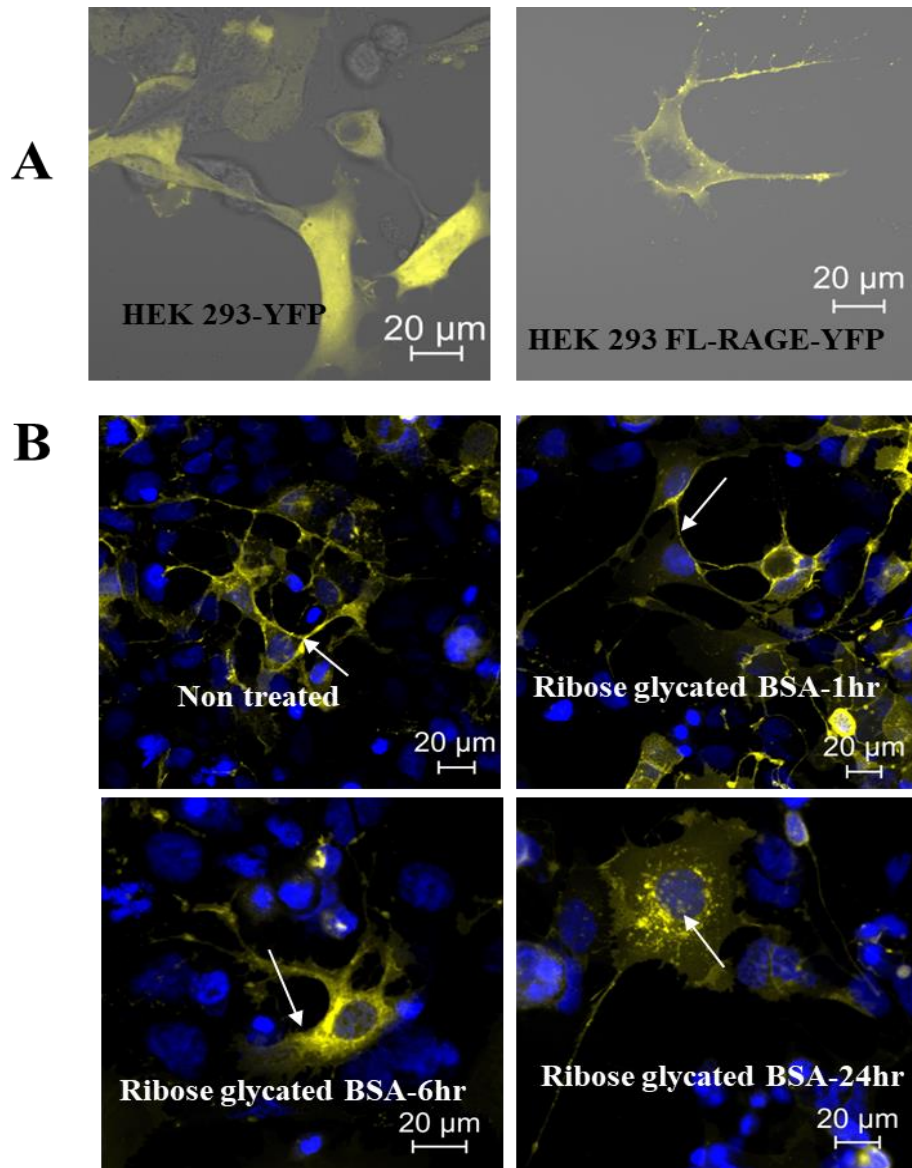


Figure 4.2: Confocal images of WT HEK 293 cells transfected with (A) control, YFP, and FL-RAGE-YFP plasmids. (B) Images of cells transfected with FL-RAGE-YFP and treated with ribose glycosylated BSA at different time points (1, 6, and 24 hours). (C) 3D image of cells transfected with FL-RAGE and treated with ribose glycosylated BSA for 24 hours.

Without AGE treatment, RAGE was localized to the membrane. After 6 hours of AGE treatment (500 μg/ml), RAGE internalization was observed with increased intracellular RAGE localization. Spots of nuclear localization of RAGE-ICD were observed after 24 hours of ribose glycosylated BSA treatment (shown in 3D image). Images from different experiments under the same conditions are included in appendix figure A7.

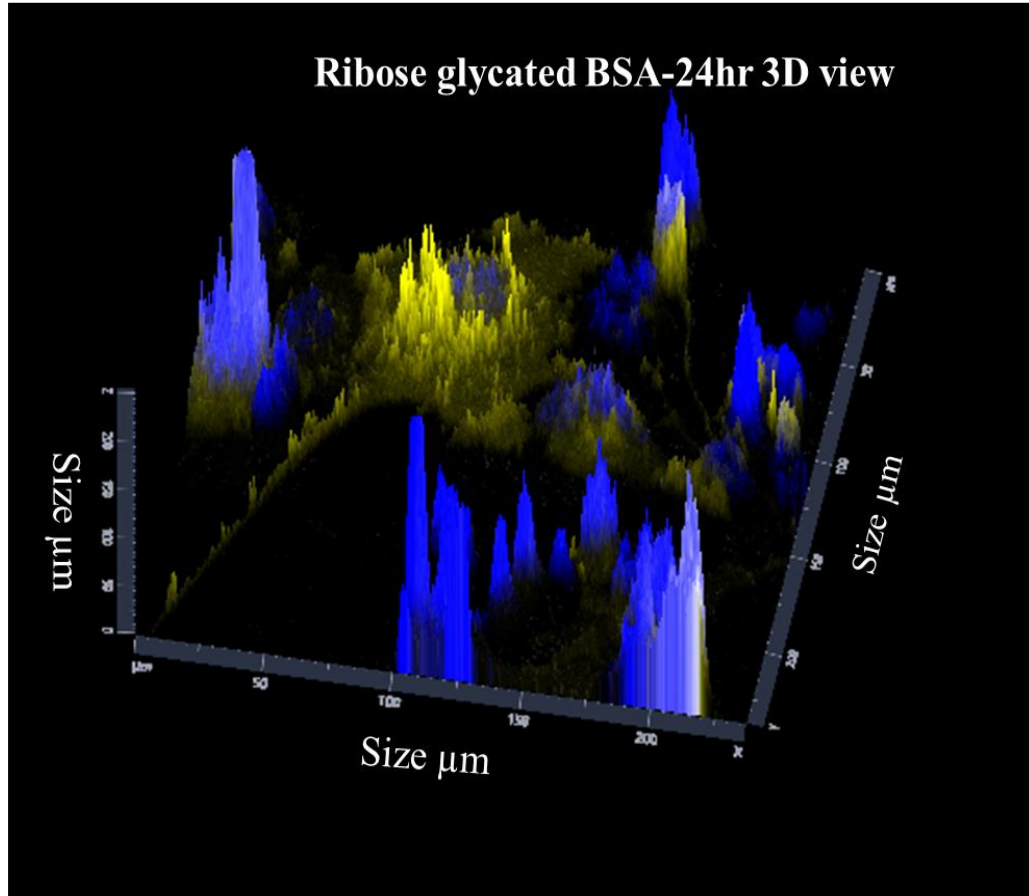
C

Figure 4.2: Confocal images of WT HEK 293 cells transfected with (A) control, YFP, and FL-RAGE-YFP plasmids. (B) Images of cells transfected with FL-RAGE-YFP and treated with ribose glycosylated BSA at different time points (1, 6, and 24 hours). (C) 3D image of cells transfected with FL-RAGE and treated with ribose glycosylated BSA for 24 hours (continued).

Without AGE treatment, RAGE was localized to the membrane. After 6 hours of AGE treatment (500 μ g/ml), RAGE internalization was observed with increased intracellular RAGE localization. Spots of nuclear localization of RAGE-ICD were observed after 24 hours of ribose glycosylated BSA treatment (shown in 3D image). Images from different experiments under the same conditions are included in appendix figure A7.

Expression of RAGE-ICD showed nuclear translocation without ribose glycosylated BSA

treatment in HEK 293 and CHO cells

The results from the image analysis of FL-RAGE-YFP suggested nuclear localization of RAGE after 24 hrs, so we took this as our reference timepoint and monitored RAGE ICD localization. Immunofluorescence data (chapter 3) of the TmCyto-RAGE variant showed intracellular and nuclear localization. But in this case, we observed localization of RAGE-ICD-

CYAN mostly in the nucleus (Figure 4.3). We investigated if the same phenomenon can be replicated in a different cell line that has no endogenous RAGE and has properties similar to HEK 293 cells. We chose Chinese hamster ovary (CHO) cells as the second cell line and expressed RAGE-ICD-CYAN. It was observed after 24 hours of transfection RAGE-ICD-CYAN transfected CHO cells also showed nuclear localization. This suggests that RAGE-ICD can translocate into the nucleus in different cell types.

We hypothesized that a nuclear localization signal (NLS) exists in the RAGE-ICD sequence. SeqNLS, an online NLS predicting software, was used. SeqNLS is based on frequent pattern mining and linear motif scoring (274). This software uses the amino acid sequence as the bait queue and compares it to a library of known NLS sequences. The output from SeqNLS analysis is shown as color-coded score number from calculating all the positively charged lysine and arginine residues from the sequence. A score of >0.89 corresponds to strong NLS, and the sequence is shown in red. We compared the RAGE-ICD sequence to EpCAM, which has a RIP substrate ICD sequence confirmed to have nuclear localization. We found that the size of EpCAM-ICD (260) was similar to RAGE-ICD sequence. Comparing the ICDs of these two proteins in SeqNLS gave a prediction score of about 0.9, corresponding to strong NLS (Figure 4.3). The NLS sequence RRQR in RAGE ICD corresponds to amino acid residues 365-368. It was also observed that the start and the stop amino acid residues in RAGE-ICD and EpCAM-ICD were arginines. These results show that RAGE-ICD could potentially translocate to the nucleus through its NLS sequence.

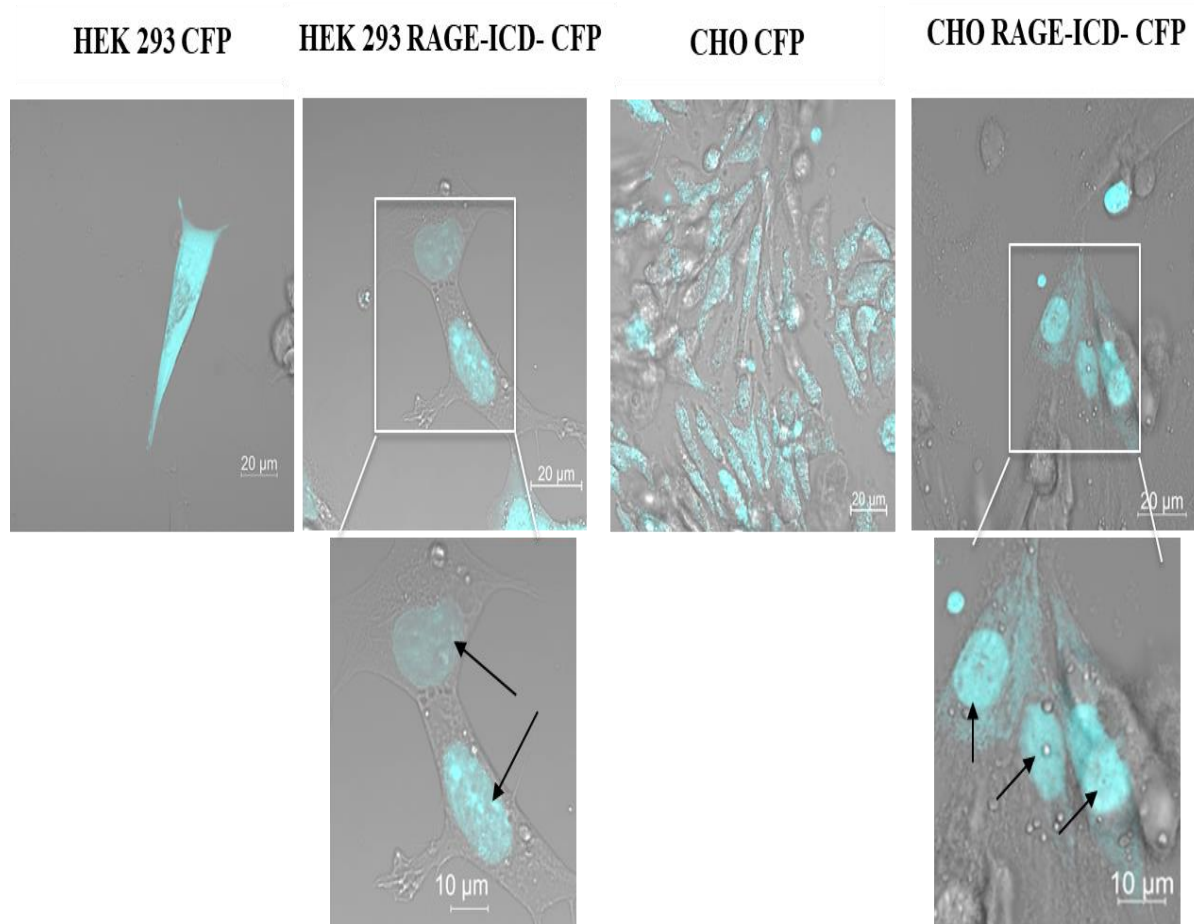


Figure 4.3: Confocal microscopy images of cells transfected with control plasmid containing only cyan fluorescent protein (CFP) tagging and RAGE-ICD CFP in HEK 293 (left) and CHO cells (right).

HEK 293 and CHO cells were transfected with CFP and RAGE-ICD CFP plasmids for 24 hours. Image analysis showed distinct nuclear localization of the CFP in cells transfected with RAGE-ICD-CFP (image enlarged below). In contrast, the control plasmid transfected cells showed no distinct cellular localization of the fluorescent protein. Images from different experiments under the same conditions are included in appendix figure A8.

SeqNLS: Nuclear Localization Signal (NLS) Prediction software

EpCAM intracellular cytoplasmic domain amino acid sequence

P16422: **SRKKR**MAKYEKAEIKEMGEMHRELNA

Protein ID	Predicted NLS	Start	Stop	The highest score of matches within the prediction
P16422	RKKR	2	5	0.902

score range	color
0.1-0.3	dark blue
0.3-0.5	blue
0.5-0.7	cyan
0.7-0.8	green
0.8-0.86	yellow
0.86-0.89	orange
>0.89	red

RAGE intracellular cytoplasmic domain (RAGE-ICD) amino acid sequence

Q15109: Q**RRQR**GEERKAPENQEEEEERAELNQSEEPAGESSTGGP

Protein ID	Predicted NLS	Start	Stop	The highest score of matches within the prediction
Q15109	RRQR	2	5	0.904

Figure 4.4: Data from the SeqNLS software.

Processed data from SeqNLS software indicating NLS in ICD sequence of EpCAM and RAGE. The highest NLS prediction score in both was observed to be 0.9, which corresponds to a strong NLS amino acid sequence (indicated in red) (274).

FL-RAGE undergoes intramembrane proteolysis upon treatment with ribose glycated BSA and leads to the nuclear translocation of its ICD

Image analysis of the FL-RAGE tagged with EGFP, and RFP (EGFP-FL- RAGE-RFP) showed superimposed fluorescence of two fluorescence signals giving a yellow false color image at the cell membrane without ligand stimulation (Figure 4.5). The data is in line with our previous data from the image analysis of FL-RAGE-YFP, which showed membrane localization before treatment. It also demonstrates that FL-RAGE is intact with all its domains at the cell surface and clustered at cell-cell contacts. After 12 hours of treatment with ribose glycated BSA, a proteolytic

cleavage in FL-RAGE was inferred by the distinct localization of EGFP and RFP. In particular, the cleaved C-terminal RFP fragment from the FL-RAGE appeared to be localized in the nucleus. The N-terminal tagged EGFP localization appeared diffused and remained more at the surface. The nuclear localization of the cleaved C-terminal tagged RFP fragment was observed to be time dependent and appeared to occur after 24 hrs of ligand treatment. The nuclear localized RAGE C-terminal RFP fragment appeared as intensely concentrated spots rather than homogenous distribution. It prompted us to investigate further the intranuclear localization of RAGE ICD, which can be important in delineating the role of ICD in the nucleus. Our data demonstrate intramembrane proteolysis in FL-RAGE and liberation of its ICD fragment upon treatment with ribose glycosylated BSA. We also show the nuclear translocation of liberated RAGE-ICD.

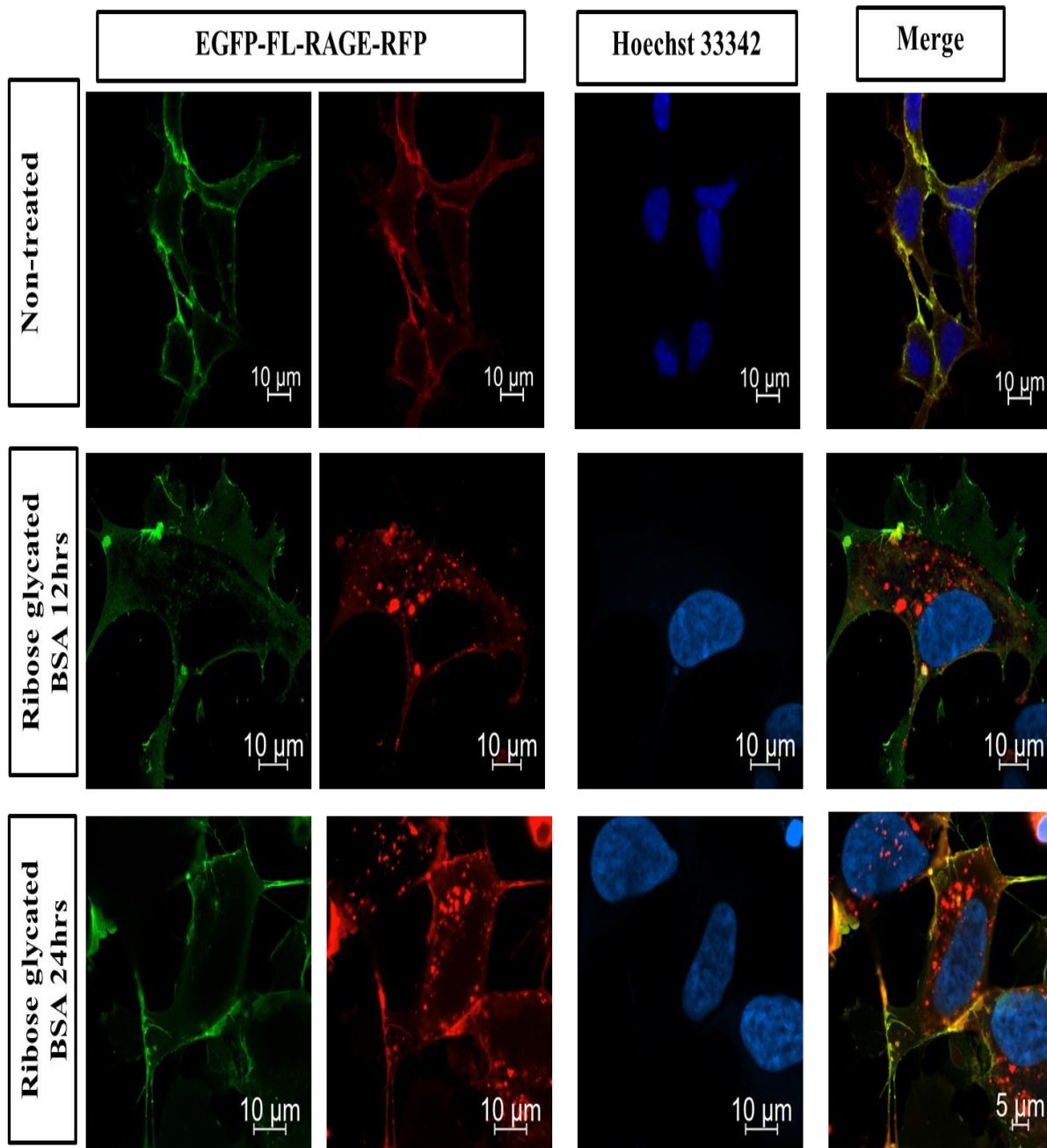
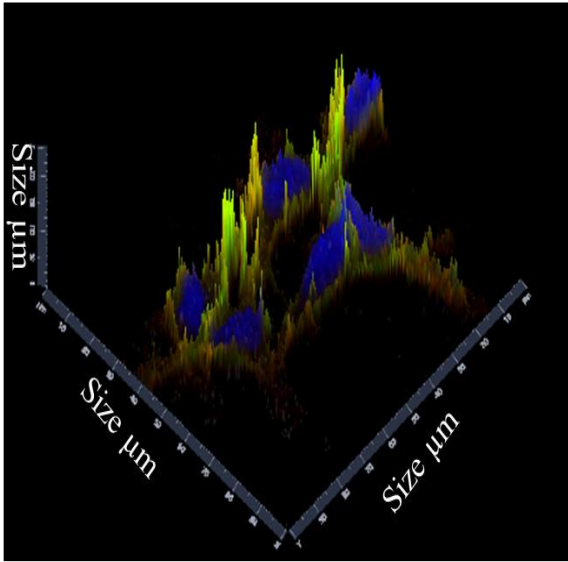


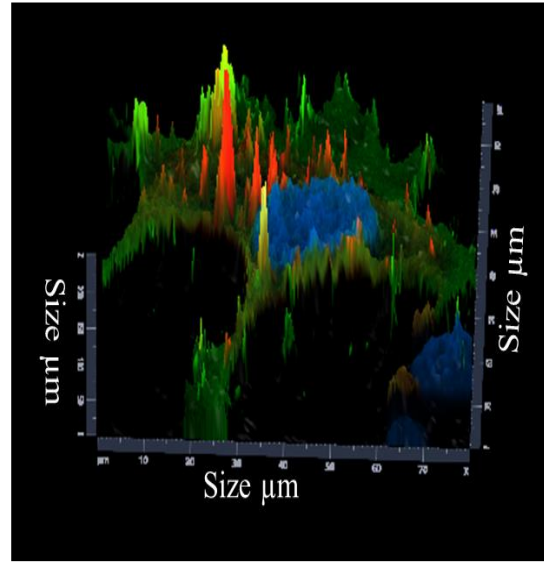
Figure 4.5: Confocal images (2D and 3D view) of WT HEK 293 cells transfected with EGFP-FL-RAGE-RFP in non-treated and ribose glycated BSA treated conditions.

In non-treated conditions, both EGFP and RFP colocalized to the membrane. The enlarged image beside shows increased colocalization of both fluorescent proteins indicating RAGE clustering at cell-cell contacts. With ribose glycated BSA treatment (500 μ g/ml) at 12 hours and 24 hours induced cleavage of RAGE, and this led to distinct localization of EGFP and RFP. After 24 hours, the RFP tagged to C-terminus of RAGE shows nuclear localization. The 3D rendering of the corresponding images was shown beside the treated conditions (Images from different experiments under the same conditions are included in appendix figure A9).

Non-treated - 3D view



Ribose glycosylated BSA 12hrs - 3D view



Ribose glycosylated BSA 24hrs - 3D view

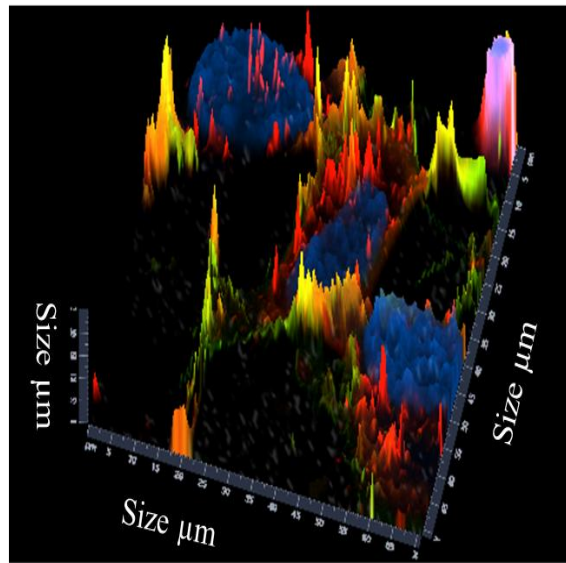


Figure 4.5: Confocal images (2D and 3D view) of WT HEK 293 cells transfected with EGFP-FL- RAGE-RFP plasmid in non-treated and ribose glycosylated BSA treated conditions (continued). In non-treated conditions, both EGFP and RFP colocalized to the membrane. The enlarged image beside shows increased colocalization of both fluorescent proteins indicating RAGE clustering at cell-cell contacts. With ribose glycosylated BSA treatment (500 μ g/ml) for 12 hours and 24 hours, RAGE induced cleavage, which led to distinct localization of EGFP and RFP. After 24 hours, the RFP tagged to the C-terminus of RAGE shows nuclear localization. The 3D rendering of the corresponding images was shown beside the treated conditions (Images from different experiments under the same conditions are included in appendix figure A9).

Characterizing the intranuclear localization of RAGE-ICD revealed localization in the nucleolus.

Data from the image analysis of nuclear localized RAGE showed heterogeneous distribution (Figure 4.2 and Figure 4.5). We initially investigated the intranuclear localization of RAGE ICD in the nucleolus, a prominent subnuclear compartment that contains genes for ribosome biosynthesis. Fibrillarin is a specific marker for the nucleolus. HEK 293 cells were cotransfected with RAGE-ICD-EGFP and the nucleolus marker, mTagRFP-T-Fibrillarin-7. We used the EGFP tagged RAGE-ICD as they emit at a longer wavelength than CFP. It is beneficial in our study as fluorescence proteins with longer wavelengths have reduced autofluorescence upon exposure to UV or visible radiation (275). After 36 hours, RAGE-ICD showed nuclear localization and appeared more concentrated in the nucleolus (Figure 4.6).

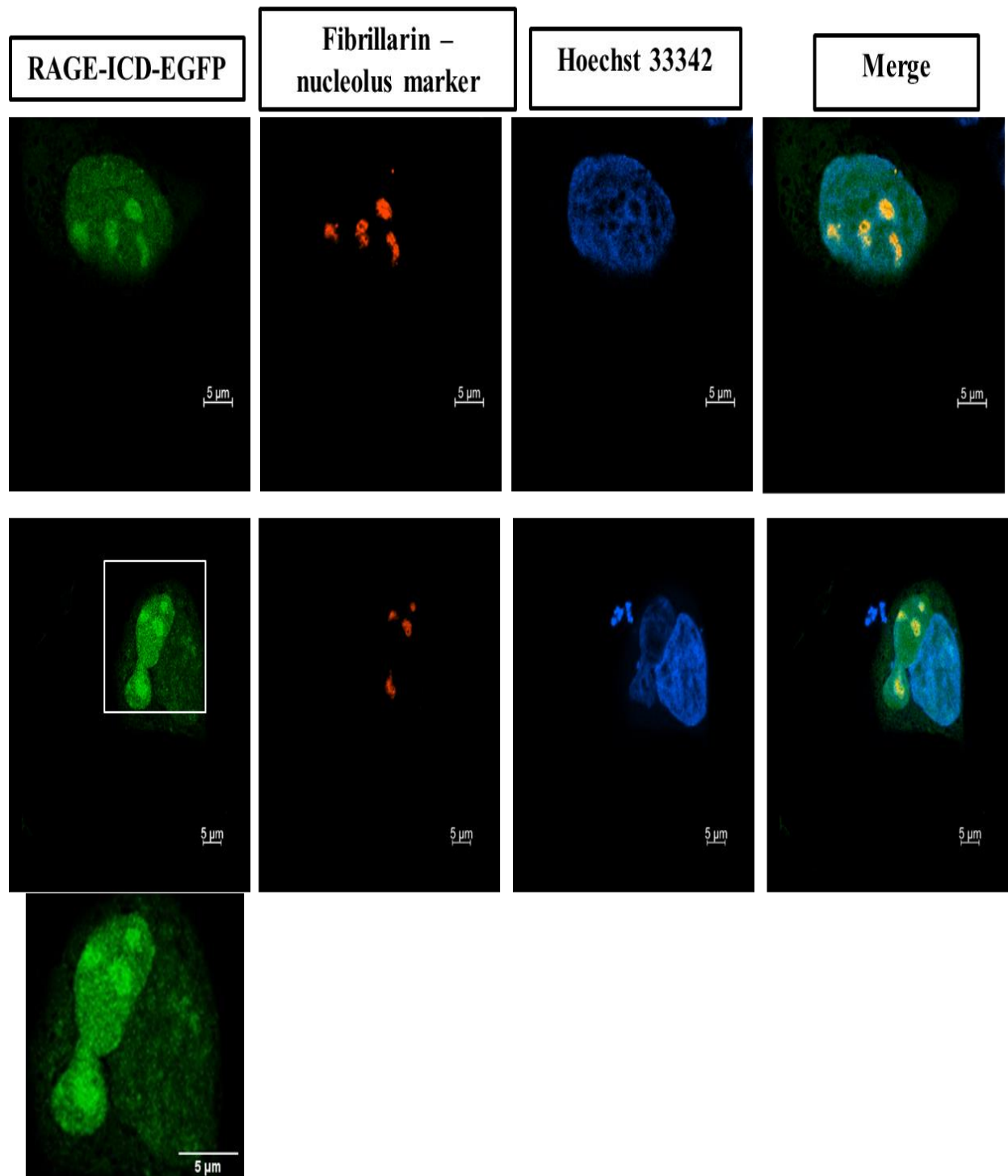


Figure 4.6: Confocal microscopy images of WT HEK 293 cells co-transfected with RAGE-ICD-CFP and mTagRFP-T-Fibrillarin-7.

After 36 hours of co-transfecting RAGE-ICD-EGFP with mTagRFP-T-Fibrillarin-7 (Addgene #58016), cells were fixed, nuclei were stained, and imaged. The enlarged image shows nuclear and nucleolar localization of RAGE-ICD-EGFP.

We questioned if FL-RAGE could have the same effect upon ribose glycated BSA treatment for 36 hours. After 36 hrs of treatment with ribose glycated BSA, FL-RAGE showed clear nucleolar localization (Figure 4.7). However, membrane bound RAGE expression was still observed in this case. The change from nuclear to nucleolar localization appears to occur in a time dependent manner for both FL-RAGE and RAGE-ICD. The Pearson overall co-localization value within the nucleolus ROI was 0.9 for RAGE-ICD-CFP (Figure 4.8) and 0.98 for FL-RAGE-YFP transfected cells.

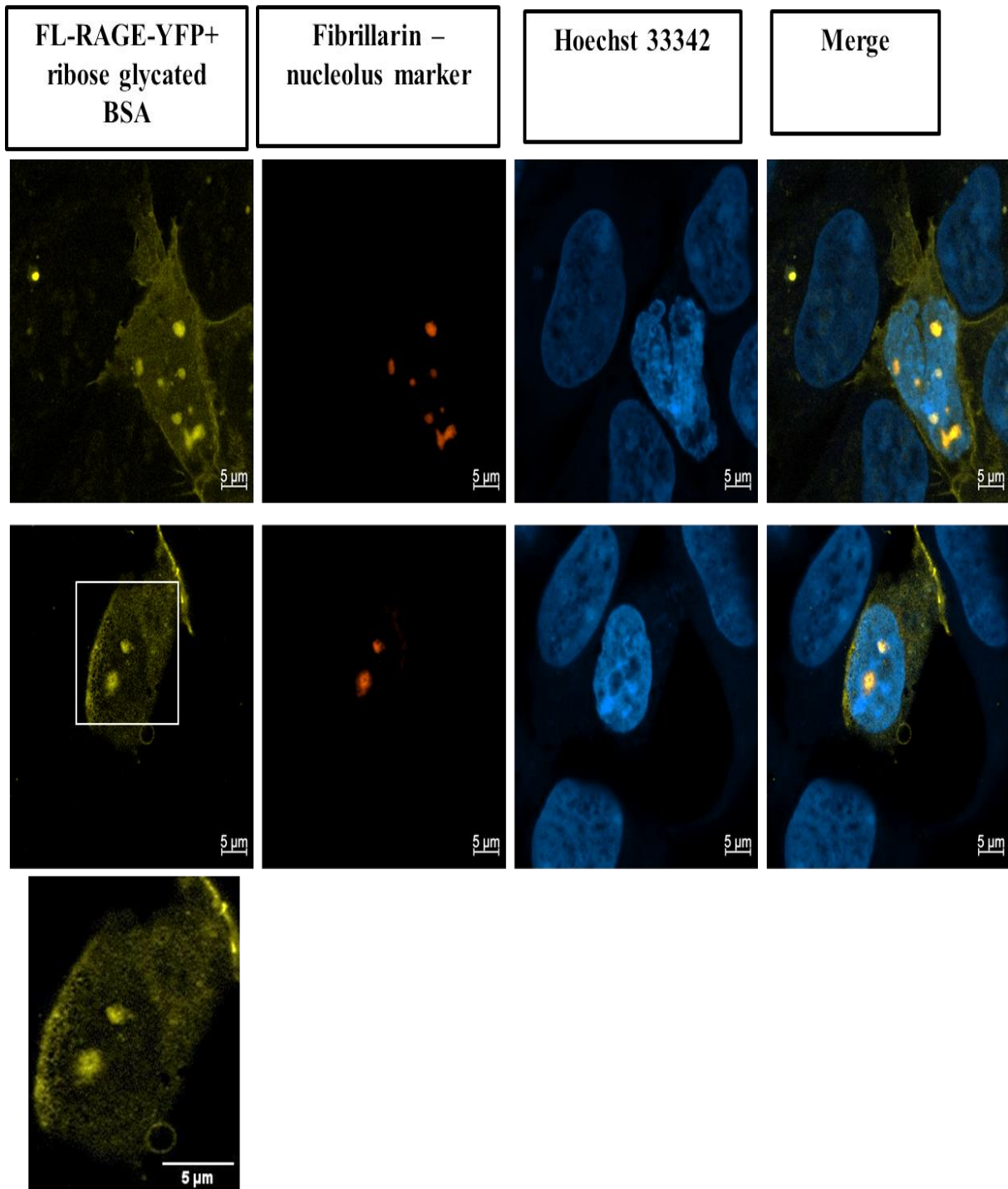


Figure 4.7: Confocal microscopy images of HEK 293 cells co-transfected with FL-RAGE-YFP and mTagRFP-T-Fibrillarin-7, treated with ribose glycated BSA. After 36 hours of co-transfecting RAGE-ICD-EGFP with mTagRFP-T-Fibrillarin-7 (Addgene #58016), cells were fixed, nuclei were stained, and imaged. The enlarged image below shows the nucleolar localization of RAGE-ICD-EGFP.

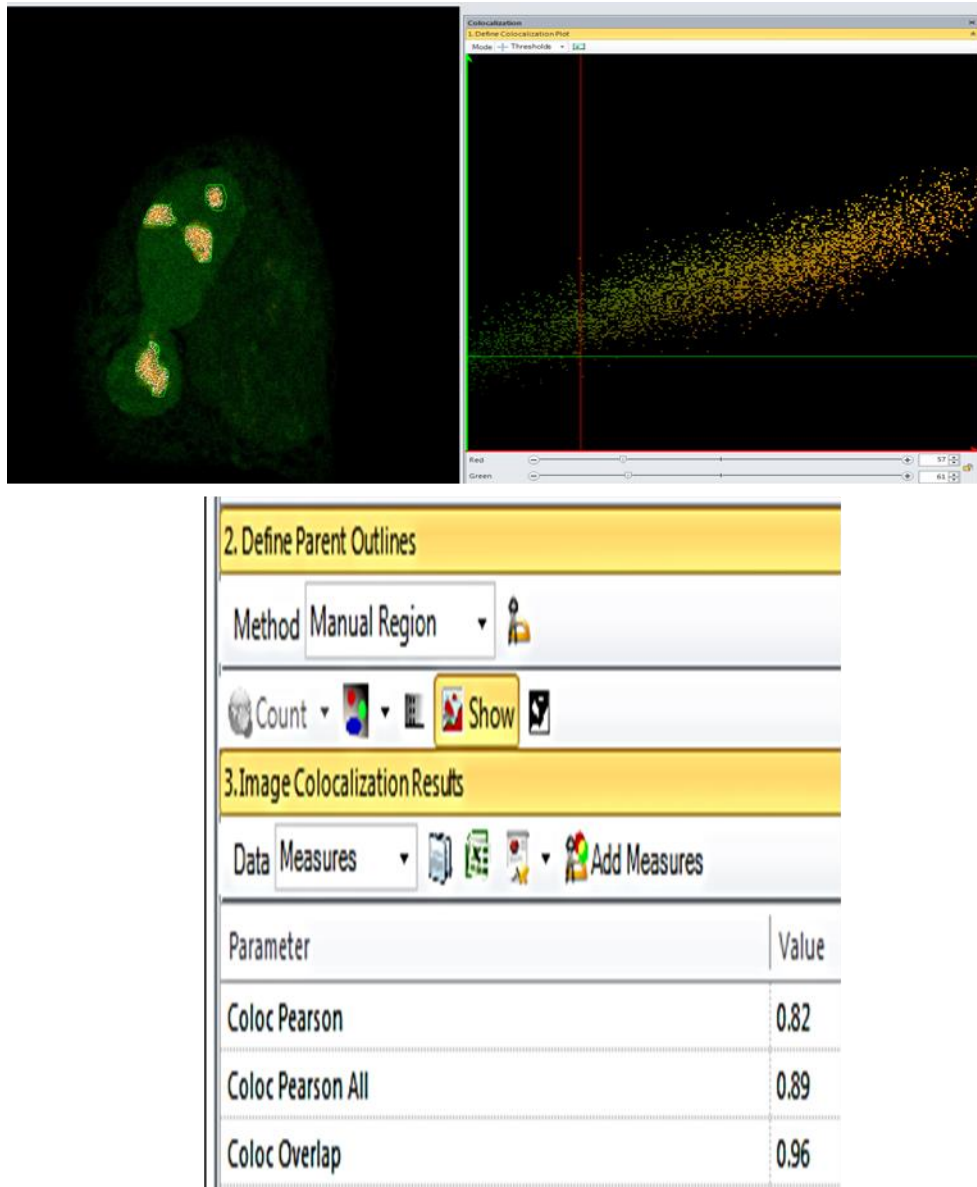


Figure 4.8: Colocalization analysis of RAGE-ICD-EGFP and mTagRFP-T-Fibrillarin-7 using Image Pro Premier software.

Representative images showing a manual selection of nucleolus ROI (top left). Corresponding colocalization plot for the selected ROI and the screenshot results from Image Pro Premier software (Media Cybernetics) are shown below the images indicating the Pearson overall colocalization value.

Similar to nuclear localization signal predictors, there are online tools to detect nucleolar localization sequences in a protein. Using a Nucleolar localization sequence Detector (NoD) two nucleolar localization sequences were detected in RAGE (276). One in the V domain and the other

in the intracellular cytoplasmic domain. The NLS sequence residue region exactly matched the nucleolar localization signal (Figure 4.9). This further complemented our observation of the nucleolus localization of RAGE-ICD.

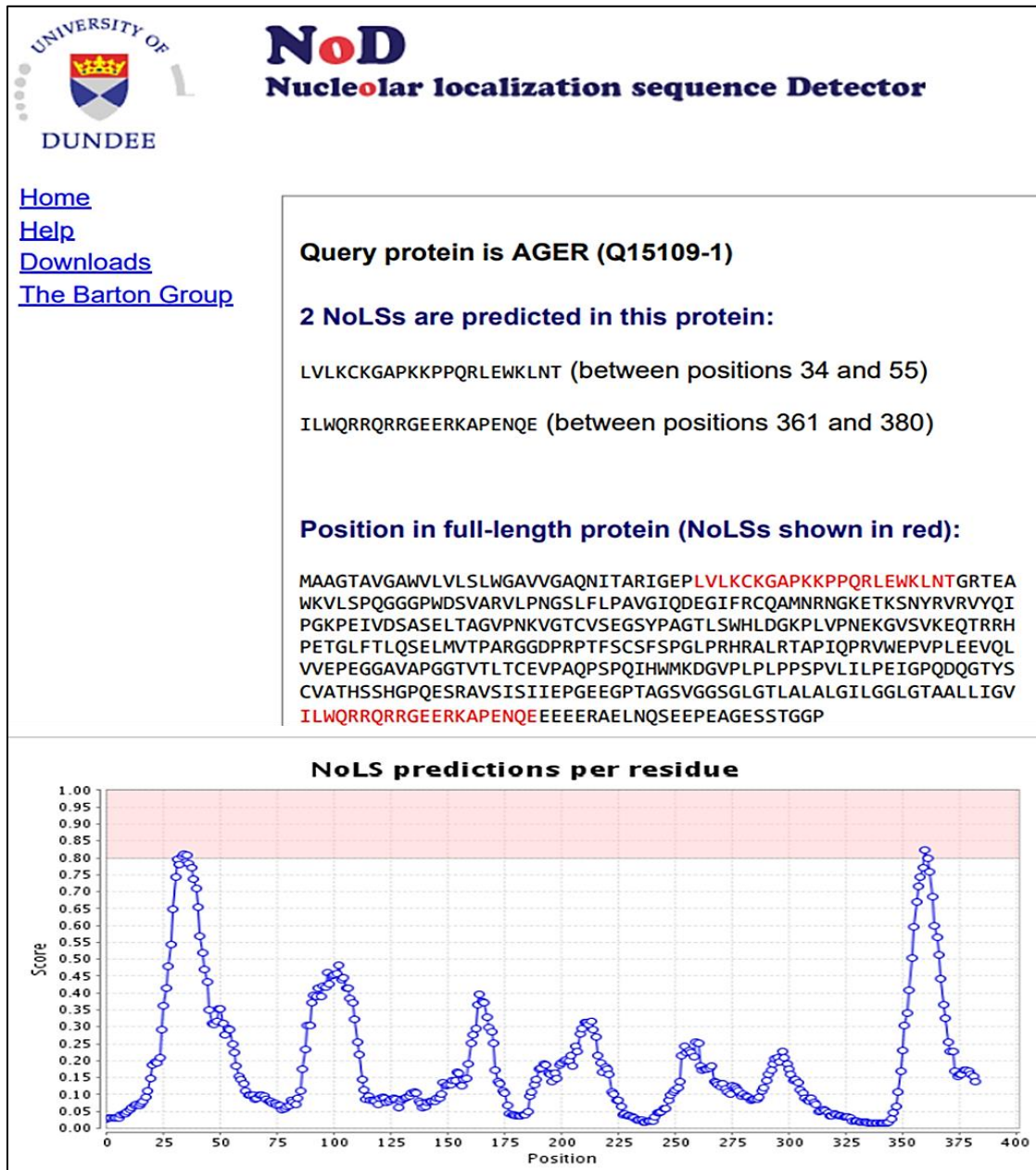


Figure 4.9: Screenshot of the output window from the Nucleolar localization sequence Detector (NoD) online software.

The software predicted two nucleolar localization signals in the RAGE protein sequence, one in the V domain and the other in the intracellular cytoplasmic domain. The plot below shows the prediction scores for each protein residue (276).

Discussion

The data from our image studies provide strong evidence for intramembrane proteolysis of RAGE. Our results indicate that the fluorescent protein labeled RAGE mutants behaved like the native RAGE with predominant cell membrane localization. In response to stimulation with ribose glycosylated BSA, RAGE was internalized in the case of FL-RAGE. RAGE-ICD is localized in the nucleus even without ligand stimulation. Earlier studies on RAGE showed that ectodomain shedding occurs in the juxtamembrane region, which is the flexible region that links the C2 to the transmembrane region (196,230,269). The Western blot data from Chapter 3 indicated proteolytic cleavage in FL-RAGE, and our imaging studies on FL-RAGE-YFP showed that treatment with the RAGE ligand decreased membrane bound RAGE. Combining the results of these experiments suggests that RAGE is capable of constitutive and induced shedding.

Images from both FL-RAGE-YFP and EGFP-FL-RAGE-RFP transfected cells showed internalization of the receptor after 6 hours of treatment with ribose glycosylated BSA. This is in line with previous studies where the authors show RAGE internalization upon ligand binding (277,278). In FL-RAGE-YFP transfected cells, the internalized RAGE was translocated first to the cytoplasmic region and then to the nucleus. We showed that the internalized RAGE fragment belonged to the ICD region (Figure 4.3 & 4.5). Similar translocation was observed in CHO cells where expressing RAGE ICD also showed nuclear localization.

Several transmembrane receptors, including CAMs, were reported to undergo regulated intramembrane, and their ICD was found to have nuclear localization (251,252,260,262). Investigating the RAGE ICD sequence revealed the presence of a nuclear localization signal, which corresponded to the sequence RRQR of amino acid residues 365-368. The NLS of RAGE ICD resembled that of EpCAM ICD, with arginine being the start and end residues. EpCAM is a

transmembrane receptor, and upon intramembrane proteolysis, the liberated ICD was identified to form a multiprotein complex with Wnt signaling associated molecules before translocating into the nucleus. In the nucleus, EpCAM ICD was reported to regulate the expression of genes involved in oncogenic signaling (260). Our data suggest that further investigations are needed to understand how the RAGE-ICD is translocated into the nucleus. We also suspect the involvement of complex formation with other cytoplasmic proteins for nuclear translocation of the RAGE (279).

Upon identifying the intranuclear localization of the RAGE-ICD, we observed that this domain is concentrated in the nucleolus. The nucleolus is a prominent, non-membrane nuclear subcompartment and is primarily the site for ribosome biogenesis (280). The hallmarks of nucleolar stress are the p53 signaling pathway inducing apoptosis, autophagy, DNA damage, and senescence. Nucleolar stress is a common event in various neurological disorders and cancers (281,282). Studies from multiple groups suggest that RAGE is a central regulator of apoptosis and autophagy by modulating p53, mTOR, Beclin, NF- κ B signaling pathways (100,283,284). The result from our study suggests an alternative mechanism of RAGE signaling in which the ICD localization in the nucleolus might contribute to nucleolar stress signaling.

Conclusion

This chapter aimed to investigate ectodomain shedding in RAGE and monitor the changes in the membrane localized RAGE. Our data showed that FL-RAGE is capable of both constitutive and induced cleavage. On treating FL-RAGE with ribose BSA induced intramembrane proteolysis. The increased intracellular localization of the FL-RAGE was accompanied by decreased cell surface RAGE localization. The internalized RAGE fragment was determined to be the ICD and showed a time dependent localization into the nucleus. Our data suggest that the RAGE-ICD can function as an independent fragment and, when expressed as FL-RAGE by translocating to the

nucleus in the two different lines HEK 293 and CHO. The NLS in RAGE-ICD sequence was mapped to residues 365-368 (RRQR) using seqNLS which showed a similar residue arrangement as the ICD of EpCAM. The exact mechanism of how RAGE-ICD is translocated into the nucleus is still not clear. We believe that RAGE-ICD forms a complex with other protein/s, and this complex could mediate the shuttling into the nucleus. Upon characterizing the intranuclear localization, we also discovered that RAGE-ICD accumulated in the nucleolus. Overall, our study suggests a new mechanism of RAGE signaling through cleaved ICD. We suggest that the liberated RAGE-ICD forms a complex with other proteins and that this complex is then translocated to the nucleus and nucleolus of the cells (summarized in Figure 4.10).

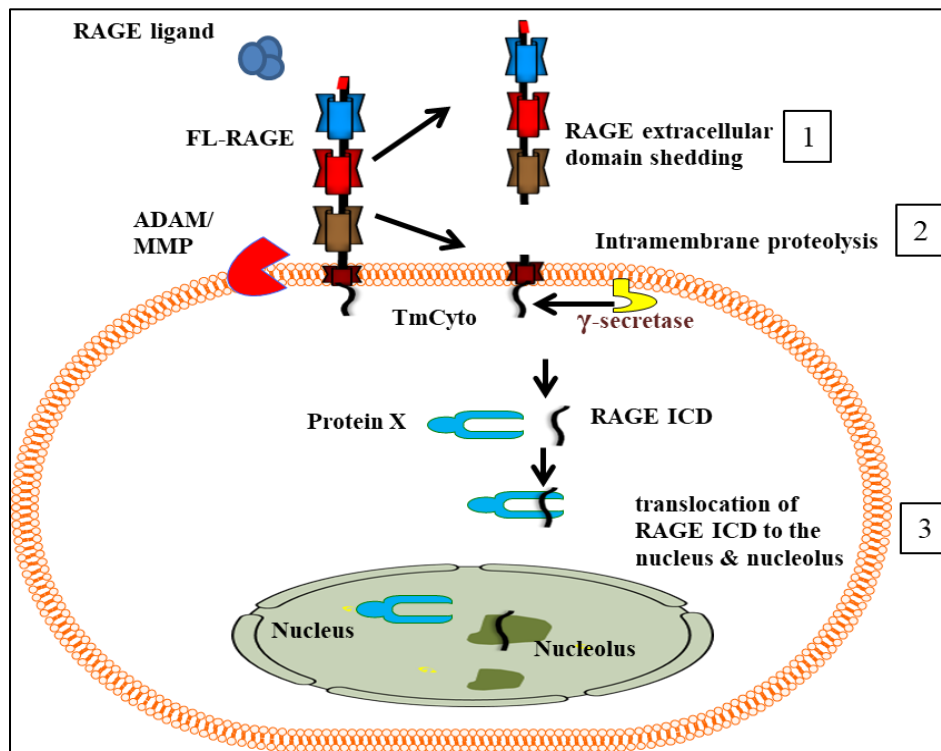


Figure 4.10: Proposed mechanism for nucleolar localization of RAGE through intramembrane proteolysis.

The extracellular domains of RAGE were cleaved by (1) ADAM10 or MMP9. The remaining membrane bound portion was proteolytically cleaved by (2) γ -secretase to liberate the ICD. The liberated ICD forms a complex with other proteins, and it is (3) translocated into the nucleus and nucleolus.

**CHAPTER 5. IDENTIFYING DIFFERENTIALLY EXPRESSED GENES AND
PROTEINS INVOLVED IN RAGE MEDIATED REGULATION OF CELL ADHESION
PROPERTIES**

Introduction

Increasing evidence shows the role of proteolytic cleavage in regulating the function of RAGE in both the extracellular and intracellular space (196,269). Lower levels of membrane bound RAGE were reported to promote myoblast differentiation via NF- κ B-dependent activation of MyoD (and myogenin) expression in aged human muscle satellite cells. However, this effect was not reversed when cells were forced to overexpress the DN-RAGE isoform. It suggests that the cleaved cytoplasmic region in RAGE is capable of signaling in these cells (285). A recent study on neuroinflammation in schizophrenia patients showed a direct involvement of RAGE shedding via matrix metalloproteinase 9 (MMP9) in promoting inflammatory responses through NF- κ B signaling (273). Expression of an ectodomain shedding resistant variant of RAGE was observed to impair RAGE ligand dependent cell signaling, actin cytoskeleton reorganization, and cell migration (196).

RAGE signaling utilizes different cellular pathways, including activation of MAPKs, PI3K/Akt, Rho GTPases, Jak/STAT, and Src family kinases (132,286). The AGE-RAGE axis has been well documented. AGE-RAGE signaling was reported to interfere with the adipogenesis process by modulating p53 function (287). AGE-RAGE interactions were also reported to generate a specific NF- κ B RelA “barcode” that regulates ECM turnover (243,288).

With the data from published studies and the results from our cell adhesion and spreading assays, we hypothesize that arginine-glycine-aspartic acid (RGD) and collagen receptors could be involved. The RGD receptors recognize the tripeptide sequence in their adhesion protein ligands,

and they are the cell attachment site for many adhesive ECM (fibronectin, vitronectin, and laminin) and cell surface proteins. Nearly half of the integrins receptors are categorized as RGD receptors (289). Similarly, diverse families of receptors, including integrins, immunoglobulin-like receptors, and receptor tyrosine kinases, bind to collagen (290). We hypothesized that RAGE could contribute to changes in the expression of adhesion-relevant surface proteins to mediate cell adhesion, as our data confirmed RAGE is not directly involved in mediating cell adhesion. To test our hypothesis, we utilized qPCR and proteomics to determine changes in the expression of adhesion relevant genes in WT and RAGE HEK 293 cells. We also tested if RAGE is responsible for regulating these changes in these cells by silencing RAGE.

Screening of RAGE regulated transcription of adhesion relevant genes

Experimental design

Gene expression analysis using qPCR

RNA extraction, cDNA synthesis, and qPCR reaction were performed as described under methods in Chapter 2. The changes in the transcription levels of cell adhesion molecules between WT HEK 293 and RAGE HEK 293 were determined using a normalizer/reference gene. A normalizer/reference gene was necessary to correct fluctuations due to technical variations, RNA quality, and reverse transcription efficiency between samples (291-293). For the initial screening, a list of 15 commonly used housekeeping genes (HKGs) (292) was selected to determine the expression pattern in WT HEK 293 and RAGE HEK 293 (appendix C). The melting curves were recorded for each HKG, and an agarose gel was run using the qPCR products to determine the quality of the amplified products and the amplification specificity. Using the Minitab software, a linear regression model with a 95% confidence interval (CI) was employed to compare mean Ct values of HKG from WT HEK 293 and RAGE HEK 293 samples to identify the stable ones for

the analysis. A list of 67 candidate genes of interest was selected based on literature studies. These genes were reported to have a role in cell adhesion (appendix D) (21,25,82,294-296). The fold change for these cell adhesion molecules in RAGE HEK 293 and WT HEK 293 was calculated as described in chapter 2. Here the $\Delta\Delta\text{Ct}$ calculated from all the selected HKG from the linear regression model were averaged for the fold change calculation.

Results

Validation using the linear regression model identified 7 housekeeping genes as stable candidate reference genes

Plotting the mean Ct values of 15 HKGs from WT HEK 293 and RAGE HEK 293 cells (Table 5.1) as a scatter plot showed linear correlation. Expression stability of the candidate HKGs in WT HEK 293 and RAGE HEK 293 cells using linear regression analysis with a 95% confidence interval gave a R^2 value of 70% (Figure 5.1.). R^2 value indicates how well the regression model fits a given dataset. A list of 7 housekeeping genes whose mean Ct fell within the 95% confidence interval from regression analysis was selected. These genes include ACTB, GAPDH, HSP90B1 – V2, LDHA, PGK1, RPLPO, and RPS18. Other 8 HKGs (B2M, GUSB, HPRT1, HSP90AB1, HSP90B1 – V1, HSP90B1 – V3, RPL13A, and PPIA) were excluded from the analysis.

Table 5.1: Ct values of housekeeping genes (HKGs) in WT HEK 293 and RAGE HEK 293 cells expressed as mean±SEM (n=3).

Gene (Gene ID)	WT HEK 293 Ct values	RAGE HEK 293 Ct values
ACTB (NM-001101)	21.60±0.57	22.85±0.49
B2M (NM_004048)	20.45±0.07	22.80±0.42
GAPDH (NM_008084)	19.05±0.07	19.35±0.07
GUSB (NM_000181)	22.05±0.99	22.15±0.21
HPRT1 (NM_000194)	21.30±0.14	23.70±0.85
HSP90AB1 (NM_007355)	20.05±0.21	21.40±0.14
HSP90B1 – V1 (NM_003299.3)	19.25±0.07	21.05±0.07
HSP90B1 – V2 (NM_003299.3)	19.90±0.14	19.75±0.14
HSP90B1 – V3 (NM_003299.3)	19.90±0.14	19.70±0.14
LDHA (NM_005566)	22.20±0.21	21.70±0.21
PGK1 (NM_000291)	20.50±0.35	20.95±0.07
PPIA (NM_021130)	22.20±0.07	22.00±0.00
RPL13A (NM_012423)	20.26±0.34	22.00±0.34
RPLP0 (NM_001002)	19.15±0.07	19.70±0.28
RPS18 (NM_022551)	17.55±0.07	17.40±0.57

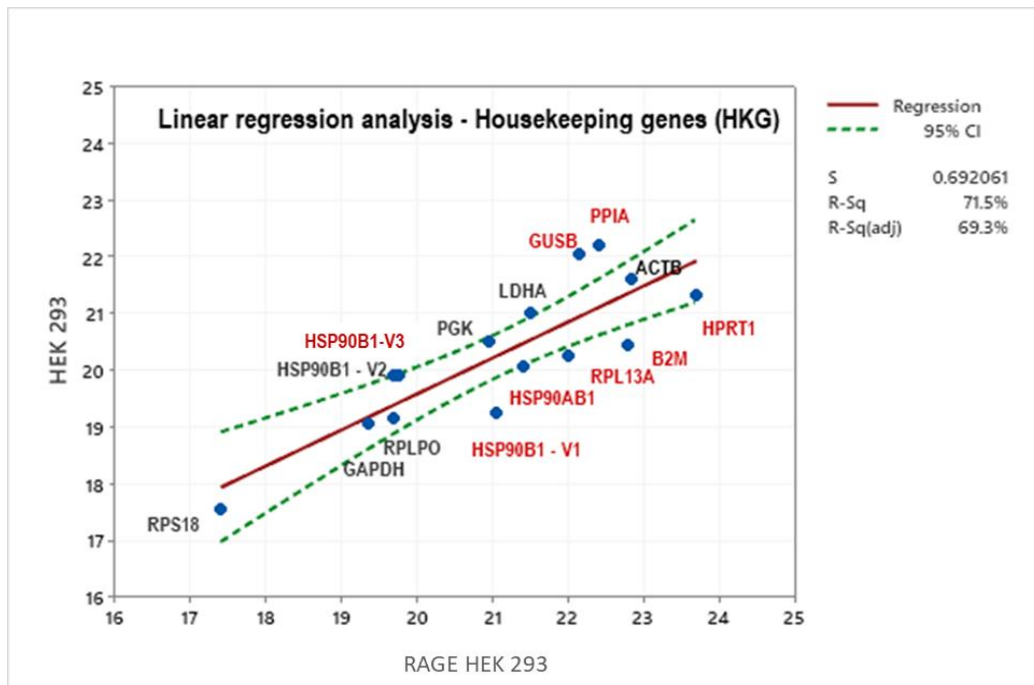


Figure 5.1: Expression correlation plot with the mean Ct values of the 15 housekeeping genes from WT HEK 293 and RAGE HEK 293 cells.

The plot was generated in Minitab using linear regression analysis at a 95% confidence interval and identified 7 HKG (ACTB, GAPDH, HSP90B1 – V2, LDHA, PGK1, RPLP0, and RPS18) labeled in black as stable candidate reference genes. Other tested HKG labeled in red were excluded from the analysis as they failed to fit in the linear regression model and not categorized as stable genes.

qPCR analysis showed selective regulation of cell adhesion molecule (CAM) gene expression in RAGE HEK 293 cells

The qPCR analysis of 67 genes mediating cell-cell and cell-extracellular matrix in WT HEK 293 and RAGE HEK 293 cells showed large variations in gene transcript levels, and the mean Ct values ranged from 21 to 33 (Table 5.2). In these experiments, relative expression of RAGE was used as an internal control. The average Ct value of RAGE in WT HEK 293 was 28.1 ± 1.8 compared to RAGE HEK 293, which was 19.0 ± 1.4 and corresponded to a 500 fold increase fold of RAGE in these cells. The CD36 gene had the maximum Ct in both WT (36.4 ± 1.7) and in RAGE HEK 293 (37.1 ± 1.5) cells, indicating low transcription levels in both these cell types.

Interestingly, a list of few candidate genes, integrin alpha 8 (ITGA8), contactin 1 (CNTN1), melanoma cell adhesion molecule (MCAM & MUC18), fibronectin1 (FN1), and thrombospondin-1 (THBS1) were found to be differentially expressed between WT HEK 293 and RAGE HEK 293 cells. ITGA8 and CNTN1 showed 4.6 ± 0.8 and 3.1 ± 0.7 increased expression in RAGE HEK 293 cells, and the changes were statistically significant (Figure 5.2). In striking contrast, the MCAM & MUC18, FN1, and THBS1 genes were found to be downregulated in RAGE HEK 293 compared to WT HEK 293 cells. The changes in transcription for these genes were MCAM 0.089 ± 0.02 ; MUC18 0.117 ± 0.5 ; FN1 0.45 ± 1.3 ; THBS1 0.064 ± 1.1 (Figure 5.3). Western blot analysis was performed in parallel for the ITAG8 and CNTN1 genes to confirm that the effect observed at the gene level represented their protein levels. It was observed that ITGA8 and CNTN1 showed increased expression at the protein levels by 8.0 and 5.2 fold, respectively (Figure 5.4). The Ct values of other genes belonging to different classes of cell adhesion molecules such as integrins, the cluster of differentiation (CD) receptors, and the IgG receptor superfamily showed no significant changes in the expression between WT HEK 293 and RAGE HEK 293 cells. The fold

change in the expression of these genes between HEK 293 and HEK 293 RAGE varied by a factor of 1 ± 0.5 .

Table 5.2: C_t values of genes mediating cell adhesion in WT HEK 293 and RAGE HEK 293 cells expressed as mean \pm SEM (n=3).

	Gene (Gene ID)	WT HEK 293 C_t values	RAGE HEK 293 C_t values
1	ADAMTS13 (NM_139026)	28.5 \pm 1.0	27.9 \pm 0.9
2	ALCAM (NM_001243281)	24.7 \pm 1.5	24.7 \pm 1.0
3	CD133 (NM_001145847)	30.5 \pm 0.6	29.3 \pm 0.7
4	CD24 (NM_013230)	25.6 \pm 0.9	27.2 \pm 0.8
5	CD36 (NM_001001548)	36.4 \pm 1.7	37.1 \pm 1.5
6	CD44 (NM_000610)	30.1 \pm 1.6	30.2 \pm 0.5
7	CDH1 (NM_004360)	28.1 \pm 2.0	27.7 \pm 0.5
8	CDH2 (NM_021248)	32.6 \pm 2.6	32.3 \pm 0.6
9	CDH12 (NM_004061)	31.1 \pm 2.0	30.8 \pm 0.5
10	CNTN1 (NM_175038)	29.7 \pm 0.4	26.7 \pm 0.8
11	Cola1h (NM_005261180)	29.5 \pm 0.9	31.1 \pm 0.6
12	CTGF (NM_001901)	23.0 \pm 2.2	25.5 \pm 1.8
13	CTNNA1 (NM_004903)	22.1 \pm 1.4	22.6 \pm 0.8
14	CTNNB1 (NM_001098209)	25.3 \pm 3.9	24.1 \pm 2.4
15	CTNNB1 (NM_001098209)	26.7 \pm 1.8	28.0 \pm 3.5
16	CTNND1 (NM_001085467)	23.2 \pm 0.8	23.4 \pm 1.4
17	DDR1 (NM_001202523)	25.0 \pm 1.2	24.9 \pm 0.5
18	DDR2 (NM_001014796)	29.4 \pm 1.0	28.7 \pm 1.3
19	DESP/DSP (NM_004415)	23.4 \pm 1.9	24.0 \pm 0.9
20	ECAD (NM_004360)	27.2 \pm 1.2	27.8 \pm 0.8
21	EPCAM (NM_002354)	22.0 \pm 1.5	23.1 \pm 1.0
22	EZR (NM_003379)	22.6 \pm 1.0	23.4 \pm 0.8
23	FN1 (NM_212482)	22.7 \pm 0.8	25.3 \pm 0.5
24	HAS3 (NM_005329)	27.1 \pm 0.6	27.5 \pm 0.6
25	ICAM1 (NM_000201)	30.2 \pm 1.8	29.2 \pm 1.0
26	ITGA1 (NM_181501.1)	28.0 \pm 2.1	29.0 \pm 1.0
27	ITGA2 (NM_002203)	29.8 \pm 2.1	30.1 \pm 1.0
28	ITGA3 (NM_005501)	31.3 \pm 2.6	31.4 \pm 0.9
29	ITGA4 (NM_000885)	27.1 \pm 1.5	27.3 \pm 1.1
30	ITGA5 (NM_002205)	29.5 \pm 2.2	30.4 \pm 1.1
31	ITGA7 (NM_001144997)	26.1 \pm 0.9	26.2 \pm 0.6
32	ITGA8 (NM_0032638)	29.3 \pm 0.7	25.8 \pm 0.7
33	ITGA10 (NM_003637)	29.3 \pm 2.1	29.5 \pm 0.7
34	ITGA11 (NM_001004439)	25.4 \pm 1.9	26.4 \pm 2.5
35	ITGAL (NM_001114380)	30.8 \pm 2.7	30.5 \pm 1.0
36	ITGAM (NM_000632)	30.8 \pm 3.2	30.2 \pm 1.2
37	ITGAM (NM_001145808)	32.6 \pm 2.2	33.0 \pm 0.7
38	ITGAV (NM_001145000)	25.0 \pm 0.7	26.4 \pm 0.5
39	ITGB1 (NM_002211)	27.0 \pm 0.8	27.8 \pm 0.6
40	ITGB2 (NM_000211)	32.2 \pm 3.4	33.0 \pm 1.6

Table 5.2: C_t values of genes mediating cell adhesion in WT HEK 293 and RAGE HEK 293 cells expressed as mean \pm SEM (n=3) (continued).

	Gene (Gene ID)	WT HEK 293 C_t values	RAGE HEK 293 C_t values
41	ITGB2 (NM_000211)	31.5 \pm 1.0	31.3 \pm 2.7
42	ITGB3 (NM_000212)	26.4 \pm 0.9	27.8 \pm 0.5
43	ITGB4 (NM_001005619)	25.9 \pm 1.4	26.4 \pm 0.8
44	ITGB5 (NM_002213)	25.4 \pm 0.8	25.7 \pm 0.6
45	MCAM (NM_006500)	26.9 \pm 1.1	29.5 \pm 0.7
46	MPZL1 (NM_001146191)	23.5 \pm 1.3	24.0 \pm 0.9
47	MSN (NM_002444)	23.4 \pm 0.7	23.4 \pm 0.4
48	MUC18 (NM_006500)	26.4 \pm 1.6	29.2 \pm 1.2
49	NCAM1 (NM_001076682)	27.8 \pm 4.2	28.7 \pm 4.0
50	NPTN (NM_017455)	22.9 \pm 1.3	23.5 \pm 1.0
51	PCDHA3 (NM_031497)	31.9 \pm 2.8	31.2 \pm 1.1
52	PECAM1 (NM_000442)	26.3 \pm 1.1	27.0 \pm 1.3
53	PLXB2 (NM_012401)	27.6 \pm 1.9	27.4 \pm 0.5
54	PNN (NM_002687.3)	25.3 \pm 0.3	26.0 \pm 1.7
55	RAGE (NM_001136)	28.1 \pm 1.8	19.0 \pm 1.4
56	RDX (NM_002906)	21.5 \pm 0.6	22.5 \pm 0.4
57	SELE (NM_000450)	29.2 \pm 2.7	28.3 \pm 1.0
58	SELL (NM_000655)	29.8 \pm 2.4	29.7 \pm 1.0
59	SELP (NM_003005)	29.7 \pm 3.6	29.4 \pm 1.7
60	SGCE (NM_001099400)	27.1 \pm 4.0	26.5 \pm 3.1
61	THBS1 (NM_003246)	25.4 \pm 0.8	28.9 \pm 0.5
62	THBS2 (NM_003247)	28.8 \pm 1.9	28.4 \pm 0.7
63	THBS3 (NM_001252607)	29.9 \pm 1.1	28.8 \pm 0.6
64	VCAM1 (NM_001078)	30.0 \pm 1.7	29.3 \pm 0.8
65	VCAN (NM_004385)	25.0 \pm 0.5	24.9 \pm 0.6
66	VIM (NM_003380)	24.3 \pm 1.2	25.2 \pm 0.5
67	VTN (NM_000638)	27.0 \pm 1.5	26.2 \pm 1.1

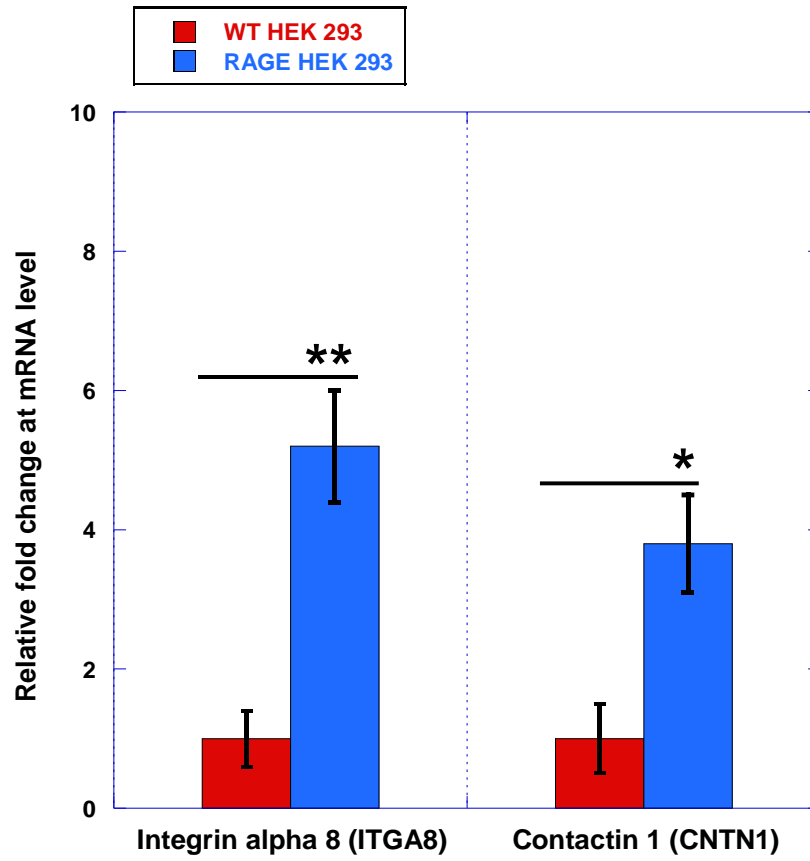


Figure 5.2: Gene expression of integrin alpha 8 (ITGA8) and contactin 1 (CNTN 1) in WT HEK 293 and RAGE HEK 293 cells.

The plot represents the average fold change from 3 independent experiments (n=3) where ** P<0.01, * P<0.05.

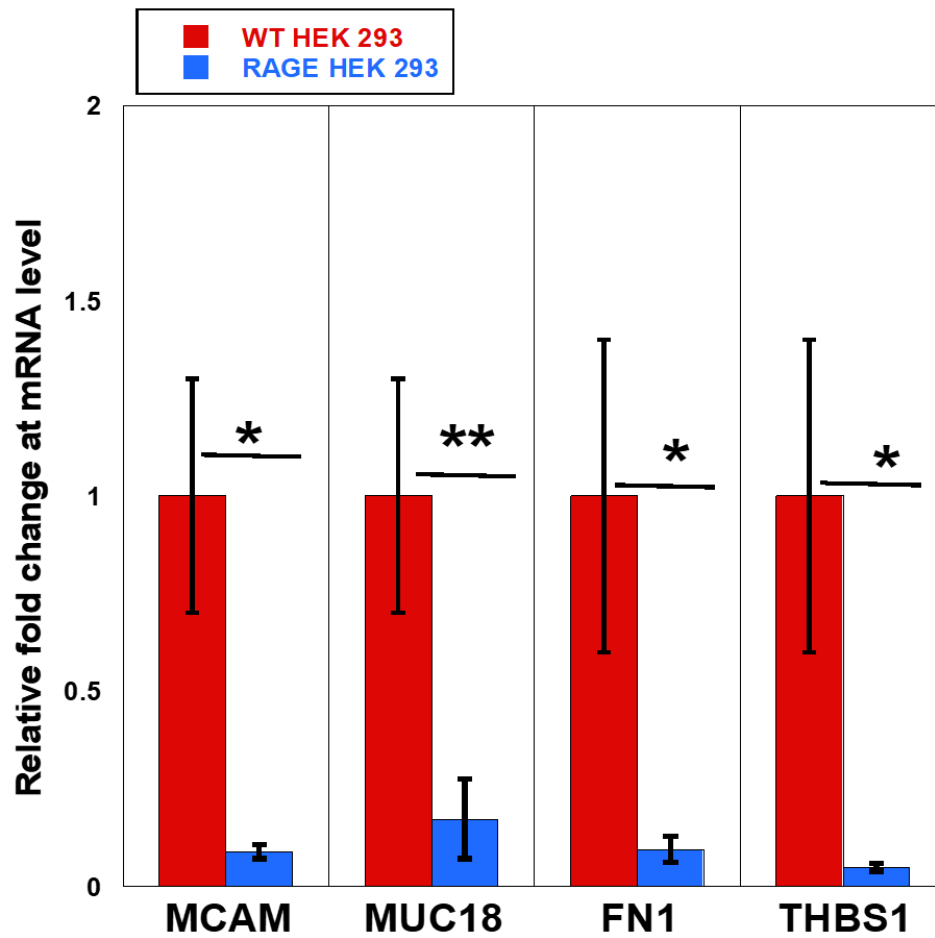


Figure 5.3: Change in the gene expression of melanoma cell adhesion molecules – (MCAM & MUC18) (left), fibronectin 1 (FN1), and thrombospondin-1 (THBS1) between WT HEK 293 and RAGE HEK 293 cells. The plot represents the average fold change from 3 independent experiments (n=3) where ** P<0.01, * P<0.05.

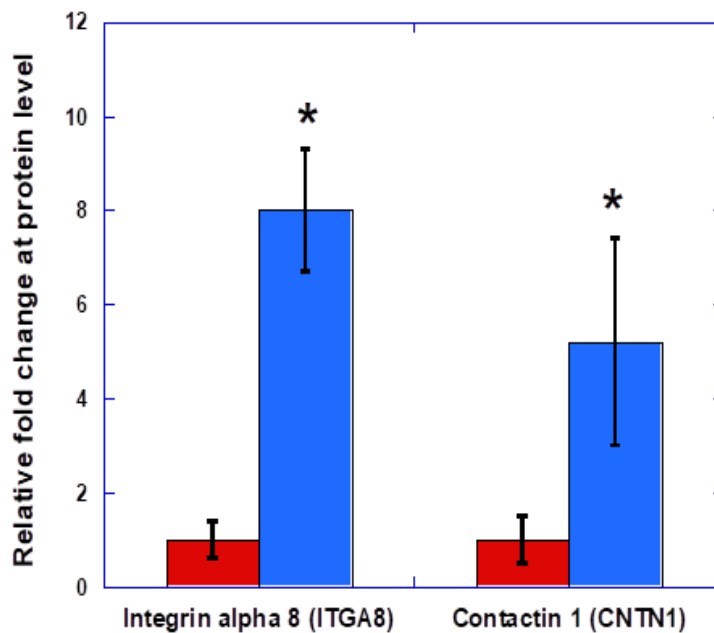
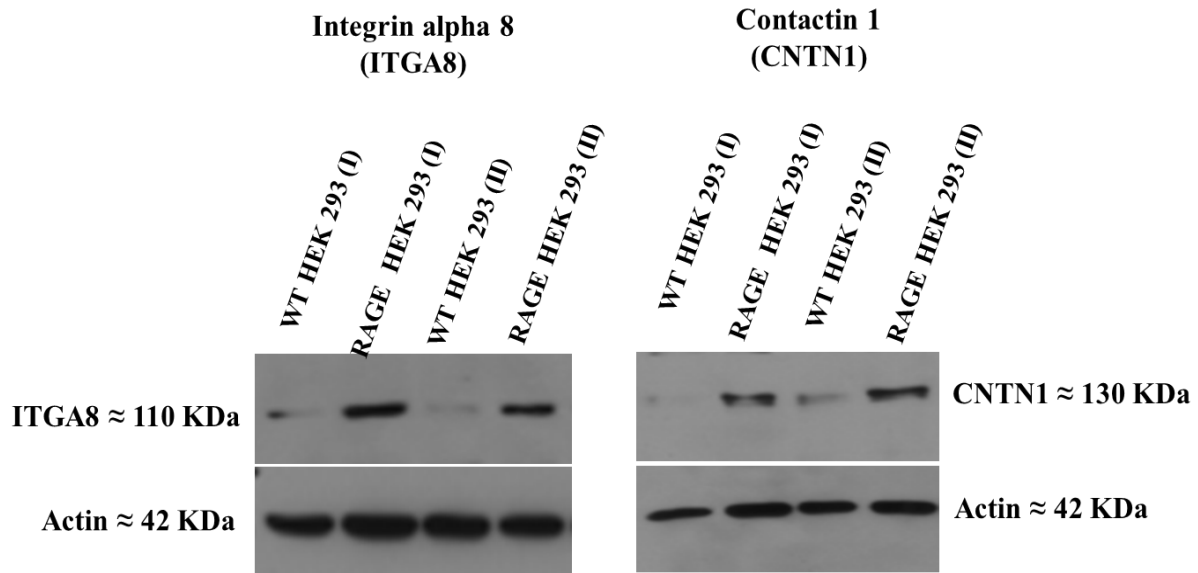


Figure 5.4: Western blot against ITGA8 and CNTN1 in WT HEK 293 and RAGE HEK 293 cells. The plot shows the relative quantification of the ITGA8 and CNTN1 expression from 2 (n=2) independent experiments where, * P<0.05. Expression of ITGA8 and CNTN1 were detected using human ITGA8 antibody (MAB6194) and human CNTN1 antibody (AF904). Actin was used as the loading control.

Discussion

Our results showed that RAGE expression in HEK 293 cells modulated the transcription levels of specific CAM genes. Out of 67 tested adhesion relevant genes, 6 were found to be significantly regulated in RAGE HEK 293 cells compared to WT HEK 293. RAGE HEK 293 samples exhibited increased expression of integrin alpha 8 (ITGA8) and contactin1 (CNTN1) at both mRNA and protein levels. Both genes were reported to have important roles in mediating cell-cell and cell-extracellular matrix adhesion (297-300). ITGA8 is expressed in epithelial and mesenchymal cells and forms a functional heterodimer by associating with integrin beta 1 (ITGB1). ITGB1 and ITGA8 heterodimer was reported to bind to the RGD sites of extracellular matrix molecules such as fibronectin and vitronectin (301-305). However, the data from our qPCR analysis showed no increase in the transcription for ITGB1 in RAGE HEK 293 samples.

CNTN1 belongs to neural adhesion molecule of the immunoglobulin (Ig) superfamily and is highly expressed in neuronal tissues. CNTN1 associates with other cell surface proteins like tenascin-C, tenascin-R, and receptor protein tyrosine phosphatase β (RPTP β) to initiate signaling as it lacks a functional intracellular domain. CNTN1 binding to ECM has been reported to promote axonal growth and neurite adhesion (306). RAGE expression in neuronal cells was also reported to influence axonal growth by binding to its ligands S100B and HMGB1 through the NF- κ B axis (307,308). Additionally, our findings suggest that RAGE may signal axonal growth via CNTN1. Deregulation of both ITGA8 and CNTN1 was reported to play an important role in cancer EMT transition and in cancer cell metastasis by altering the gene expression of EMT associated markers such as Snail, E-cadherin, and N-cadherin (309-311). Interestingly, RAGE was also reported to induce EMT transition, and the results from our data suggest that RAGE may cross talk with ITGA8 and CNTN1 to modulate oncogenic signaling (165,312).

We also observed decreased gene expression in melanoma cell adhesion molecule (MUC18/MCAM), fibronectin1 (FN1), and thrombospondin-1 (THBS1) in RAGE HEK 293 cells. Until now, no study has shown the direct relation of the expression of these genes in the context of RAGE signaling. Few studies reported that RAGE shared structural homology with MCAM/MUC1. Furthermore, RAGE and MCAM have also been reported to bind to S100A8/A9 protein heterodimers to mediate signaling in malignant melanoma (57,207). FN1 and THBS1 have been reported to have an important role in tissue repair and wound healing response (313,314). Our data suggest that RAGE expression could modulate the function of these genes. Overall, our qPCR analysis showed increased expression of ITGA8 and CNTN 1 with simultaneous downregulation of MUC18/MCAM, FN1, and THBS1 genes. The changes in protein expression levels of ITGA8 and CNTN1 in RAGE HEK 293 cells corresponded to the changes observed at the transcriptional level.

A proteomics approach to identify adhesion relevant cell surface protein regulated by RAGE

Experimental design

Cell surface proteomics

Cell surface proteomics is a powerful technique to characterize the entire surface proteome using effective labeling strategies. Recent studies on comprehensive surface proteome analysis reported a drastic change in the expression and abundance of cell surface proteins in various disease models compared to healthy controls (315-317).

For this study, we employed a cell surface biotin labeling procedure using two commercially available biotin reagents, EZ-Link Sulfo-NHS-LC-LC-Biotin, and aminoxy biotin. EZ-Link Sulfo-NHS-LC-Biotin reagent labels the primary amines of exposed surface proteins,

whereas aminoxy biotin covalently attaches biotin to aldehyde or ketone groups of glycosylated surface proteins. From initial screening experiments, we found that aminoxy biotin showed less cytoplasmic protein contamination and was chosen for further experiments. The labeling, enrichment, and sample processing for MS were performed as described in Chapter 2 under cell surface proteomics (Figure 5.5). Various factors affect the labeling procedure for surface proteomics, such as the number of cells, concentration of biotin used, biotinylation and quenching reaction time, enrichment of the labeled surface proteins, and trypsin digestion. Therefore, we optimized every step of the sample preparation process by performing appropriate control experiments.

The MS-sample run and peptide data analysis from the MS spectra was performed by Dr. Golovko (Associate Professor, Director of Mass Spectrometry Core Facility, University of North Dakota, ND, USA). A screening strategy was employed for the MS data sets by manually entering identified proteins in UniProt knowledgebase and sorting adhesion relevant surface proteins found in WT HEK 293 and RAGE HEK 293 cells. After the initial sorting, the proteins identified at least in two of the three experiments in data sets of the samples were considered for analysis. Proteins that were identified only in a single experiment data set were excluded from the analysis. Next, the common proteins in both WT HEK 293 and RAGE HEK 293 were normalized using Na, K-ATPase alpha 1 subunit (ATP1A1) (uniport entry: P05023), a prominent cell surface protein marker (226), and a loading control in our experiment. Proteins identified only in WT HEK 293, and RAGE HEK 293 were reported separately.

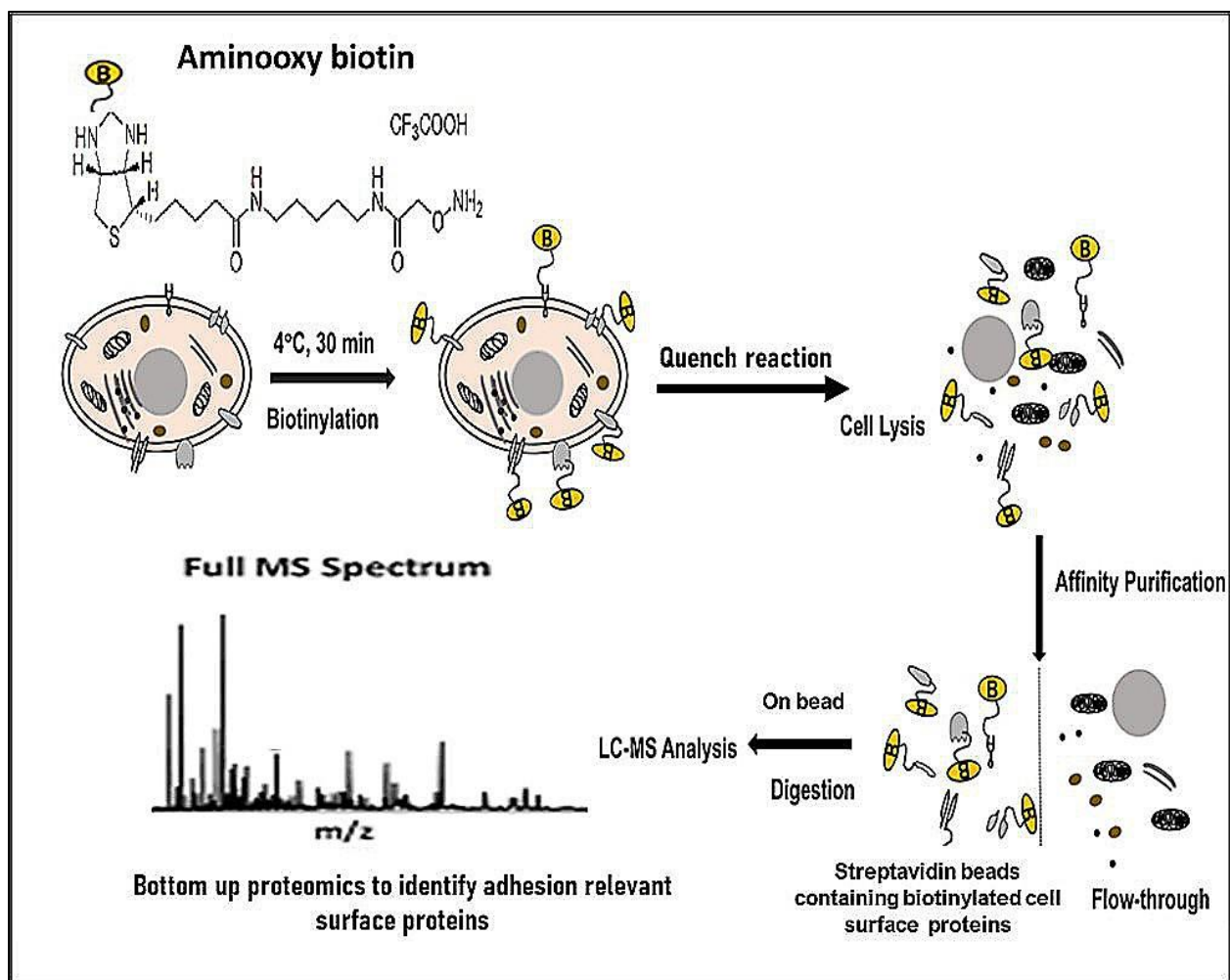


Figure 5.5: Schematic illustration of sample preparation and processing for cell surface proteomics.

The cells were biotinylated using aminoxy biotin, which selectively labels the cell surface proteins. This was followed by quenching the biotinylation reaction using 0.1% ethylene glycol, lysing of cells, and enrichment and affinity purification of the biotinylated sample using streptavidin beads overnight. Trypsin was used for on-bead digestion (18-20hrs at 37 °C), and sample fractions were collected. A bottom-up proteomics strategy was employed to identify the adhesion relevant surface proteins between WT HEK 293 and RAGE HEK 293 cells. Modified from (315).

Results

Validation of cell surface protein labeling, enrichment, and digestion

For the initial analysis, we compared two biotin reagents based on their ability to selectively label membrane proteins. This was determined using Western blot against a well-known cytoplasmic marker GAPDH (Cell Signaling Technology #5174). Biotinylated sample

from EZ-Link Sulfo-NHS-LC-Biotin labeling showed increased GAPDH presence compared to aminoxy biotin (appendix figure A10). The results from this data prompted us to proceed with aminoxy biotin for our future experiments. We further determined the optimized conditions for surface protein labeling of aminoxy biotin using its fluorescent analog compound, aminoxy TAMRA. First, the surface labeling specificity was verified using confocal imaging and was observed to be on the cell surface. We then determined that a total of 8 wash steps were required to remove excess labeling reagent from the reaction by measuring the fluorescence from the supernatant of the wash fractions at 540 nm (excitation) and 560 nm (emission).

Aminoxy biotin labeling was performed in cells using these optimized conditions. Following labeling and lysing of cells, the protein fractions from the total, membrane, and cytoplasmic proteins were tested by Western blot using a streptavidin-conjugated HRP antibody. It is done to detect the presence of biotinylated proteins in all these fractions. Biotin binds strongly to streptavidin, and their abundance would correspond to the signal in these protein fractions from the Western blot. From the Western blot data, we observed only the total, and the membrane protein fractions showed strong signals. No signal was observed in the cytoplasmic fraction of the proteins. The success of trypsin digestion in samples was checked by silver nitrate staining of digested and undigested samples. The staining showed bands present only in the undigested sample. A band around 25 kDa was observed in the digested sample, which corresponded to excess trypsin from the digestion reaction (Figure 5.6).

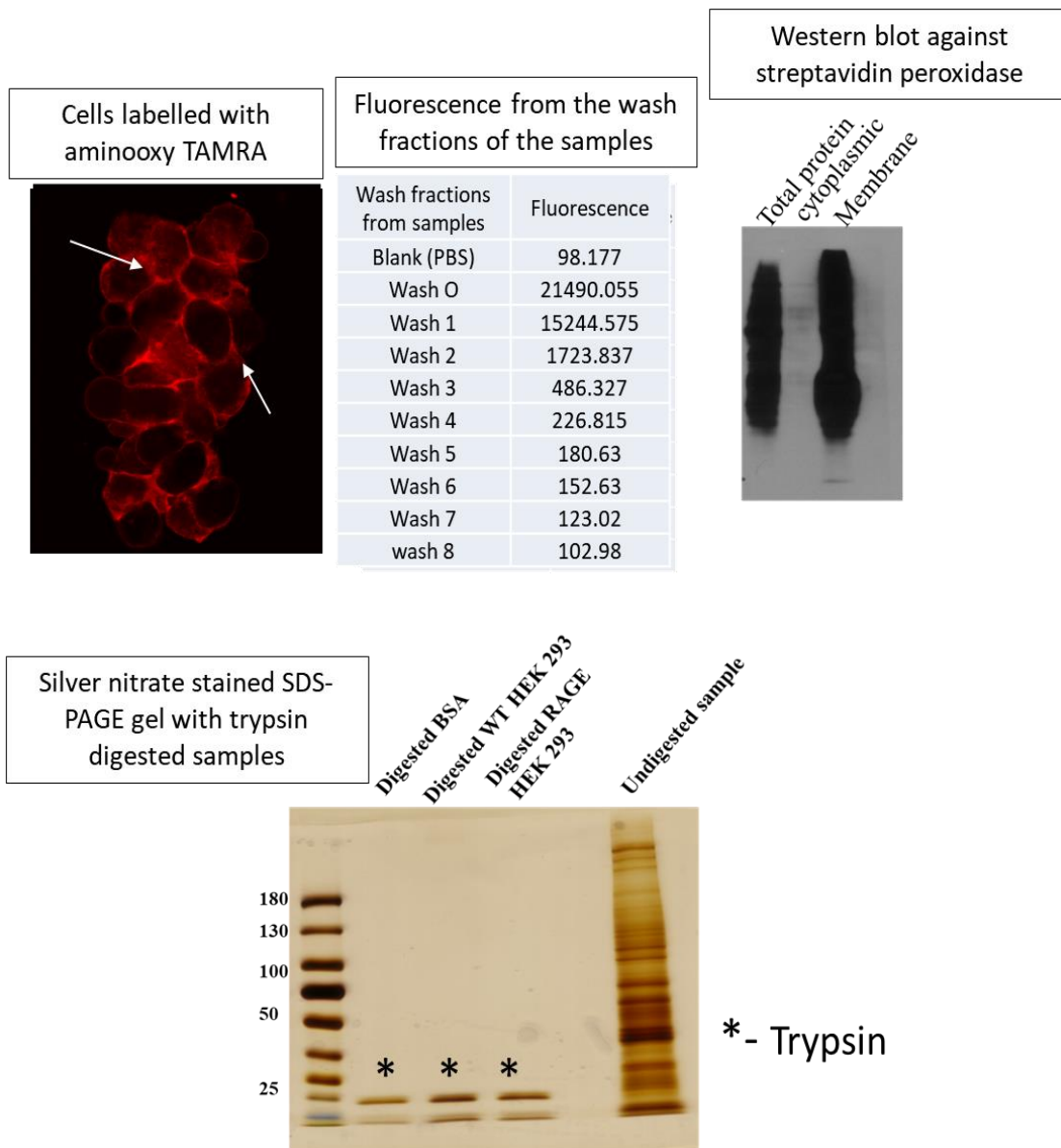


Figure 5.6: Results from optimization of cell surface protein labeling for proteomics experiment. From top left: confocal microscopy image of aminooxy TAMRA labeled cells shows selective surface labeling indicated by arrows. Fluorescence measurement from the wash fractions was evaluated to determine the number of washes required to remove free aminooxy TAMRA left in the sample after labeling. Western blot against HRP streptavidin in total, cytoplasmic, membrane protein fractions of aminooxy biotin labeled samples. Bottom center: Protein gel with digested and undigested samples. The band in the digested samples is identified as free trypsin left after the digestion.

RAGE HEK 293 cells showed altered expression of adhesion relevant proteins

Data analysis from all 3 independent experiments showed that almost 50% of the adhesion relevant proteins were found in both WT and RAGE HEK 293 cells. It was also noticed that RAGE expression in HEK 293 cells increased the expression of selective adhesion relevant proteins that were found to be absent in WT HEK 293 cells. Comparing the results within individual sample sets showed that 29 proteins were identified from all 3 experiments in RAGE HEK 293 and 24 proteins in WT HEK 293 samples (appendix figure A12).

From the total list of identified proteins in 3 independent experiments, 12 proteins were found in both WT and RAGE HEK 293 cells. These proteins include neural cell adhesion molecule (NCAM), cell adhesion molecule 1 (CAM1), basigin (BSG), dystroglycan (DAG1), integrin alpha 5 (ITGA5), integrin beta 1 (ITGB1), activated leukocyte cell adhesion molecule (ALCAM/CD166), leukocyte surface antigen CD47 (CD 47), integrin alpha 2 (ITGA2), plexin-B2 (PLXB2), cadherin-2 (CADH2), and integrin alpha 1 (ITGA1). Of these proteins, cadherin-2 showed no change in expression, and plexin-B2 was downregulated by half fold (0.5 ± 0.2) in RAGE HEK 293. The remaining proteins were upregulated in RAGE HEK 293, and of these proteins, NCAM, dystroglycan, ITGA2, and ITGA1 showed fold changes greater than 3.5 ± 0.7 that were statistically significant. Adhesion proteins CAM1, basigin, ITGA5, ITGB1, CD166, and CD 47 had a slight increase in fold change in the range of 1.5-2.0 (Figure 5.7).

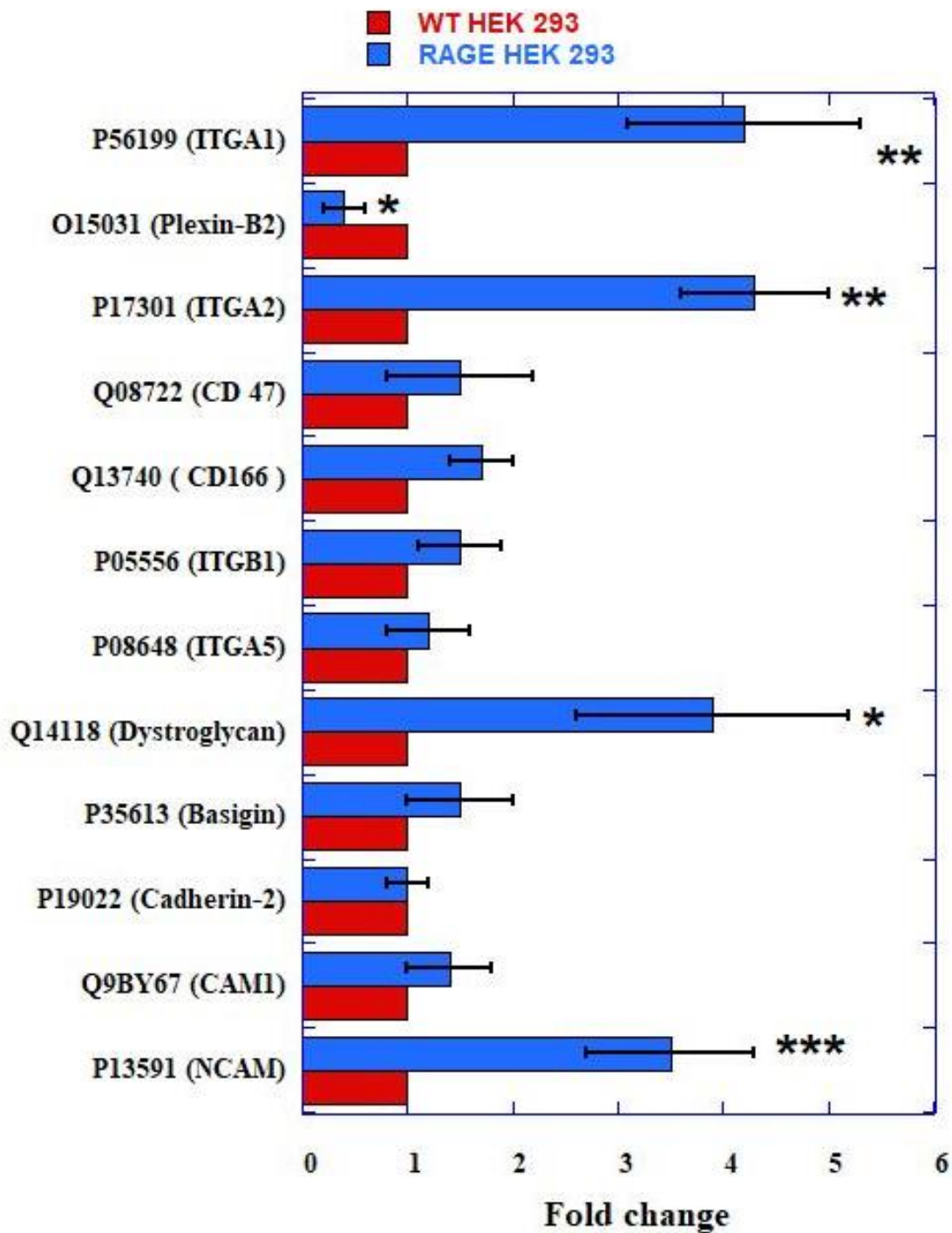


Figure 5.7: Differentially expressed adhesion relevant proteins in WT and RAGE HEK 293 cells identified by LC-MS-MS proteomics. The plot represents the normalized average fold change from 3 experiments (n=3) where *** P<0.001, ** P<0.01, * P<0.05.

Interestingly, in RAGE HEK 293 cells, a set of cell adhesion proteins were identified that were not found in WT HEK 293 cells; epidermal growth factor receptor (EGFR), CD44 antigen (CD44), ephrin-B1 (EFNB1); trophoblast glycoprotein (TPBG); podocalyxin-like protein 2 (PODXL2), neuroligin (NPTN), CD99 antigen (CD99), integrin alpha-8 (ITGA8), filamin-A (FLNA), integrin alpha-V (ITGAV), and inactive tyrosine-protein kinase 7 (PTK7). Also, it was noted that RAGE expression in HEK 293 completely abolished the expression of a set of proteins, including ephrin type-A receptor 2 (EPHA2), ephrin type-A receptor 3 (EPHA3), ephrin type-A receptor 8 (EPHA8), ephrin type-B receptor 1 (EPHB1), ephrin type-B receptor 3 (EPHB3), and ephrin type-B receptor 4 (EPHB4) (figure 5.8). Using the Panther classification system, the functional classification of these differentially expressed genes towards pathway analysis predicted the involvement of integrin mediated signaling pathways along with presenilin/ γ -secretase and inflammation pathways from cytokines. Overall results from our proteomics study suggest that RAGE expression in HEK 293 cells differentially regulates the expression of adhesion relevant surface proteins, as listed in figure 5.8.

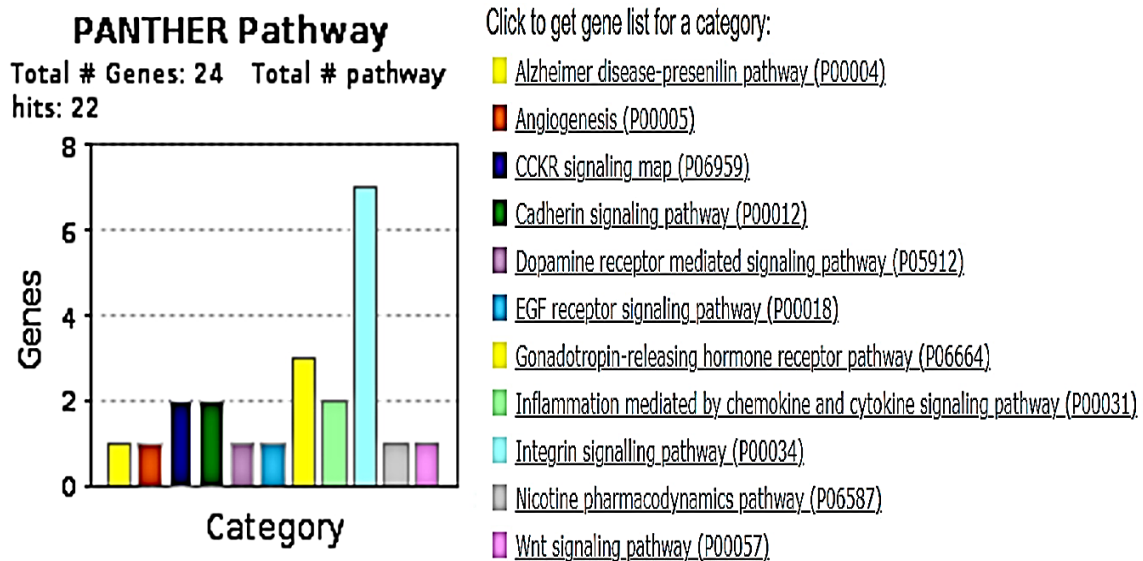
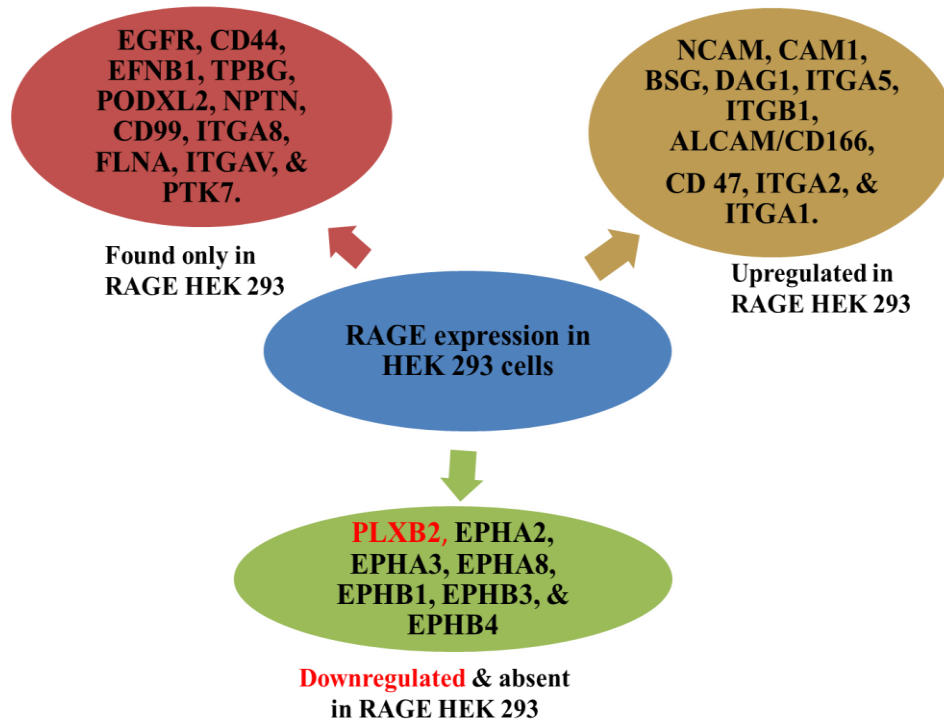


Figure 5.8: Differentially expressed adhesion proteins upon RAGE expression in HEK 293 cells by cell surface proteomics (top). Pathway analysis using the Panther classification system on the genes identified in RAGE HEK 293 cells (bottom).

Discussion

The results from cell surface proteomics showed that RAGE expression in HEK 293 cells regulates the expression of surface proteins which are suggested to have an important role in cell-cell and cell-matrix adhesion. Studies reported that there is an apparent interdependence in RAGE signaling and the cell surface proteins identified. For example, in addition to signaling to proinflammatory pathways, AGE-RAGE is also reported to mediate leukocyte recruitment via RAGE expression and binding to Mac-1, a leukocyte adhesion molecule (318,319). Furthermore, RAGE expression in HEK 293 significantly upregulated the expression of the following adhesion molecules; NCAM, ITGA2, DAG1, and ITGA1. However, our qPCR analysis for the same genes showed no significant upregulation in their transcriptional level compared to WT HEK 293. The plausible scientific explanation is that a gene's transcript level is not the only factor affecting protein levels. The expression level of proteins is also affected by their translation rates and degradation rates (320).

Consistent with the upregulation of adhesion relevant surface proteins, RAGE also induced expression of genes that were not found in WT HEK 293 cells. The data suggest that RAGE can modulate the translational levels of these genes, although their transcriptional levels remain constant. From the list of identified proteins in RAGE HEK 293 cells, only ITGA8 protein levels matched with its mRNA levels, and the result was also supported by Western blot analysis. Other identified proteins such as FLNA, CD44, NPTN were observed to have mRNA expression in the WT HEK 293 cells but were not found in the protein levels. To our surprise, we did not find CNTN1 from the proteomics data, although, from our Western blot analysis, we were able to identify its expression. A possible explanation could be the absence of surface localization as these proteins are reported to form complexes with other surface proteins such as Notch, which rapidly

undergoes RIP processing (321). In the vasculature, RAGE expression was reported to stimulate VCAM1 and ICAM1 expression. From our data, we did not find VCAM1 and ICAM1 at both transcript and protein levels in RAGE HEK 293 cells suggesting that RAGE regulation of these two CAMs is dependent on the tissue type (322). We expected to observe an increased expression of MUC18/MCAM, FN1, and THBS1 based on the result from our qPCR data in WT HEK 293 cells, but we could not identify these proteins in our proteomics study. However, WT HEK 293 cells were found to express high levels of ephrin type A and B receptors which were not found in RAGE HEK 293 cells. Overall, our data suggests that RAGE regulates the expression of cell surface adhesion receptors differently.

Effect of RAGE knockdown in cell adhesion and ITGA8 expression

Experimental design

Knockdown of RAGE using shRNA

Knockdown of RAGE was performed using shRNA plasmid targeted against RAGE (Genecopoeia, product# HSH094823-CU6). RAGE HEK 293 cells and MiaPaCa2 cells were transiently transfected as described in chapter 2 with some modifications. Cells were transfected for 72 hours and processed for RNA extraction for qPCR and protein extraction for Western blot analysis to determine the knockdown efficiency. Changes in cell adhesion to ECM coated surfaces (collagen IV, collagen I, and fibronectin) and ITGA8 expression was investigated upon RAGE knockdown in these cells. Scrambled shRNA was used as a control in this study (Genecopoeia, product# CSHCTR001-CU6).

Results

RAGE knockdown reduced cell adhesion, cell spreading to ECM, and downregulation of ITGA8

Out of the 3 RAGE shRNA plasmids tested, clone 'C' showed maximum knockdown efficiency and was used for subsequent experiments (appendix figure A12). Knockdown efficiency of 40% was observed at the transcript level and 54% at the translational level (Figure 5.9).

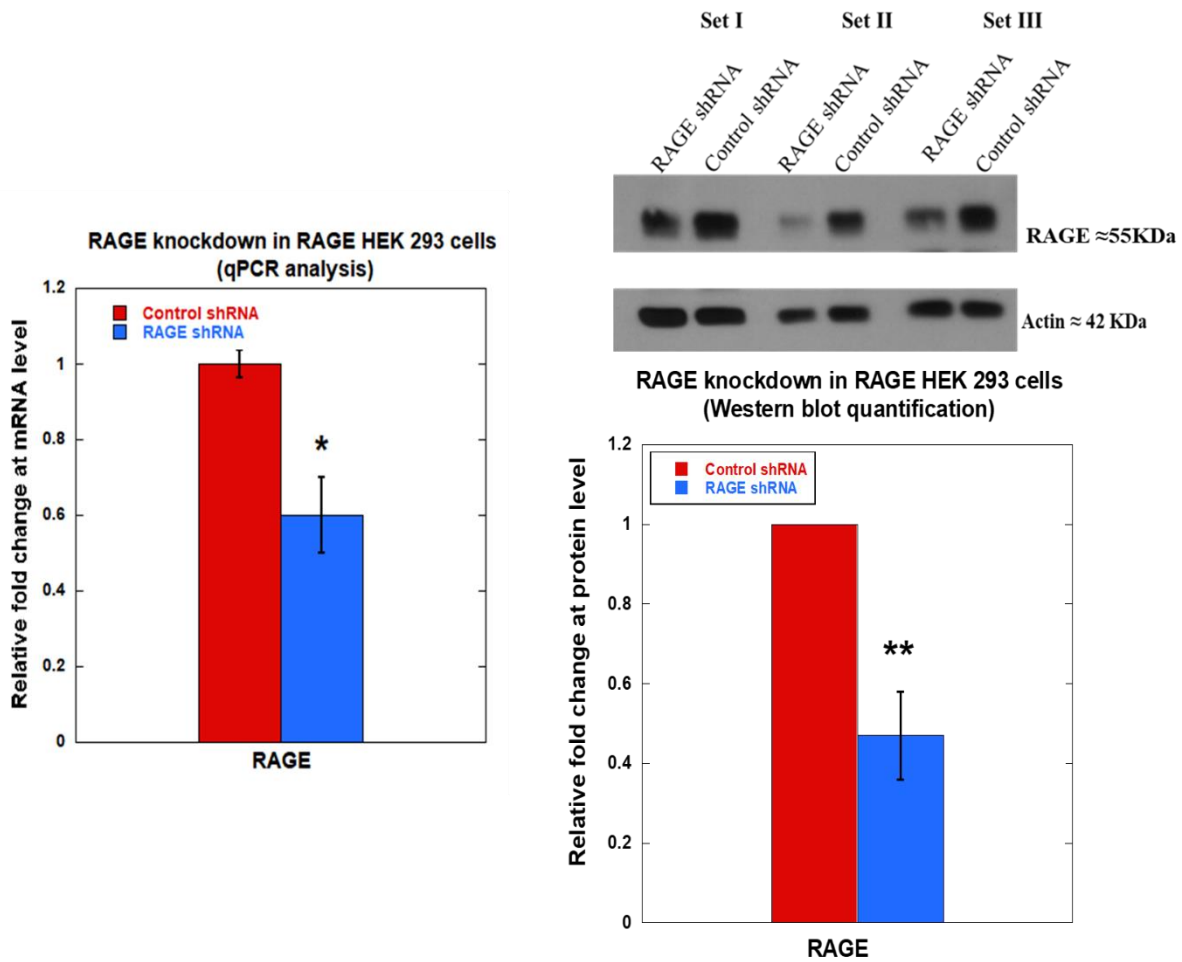


Figure 5.9: qPCR and Western blot data showing relative fold change in RAGE expression after shRNA knockdown in RAGE HEK 293 cells.

The plots represent the average of 3 independent experiments (n=3) where ** P<0.01, * P<0.05. AntiRAGE D1A12 antibody was used to detect RAGE in these samples.

Knocking down RAGE reduced cell adhesion in RAGE HEK 293 cells to different ECM proteins (Figure 5.10). The RAGE shRNA transfected cells showed a reduced adherence of about 40% to the ECM proteins. It was also noticed that adherence to collagen IV was slightly higher than to collagen I or fibronectin 1 during the 5 min time point with control shRNA transfected RAGE HEK 293 cells. With fibronectin and collagen I coated surfaces the control shRNA transfected cells adhered at the same rate. Cells transfected with RAGE shRNA showed reduced binding between 5-10 minute time points to collagen I changing from 20 to 24%, but with fibronectin, the adherence was comparatively higher in the initial time points. Data obtained for cell spreading assays mirrored the results of the adhesion assay (Figure 5.11). Overall, RAGE knockdown decreased the cell polarization, and cells appeared circular. However, control shRNA transfected RAGE HEK 293 cells maintained a dense, almost neuronal-like spread pattern typical for RAGE expressing HEK 293 cells. The observed circularity value for RAGE shRNA transfected cells were >0.8 , whereas the control shRNA transfected cells had a value of <0.5 .

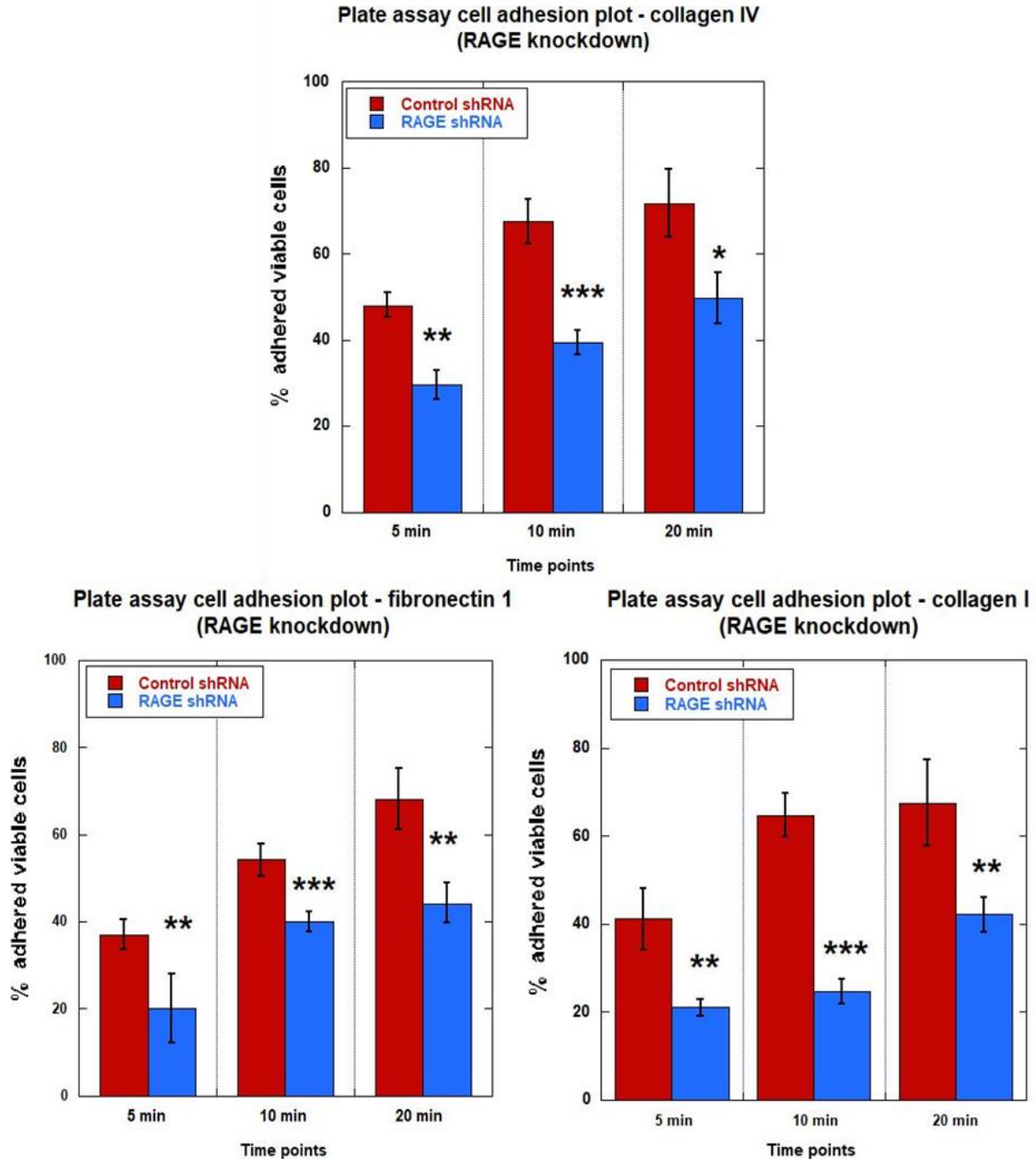


Figure 5.10: Plots from cell adhesion plate assay with RAGE HEK 293 cells transfected with control and RAGE shRNA to collagen IV (top center), fibronectin (bottom left), and collagen I (bottom right) coated surfaces.

This plot represents the average of all three independent experiments (n=3). Statistical analysis was performed using Student t-test; *p<0.05, **p<0.01, ***p<0.001.

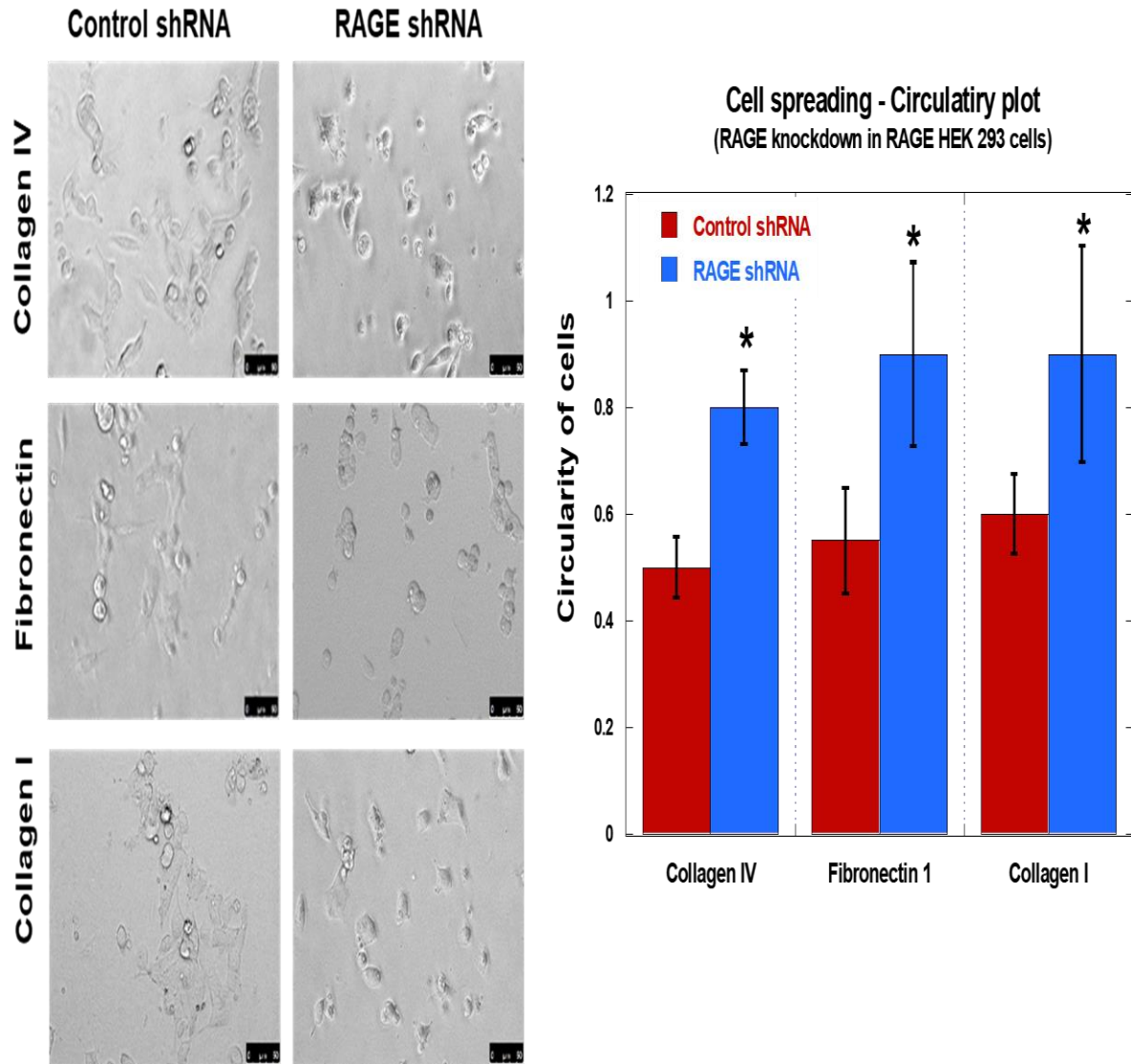


Figure 5.11: Images from cell spreading assay in RAGE HEK 293 cells transfected with control and RAGE shRNA.

After 72hrs of transfection, cells were seeded onto different ECM protein coatings and imaged after 3 hrs. Results from the image analysis of a single experiment demonstrated that RAGE knockdown inhibited cell polarization and was observed to have circular shaped morphology. Quantitative analysis of circularity of cells was shown beside. The bar graph represents the average cell circularity values from all three independent experiments using Image J software. A circularity value of 1 denotes the perfect circular shape of a cell. Statistical analysis was performed using Student t-test; n=3 and *p<0.05. Scale bar 25µm.

As our next step, we investigated the effect of RAGE knockdown on ITGA8 level in RAGE HEK 293 cells using Western blot analysis. RAGE knockdown significantly downregulated ITGA8 expression by 60% (Figure 5.12). To further investigate the functional dependency of

RAGE and ITGA8, we used the pancreatic cancer cell line, MIA PaCa-2. Endogeneous expression of RAGE and ITGA8 expression were determined in MIA PaCa-2 cells (Figure 5.13). Western blot analysis using antiRAGE D1A12 antibody showed a RAGE band around 55 Kda from MIA PaCa-2 lysate. Immunofluorescence analysis showed that RAGE localized mainly in the intracellular region, and some fluorescence was observed in the nucleus. ITGA8 expression was confirmed by Western blot and by flow cytometry analysis.

We observed about 40% knockdown of RAGE in MIA PaCa-2 cells by Western blot analysis. Furthermore, as observed in RAGE HEK 293 cells, knocking down RAGE in MIA PaCa-2 cells also reduced ITGA8 levels by 80% (Figure 5.14). Overall, our results showed that RAGE knockdown reduced cell adhesion and cell spreading, which might be resulted from the downregulation of ITGA8.

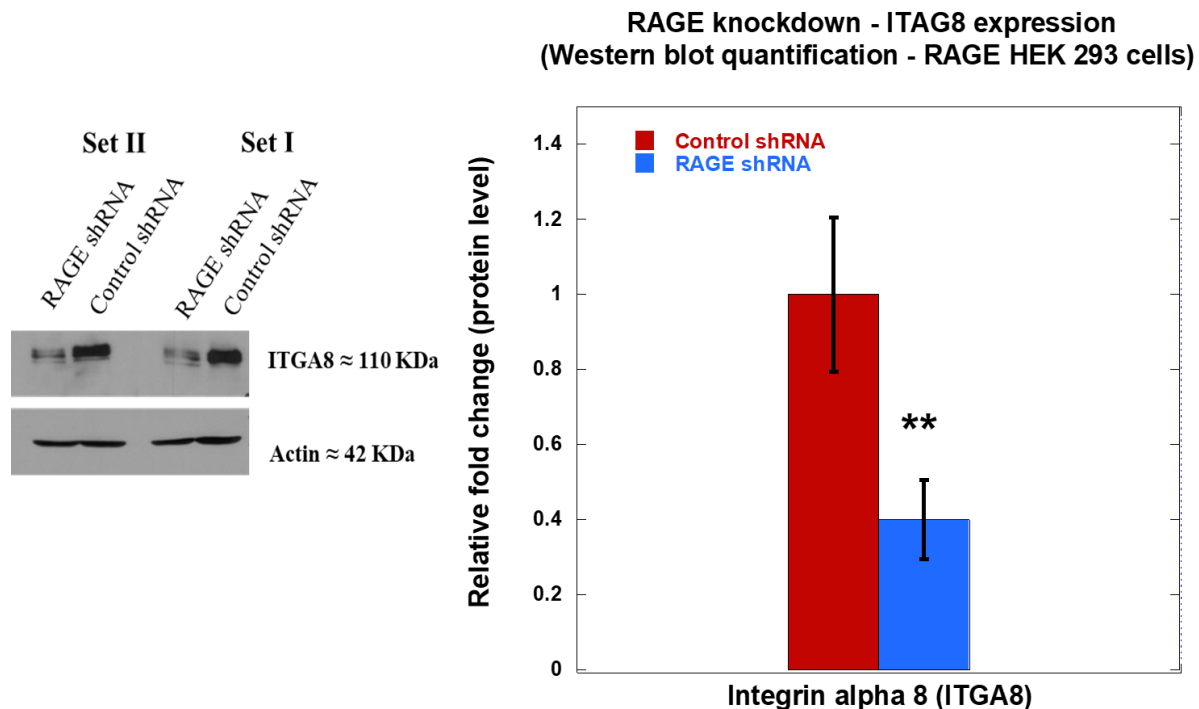


Figure 5.12: Western blot against ITGA8 in RAGE HEK 293 cells transfected with control/scrambled and RAGE shRNA.

Actin was used as the loading control. The plot below shows the relative quantification of the ITAG8 expression from 2 independent experiments (n=2) where ** P<0.01. Human ITGA8 antibody (MAB6194) was used to detect ITGA8 in these samples.

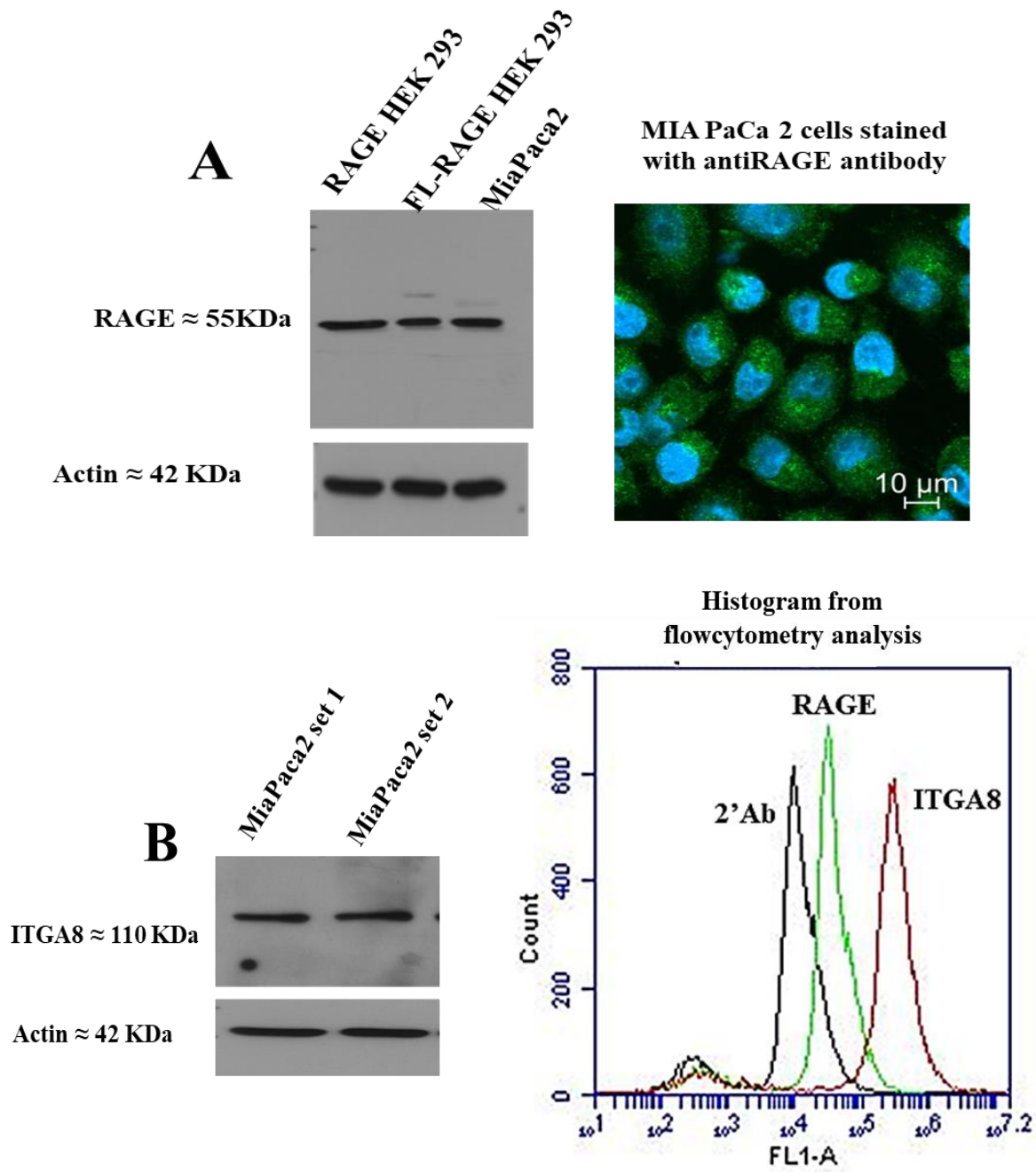


Figure 5.13: Validation of endogenous expression of RAGE and ITGA8 in MIA PaCa-2 cells. (A) Western blot against RAGE in RAGE HEK 293 and MIA PaCa-2 lysates; Immunofluorescence analysis of RAGE in MIA PaCa-2 cells. AntiRAGE D1A12 antibody was used to detect RAGE in these samples. (B) Western blot against ITGA8 in MIA PaCa-2 lysates; Histogram from flow cytometry analysis of cell surface RAGE and ITGA8 in MIA PaCa-2 cells in non-permeabilized condition. AntiRAGE 9A11 was used to detect RAGE, and human ITGA8 antibody (MAB6194) was used to detect ITGA8 in these samples.

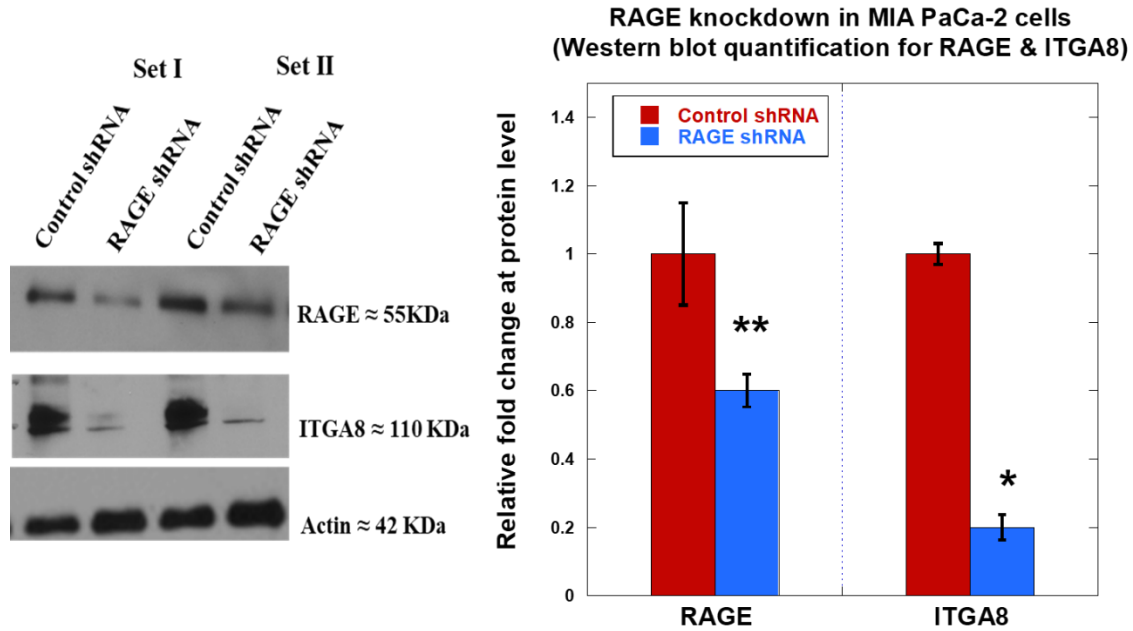


Figure 5.14: Western blot showing expression of RAGE and ITGA8 in MIA PaCa-2 cells after RAGE knockdown.

The plot shows the quantification of these respective proteins and represents the average of 2 independent experiments (n=2) where ** P<0.01, * P<0.05. AntiRAGE D1A12 was used to detect RAGE, and human ITGA8 antibody (MAB6194) was used to detect ITGA8 in these samples.

Discussion

Our study demonstrated successful knockdown of RAGE in both RAGE HEK 293 and MIA PaCa-2 cells. RAGE HEK 293 cells showed a slightly higher knockdown level of RAGE in protein levels (~60%) compared to MIA PaCa-2 cells (~40%) which could be due to differences in the transfection efficiency between these cell types (323). RAGE knockdown reduced cell adhesion compared to the control shRNA transfected cells. The data is in line with our findings in chapter 3, where we observed that overexpression of RAGE significantly improved adherence of cells. The data from the cell spreading assay showed that RAGE knockdown decreased the cell's ability to polarize. These cells had circularity values corresponding to those of mock and DN-RAGE expressing cells from chapter 3.

Data from the qPCR and proteomics studies showed that RAGE expression increased the expression of ITGA8 both at the transcript and translational levels. We investigated levels of ITGA8 upon RAGE knockdown in RAGE HEK 293 cells and in the pancreatic cancer cell line Mia PaCa2-2 which is reported to express endogenous RAGE. It was observed that silencing RAGE downregulated ITGA8 levels in these cells (324). Western blot analysis showed endogenous expression of ITGA8 in MIA PaCa-2 cells. It was also previously reported that altered integrin expression in pancreatic cancer contributes to cancer cell invasion and metastasis (325). RAGE knockdown reduced the expression of ITGA8 in Mia PaCa-2 cells suggesting that RAGE modulates ITGA8 expression in these cells. A recent study described that endogenous RAGE in podocyte co-immunoprecipitates with $\alpha V\beta 3$ -integrin. $\alpha V\beta 3$ -integrin associates with soluble urokinase plasminogen activator receptor (suPAR) to mediate pathological signaling. This study identified that RAGE is an essential co-receptor for suPAR as blocking RAGE using its inhibitor, azeliragon, and silencing RAGE inhibited the signaling (326). Our data suggest that RAGE can directly or indirectly affect integrins in mediating signaling response.

The overall result from this study demonstrates that RAGE knockdown suppresses cell adhesion and cell spreading by downregulating ITGA8 expression.

Conclusion

The overall goal of this study was to identify differentially expressed adhesion relevant surface proteins upon RAGE expression. We investigated the above at the transcriptional and protein levels. We utilized qPCR to evaluate the transcriptional changes using a list of selected genes relevant to cell adhesion. Our results from the qPCR analysis showed increased transcript levels of ITGA8 and CNTN1 in RAGE HEK 293 cells and downregulated the levels of MCAM/MUC18, FN1, and THBS1 in these cells compared to WT HEK 293. Since transcript

levels do not always replicate the protein levels of a gene, we used cell surface proteomics as a complementary approach.

Data analysis from the proteomics study showed that RAGE expression differentially altered the expression of adhesion relevant cell surface proteins, which fell into 3 categories; proteins that were (1) common in both the cell types, (2) identified only in RAGE HEK 293, and (3) WT HEK 293. From the analysis, we identified 12 proteins in both WT and RAGE HEK 293 cells: NCAM, CAM1, BSG, DAG1, ITGA5, ITGB1, ALCAM/CD166, CD 47, ITGA2, PLXB2, CADH2, and ITGA1. Except for PLXB2, all proteins were upregulated, in particular NCAM, ITGA1, and ITGA2, which showed fold changes greater than 3.5. However, their transcript levels did not show significant changes when compared to the WT HEK 293 cells. In addition, RAGE expression induced the expression of certain proteins that were absent in WT HEK 293 cells. The genes include, EGFR, CD44, EFNB1, TPBG, PODXL2, NPTN, CD99, ITGA8, FLNA, ITGAV, and PTK7. Ephrin type A and B receptor proteins (EPHA & EPHB) were found only in WT HEK 293 cells but not in RAGE HEK 293 cells.

A knockdown study approach was utilized to understand the functional relevance of RAGE expression towards cell adhesion and the molecular mechanism involved. Based on the result from pathway ontology using the panther classification system, we linked changes in ITGA8 and RAGE to cell adhesion in HEK 293 and in MIA PaCa2 cells. As expected, knocking down RAGE resulted in reduced adherence and impairment in cell polarization in RAGE HEK 293 cells. Furthermore, we observed a direct correlation between RAGE and ITGA8 expression and knocking down RAGE reduced the expression of ITGA8.

Collectively, the results of this study suggest that RAGE expression alters global changes in the surface proteome of the cells, and ITGA8 was identified as one of the adhesion proteins. We

also demonstrated ITGA8 expression to correlate with RAGE expression changes directly and further suggest a functional dependency between them (Summarized in Figure 5.15). However, we could not come to a definite conclusion about this as the effect of ITGA8 expression on RAGE was not evaluated.

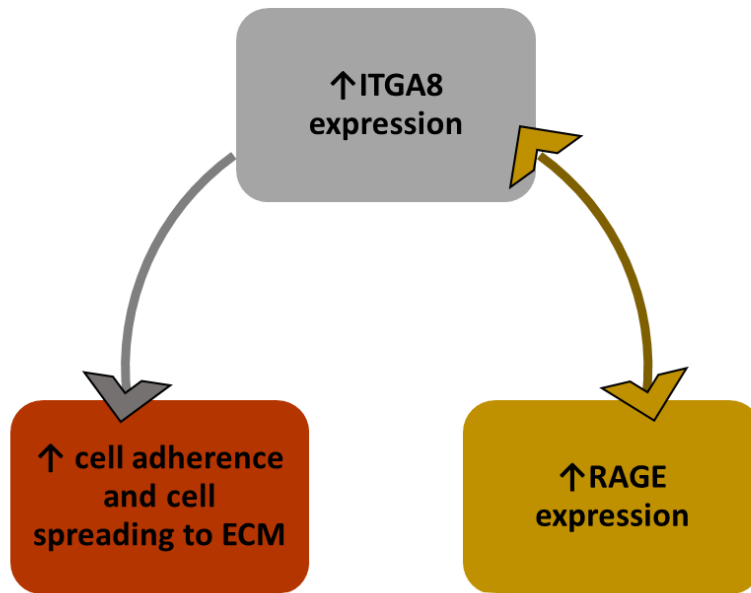


Figure 5.15: Overall findings from Chapter 5 show RAGE expression increases cell adhesion and cell spreading to ECM by regulating ITGA8 expression. Our data suggest that RAGE regulates ITGA8 expression in RAGE HEK 293 and Mia PaCa-2 cells. We propose that this might contribute to increased cell adhesion and spreading to ECM.

CHAPTER 6. SUMMARY AND CONCLUSIONS; CLINICAL RELEVANCE; LIMITATIONS; AND FUTURE DIRECTIONS

Summary and conclusion

This project provides novel insights into the role of different domains of RAGE and the underlining mechanism involved in RAGE mediated cell adhesion.

RAGE is a pattern recognition receptor comprising three Ig-like extracellular domains, V, C1, and C2, a single transmembrane domain, and an intracellular cytoplasmic domain (ICD) (104,105). RAGE is known to interact with a wide range of ligands and activates multiple signaling pathways (109,134). RAGE associated signaling has significant roles in human pathogenesis, including diabetic complications (146,147), neurodegenerative diseases (148,149), and certain cancers (150,152,327). Blocking RAGE activation and signaling has been shown to reduce or prevent the development of these pathological conditions in *in vitro* and *in vivo* models (134,204,328-330). Despite the prominent role of RAGE in pathological complications, studies have also shown that RAGE expressing cells had increased adherence and spreading in the presence of extracellular matrix (ECM) proteins (196,205-207).

An elaborate investigation of the importance of the different domains of RAGE in cell adhesion was performed using domain deletion variants of RAGE; (FL-, DN-, Δ V-, Δ C1, Δ C2, and TmCyto-). Deletion of the V domain of RAGE impaired the membrane localization of RAGE, suggesting the function of the V domain in RAGE localization. To evaluate the adhesion upon expression of these variants, we utilized the real time cell analyzer Xcelligence dp system, which is capable of recording small changes in cell adhesion. The results from cell adhesion and cell spreading data highlighted the importance of the ICD and demonstrated that the presence of membrane bound RAGE or its extracellular domains was not necessary to mediate cell-cell and

cell-extracellular matrix interactions. Another observation from this study was that the ICD of RAGE, even when expressed individually, was able to function as the full-length receptor. The striking difference between these variants is their difference in localization, with the expression of FL-RAGE localized primarily at the plasma membrane and the TmCyto-RAGE localized in the intracellular region.

Studies reported the occurrence of metalloprotease mediated ectodomain shedding/cleavage in RAGE upon stimulation (269). This extracellular shedding is often associated with intramembrane proteolysis in many transmembrane receptors and reported to liberate the intracellular cytoplasmic domain which upon nuclear localization signals to alter cellular events including gene expression, cell adhesion and migration (262,267). Ligand stimulation in FL-RAGE induced intramembrane proteolysis and nuclear translocation. However, in the case of the cytoplasmic domain, it was observed that the intramembrane proteolysis occurred without stimulation and showed selective nuclear localization.

Furthermore, in the nucleus, the ICD was found to concentrate in the nucleolus, and this is the first study to report the nucleolar localization of RAGE ICD. The findings were also complemented by the NLS prediction software, which reported residues 365-368 (RRQR) in the RAGE ICD as an NLS sequence. Interestingly, a nucleolar localization signal was also mapped in this same region.

Next, RAGE expression and its effects on global changes in the expression of adhesion relevant surface proteins were investigated. ITGA8 and CNTN1 were found to be upregulated in their mRNA and protein levels. Also, it was observed that the genes such as MCAM, FN1, and THBS1 were downregulated upon RAGE expression. The cell surface proteomics study identified cell adhesion molecules that were upregulated upon RAGE expression. NCAM, ITGA1, and

ITGA2 showed greater than 3-fold change. Interestingly, RAGE expression also induced the expression of adhesion molecules EGFR, CD44, EFNB1, TPBG, PODXL2, NPTN, CD99, ITGA8, FLNA, ITGAV, and PTK7. Multiple studies showed that the identified genes are important contributors to neurologic disorders and cancer metastasis (52,259,309,331,332). Also, half of the identified proteins were reported to undergo intermembrane proteolysis and signal important biological functions such as cell adhesion, proliferation, and migration (267).

Lastly, the functional dependency of RAGE towards changes in adhesion and spreading was assessed using the gene knockdown approach. RAGE knockdown significantly reduced adherence of the cells to ECM proteins and completely abolished polarization of the cells. Furthermore, the protein levels of ITGA8 correlated with RAGE expression, as knocking down RAGE in both RAGE HEK 293 and MIA PaCa2 cells reduced integrin expression. Our data suggest an interplay between RAGE and ITGA8 in mediating cell adhesion.

Collectively, these data propose a new model of RAGE signaling via ectodomain shedding and intramembrane proteolysis that is distinct from classical signaling. The liberated RAGE ICD upon nuclear and nucleolar translocation regulates the expression of adhesion molecules on the cell surface, such as ITGA8(Summarized in Figure 6.1).

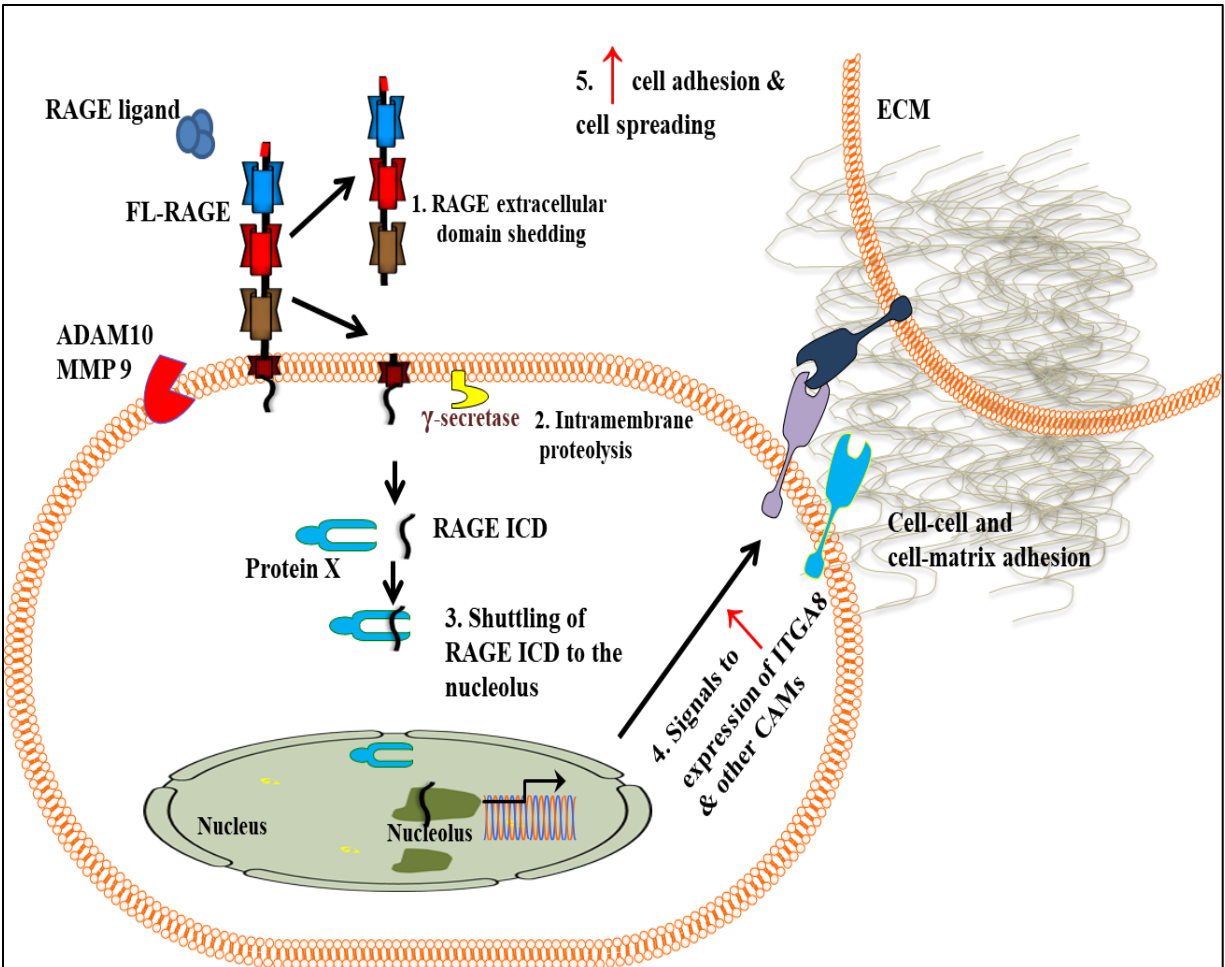


Figure 6.1: Overall findings and proposed model of RAGE signaling to cell adhesion by intramembrane proteolysis.

(1) RAGE-ligand association induces ectodomain shedding by ADAM10 or MMP9. (2) The cytoplasmic tail of RAGE is liberated upon regulated intramembrane proteolysis (RIP) by γ -secretase. (3) The liberated cytoplasmic tail forms an association with a cytoplasmic protein partner (Protein X) and is translocated to the nucleus. (4 & 5) In the nucleus, RAGE ICD drives transcription factors to signal to induce expression of ITGA8 and other CAMs, which contributes to increased cell adherence and cell spreading in the presence of ECM.

Clinical relevance

RAGE is implicated in diverse chronic inflammatory states, and the clinical relevance of RAGE in these inflammatory diseases is being demonstrated in clinical trials of novel small-molecule RAGE inhibitors. Several of these inhibitors (Table 1.2) were developed to target the ligand binding sites in the extracellular domains of RAGE. For example, Azeliragon is an

orally bioavailable inhibitor of RAGE targeting its VC1 domain and has undergone phase 3 clinical trials for Alzheimer's disease (ClinicalTrials.gov identifier: NC02080364). The study was terminated due to its failure to slow the decline on the Alzheimer's disease assessment scale (333). The result suggests that an alternative strategy is needed to block RAGE from signaling in pathological conditions.

The results from our data suggest an alternative mechanism in RAGE signaling involving nuclear translocation of its ICD. Our study also demonstrated the functional dependency of RAGE with integrins, and further investigations on this would be beneficial to understanding RAGE's signaling and cross talks.

Overall, our study suggests that targeting ectodomain shedding and intramembrane proteolysis along with small molecule inhibitors might be effective in blocking RAGE signaling in pathological conditions.

Limitations

Although this study resulted in novel findings, there were limitations associated with it.

The major limitation of this study is that all of the experiments have been carried out in cell culture models. Another limitation is that our study used only one disease cell model (Mia PaCa2 – pancreatic cancer cell) to correlate changes in RAGE expression to ITGA8. Also, additional studies would be required to translate the proposed RAGE signaling model to *in vitro* and *in vivo* disease models.

A second limitation was that we could not identify a mechanism behind the nuclear translocation of the RAGE ICD. Although we show the presence of NLS, it is not clear if the ICD translocates on its own into the nucleus or forms a complex with another cytoplasmic protein for nuclear translocation.

Third, we did not check the changes in expression of adhesion relevant genes in disease models that express endogenous RAGE. We also did not check the functional dependency of other identified proteins from our surface proteomics study. Therefore, this limited our understanding of the dependency between RAGE and other adhesion molecules.

Future directions

It would be beneficial to investigate the mechanism behind the nuclear translocation of RAGE and to identify the associated cytoplasmic binding partners in mediating this translocation. This can be done by affinity tagging the cytoplasmic domain followed by an immunoprecipitation-based purification technique for studying protein–protein interactions.

Next, it would be valuable to investigate if blocking the extracellular ligand binding region and inhibiting the RAGE ICD nuclear translocation could disrupt RAGE signaling in HEK 293 cells. This can be done by mutating the NLS sequence (RRQR) in the cytoplasmic domain (residue 365-368) and blocking the ligand binding V domain using antiRAGE antibodies, followed by monitoring changes in the expression of ITGA8. The results from the above experiment would answer if nuclear translocation of RAGE-ICD is the reason behind changes in expression of ITGA8 and other adhesion relevant proteins.

Finally, an in-depth study investigating the effect of RAGE expression and activation of adhesion molecule transcription and expression in specific disease models would be important. Such a study could use RNAseq and the targeted proteomics approaches in cell based and mouse disease models.

REFERENCES

1. Frantz, C., Stewart, K. M., and Weaver, V. M. (2010) The extracellular matrix at a glance. *Journal of Cell Science* **123**, 4195–4200.
2. Schaefer, L., and Schaefer, R. M. (2010) Proteoglycans: from structural compounds to signaling molecules. *Cell Tissue Res* **339**, 237-246
3. Yue, B. (2014) Biology of the extracellular matrix: an overview. *J Glaucoma* **23**, 20-23
4. Gordon, M. K., and Hahn, R. A. (2010) Collagens. *Cell Tissue Res* **339**, 247-257
5. Kadler, K. E., Hill, A., and Canty-Laird, E. G. (2008) Collagen fibrillogenesis: fibronectin, integrins, and minor collagens as organizers and nucleators. *Current Opinion in Cell Biology* **20**, 495-501
6. Wierzbicka-Patynowski, I., and Schwarzbauer, J. E. (2003) The ins and outs of fibronectin matrix assembly. *Journal of Cell Science* **116**, 3269-3276
7. Singh, P., Carraher, C., and Schwarzbauer, J. E. (2010) Assembly of Fibronectin Extracellular Matrix. *Annual Review of Cell and Developmental Biology* **26**, 397-419
8. Karamanos, N. K., Theocharis, A. D., Piperigkou, Z., Manou, D., Passi, A., Skandalis, S. S., Vynios, D. H., Orian-Rousseau, V., Ricard-Blum, S., Schmelzer, C. E. H., Duca, L., Durbeej, M., Afratis, N. A., Troeberg, L., Franchi, M., Masola, V., and Onisto, M. (2021) A guide to the composition and functions of the extracellular matrix. *The FEBS Journal* **288**, 6850-6912
9. Durbeej, M. (2010) Laminins. *Cell Tissue Res* **339**, 259-268
10. Chothia, C., and Jones, E. Y. (1997) The molecular structure of cell adhesion molecules. *Annu Rev Biochem* **66**, 823-862
11. Hynes, R. O., and Zhao, Q. (2000) The Evolution of Cell Adhesion. *Journal of Cell Biology* **150**, 89-96
12. Yamada, K. M. (2003) Cell Adhesion. *Current Protocols in Cell Biology* **18**, 901-909
13. Vitte, J., Benoliel, A. M., Pierres, A., and Bongrand, P. (2005) Regulation of cell adhesion. *Clin Hemorheol Microcirc* **33**, 167-188
14. Edelman Gerald, M. (1983) Cell Adhesion Molecules. *Science* **219**, 450-457
15. Alberts B, J. A., Lewis J, et al. (2002) Cell Junctions, Cell Adhesion, and the Extracellular Matrix. in *Molecular biology of the cell*, 4th Ed., Garland Science, New York. pp 2700-2857
16. Spiller, S., Clauder, F., Bellmann-Sickert, K., and Beck-Sickinger, A. G. (2021) Improvement of wound healing by the development of ECM-inspired biomaterial coatings and controlled protein release. *Biological Chemistry* **402**, 1271-1288
17. Petruzzelli, L., Takami, M., and Humes, H. D. (1999) Structure and function of cell adhesion molecules. *The American Journal of Medicine* **106**, 467-476
18. Humphries, M. J., and Newham, P. (1998) The structure of cell-adhesion molecules. *Trends Cell Biol* **8**, 78-83
19. Smith, C. W. (2008) 3. Adhesion molecules and receptors. *Journal of Allergy and Clinical Immunology* **121**, S375-S379
20. Foty, R. A., and Steinberg, M. S. (2005) The differential adhesion hypothesis: a direct evaluation. *Developmental Biology* **278**, 255-263
21. Lodish, H., Berk, A., Matsudaira, P., Kaiser, C.A., Krieger, M., Scott, M.P., et al. (2005) Cell–Cell and Cell–Matrix Adhesion: An Overview. in *Molecular Cell Biology*, 5th Ed., W.H. Freeman and Co., New York. pp 215-217

22. Honig, B., and Shapiro, L. (2020) Adhesion Protein Structure, Molecular Affinities, and Principles of Cell-Cell Recognition. *Cell* **181**, 520-535
23. (2020) Cell Adhesion and the Extracellular Matrix. in *Goodman's Medical Cell Biology* (Goodman, S. R. ed.), 4th Ed., Academic Press. pp 203-247
24. Sainio, A., and Järveläinen, H. (2020) Extracellular matrix-cell interactions: Focus on therapeutic applications. *Cellular Signalling* **66**, 109487
25. Albelda, S. M., and Buck, C. A. (1990) Integrins and other cell adhesion molecules. *The FASEB Journal* **4**, 2868-2880
26. De Grandis, M., Lhoumeau, A. C., Mancini, S. J., and Aurrand-Lions, M. (2016) Adhesion receptors involved in HSC and early-B cell interactions with bone marrow microenvironment. *Cell Mol Life Sci* **73**, 687-703
27. Shapiro, L., and Weis, W. I. (2009) Structure and biochemistry of cadherins and catenins. *Cold Spring Harbor Perspectives Biology* **1**, a003053
28. Oda, H., and Takeichi, M. (2011) Structural and functional diversity of cadherin at the adherens junction. *Journal of Cell Biology* **193**, 1137-1146
29. Truong, K., and Ikura, M. (2002) The cadherin superfamily database. *J Struct Funct Genomics* **2**, 135-143
30. Kim, S. A., Tai, C. Y., Mok, L. P., Mosser, E. A., and Schuman, E. M. (2011) Calcium-dependent dynamics of cadherin interactions at cell-cell junctions. *Proc Natl Acad Sci USA* **108**, 9857-9862
31. Prakasam, A. K., Maruthamuthu, V., and Leckband, D. E. (2006) Similarities between heterophilic and homophilic cadherin adhesion. *Proc Natl Acad Sci USA* **103**, 15434-15439
32. McCrea, P. D., Maher, M. T., and Gottardi, C. J. (2015) Nuclear signaling from cadherin adhesion complexes. *Current topics in developmental biology* **112**, 129-196
33. Klezovitch, O., and Vasioukhin, V. (2015) Cadherin signaling: keeping cells in touch. *F1000Research* **4**, 550
34. Bruner, H. C., and Derksen, P. W. B. (2018) Loss of E-Cadherin-Dependent Cell-Cell Adhesion and the Development and Progression of Cancer. *Cold Spring Harbor Perspectives in Biology* **10**, a029330
35. Jiang, J., Dean, D., Burghardt, R. C., and Parrish, A. R. (2004) Disruption of Cadherin/Catenin Expression, Localization, and Interactions During HgCl₂-Induced Nephrotoxicity. *Toxicological Sciences* **80**, 170-182
36. Sisto, M., Ribatti, D., and Lisi, S. (2021) Cadherin Signaling in Cancer and Autoimmune Diseases. *International Journal of Molecular Sciences* **22**, 13358
37. Lasky, L. A. (1995) Selectin-carbohydrate interactions and the initiation of the inflammatory response. *Annu Rev Biochem* **64**, 113-139
38. (2021) Chapter 7 - Cell Adhesion and the Extracellular Matrix. in *Goodman's Medical Cell Biology (Fourth Edition)* (Goodman, S. R. ed.), Academic Press. pp 203-247
39. Alberts, B., Johnson, A., Lewis, J., Raff, M., Roberts, K. and Walter, P. (2003) Molecular biology of the cell. 4th edn. *Annals of Botany* **91**, 2767-2788
40. Kansas, G. S. (1992) Structure and function of L-selectin. *Apmis* **100**, 287-293
41. McEver, R. P., and Zhu, C. (2010) Rolling cell adhesion. *Annu Rev Cell Dev Biol* **26**, 363-396
42. Tvaroška, I., Selvaraj, C., and Koča, J. (2020) Selectins-The Two Dr. Jekyll and Mr. Hyde Faces of Adhesion Molecules-A Review. *Molecules (Basel, Switzerland)* **25**, 2835

43. Borsig, L. (2018) Selectins in cancer immunity. *Glycobiology* **28**, 648-655
44. Siddiqui, K., George, T. P., Nawaz, S. S., and Joy, S. S. (2019) VCAM-1, ICAM-1 and selectins in gestational diabetes mellitus and the risk for vascular disorders. *Future Cardiol* **15**, 339-346
45. Smith, B. A. H., and Bertozzi, C. R. (2021) The clinical impact of glycobiology: targeting selectins, Siglecs and mammalian glycans. *Nature Reviews. Drug Discovery* **20**, 217-243
46. Hunkapiller, T., and Hood, L. (1989) Diversity of the immunoglobulin gene superfamily. *Adv Immunol* **44**, 1-63
47. Shimono, Y., Rikitake, Y., Mandai, K., Mori, M., and Takai, Y. (2012) Immunoglobulin superfamily receptors and adherens junctions. *Subcell Biochem* **60**, 137-170
48. Marchalonis, J. J., Hohman, V. S., Kaymaz, H., Schluter, S. F., and Edmundson, A. B. (1994) Cell surface recognition and the immunoglobulin superfamily. *Ann N Y Acad Sci* **712**, 20-33
49. Muller, W. A. (2013) Getting leukocytes to the site of inflammation. *Vet Pathol* **50**, 7-22
50. Cayrol, R., Wosik, K., Berard, J. L., Dodelet-Devillers, A., Ifergan, I., Kebir, H., Haqqani, A. S., Kreymborg, K., Krug, S., Moumdjian, R., Bouthillier, A., Becher, B., Arbour, N., David, S., Stanimirovic, D., and Prat, A. (2008) Activated leukocyte cell adhesion molecule promotes leukocyte trafficking into the central nervous system. *Nat Immunol* **9**, 137-145
51. Ebnet, K., Suzuki, A., Ohno, S., and Vestweber, D. (2004) Junctional adhesion molecules (JAMs): more molecules with dual functions? *Journal of Cell Science* **117**, 19-29
52. Wai Wong, C., Dye, D. E., and Coombe, D. R. (2012) The Role of Immunoglobulin Superfamily Cell Adhesion Molecules in Cancer Metastasis. *International Journal of Cell Biology* **2012**, 340296
53. Roland, C. L., Harken, A. H., Sarr, M. G., and Barnett Jr, C. C. (2007) ICAM-1 expression determines malignant potential of cancer. *Surgery* **141**, 705-707
54. Swart, G. W. M. (2002) Activated leukocyte cell adhesion molecule (CD166/ALCAM): Developmental and mechanistic aspects of cell clustering and cell migration. *European Journal of Cell Biology* **81**, 313-321
55. Weichert, W., Knösel, T., Bellach, J., Dietel, M., and Kristiansen, G. (2004) ALCAM/CD166 is overexpressed in colorectal carcinoma and correlates with shortened patient survival. *Journal of clinical pathology* **57**, 1160-1164
56. Jezierska, A., Matysiak, W., and Motyl, T. (2006) ALCAM/CD166 protects breast cancer cells against apoptosis and autophagy. *Med Sci Monit* **12**, 263-273
57. Ruma, I. M., Putranto, E. W., Kondo, E., Murata, H., Watanabe, M., Huang, P., Kinoshita, R., Futami, J., Inoue, Y., Yamauchi, A., Sumardika, I. W., Youyi, C., Yamamoto, K., Nasu, Y., Nishibori, M., Hibino, T., and Sakaguchi, M. (2016) MCAM, as a novel receptor for S100A8/A9, mediates progression of malignant melanoma through prominent activation of NF- κ B and ROS formation upon ligand binding. *Clin Exp Metastasis* **33**, 609-627
58. O'Brien, K. D., Allen, M. D., McDonald, T. O., Chait, A., Harlan, J. M., Fishbein, D., McCarty, J., Ferguson, M., Hudkins, K., Benjamin, C. D., and et al. (1993) Vascular cell adhesion molecule-1 is expressed in human coronary atherosclerotic plaques. Implications for the mode of progression of advanced coronary atherosclerosis. *J Clin Invest* **92**, 945-951

59. Printseva, O., Peclo, M. M., and Gown, A. M. (1992) Various cell types in human atherosclerotic lesions express ICAM-1. Further immunocytochemical and immunochemical studies employing monoclonal antibody 10F3. *Am J Pathol* **140**, 889-896
60. Krieglstein, C. F., and Granger, D. N. (2001) Adhesion molecules and their role in vascular disease. *American Journal of Hypertension* **14**, 44-54
61. Brady, H. R. (1994) Leukocyte adhesion molecules and kidney diseases. in *Kidney Int*, United States. pp 1285-1300
62. Seron, D., Cameron, J. S., and Haskard, D. O. (1991) Expression of VCAM-1 in the normal and diseased kidney. *Nephrology Dialysis Transplantation* **6**, 917-922
63. Jonckheere, N., Skrypek, N., Frénois, F., and Van Seuningen, I. (2013) Membrane-bound mucin modular domains: From structure to function. *Biochimie* **95**, 1077-1086
64. Seregini, E., Botti, C., Massaron, S., Lombardo, C., Capobianco, A., Bogni, A., and Bombardieri, E. (1997) Structure, function and gene expression of epithelial mucins. *Tumori* **83**, 625-632
65. Hori, Y. (2018) Secreted Mucins on the Ocular Surface. *Investigative Ophthalmology & Visual Science* **59**, 151-156
66. Hilkens, J., Ligtenberg, M. J. L., Vos, H. L., and Litvinov, S. V. (1992) Cell membrane-associated mucins and their adhesion-modulating property. *Trends in Biochemical Sciences* **17**, 359-363
67. Van Klinken, B. J., Dekker, J., Büller, H. A., and Einerhand, A. W. (1995) Mucin gene structure and expression: protection vs. adhesion. *Am J Physiol* **269**, G613-627
68. Kufe, D. W. (2009) Mucins in cancer: function, prognosis and therapy. *Nature Reviews. Cancer* **9**, 874-885
69. van Putten, J. P. M., and Strijbis, K. (2017) Transmembrane Mucins: Signaling Receptors at the Intersection of Inflammation and Cancer. *Journal of Innate Immunity* **9**, 281-299
70. Luo, B. H., Carman, C. V., and Springer, T. A. (2007) Structural basis of integrin regulation and signaling. *Annu Rev Immunol* **25**, 619-647
71. Campbell, I. D., and Humphries, M. J. (2011) Integrin structure, activation, and interactions. *Cold Spring Harbor Perspectives in Biology* **3**, a004994
72. Takada, Y., Ye, X., and Simon, S. (2007) The integrins. *Genome Biology* **8**, 215
73. Hynes, R. O. (2004) The emergence of integrins: a personal and historical perspective. *Matrix biology: Journal of the International Society for Matrix Biology* **23**, 333-340.
74. Barczyk, M., Carracedo, S., and Gullberg, D. (2010) Integrins. *Cell Tissue Res* **339**, 269-280
75. Arias-Salgado, E. G., Lizano, S., Sarkar, S., Brugge, J. S., Ginsberg, M. H., and Shattil, S. J. (2003) Src kinase activation by direct interaction with the integrin beta cytoplasmic domain. *Proc Natl Acad Sci USA* **100**, 13298-13302
76. Arnaout, M. A., Goodman, S. L., and Xiong, J.-P. (2007) Structure and mechanics of integrin-based cell adhesion. *Current Opinion in Cell Biology* **19**, 495-507
77. Bachmann, M., Kukkurainen, S., Hytönen, V. P., and Wehrle-Haller, B. (2019) Cell Adhesion by Integrins. *Physiological Reviews* **99**, 1655-1699
78. Mezu-Ndubuisi, O. J., and Maheshwari, A. (2021) The role of integrins in inflammation and angiogenesis. *Pediatric Research* **89**, 1619-1626
79. Desgrosellier, J. S., and Chersesh, D. A. (2010) Integrins in cancer: biological implications and therapeutic opportunities. *Nature reviews. Cancer* **10**, 9-22

80. Hamidi, H., and Ivaska, J. (2018) Every step of the way: integrins in cancer progression and metastasis. *Nature reviews. Cancer* **18**, 533-548
81. Cooper, J., and Giancotti, F. G. (2019) Integrin Signaling in Cancer: Mechanotransduction, Stemness, Epithelial Plasticity, and Therapeutic Resistance. *Cancer Cell* **35**, 347-367
82. Pozzi, A., and Zent, R. (2013) Integrins in Kidney Disease. *Journal of the American Society of Nephrology* **24**, 1034-1039
83. Sheppard, D. (2008) The role of integrins in pulmonary fibrosis. *European Respiratory Review* **17**, 157-162
84. Schnittert, J., Bansal, R., Storm, G., and Prakash, J. (2018) Integrins in wound healing, fibrosis and tumor stroma: High potential targets for therapeutics and drug delivery. *Advanced Drug Delivery Reviews* **129**, 37-53
85. Guerrero, P. A., and McCarty, J. H. (2018) Chapter Five - Integrins in Vascular Development and Pathology. in *Advances in Pharmacology* (Khalil, R. A. ed.), Academic Press. pp 129-153
86. Hamidi, H., and Ivaska, J. (2017) Vascular Morphogenesis: An Integrin and Fibronectin Highway. *Current Biology* **27**, 158-161
87. Finney, A. C., Stokes, K. Y., Pattillo, C. B., and Orr, A. W. (2017) Integrin signaling in atherosclerosis. *Cell Mol Life Sci* **74**, 2263-2282
88. Wu, X., and Reddy, D. S. (2012) Integrins as receptor targets for neurological disorders. *Pharmacology and Therapeutics* **134**, 68-81
89. Lilja, J., and Ivaska, J. (2018) Integrin activity in neuronal connectivity. *Journal of Cell Science* **131**
90. Jaudon, F., Thalhammer, A., and Cingolani, L. A. (2021) Integrin adhesion in brain assembly: From molecular structure to neuropsychiatric disorders. *European Journal of Neuroscience* **53**, 3831-3850
91. Cox, D., Brennan, M., and Moran, N. (2010) Integrins as therapeutic targets: lessons and opportunities. *Nature Reviews Drug Discovery* **9**, 804-820
92. Goodman, S. L., and Picard, M. (2012) Integrins as therapeutic targets. *Trends in Pharmacological Sciences* **33**, 405-412
93. Huang, R., and Rofstad, E. K. (2018) Integrins as therapeutic targets in the organ-specific metastasis of human malignant melanoma. *Journal of Experimental & Clinical Cancer Research* **37**, 92
94. Neeper, M., Schmidt, A. M., Brett, J., Yan, S. D., Wang, F., Pan, Y. C., Elliston, K., Stern, D., and Shaw, A. (1992) Cloning and expression of a cell surface receptor for advanced glycosylation end products of proteins. *Journal of Biological Chemistry* **267**, 14998-15004
95. Bierhaus, A., Humpert, P. M., Morcos, M., Wendt, T., Chavakis, T., Arnold, B., Stern, D. M., and Nawroth, P. P. (2005) Understanding RAGE, the receptor for advanced glycation end products. *Journal of Molecular Medicine* **83**, 876-886
96. Roh, J. S., and Sohn, D. H. (2018) Damage-Associated Molecular Patterns in Inflammatory Diseases. *Immune network* **18**, e27
97. Leclerc, E., Fritz, G., Vetter, S. W., and Heizmann, C. W. (2009) Binding of S100 proteins to RAGE: An update. *Biochimica et Biophysica Acta (BBA) - Molecular Cell Research* **1793**, 993-1007

98. Huttunen, H. J., Fages, C., and Rauvala, H. (1999) Receptor for advanced glycation end products (RAGE)-mediated neurite outgrowth and activation of NF-kappaB require the cytoplasmic domain of the receptor but different downstream signaling pathways. *Journal of Biological Chemistry* **274**, 19919-19924
99. Rojas, A., Figueroa, H., and Morales, E. (2010) Fueling inflammation at tumor microenvironment: the role of multiligand/rage axis. *Carcinogenesis* **31**, 334-341
100. Kang, R., Tang, D., Schapiro, N. E., Livesey, K. M., Farkas, A., Loughran, P., Bierhaus, A., Lotze, M. T., and Zeh, H. J. (2010) The receptor for advanced glycation end products (RAGE) sustains autophagy and limits apoptosis, promoting pancreatic tumor cell survival. *Cell Death Differ* **17**, 666-676
101. Yan, S. F., Yan, S. D., Ramasamy, R., and Schmidt, A. M. (2009) Tempering the wrath of RAGE: an emerging therapeutic strategy against diabetic complications, neurodegeneration, and inflammation. *Ann Med* **41**, 408-422
102. Sterenczak, K. A., Nolte, I., and Escobar, H. M. (2013) RAGE Splicing Variants in Mammals. in *Calcium-Binding Proteins and RAGE: From Structural Basics to Clinical Applications* (Heizmann, C. W. ed.), Humana Press, Totowa, NJ. pp 265-276
103. Dattilo, B. M., Fritz, G., Leclerc, E., Vander Kooi, C. W., Heizmann, C. W., and Chazin, W. J. (2007) The Extracellular Region of the Receptor for Advanced Glycation End Products is Comprised of Two Independent Structural Units. *Biochemistry* **46**, 6957-6970
104. Koch, M., Chitayat, S., Dattilo, B. M., Schiefner, A., Diez, J., Chazin, W. J., and Fritz, G. (2010) Structural Basis for Ligand Recognition and Activation of RAGE. *Structure* **18**, 1342-1352
105. Park, H., Adsit, F. G., and Boyington, J. C. (2010) The 1.5 Å crystal structure of human receptor for advanced glycation endproducts (RAGE) ectodomains reveals unique features determining ligand binding. *Journal of Biological Chemistry* **285**, 40762-40770
106. Matsumoto, S., Yoshida, T., Murata, H., Harada, S., Fujita, N., Nakamura, S., Yamamoto, Y., Watanabe, T., Yonekura, H., Yamamoto, H., Ohkubo, T., and Kobayashi, Y. (2008) Solution Structure of the Variable-Type Domain of the Receptor for Advanced Glycation End Products: New Insight into AGE-RAGE Interaction. *Biochemistry* **47**, 12299-12311
107. Srikrishna, G., Huttunen, H. J., Johansson, L., Weigle, B., Yamaguchi, Y., Rauvala, H., and Freeze, H. H. (2002) N -Glycans on the receptor for advanced glycation end products influence amphoterin binding and neurite outgrowth. *J Neurochem* **80**, 998-1008
108. Xu, D., Young, J. H., Krahn, J. M., Song, D., Corbett, K. D., Chazin, W. J., Pedersen, L. C., and Esko, J. D. (2013) Stable RAGE-Heparan Sulfate Complexes are Essential for Signal Transduction. *ACS Chem Biol* **8**, 1611-1620
109. Fritz, G. (2011) RAGE: a single receptor fits multiple ligands. *Trends in Biochemical Sciences* **36**, 625-632
110. Brett, J., Schmidt, A. M., Yan, S. D., Zou, Y. S., Weidman, E., Pinsky, D., Nowygrod, R., Neeper, M., Przysiecki, C., Shaw, A., and et al. (1993) Survey of the distribution of a newly characterized receptor for advanced glycation end products in tissues. *The American Journal of Pathology* **143**, 1699-1712
111. Kaji, Y., Amano, S., Usui, T., Oshika, T., Yamashiro, K., Ishida, S., Suzuki, K., Tanaka, S., Adamis, A. P., Nagai, R., and Horiuchi, S. (2003) Expression and Function of Receptors for Advanced Glycation End Products in Bovine Corneal Endothelial Cells. *Investigative Ophthalmology & Visual Science* **44**, 521-528

112. Cheng, C., Tsuneyama, K., Kominami, R., Shinohara, H., Sakurai, S., Yonekura, H., Watanabe, T., Takano, Y., Yamamoto, H., and Yamamoto, Y. (2005) Expression profiling of endogenous secretory receptor for advanced glycation end products in human organs. *Modern Pathology* **18**, 1385-1396
113. Katsuoka, F., Kawakami, Y., Arai, T., Imuta, H., Fujiwara, M., Kanma, H., and Yamashita, K. (1997) Type II alveolar epithelial cells in lung express receptor for advanced glycation end products (RAGE) gene. *Biochem Biophys Res Commun* **238**, 512-516
114. Buckley, S. T., and Ehrhardt, C. (2010) The Receptor for Advanced Glycation End Products (RAGE) and the Lung. *Journal of Biomedicine and Biotechnology* **2010**, 917108
115. Queisser, M. A., Kouri, F. M., Königshoff, M., Wygrecka, M., Schubert, U., Eickelberg, O., and Preissner, K. T. (2008) Loss of RAGE in pulmonary fibrosis: molecular relations to functional changes in pulmonary cell types. *Am J Respir Cell Mol Biol* **39**, 337-345
116. Perkins, T. N., and Oury, T. D. (2021) The perplexing role of RAGE in pulmonary fibrosis: causality or casualty? *Therapeutic Advances in Respiratory Disease* **15**
117. Hudson B.I., C. A. M., Harja E., Kalea A.Z., Arriero M., Yang H., Grant P.J., Schmidt A.M. (2008) Identification, classification, and expression of RAGE gene splice variants. *The FASEB Journal* **22**, 1572-1580
118. Yonekura, H., Yamamoto, Y., Sakurai, S., Petrova, R. G., Abedin, M. J., Li, H., Yasui, K., Takeuchi, M., Makita, Z., Takasawa, S., Okamoto, H., Watanabe, T., and Yamamoto, H. (2003) Novel splice variants of the receptor for advanced glycation end-products expressed in human vascular endothelial cells and pericytes, and their putative roles in diabetes-induced vascular injury. *The Biochemical Journal* **370**, 1097-1109
119. Ding, Q., and Keller, J. N. (2005) Evaluation of rage isoforms, ligands, and signaling in the brain. *Biochimica et Biophysica Acta (BBA) - Molecular Cell Research* **1746**, 18-27
120. Sparvero, L. J., Asafu-Adjei, D., Kang, R., Tang, D., Amin, N., Im, J., Rutledge, R., Lin, B., Amoscato, A. A., Zeh, H. J., and Lotze, M. T. (2009) RAGE (Receptor for Advanced Glycation Endproducts), RAGE ligands, and their role in cancer and inflammation. *Journal of Translational Medicine* **7**, 17
121. Harja, E., Bu, D.-x., Hudson, B. I., Chang, J. S., Shen, X., Hallam, K., Kalea, A. Z., Lu, Y., Rosario, R. H., Oruganti, S., Nikolla, Z., Belov, D., Lalla, E., Ramasamy, R., Yan, S. F., and Schmidt, A. M. (2008) Vascular and inflammatory stresses mediate atherosclerosis via RAGE and its ligands in apoE^{-/-} mice. *The Journal of clinical investigation* **118**, 183-194
122. Jangde, N., Ray, R., Sinha, S., Rana, K., Singh, S. K., Khandagale, P., Acharya, N., and Rai, V. (2018) Cysteine mediated disulfide bond formation in RAGE V domain facilitates its functionally relevant dimerization. *Biochimie* **154**, 55-61
123. Wei, W., Lampe, L., Park, S., Vangara, B. S., Waldo, G. S., Cabantous, S., Subaran, S. S., Yang, D., Lakatta, E. G., and Lin, L. (2012) Disulfide Bonds within the C2 Domain of RAGE Play Key Roles in Its Dimerization and Biogenesis. *PLOS ONE* **7**, e50736
124. Yatime, L., and Andersen, G. R. (2013) Structural insights into the oligomerization mode of the human receptor for advanced glycation end-products. *The FEBS Journal* **280**, 6556-6568

125. Moysa, A., Hammerschmid, D., Szczepanowski, R. H., Sobott, F., and Dadlez, M. (2019) Enhanced oligomerization of full-length RAGE by synergy of the interaction of its domains. *Scientific Reports* **9**, 20332
126. Sitkiewicz, E., Tarnowski, K., Poznański, J., Kulma, M., and Dadlez, M. (2013) Oligomerization Interface of RAGE Receptor Revealed by MS-Monitored Hydrogen Deuterium Exchange. *PLOS ONE* **8**, e76353
127. Xie, J., Reverdatto, S., Frolov, A., Hoffmann, R., Burz, D. S., and Shekhtman, A. (2008) Structural basis for pattern recognition by the receptor for advanced glycation end products (RAGE). *Journal of Biological Chemistry* **283**, 27255-27269
128. Wilton, R., Yousef, M. A., Saxena, P., Szpunar, M., and Stevens, F. J. (2006) Expression and purification of recombinant human receptor for advanced glycation endproducts in *Escherichia coli*. *Protein Expression and Purification* **47**, 25-35
129. Degani, G., Barbiroli, A., Magnelli, P., Digiovanni, S., Altomare, A., Aldini, G., and Popolo, L. (2019) Insights into the effects of N-glycosylation on the characteristics of the VC1 domain of the human receptor for advanced glycation end products (RAGE) secreted by *Pichia pastoris*. *Glycoconjugate Journal* **36**, 27-38
130. Land, W. G. (2015) The Role of Damage-Associated Molecular Patterns (DAMPs) in Human Diseases: Part II: DAMPs as diagnostics, prognostics and therapeutics in clinical medicine. *Sultan Qaboos University Medical Journal* **15**, 157-170
131. Jules, J., Maignel, D., and Hudson, B. I. (2013) Alternative Splicing of the RAGE Cytoplasmic Domain Regulates Cell Signaling and Function. *PLOS ONE* **8**, e78267
132. Kim, H. J., Jeong, M. S., and Jang, S. B. (2021) Molecular Characteristics of RAGE and Advances in Small-Molecule Inhibitors. *International Journal of Molecular Sciences* **22**, 6904
133. Zong, H., Madden, A., Ward, M., Mooney, M. H., Elliott, C. T., and Stitt, A. W. (2010) Homodimerization is essential for the receptor for advanced glycation end products (RAGE)-mediated signal transduction. *Journal of Biological Chemistry* **285**, 23137-23146
134. Bongarzone, S., Savickas, V., Luzi, F., and Gee, A. D. (2017) Targeting the Receptor for Advanced Glycation Endproducts (RAGE): A Medicinal Chemistry Perspective. *Journal of medicinal chemistry* **60**, 7213-7232
135. Bianchi, R., Kastrisianaki, E., Giambanco, I., and Donato, R. (2011) S100B protein stimulates microglia migration via RAGE-dependent up-regulation of chemokine expression and release. *Journal of Biological Chemistry* **286**, 7214-7226
136. Sakaguchi, M., Murata, H., Yamamoto, K., Ono, T., Sakaguchi, Y., Motoyama, A., Hibino, T., Kataoka, K., and Huh, N. H. (2011) TIRAP, an adaptor protein for TLR2/4, transduces a signal from RAGE phosphorylated upon ligand binding. *PLOS ONE* **6**, e23132
137. Sorci, G., Riuzzi, F., Giambanco, I., and Donato, R. (2013) RAGE in tissue homeostasis, repair and regeneration. *Biochimica et Biophysica Acta (BBA) - Molecular Cell Research* **1833**, 101-109
138. Rouhiainen, A., Kuja-Panula, J., Tumova, S., and Rauvala, H. (2013) RAGE-mediated cell signaling. *Methods Mol Biol* **963**, 239-263
139. Schmidt, A. M., Yan, S. D., Yan, S. F., and Stern, D. M. (2001) The multiligand receptor RAGE as a progression factor amplifying immune and inflammatory responses. *J Clin Invest* **108**, 949-955

140. Barbel, L.-S., Markus, S., and Peter Nawroth and Angelika, B. (2007) RAGE Signaling in Cell Adhesion and Inflammation. *Current Pediatric Reviews* **3**, 1-9
141. Xue, J., Manigrasso, M., Scalabrin, M., Rai, V., Reverdatto, S., Burz, David S., Fabris, D., Schmidt, Ann M., and Shekhtman, A. (2016) Change in the Molecular Dimension of a RAGE-Ligand Complex Triggers RAGE Signaling. *Structure* **24**, 1509-1522
142. Ramasamy, R., Shekhtman, A., and Schmidt, A. M. (2022) The RAGE/DIAPH1 Signaling Axis & Implications for the Pathogenesis of Diabetic Complications. *International Journal of Molecular Sciences* **23**, 4579
143. Manigrasso, M. B., Rabbani, P., Egaña-Gorroño, L., Quadri, N., Frye, L., Zhou, B., Reverdatto, S., Ramirez, L. S., Dansereau, S., Pan, J., Li, H., D'Agati, V. D., Ramasamy, R., DeVita, R. J., Shekhtman, A., and Schmidt, A. M. (2021) Small-molecule antagonism of the interaction of the RAGE cytoplasmic domain with DIAPH1 reduces diabetic complications in mice. *Sci Transl Med* **13**, eabf7084
144. Manigrasso, M. B., Friedman, R. A., Ramasamy, R., D'Agati, V., and Schmidt, A. M. (2018) Deletion of the formin Diaph1 protects from structural and functional abnormalities in the murine diabetic kidney. *American Journal of Physiology. Renal Physiology* **315**, F1601-F1612
145. Yatime, L., Betzer, C., Jensen, R. K., Mortensen, S., Jensen, P. H., and Andersen, G. R. (2016) The Structure of the RAGE:S100A6 Complex Reveals a Unique Mode of Homodimerization for S100 Proteins. *Structure* **24**, 2043-2052
146. Yan, S. F., Yan, S. D., Ramasamy, R., and Schmidt, A. M. (2009) Tempering the wrath of RAGE: An emerging therapeutic strategy against diabetic complications, neurodegeneration, and inflammation. *Annals of Medicine* **41**, 408-422
147. Litwinoff, E. M. S., Hurtado del Pozo, C., Ramasamy, R., and Schmidt, A. M. (2015) Emerging Targets for Therapeutic Development in Diabetes and Its Complications: The RAGE Signaling Pathway. *Clinical Pharmacology and Therapeutics* **98**, 135-144
148. Schmidt, A. M., Sahagan, B., Nelson, R. B., Selmer, J., Rothlein, R., and Bell, J. M. (2009) The role of RAGE in amyloid-beta peptide-mediated pathology in Alzheimer's disease. *Curr Opin Investig Drugs* **10**, 672-680
149. Ali, T., Badshah, H., Kim, T. H., and Kim, M. O. (2015) Melatonin attenuates D-galactose-induced memory impairment, neuroinflammation and neurodegeneration via RAGE/NF-KB/JNK signaling pathway in aging mouse model. *Journal of Pineal Research* **58**, 71-85
150. Sims, G. P., Rowe, D. C., Rietdijk, S. T., Herbst, R., and Coyle, A. J. (2010) HMGB1 and RAGE in Inflammation and Cancer. *Annual Review of Immunology* **28**, 367-388
151. Nasser, M. W., Wani, N. A., Ahirwar, D. K., Powell, C. A., Ravi, J., Elbaz, M., Zhao, H., Padilla, L., Zhang, X., Shilo, K., Ostrowski, M., Shapiro, C., Carson, W. E., 3rd, and Ganju, R. K. (2015) RAGE mediates S100A7-induced breast cancer growth and metastasis by modulating the tumor microenvironment. *Cancer Res* **75**, 974-985
152. Azizan, N., Suter, M. A., Liu, Y., and Logsdon, C. D. (2017) RAGE maintains high levels of NFκB and oncogenic Kras activity in pancreatic cancer. *Biochemical and Biophysical Research Communications* **493**, 592-597
153. Kay, A. M., Simpson, C. L., and Stewart, J. A., Jr. (2016) The Role of AGE/RAGE Signaling in Diabetes-Mediated Vascular Calcification. *J Diabetes Res* **2016**, 6809703
154. Bucciarelli, L. G., Wendt, T., Qu, W., Lu, Y., Lalla, E., Rong, L. L., Goova, M. T., Moser, B., Kislinger, T., Lee, D. C., Kashyap, Y., Stern, D. M., and Schmidt, A. M.

- (2002) RAGE Blockade Stabilizes Established Atherosclerosis in Diabetic Apolipoprotein E–Null Mice. *Circulation* **106**, 2827-2835
155. Zhang, X., Cheng, M., Tong, F., and Su, X. (2019) Association between RAGE variants and the susceptibility to atherosclerotic lesions in Chinese Han population. *Exp Ther Med* **17**, 2019-2030
 156. Chuah, Y. K., Basir, R., Talib, H., Tie, T. H., and Nordin, N. (2013) Receptor for Advanced Glycation End Products and Its Involvement in Inflammatory Diseases. *International Journal of Inflammation* **2013**, 403460
 157. Fukami, K., Yamagishi, S., and Okuda, S. (2014) Role of AGEs-RAGE system in cardiovascular disease. *Curr Pharm Des* **20**, 2395-2402
 158. Wautier, J. L., and Wautier, M. P. (2020) Cellular and Molecular Aspects of Blood Cell-Endothelium Interactions in Vascular Disorders. *International Journal of Molecular Sciences* **21**
 159. Juranek, J. K., Daffu, G. K., Wojtkiewicz, J., Lacomis, D., Kofler, J., and Schmidt, A. M. (2015) Receptor for Advanced Glycation End Products and its Inflammatory Ligands are Upregulated in Amyotrophic Lateral Sclerosis. *Frontiers in Cellular Neuroscience* **9**, 485
 160. Juranek, J. K., Kothary, P., Mehra, A., Hays, A., Brannagan, T. H., 3rd, and Schmidt, A. M. (2013) Increased expression of the receptor for advanced glycation end-products in human peripheral neuropathies. *Brain Behav* **3**, 701-709
 161. Kouidrat, Y., Amad, A., Arai, M., Miyashita, M., Lalau, J. D., Loas, G., and Itokawa, M. (2015) Advanced glycation end products and schizophrenia: A systematic review. *J Psychiatr Res* **66-67**, 112-117
 162. Deane, R., Du Yan, S., Subramanian, R. K., LaRue, B., Jovanovic, S., Hogg, E., Welch, D., Manness, L., Lin, C., Yu, J., Zhu, H., Ghiso, J., Frangione, B., Stern, A., Schmidt, A. M., Armstrong, D. L., Arnold, B., Liliensiek, B., Nawroth, P., Hofman, F., Kindy, M., Stern, D., and Zlokovic, B. (2003) RAGE mediates amyloid-beta peptide transport across the blood-brain barrier and accumulation in brain. *Nat Med* **9**, 907-913
 163. Sasaki, N., Toki, S., Chowei, H., Saito, T., Nakano, N., Hayashi, Y., Takeuchi, M., and Makita, Z. (2001) Immunohistochemical distribution of the receptor for advanced glycation end products in neurons and astrocytes in Alzheimer's disease. *Brain Res* **888**, 256-262
 164. Kang, R., Hou, W., Zhang, Q., Chen, R., Lee, Y. J., Bartlett, D. L., Lotze, M. T., Tang, D., and Zeh, H. J. (2014) RAGE is essential for oncogenic KRAS-mediated hypoxic signaling in pancreatic cancer. *Cell Death Dis* **5**, e1480
 165. Swami, P., Thiagarajan, S., Vidger, A., Indurthi, V. S. K., Vetter, S. W., and Leclerc, E. (2020) RAGE Up-Regulation Differently Affects Cell Proliferation and Migration in Pancreatic Cancer Cells. *International Journal of Molecular Sciences* **21**, 7723
 166. Nankali, M., Karimi, J., Goodarzi, M. T., Saidijam, M., Khodadadi, I., Razavi, A. N., and Rahimi, F. (2016) Increased Expression of the Receptor for Advanced Glycation End-Products (RAGE) Is Associated with Advanced Breast Cancer Stage. *Oncol Res Treat* **39**, 622-628
 167. Palanissami, G., and Paul, S. F. D. (2018) RAGE and Its Ligands: Molecular Interplay Between Glycation, Inflammation, and Hallmarks of Cancer—a Review. *Hormones and Cancer* **9**, 295-325
 168. Olaoba, O. T., Kadasah, S., Vetter, S. W., and Leclerc, E. (2020) RAGE Signaling in Melanoma Tumors. *International Journal of Molecular Sciences* **21**, 8989

169. Meghnani, V., Vetter, S. W., and Leclerc, E. (2014) RAGE overexpression confers a metastatic phenotype to the WM115 human primary melanoma cell line. *Biochimica et Biophysica Acta (BBA)* **1842**, 1017-1027
170. Li, J., Wu, P.-W., Zhou, Y., Dai, B., Zhang, P.-F., Zhang, Y.-H., Liu, Y., and Shi, X.-L. (2018) Rage induces hepatocellular carcinoma proliferation and sorafenib resistance by modulating autophagy. *Cell Death & Disease* **9**, 225
171. Pusterla, T., Nèmeth, J., Stein, I., Wiechert, L., Knigin, D., Marhenke, S., Longerich, T., Kumar, V., Arnold, B., Vogel, A., Bierhaus, A., Pikarsky, E., Hess, J., and Angel, P. (2013) Receptor for advanced glycation endproducts (RAGE) is a key regulator of oval cell activation and inflammation-associated liver carcinogenesis in mice. *Hepatology* **58**, 363-373
172. El-Far, A. H., Sroga, G., Jaouni, S. K. A., and Mousa, S. A. (2020) Role and Mechanisms of RAGE-Ligand Complexes and RAGE-Inhibitors in Cancer Progression. *International journal of molecular sciences* **21**, 3613
173. Matou-Nasri, S., Sharaf, H., Wang, Q., Almobadel, N., Rabhan, Z., Al-Eidi, H., Yahya, W. B., Trivilegio, T., Ali, R., Al-Shanti, N., and Ahmed, N. (2017) Biological impact of advanced glycation endproducts on estrogen receptor-positive MCF-7 breast cancer cells. *Biochimica et Biophysica Acta (BBA) - Molecular Cell Research* **1863**, 2808-2820
174. Muthyalaiyah, Y. S., Jonnalagadda, B., John, C. M., and Arockiasamy, S. (2021) Impact of Advanced Glycation End products (AGEs) and its receptor (RAGE) on cancer metabolic signaling pathways and its progression. *Glycoconjugate Journal* **38**, 717-734
175. Allegra, A., Musolino, C., Pace, E., Innao, V., Di Salvo, E., Ferraro, M., Casciaro, M., Spatari, G., Tartarisco, G., Allegra, A. G., and Gangemi, S. (2019) Evaluation of the AGE/sRAGE Axis in Patients with Multiple Myeloma. *Antioxidants (Basel, Switzerland)* **8**, 55
176. Ahmad, S., Khan, H., Siddiqui, Z., Khan, M. Y., Rehman, S., Shahab, U., Godovikova, T., Silnikov, V., and Moinuddin. (2018) AGEs, RAGEs and s-RAGE; friend or foe for cancer. *Semin Cancer Biol* **49**, 44-55
177. Yamaguchi, K., Iwamoto, H., Mazur, W., Miura, S., Sakamoto, S., Horimasu, Y., Masuda, T., Miyamoto, S., Nakashima, T., Ohshimo, S., Fujitaka, K., Hamada, H., and Hattori, N. (2020) Reduced endogenous secretory RAGE in blood and bronchoalveolar lavage fluid is associated with poor prognosis in idiopathic pulmonary fibrosis. *Respiratory Research* **21**, 145
178. Machahua, C., Montes-Worboys, A., Llatjos, R., Escobar, I., Dorca, J., Molina-Molina, M., and Vicens-Zygmunt, V. (2016) Increased AGE-RAGE ratio in idiopathic pulmonary fibrosis. *Respiratory Research* **17**, 144
179. Ruiz, H. H., Nguyen, A., Wang, C., He, L., Li, H., Hallowell, P., McNamara, C., and Schmidt, A. M. (2021) AGE/RAGE/DIAPH1 axis is associated with immunometabolic markers and risk of insulin resistance in subcutaneous but not omental adipose tissue in human obesity. *International Journal of Obesity* **45**, 2083-2094
180. Feng, Z., Du, Z., Shu, X., Zhu, L., Wu, J., Gao, Q., Wang, L., Chen, N., Li, Y., Luo, M., Hill, M. A., and Wu, J. (2021) Role of RAGE in obesity-induced adipose tissue inflammation and insulin resistance. *Cell Death Discovery* **7**, 305
181. Ozgor, O., Akoglu, G., Sungu, N., Karaismailoglu, E., and Aktas, A. (2017) Receptor for advanced glycation end products is overexpressed in psoriatic plaques independent of disease severity. *Indian J Dermatol Venereol Leprol* **83**, 556-560

182. Papagrigoraki, A., Maurelli, M., Del Giglio, M., Gisondi, P., and Girolomoni, G. (2017) Advanced Glycation End Products in the Pathogenesis of Psoriasis. *International Journal of Molecular Sciences* **18**, 2471
183. Koyama, H., Yamamoto, H., and Nishizawa, Y. (2007) RAGE and soluble RAGE: potential therapeutic targets for cardiovascular diseases. *Molecular medicine (Cambridge, Mass.)* **13**, 625-635
184. Vazzana, N., Santilli, F., Cuccurullo, C., and Davì, G. (2009) Soluble forms of RAGE in internal medicine. *Internal and Emergency Medicine* **4**, 389-401
185. Tanji, N., Markowitz, G. S., Fu, C., Kislinger, T., Taguchi, A., Pischetsrieder, M., Stern, D., Schmidt, A. M., and D'Agati, V. D. (2000) Expression of advanced glycation end products and their cellular receptor RAGE in diabetic nephropathy and nondiabetic renal disease. *J Am Soc Nephrol* **11**, 1656-1666
186. Wendt, T. M., Tanji, N., Guo, J., Kislinger, T. R., Qu, W., Lu, Y., Bucciarelli, L. G., Rong, L. L., Moser, B., Markowitz, G. S., Stein, G., Bierhaus, A., Liliensiek, B., Arnold, B., Nawroth, P. P., Stern, D. M., D'Agati, V. D., and Schmidt, A. M. (2003) RAGE drives the development of glomerulosclerosis and implicates podocyte activation in the pathogenesis of diabetic nephropathy. *Am J Pathol* **162**, 1123-1137
187. Barile, G. R., Pachydaki, S. I., Tari, S. R., Lee, S. E., Donmoyer, C. M., Ma, W., Rong, L. L., Buciarelli, L. G., Wendt, T., Hörig, H., Hudson, B. I., Qu, W., Weinberg, A. D., Yan, S. F., and Schmidt, A. M. (2005) The RAGE axis in early diabetic retinopathy. *Invest Ophthalmol Vis Sci* **46**, 2916-2924
188. Zhang, J., Xu, X., Rao, N. V., Argyle, B., McCoard, L., Rusho, W. J., Kennedy, T. P., Prestwich, G. D., and Krueger, G. (2011) Novel Sulfated Polysaccharides Disrupt Cathelicidins, Inhibit RAGE and Reduce Cutaneous Inflammation in a Mouse Model of Rosacea. *PLOS ONE* **6**, e16658
189. Cui, L., Cai, Y., Cheng, W., Liu, G., Zhao, J., Cao, H., Tao, H., Wang, Y., Yin, M., Liu, T., Liu, Y., Huang, P., Liu, Z., Li, K., and Zhao, B. (2017) A Novel, Multi-Target Natural Drug Candidate, Matrine, Improves Cognitive Deficits in Alzheimer's Disease Transgenic Mice by Inhibiting A β Aggregation and Blocking the RAGE/A β Axis. *Mol Neurobiol* **54**, 1939-1952
190. Mizumoto, S., Takahashi, J., and Sugahara, K. (2012) Receptor for advanced glycation end products (RAGE) functions as receptor for specific sulfated glycosaminoglycans, and anti-RAGE antibody or sulfated glycosaminoglycans delivered in vivo inhibit pulmonary metastasis of tumor cells. *Journal of Biological Chemistry* **287**, 18985-18994
191. Galasko, D., Bell, J., Mancuso, J. Y., Kupiec, J. W., Sabbagh, M. N., van Dyck, C., Thomas, R. G., Aisen, P. S., and Alzheimer's Disease Cooperative, S. (2014) Clinical trial of an inhibitor of RAGE-A β interactions in Alzheimer disease. *Neurology* **82**, 1536-1542
192. Burstein, A. H., Grimes, I., Galasko, D. R., Aisen, P. S., Sabbagh, M., and Mjalli, A. M. (2014) Effect of TTP488 in patients with mild to moderate Alzheimer's disease. *BMC Neurol* **14**, 12
193. Han, Y. T., Choi, G. I., Son, D., Kim, N. J., Yun, H., Lee, S., Chang, D. J., Hong, H. S., Kim, H., Ha, H. J., Kim, Y. H., Park, H. J., Lee, J., and Suh, Y. G. (2012) Ligand-based design, synthesis, and biological evaluation of 2-aminopyrimidines, a novel series of receptor for advanced glycation end products (RAGE) inhibitors. *J Med Chem* **55**, 9120-9135

194. Han, Y. T., Kim, K., Choi, G. I., An, H., Son, D., Kim, H., Ha, H. J., Son, J. H., Chung, S. J., Park, H. J., Lee, J., and Suh, Y. G. (2014) Pyrazole-5-carboxamides, novel inhibitors of receptor for advanced glycation end products (RAGE). *Eur J Med Chem* **79**, 128-142
195. Deane, R., Singh, I., Sagare, A. P., Bell, R. D., Ross, N. T., LaRue, B., Love, R., Perry, S., Paquette, N., Deane, R. J., Thiyagarajan, M., Zarcone, T., Fritz, G., Friedman, A. E., Miller, B. L., and Zlokovic, B. V. (2012) A multimodal RAGE-specific inhibitor reduces amyloid β -mediated brain disorder in a mouse model of Alzheimer disease. *J Clin Invest* **122**, 1377-1392
196. Braley, A., Kwak, T., Jules, J., Harja, E., Landgraf, R., and Hudson, B. I. (2016) Regulation of Receptor for Advanced Glycation End Products (RAGE) Ectodomain Shedding and Its Role in Cell Function. *Journal of Biological Chemistry* **291**, 12057-12073
197. Arumugam, T., Ramachandran, V., Gomez, S. B., Schmidt, A. M., and Logsdon, C. D. (2012) S100P-derived RAGE antagonistic peptide reduces tumor growth and metastasis. *Clin Cancer Res* **18**, 4356-4364
198. Huttunen, H. J., Fages, C., Kuja-Panula, J., Ridley, A. J., and Rauvala, H. (2002) Receptor for advanced glycation end products-binding COOH-terminal motif of amphoterin inhibits invasive migration and metastasis. *Cancer Res* **62**, 4805-4811
199. Manigrasso, M. B., Pan, J., Rai, V., Zhang, J., Reverdatto, S., Quadri, N., DeVita, R. J., Ramasamy, R., Shekhtman, A., and Schmidt, A. M. (2016) Small Molecule Inhibition of Ligand-Stimulated RAGE-DIAPH1 Signal Transduction. *Scientific Reports* **6**, 22450
200. Zhu, Q., and Smith, E. A. (2019) Diaphanous-1 affects the nanoscale clustering and lateral diffusion of receptor for advanced glycation endproducts (RAGE). *Biochimica et Biophysica Acta (BBA) - Biomembranes* **1861**, 43-49
201. Yan, Z., Luo, H., Xie, B., Tian, T., Li, S., Chen, Z., Liu, J., Zhao, X., Zhang, L., Deng, Y., Billiar, T. R., and Jiang, Y. (2021) Targeting adaptor protein SLP76 of RAGE as a therapeutic approach for lethal sepsis. *Nature Communications* **12**, 308
202. Zheng, J., Zhu, W., He, F., Li, Z., Cai, N., and Wang, H. H. (2021) An Aptamer-Based Antagonist against the Receptor for Advanced Glycation End-Products (RAGE) Blocks Development of Colorectal Cancer. *Mediators Inflamm* **2021**, 9958051
203. Senatus, L. M., and Schmidt, A. M. (2017) The AGE-RAGE Axis: Implications for Age-Associated Arterial Diseases. *Frontiers in Genetics* **8**, 187
204. Deane, R., Singh, I., Sagare, A. P., Bell, R. D., Ross, N. T., LaRue, B., Love, R., Perry, S., Paquette, N., Deane, R. J., Thiyagarajan, M., Zarcone, T., Fritz, G., Friedman, A. E., Miller, B. L., and Zlokovic, B. V. (2012) A multimodal RAGE-specific inhibitor reduces amyloid β -mediated brain disorder in a mouse model of Alzheimer disease. *The Journal of Clinical Investigation* **122**, 1377-1392
205. Demling, N., Ehrhardt, C., Kasper, M., Laue, M., Knels, L., and Rieber, E. P. (2006) Promotion of cell adherence and spreading: a novel function of RAGE, the highly selective differentiation marker of human alveolar epithelial type I cells. *Cell and Tissue Research* **323**, 475-488
206. Buckley, S. T., Medina, C., Kasper, M., and Ehrhardt, C. (2010) Interplay between RAGE, CD44, and focal adhesion molecules in epithelial-mesenchymal transition of alveolar epithelial cells. *American Journal of Physiology-Lung Cellular and Molecular Physiology* **300**, L548-L559

207. Sessa, L., Gatti, E., Zeni, F., Antonelli, A., Catucci, A., Koch, M., Pompilio, G., Fritz, G., Raucci, A., and Bianchi, M. E. (2014) The Receptor for Advanced Glycation End-Products (RAGE) Is Only Present in Mammals, and Belongs to a Family of Cell Adhesion Molecules (CAMs). *PLOS ONE* **9**, e86903
208. Yan, S. F., Ramasamy, R., Naka, Y., and Schmidt, A. M. (2003) Glycation, Inflammation, and RAGE. *Circulation Research* **93**, 1159-1169
209. Srikrishna, G., Nayak, J., Weigle, B., Temme, A., Foell, D., Hazelwood, L., Olsson, A., Volkmann, N., Hanein, D., and Freeze, H. H. (2010) Carboxylated N-glycans on RAGE promote S100A12 binding and signaling. *Journal of cellular biochemistry* **110**, 645-659
210. Videira, P. A. Q., and Castro-Caldas, M. (2018) Linking Glycation and Glycosylation With Inflammation and Mitochondrial Dysfunction in Parkinson's Disease. *Frontiers in Neuroscience* **12**, 381
211. Popa, I., Ganea, E., and Petrescu, S. M. (2014) Expression and subcellular localization of RAGE in melanoma cells. *Biochemistry and Cell Biology* **92**, 127-136
212. Ruelas Cinco, E. D. C., Ruíz Madrigal, B., Domínguez Rosales, J. A., Maldonado González, M., De la Cruz Color, L., Ramírez Meza, S. M., Torres Baranda, J. R., Martínez López, E., and Hernández Nazará, Z. H. (2019) Expression of the receptor of advanced glycation end-products (RAGE) and membranal location in peripheral blood mononuclear cells (PBMC) in obesity and insulin resistance. *Iranian Journal of Basic Medical Sciences* **22**, 623-630
213. Xiong, F., Leonov, S., Howard, A. C., Xiong, S., Zhang, B., Mei, L., McNeil, P., Simon, S., and Xiong, W.-C. (2011) Receptor for advanced glycation end products (RAGE) prevents endothelial cell membrane resealing and regulates F-actin remodeling in a beta-catenin-dependent manner. *Journal of Biological Chemistry* **286**, 35061-35070
214. Linask, K. K., Manisastry, S., and Han, M. (2005) Cross Talk between Cell–Cell and Cell–Matrix Adhesion Signaling Pathways during Heart Organogenesis: Implications for Cardiac Birth Defects. *Microscopy and Microanalysis* **11**, 200-208
215. Sheikh, F., Ross, R. S., and Chen, J. (2009) Cell-Cell Connection to Cardiac Disease. *Trends in Cardiovascular Medicine* **19**, 182-190
216. Brooke, M. A., Nitoiu, D., and Kelsell, D. P. (2012) Cell–cell connectivity: desmosomes and disease. *The Journal of Pathology* **226**, 158-171
217. Waanders, E., Van Krieken, J. H. J. M., Lameris, A. L. L., and Drenth, J. P. H. (2008) Disrupted cell adhesion but not proliferation mediates cyst formation in polycystic liver disease. *Modern Pathology* **21**, 1293-1302
218. Onori, P., Franchitto, A., Mancinelli, R., Carpino, G., Alvaro, D., Francis, H., Alpini, G., and Gaudio, E. (2010) Polycystic liver diseases. *Digestive and Liver Disease* **42**, 261-271
219. Sousa, B., Pereira, J., and Paredes, J. (2019) The Crosstalk Between Cell Adhesion and Cancer Metabolism. *International Journal of Molecular Sciences* **20**, 1933
220. Schwager, S. C., Taufalele, P. V., and Reinhart-King, C. A. (2019) Cell–Cell Mechanical Communication in Cancer. *Cellular and Molecular Bioengineering* **12**, 1-14
221. Cavallaro, U., and Christofori, G. (2004) Cell adhesion and signalling by cadherins and Ig-CAMs in cancer. *Nature Reviews Cancer* **4**, 118-132
222. Tang, J., Hu, M., Lee, S., and Roblin, R. (2000) A polymerase chain reaction based method for detecting Mycoplasma/Acholeplasma contaminants in cell culture. *Journal of Microbiological Methods* **39**, 121-126

223. Pfaffl, M. W. (2001) A new mathematical model for relative quantification in real-time RT-PCR. *Nucleic Acids Research* **29**, e45
224. Zeng, Y., Ramya, T. N. C., Dirksen, A., Dawson, P. E., and Paulson, J. C. (2009) High-efficiency labeling of sialylated glycoproteins on living cells. *Nature methods* **6**, 207-209
225. Hörmann, K., Stukalov, A., Müller, A. C., Heinz, L. X., Superti-Furga, G., Colinge, J., and Bennett, K. L. (2016) A Surface Biotinylation Strategy for Reproducible Plasma Membrane Protein Purification and Tracking of Genetic and Drug-Induced Alterations. *Journal of Proteome Research* **15**, 647-658
226. Ura, K., Soyano, K., Omoto, N., Adachi, S., and Yamauchi, K. (1996) Localization of Na⁺, K⁽⁺⁾-ATPase in tissues of rabbit and teleosts using an antiserum directed against a partial sequence of the alpha-subunit. *Zoolog Sci* **13**, 219-227
227. Milutinovic, P. S., Englert, J. M., Crum, L. T., Mason, N. S., Ramsgaard, L., Enghild, J. J., Sparvero, L. J., Lotze, M. T., and Oury, T. D. (2014) Clearance kinetics and matrix binding partners of the receptor for advanced glycation end products. *PLOS ONE* **9**, e88259
228. Longo, P. A., Kavran, J. M., Kim, M. S., and Leahy, D. J. (2013) Transient mammalian cell transfection with polyethylenimine (PEI). *Methods Enzymol* **529**, 227-240
229. Lin, Y.-C., Boone, M., Meuris, L., Lemmens, I., Van Roy, N., Soete, A., Reumers, J., Moisse, M., Plaisance, S., Drmanac, R., Chen, J., Speleman, F., Lambrechts, D., Van de Peer, Y., Tavernier, J., and Callewaert, N. (2014) Genome dynamics of the human embryonic kidney 293 lineage in response to cell biology manipulations. *Nature Communications* **5**, 4767
230. Zhang, L. B., Monika Kojro, Elzbieta Roth, Annette Metz, Verena V. Fahrenholz, Falk Nawroth, Peter P. Bierhaus, Angelika Postina, Rolf. (2008) Receptor for Advanced Glycation End Products Is Subjected to Protein Ectodomain Shedding by Metalloproteinases. *Journal of Biological Chemistry* **283**, 35507-35516
231. Raucci, A., Cugusi, S., Antonelli, A., Barabino, S. M., Monti, L., Bierhaus, A., Reiss, K., Saftig, P., and Bianchi, M. E. (2008) A soluble form of the receptor for advanced glycation endproducts (RAGE) is produced by proteolytic cleavage of the membrane-bound form by the sheddase a disintegrin and metalloprotease 10 (ADAM10). *The FASEB Journal* **22**, 3716-3727
232. Galichet, A., Weibel, M., and Heizmann, C. W. (2008) Calcium-regulated intramembrane proteolysis of the RAGE receptor. *Biochemical and Biophysical Research Communications* **370**, 1-5
233. Metz, V. V., Kojro, E., Rat, D., and Postina, R. (2012) Induction of RAGE Shedding by Activation of G Protein-Coupled Receptors. *PLOS ONE* **7**, e41823
234. Zong, H., Madden, A., Ward, M., Mooney, M. H., Elliott, C. T., and Stitt, A. W. (2010) Homodimerization is essential for the receptor for advanced glycation end products (RAGE)-mediated signal transduction. *The Journal of biological chemistry* **285**, 23137-23146
235. Xie, J., Méndez, J. D., Méndez-Valenzuela, V., and Aguilar-Hernández, M. M. (2013) Cellular signalling of the receptor for advanced glycation end products (RAGE). *Cellular Signalling* **25**, 2185-2197
236. Al-Robaiy, S., Weber, B., Simm, A., Diez, C., Rolewska, P., Silber, R. E., and Bartling, B. (2013) The receptor for advanced glycation end-products supports lung tissue biomechanics. *Am J Physiol Lung Cell Mol Physiol* **305**, 491-500

237. Au - Rahim, S., and Au - Üren, A. (2011) A Real-time Electrical Impedance Based Technique to Measure Invasion of Endothelial Cell Monolayer by Cancer Cells. *JoVE*, e2792
238. Xie, J., Reverdatto, S., Frolov, A., Hoffmann, R., Burz, D. S., and Shekhtman, A. (2008) Structural basis for pattern recognition by the receptor for advanced glycation end products (RAGE). *J Biol Chem* **283**, 27255-27269
239. Hudson, B. I., Kalea, A. Z., Del Mar Arriero, M., Harja, E., Boulanger, E., D'Agati, V., and Schmidt, A. M. (2008) Interaction of the RAGE cytoplasmic domain with diaphanous-1 is required for ligand-stimulated cellular migration through activation of Rac1 and Cdc42. *Journal of Biological Chemistry* **283**, 34457-34468
240. Yamamoto, K., Murata, H., Putranto, E. W., Kataoka, K., Motoyama, A., Hibino, T., Inoue, Y., Sakaguchi, M., and Huh, N. H. (2013) DOCK7 is a critical regulator of the RAGE-Cdc42 signaling axis that induces formation of dendritic pseudopodia in human cancer cells. *Oncol Rep* **29**, 1073-1079
241. Ishihara, K., Tsutsumi, K., Kawane, S., Nakajima, M., and Kasaoka, T. (2003) The receptor for advanced glycation end-products (RAGE) directly binds to ERK by a D-domain-like docking site. *The FEBS letters* **550**, 107-113
242. Riuzzi, F., Sorci, G., and Donato, R. (2006) The amphoterin (HMGB1)/receptor for advanced glycation end products (RAGE) pair modulates myoblast proliferation, apoptosis, adhesiveness, migration, and invasiveness. Functional inactivation of RAGE in L6 myoblasts results in tumor formation in vivo. *Journal of Biological Chemistry* **281**, 8242-8253
243. Serban, A. I., Stanca, L., Geicu, O. I., Munteanu, M. C., and Dinischiotu, A. (2016) RAGE and TGF- β 1 Cross-Talk Regulate Extracellular Matrix Turnover and Cytokine Synthesis in AGEs Exposed Fibroblast Cells. *PLOS ONE* **11**, e0152376
244. Winden, D. R., Ferguson, N. T., Bukey, B. R., Geyer, A. J., Wright, A. J., Jergensen, Z. R., Robinson, A. B., Stogsdill, J. A., and Reynolds, P. R. (2013) Conditional over-expression of RAGE by embryonic alveolar epithelium compromises the respiratory membrane and impairs endothelial cell differentiation. *Respiratory Research* **14**, 108
245. Kapeller, M., Gal-Oz, R., Grover, N. B., and Doljanski, F. (1973) Natural shedding of carbohydrate-containing macromolecules from cell surfaces. *Exp Cell Res* **79**, 152-158
246. Black, P. H. (1980) Shedding from normal and cancer-cell surfaces. *N Engl J Med* **303**, 1415-1416
247. Arribas, J., Coodly, L., Vollmer, P., Kishimoto, T. K., Rose-John, S., and Massagué, J. (1996) Diverse cell surface protein ectodomains are shed by a system sensitive to metalloprotease inhibitors. *Journal of Biological Chemistry* **271**, 11376-11382
248. Hayashida, K., Bartlett, A. H., Chen, Y., and Park, P. W. (2010) Molecular and cellular mechanisms of ectodomain shedding. *Anat Rec (Hoboken)* **293**, 925-937
249. Kheradmand, F., and Werb, Z. (2002) Shedding light on sheddases: role in growth and development. *Bioessays* **24**, 8-12
250. Weber, S., and Saftig, P. (2012) Ectodomain shedding and ADAMs in development. *Development* **139**, 3693-3709
251. Maretzky, T., Reiss, K., Ludwig, A., Buchholz, J., Scholz, F., Proksch, E., de Strooper, B., Hartmann, D., and Saftig, P. (2005) ADAM10 mediates E-cadherin shedding and regulates epithelial cell-cell adhesion, migration, and beta-catenin translocation. *Proc Natl Acad Sci USA* **102**, 9182-9187

252. Reiss, K., Maretzky, T., Ludwig, A., Tousseyn, T., de Strooper, B., Hartmann, D., and Saftig, P. (2005) ADAM10 cleavage of N-cadherin and regulation of cell-cell adhesion and beta-catenin nuclear signalling. *Embo j* **24**, 742-752
253. McGuire, J. K., Li, Q., and Parks, W. C. (2003) Matrilysin (matrix metalloproteinase-7) mediates E-cadherin ectodomain shedding in injured lung epithelium. *Am J Pathol* **162**, 1831-1843
254. Symowicz, J., Adley, B. P., Gleason, K. J., Johnson, J. J., Ghosh, S., Fishman, D. A., Hudson, L. G., and Stack, M. S. (2007) Engagement of collagen-binding integrins promotes matrix metalloproteinase-9-dependent E-cadherin ectodomain shedding in ovarian carcinoma cells. *Cancer Res* **67**, 2030-2039
255. Brown, M. S., Ye, J., Rawson, R. B., and Goldstein, J. L. (2000) Regulated Intramembrane Proteolysis: A Control Mechanism Conserved from Bacteria to Humans. *Cell* **100**, 391-398
256. Langosch, D., Scharnagl, C., Steiner, H., and Lemberg, M. K. (2015) Understanding intramembrane proteolysis: from protein dynamics to reaction kinetics. *Trends Biochem Sci* **40**, 318-327
257. De Strooper, B., Saftig, P., Craessaerts, K., Vanderstichele, H., Guhde, G., Annaert, W., Von Figura, K., and Van Leuven, F. (1998) Deficiency of presenilin-1 inhibits the normal cleavage of amyloid precursor protein. *Nature* **391**, 387-390
258. De Strooper, B., Annaert, W., Cupers, P., Saftig, P., Craessaerts, K., Mumm, J. S., Schroeter, E. H., Schrijvers, V., Wolfe, M. S., Ray, W. J., Goate, A., and Kopan, R. (1999) A presenilin-1-dependent gamma-secretase-like protease mediates release of Notch intracellular domain. *Nature* **398**, 518-522
259. Lammich, S., Okochi, M., Takeda, M., Kaether, C., Capell, A., Zimmer, A. K., Edbauer, D., Walter, J., Steiner, H., and Haass, C. (2002) Presenilin-dependent intramembrane proteolysis of CD44 leads to the liberation of its intracellular domain and the secretion of an Abeta-like peptide. *Journal of Biological Chemistry* **277**, 44754-44759
260. Maetzel, D., Denzel, S., Mack, B., Canis, M., Went, P., Benk, M., Kieu, C., Papior, P., Baeuerle, P. A., Munz, M., and Gires, O. (2009) Nuclear signalling by tumour-associated antigen EpCAM. *Nature Cell Biology* **11**, 162-171
261. Laurent, S. A., Hoffmann, F. S., Kuhn, P. H., Cheng, Q., Chu, Y., Schmidt-Supprian, M., Hauck, S. M., Schuh, E., Krumbholz, M., Rübsamen, H., Wanngren, J., Khademi, M., Olsson, T., Alexander, T., Hiepe, F., Pfister, H. W., Weber, F., Jenne, D., Wekerle, H., Hohlfeld, R., Lichtenthaler, S. F., and Meinl, E. (2015) γ -Secretase directly sheds the survival receptor BCMA from plasma cells. *Nature Communications* **6**, 7333
262. McCarthy, A. J., Coleman-Vaughan, C., and McCarthy, J. V. (2017) Regulated intramembrane proteolysis: emergent role in cell signalling pathways. *Biochemical Society Transactions* **45**, 1185-1202
263. Jones, J. C., Rustagi, S., and Dempsey, P. J. (2016) ADAM proteases and gastrointestinal function. *Annual review of physiology* **78**, 243-276
264. Reiss, K., and Saftig, P. (2009) The "a disintegrin and metalloprotease" (ADAM) family of sheddases: physiological and cellular functions. *Semin Cell Dev Biol* **20**, 126-137
265. Armanious, H., Gelebart, P., Anand, M., Belch, A., and Lai, R. (2011) Constitutive activation of metalloproteinase ADAM10 in mantle cell lymphoma promotes cell growth and activates the TNF α /NF κ B pathway. *Blood* **117**, 6237-6246

266. Meyer-Schwesinger, C., Seipold, L., and Saftig, P. (2022) Ectodomain shedding by ADAM proteases as a central regulator in kidney physiology and disease. *Biochimica et Biophysica Acta (BBA) - Molecular Cell Research* **1869**, 119165
267. Lal, M., and Caplan, M. (2011) Regulated Intramembrane Proteolysis: Signaling Pathways and Biological Functions. *Physiology* **26**, 34-44
268. Yang, W. S., Kim, J. J., Lee, M. J., Lee, E. K., and Park, S. K. (2018) Ectodomain Shedding of RAGE and TLR4 as a Negative Feedback Regulation in High-Mobility Group Box 1-Activated Aortic Endothelial Cells. *Cellular Physiology and Biochemistry* **51**, 1632-1644
269. Zhang, L., Postina, R., and Wang, Y. (2009) Ectodomain shedding of the receptor for advanced glycation end products: a novel therapeutic target for Alzheimer's disease. *Cellular and Molecular Life Sciences* **66**, 3923-3935
270. Geroldi, D., Falcone, C., Emanuele, E., D'Angelo, A., Calcagnino, M., Buzzi, M. P., Scioli, G. A., and Fogari, R. (2005) Decreased plasma levels of soluble receptor for advanced glycation end-products in patients with essential hypertension. *J Hypertens* **23**, 1725-1729
271. Falcone, C., Emanuele, E., D'Angelo, A., Buzzi, M. P., Belvito, C., Cuccia, M., and Geroldi, D. (2005) Plasma levels of soluble receptor for advanced glycation end products and coronary artery disease in nondiabetic men. *Arterioscler Thromb Vasc Biol* **25**, 1032-1037
272. Qin, J., Goswami, R., Dawson, S., and Dawson, G. (2008) Expression of the receptor for advanced glycation end products in oligodendrocytes in response to oxidative stress. *Journal of neuroscience research* **86**, 2414-2422
273. Dwir, D., Giangreco, B., Xin, L., Tenenbaum, L., Cabungcal, J.-H., Steullet, P., Goupil, A., Cleusix, M., Jenni, R., Chtarto, A., Baumann, P. S., Klauser, P., Conus, P., Tirouvanziam, R., Cuenod, M., and Do, K. Q. (2020) MMP9/RAGE pathway overactivation mediates redox dysregulation and neuroinflammation, leading to inhibitory/excitatory imbalance: a reverse translation study in schizophrenia patients. *Molecular Psychiatry* **25**, 2889-2904
274. Lin, J. R., and Hu, J. (2013) SeqNLS: nuclear localization signal prediction based on frequent pattern mining and linear motif scoring. *PLOS ONE* **8**, e76864
275. Miyawaki, A., Sawano, A., and Kogure, T. (2003) Lighting up cells: labelling proteins with fluorophores. *Nature Cell Biology Suppl*, S1-7
276. Scott, M. S., Troshin, P. V., and Barton, G. J. (2011) NoD: a Nucleolar localization sequence detector for eukaryotic and viral proteins. *BMC Bioinformatics* **12**, 317
277. Sevillano, N., Girón, M. D., Salido, M., Vargas, A. M., Vilches, J., and Salto, R. (2009) Internalization of the receptor for advanced glycation end products (RAGE) is required to mediate intracellular responses. *Journal of Biological Chemistry* **145**, 21-30
278. Bertheloot, D., Naumovski, A. L., Langhoff, P., Horvath, G. L., Jin, T., Xiao, T. S., Garbi, N., Agrawal, S., Kolbeck, R., and Latz, E. (2016) RAGE Enhances TLR Responses through Binding and Internalization of RNA. *The Journal of Immunology* **197**, 4118-4126
279. Lecker, S. H., Goldberg, A. L., and Mitch, W. E. (2006) Protein degradation by the ubiquitin-proteasome pathway in normal and disease states. *J Am Soc Nephrol* **17**, 1807-1819

280. Mangan, H., Gailín, M. Ó., and McStay, B. (2017) Integrating the genomic architecture of human nucleolar organizer regions with the biophysical properties of nucleoli. *The FEBS journal* **284**, 3977-3985
281. Yang, K., Yang, J., and Yi, J. (2018) Nucleolar Stress: hallmarks, sensing mechanism and diseases. *Cell stress* **2**, 125-140
282. Pfister, A. S. (2019) Emerging Role of the Nucleolar Stress Response in Autophagy. *Frontiers in Cellular Neuroscience* **13**, 156
283. Kang, R., Tang, D., Lotze, M. T., and Zeh, H. J., 3rd. (2011) RAGE regulates autophagy and apoptosis following oxidative injury. *Autophagy* **7**, 442-444
284. Swami, P., O'Connell, K. A., Thiyagarajan, S., Crawford, A., Patil, P., Radhakrishnan, P., Shin, S., Caffrey, T. C., Grunkemeyer, J., Neville, T., Vetter, S. W., Hollingsworth, M. A., and Leclerc, E. (2021) Inhibition of the Receptor for Advanced Glycation End Products Enhances the Cytotoxic Effect of Gemcitabine in Murine Pancreatic Tumors. *Biomolecules* **11**, 526
285. Beccafico, S., RiuZZi, F., Puglielli, C., Mancinelli, R., Fulle, S., Sorci, G., and Donato, R. (2011) Human muscle satellite cells show age-related differential expression of S100B protein and RAGE. *AGE* **33**, 523-541
286. Adamopoulos, C., Piperi, C., Gargalionis, A. N., Dalagiorgou, G., Spilioti, E., Korkolopoulou, P., Diamanti-Kandarakis, E., and Papavassiliou, A. G. (2016) Advanced glycation end products upregulate lysyl oxidase and endothelin-1 in human aortic endothelial cells via parallel activation of ERK1/2-NF- κ B and JNK-AP-1 signaling pathways. *Cell Mol Life Sci* **73**, 1685-1698
287. Chen, C.-Y., Abell, A. M., Moon, Y. S., and Kim, K.-H. (2012) An Advanced Glycation End Product (AGE)-Receptor for AGEs (RAGE) Axis Restores Adipogenic Potential of Senescent Preadipocytes through Modulation of p53 Protein Function. *Journal of Biological Chemistry* **287**, 44498-44507
288. Peng, Y., Kim, J.-M., Park, H.-S., Yang, A., Islam, C., Lakatta, E. G., and Lin, L. (2016) AGE-RAGE signal generates a specific NF- κ B RelA “barcode” that directs collagen I expression. *Scientific Reports* **6**, 18822
289. Ruoslahti, E. (1996) RGD and other recognition sequences for integrins. *Annual Review of Cell and Developmental Biology* **12**, 697-715
290. Elango, J., Hou, C., Bao, B., Wang, S., Maté Sánchez de Val, J. E., and Wenhui, W. (2022) The Molecular Interaction of Collagen with Cell Receptors for Biological Function. *Polymers* **14**
291. Radonić, A., Thulke, S., Mackay, I. M., Landt, O., Siegert, W., and Nitsche, A. (2004) Guideline to reference gene selection for quantitative real-time PCR. *Biochemical and Biophysical Research Communications* **313**, 856-862
292. Kozera, B., and Rapacz, M. (2013) Reference genes in real-time PCR. *Journal of Applied Genetics* **54**, 391-406
293. Dheda, K., Huggett, J. F., Bustin, S. A., Johnson, M. A., Rook, G., and Zumla, A. (2004) Validation of housekeeping genes for normalizing RNA expression in real-time PCR. *BioTechniques* **37**, 112-119
294. Dal Canton, A. (1995) Adhesion molecules in renal disease. *Kidney International* **48**, 1687-1696
295. Muller, U., and Brandli, A. W. (1999) Cell adhesion molecules and extracellular-matrix constituents in kidney development and disease. *Journal of Cell Science* **112**, 3855-3867

296. Boguslawska, J., Kedzierska, H., Poplawski, P., Rybicka, B., Tanski, Z., and Piekielko-Witkowska, A. (2016) Expression of Genes Involved in Cellular Adhesion and Extracellular Matrix Remodeling Correlates with Poor Survival of Patients with Renal Cancer. *Journal of Urology* **195**, 1892-1902
297. Schnapp, L. M., Hatch, N., Ramos, D. M., Klimanskaya, I. V., Sheppard, D., and Pytela, R. (1995) The human integrin alpha 8 beta 1 functions as a receptor for tenascin, fibronectin, and vitronectin. *Journal of Biological Chemistry* **270**, 23196-23202
298. Marek, I., Hilgers, K. F., Rascher, W., Woelfle, J., and Hartner, A. (2020) A role for the alpha-8 integrin chain (itga8) in glomerular homeostasis of the kidney. *Molecular and cellular pediatrics* **7**, 13-13
299. Shimoda, Y., and Watanabe, K. (2009) Contactins: emerging key roles in the development and function of the nervous system. *Cell Adh Migr* **3**, 64-70
300. Mohebiny, A. N., Harroch, S., and Bouyain, S. (2014) New Insights into the Roles of the Contactin Cell Adhesion Molecules in Neural Development. in *Cell Adhesion Molecules: Implications in Neurological Diseases* (Berezin, V., and Walmod, P. S. eds.), Springer New York, New York, NY. pp 165-194
301. Bossy, B., Bossy-Wetzel, E., and Reichardt, L. F. (1991) Characterization of the integrin alpha 8 subunit: a new integrin beta 1-associated subunit, which is prominently expressed on axons and on cells in contact with basal laminae in chick embryos. *Embo j* **10**, 2375-2385
302. Schnapp, L. M., Breuss, J. M., Ramos, D. M., Sheppard, D., and Pytela, R. (1995) Sequence and tissue distribution of the human integrin alpha 8 subunit: a beta 1-associated alpha subunit expressed in smooth muscle cells. *Journal of Cell Science* **108** (Pt 2), 537-544
303. Varnum-Finney, B., Venstrom, K., Muller, U., Kypta, R., Backus, C., Chiquet, M., and Reichardt, L. F. (1995) The integrin receptor alpha 8 beta 1 mediates interactions of embryonic chick motor and sensory neurons with tenascin-C. *Neuron* **14**, 1213-1222
304. Hartner, A., and Dötsch, J. (2002) Lessons in congenital and acquired renal disease from alpha8 integrin mutant mice. *Pediatr Nephrol* **17**, 882-888
305. Brandenberger, R., Schmidt, A., Linton, J., Wang, D., Backus, C., Denda, S., Müller, U., and Reichardt, L. F. (2001) Identification and characterization of a novel extracellular matrix protein nephronectin that is associated with integrin alpha8beta1 in the embryonic kidney. *The Journal of Cell Biology* **154**, 447-458
306. Gu, Y., Li, T., Kapoor, A., Major, P., and Tang, D. (2020) Contactin 1: An Important and Emerging Oncogenic Protein Promoting Cancer Progression and Metastasis. *Genes* **11**, 874
307. Meneghini, V., Bortolotto, V., Francese, M. T., Dellarole, A., Carraro, L., Terzieva, S., and Grilli, M. (2013) High-mobility group box-1 protein and β -amyloid oligomers promote neuronal differentiation of adult hippocampal neural progenitors via receptor for advanced glycation end products/nuclear factor- κ B axis: relevance for Alzheimer's disease. *J Neurosci* **33**, 6047-6059
308. Piras, S., Furfaro, A. L., Domenicotti, C., Traverso, N., Marinari, U. M., Pronzato, M. A., and Nitti, M. (2016) RAGE Expression and ROS Generation in Neurons: Differentiation versus Damage. *Oxidative Medicine and Cellular Longevity* **2016**, 9348651-9348651

309. Ryu, J., Koh, Y., Park, H., Kim, D. Y., Kim, D. C., Byun, J. M., Lee, H. J., and Yoon, S.-S. (2016) Highly Expressed Integrin- $\alpha 8$ Induces Epithelial to Mesenchymal Transition-Like Features in Multiple Myeloma with Early Relapse. *Molecules and cells* **39**, 898-908
310. Yan, J., Wong, N., Hung, C., Chen, W. X., and Tang, D. (2013) Contactin-1 reduces E-cadherin expression via activating AKT in lung cancer. *PLOS ONE* **8**, e65463
311. Liang, Y., Ma, C., Li, F., Nie, G., and Zhang, H. (2020) The Role of Contactin 1 in Cancers: What We Know So Far. *Frontiers in Oncology* **10**, 574208-574208
312. Chen, M.-C., Chen, K.-C., Chang, G.-C., Lin, H., Wu, C.-C., Kao, W.-H., Teng, C.-L. J., Hsu, S.-L., and Yang, T.-Y. (2020) RAGE acts as an oncogenic role and promotes the metastasis of human lung cancer. *Cell Death & Disease* **11**, 265
313. To, W. S., and Midwood, K. S. (2011) Plasma and cellular fibronectin: distinct and independent functions during tissue repair. *Fibrogenesis & Tissue Repair* **4**, 21
314. Kyriakides, T. R., and Maclachlan, S. (2009) The role of thrombospondins in wound healing, ischemia, and the foreign body reaction. *Journal of Cell Communication and Signaling* **3**, 215-225
315. Li, Y., Wang, Y., Mao, J., Yao, Y., Wang, K., Qiao, Q., Fang, Z., and Ye, M. (2019) Sensitive profiling of cell surface proteome by using an optimized biotinylation method. *Journal of Proteomics* **196**, 33-41
316. Ghosh, D., Funk, C. C., Caballero, J., Shah, N., Rouleau, K., Earls, J. C., Soroceanu, L., Foltz, G., Cobbs, C. S., Price, N. D., and Hood, L. (2017) A Cell-Surface Membrane Protein Signature for Glioblastoma. *Cell Syst* **4**, 516-529.e517
317. Leung, K. K., Wilson, G. M., Kirkemo, L. L., Riley, N. M., Coon, J. J., and Wells, J. A. (2020) Broad and thematic remodeling of the surfaceome and glycoproteome on isogenic cells transformed with driving proliferative oncogenes. *Proceedings of the National Academy of Sciences* **117**, 7764-7775
318. Frommhold, D., Kamphues, A., Dannenberg, S., Buschmann, K., Zablotzkaya, V., Tschada, R., Lange-Sperandio, B., Nawroth, P. P., Poeschl, J., Bierhaus, A., and Sperandio, M. (2011) RAGE and ICAM-1 differentially control leukocyte recruitment during acute inflammation in a stimulus-dependent manner. *BMC Immunology* **12**, 56
319. Schmidt, A. M., Yan, S. D., Brett, J., Mora, R., Nowygrod, R., and Stern, D. (1993) Regulation of human mononuclear phagocyte migration by cell surface-binding proteins for advanced glycation end products. *J Clin Invest* **91**, 2155-2168
320. Liu, Y., Beyer, A., and Aebersold, R. (2016) On the Dependency of Cellular Protein Levels on mRNA Abundance. *Cell* **165**, 535-550
321. Chen, D.-H., Yu, J.-W., and Jiang, B.-J. (2015) Contactin 1: A potential therapeutic target and biomarker in gastric cancer. *World journal of gastroenterology* **21**, 9707-9716
322. Kierdorf, K., and Fritz, G. (2013) RAGE regulation and signaling in inflammation and beyond. *J Leukoc Biol* **94**, 55-68
323. Yamano, S., Dai, J., and Moursi, A. M. (2010) Comparison of transfection efficiency of nonviral gene transfer reagents. *Mol Biotechnol* **46**, 287-300
324. Takada, M., Hirata, K., Ajiki, T., Suzuki, Y., and Kuroda, Y. (2004) Expression of receptor for advanced glycation end products (RAGE) and MMP-9 in human pancreatic cancer cells. *Hepatogastroenterology* **51**, 928-930
325. Walsh, N., Clynes, M., Crown, J., and O'Donovan, N. (2009) Alterations in integrin expression modulates invasion of pancreatic cancer cells. *Journal of Experimental & Clinical Cancer Research* **28**, 140-140

326. Kim, E. Y., and Dryer, S. E. (2021) RAGE and α V β 3-integrin are essential for suPAR signaling in podocytes. *Biochimica et Biophysica Acta (BBA) - Molecular Basis of Disease* **1867**, 166186
327. Nasser, M. W., Wani, N. A., Ahirwar, D. K., Powell, C. A., Ravi, J., Elbaz, M., Zhao, H., Padilla, L., Zhang, X., Shilo, K., Ostrowski, M., Shapiro, C., Carson, W. E., and Ganju, R. K. (2015) RAGE Mediates S100A7-Induced Breast Cancer Growth and Metastasis by Modulating the Tumor Microenvironment. *Cancer Research* **75**, 974
328. Chen, J., Sun, Z., Jin, M., Tu, Y., Wang, S., Yang, X., Chen, Q., Zhang, X., Han, Y., and Pi, R. (2017) Inhibition of AGEs/RAGE/Rho/ROCK pathway suppresses non-specific neuroinflammation by regulating BV2 microglial M1/M2 polarization through the NF- κ B pathway. *Journal of Neuroimmunology* **305**, 108-114
329. Hudson, B. I., and Lippman, M. E. (2018) Targeting RAGE Signaling in Inflammatory Disease. *Annual Review of Medicine* **69**, 349-364
330. Nasser, M. W., Ahirwar, D. K., and Ganju, R. K. (2016) RAGE: A novel target for breast cancer growth and metastasis. *Oncoscience* **3**, 52-53
331. Guo, P., Moses-Gardner, A., Huang, J., Smith, E. R., and Moses, M. A. (2019) ITGA2 as a potential nanotherapeutic target for glioblastoma. *Scientific Reports* **9**, 6195
332. Liu, F., Zhang, J., Deng, Y., Wang, D., Lu, Y., and Yu, X. (2011) Detection of EGFR on living human gastric cancer BGC823 cells using surface plasmon resonance phase sensing. *Sensors and Actuators B: Chemical* **153**, 398-403
333. Valcarce, C., Dunn, I., and Burstein, A. H. (2019) Linking diabetes and Alzheimer's disease through rage: a retrospective analysis of Azeliragon Phase 2 and Phase 3 studies. in *Alzheimer's Association International Conference*, 7S_Part_24 Ed.

APPENDIX A. SUPPLEMENTAL FIGURES

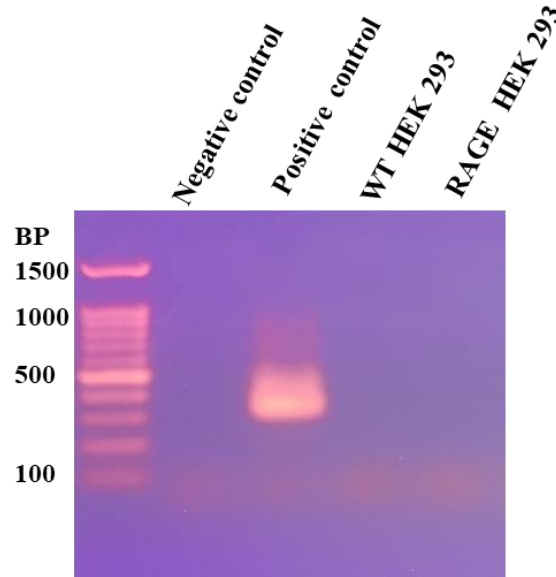


Figure A1: Agarose gel (1.5%) with the PCR products amplified from mycoplasma primers. For details, refer to cell culture conditions in chapter 2. Only the positive sample showed the PCR product, which is a single DNA amplicon ranging in 236-365 base pairs (bp). Wild type (WT) HEK 293 cells and RAGE stably transfected HEK 293 cells (RAGE HEK 293) were negative for mycoplasma contamination.

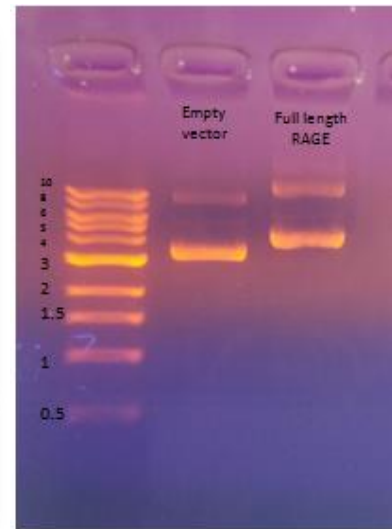
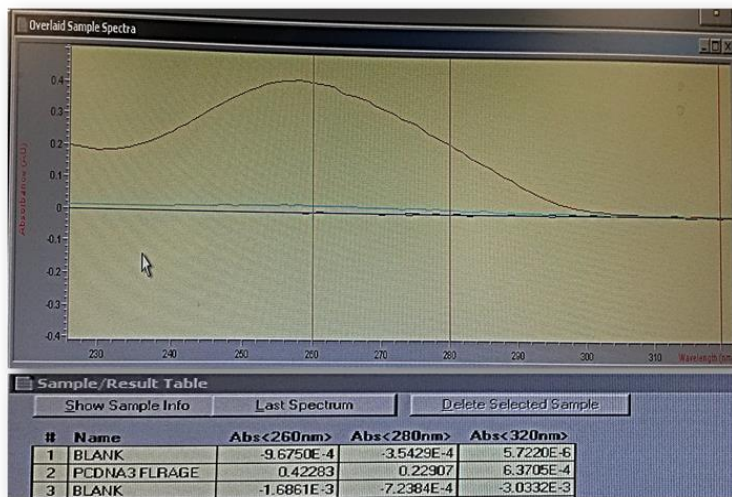


Figure A2: UV spectra of the pcDNA3 FL-RAGE plasmid (left). Extracted plasmids pcDNA3 empty vector (MOCK) and pcDNA3 full length (FL)-RAGE ran on a agarose gel (0.8%) with a 10Kbp DNA ladder (New England Biolabs) (right).

The quality of extracted plasmid was determined using the absorbance ratio of 260 to 280 nm ($0.42/0.23 = \sim 1.8$). Plasmid with a 260/280 ratio of ~ 1.8 is generally accepted as “pure” for DNA. It was observed that the plasmid sample containing FL-RAGE ran higher than the mock plasmid

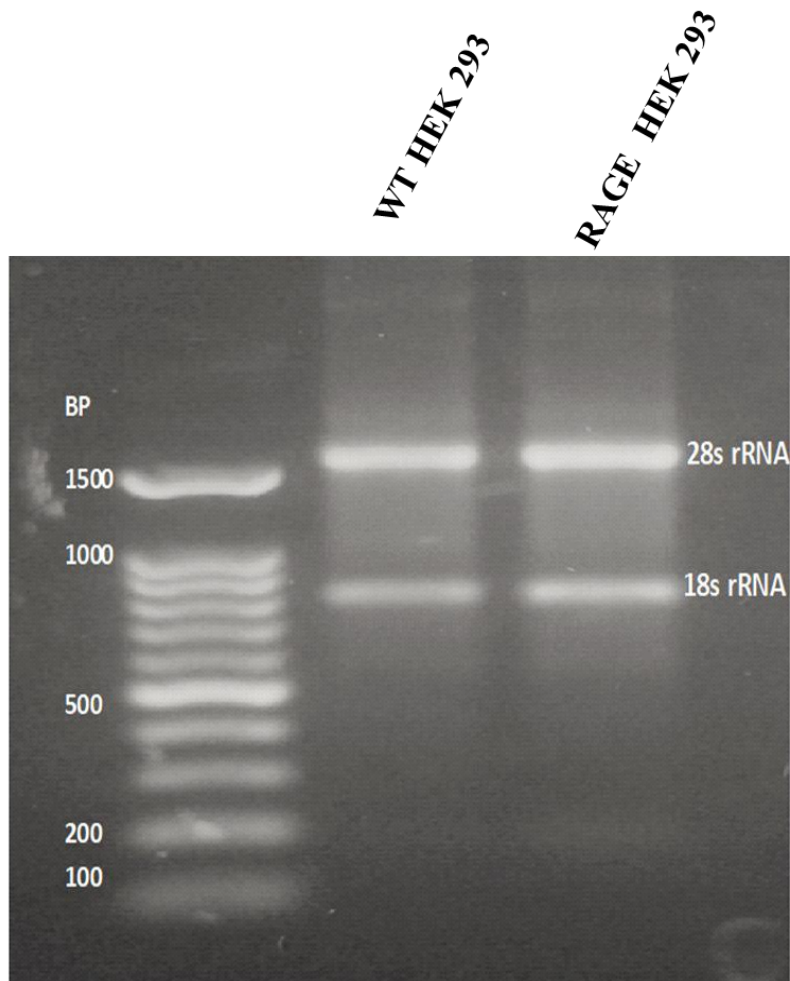


Figure A3: Extracted total RNA sample ran on a agarose gel.

200 ng of total RNA samples from WT HEK 293 and RAGE HEK 293 were run beside GoldBio.com 100bp ladder D001-500 on a 1.5% agarose gel containing 0.01% ethidium bromide. The 18S and 28S ribosomal RNA bands are clearly visible and intact in these samples. The ratios of 260/280 nm for these extracted RNA samples were found to be ~1.8

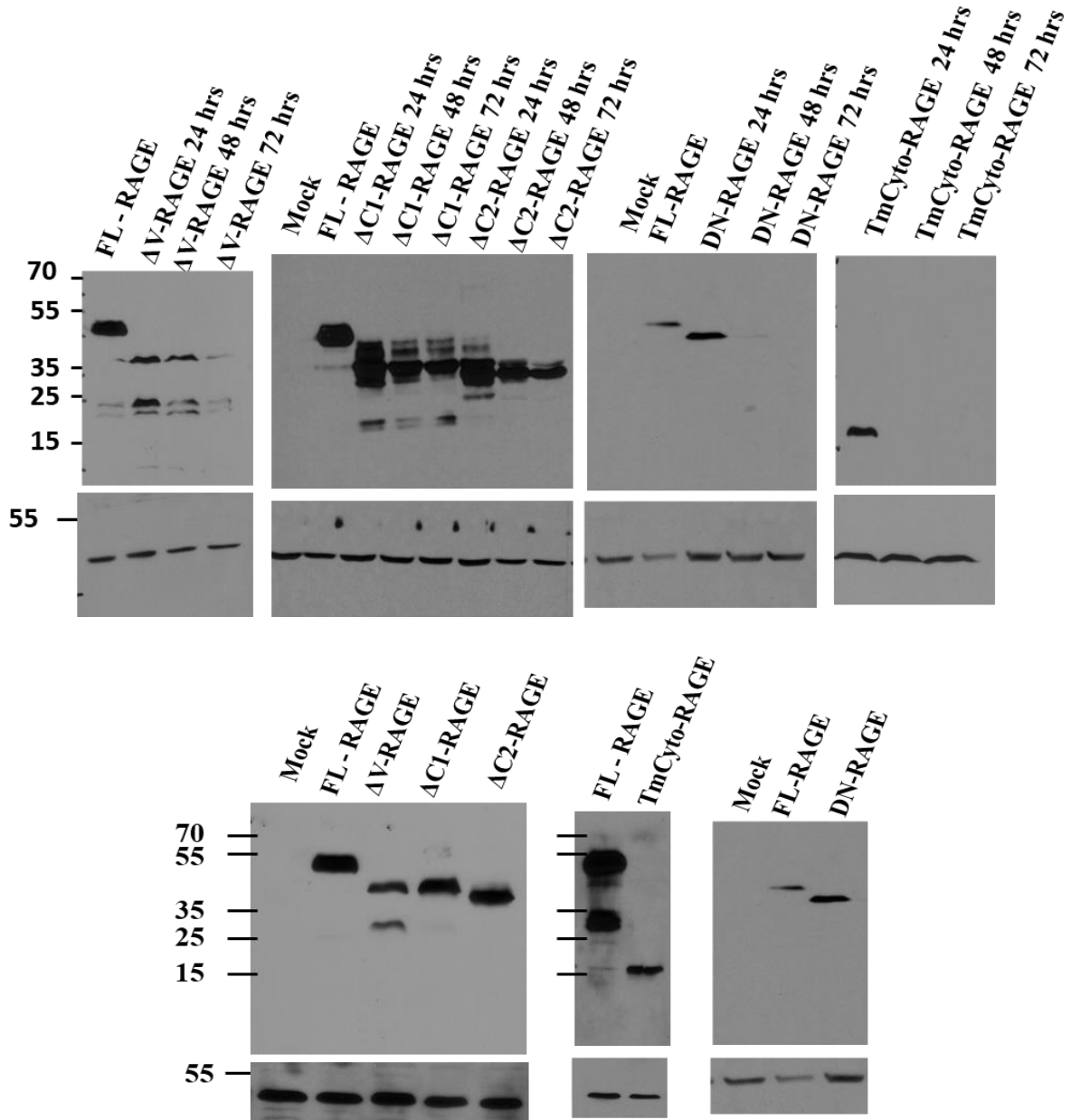


Figure A4: Additional western blot data from different experiments representing figure 3.7 of chapter 3. Protein expression in WT HEK 293 cells transfected with FL-RAGE and other RAGE variants at time points (A) 24, 48, and 72 hours and (B) at 24 hours in WT HEK 293 cells. Actin was used as the loading control. The N-terminus antiRAGE 9A11 antibody was used to determine expression in FL-RAGE and DN-RAGE. For all other RAGE domain deletion variants, including FL-RAGE, expression was detected using the C-terminus antiRAGE D1A12 antibody.

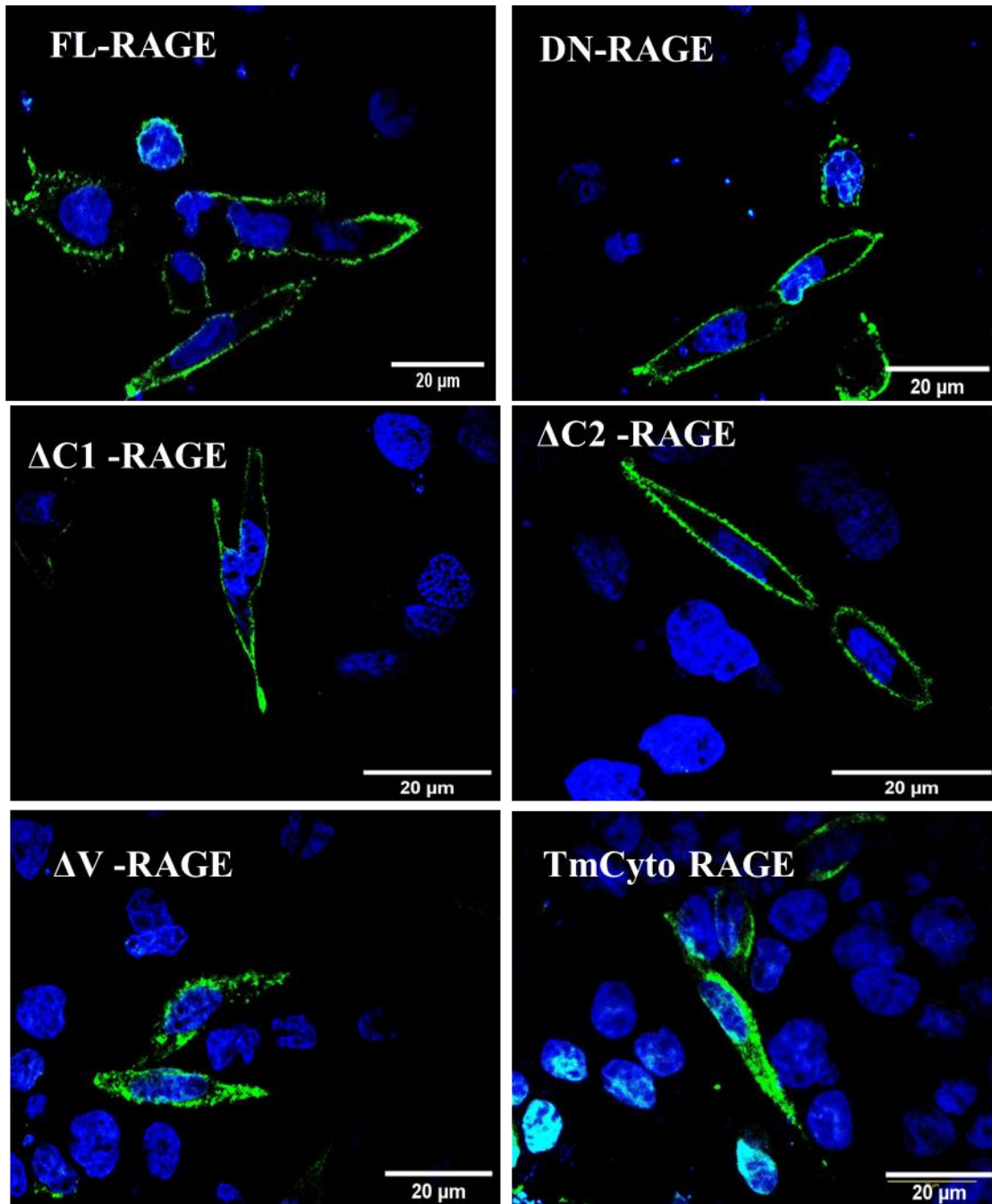


Figure A5: Additional images from different experiments representing figure 3.8 of chapter 3. Confocal microscopy images of cells expressing the FL-RAGE and different domain deletion variants.

For the DN-RAGE construct antiRAGE 9A11 antibody was used, and for all other constructs, antiRAGE D1A12 antibody was used. The images are taken at 40X objective using Olympus FV3000 at the same exposure time.

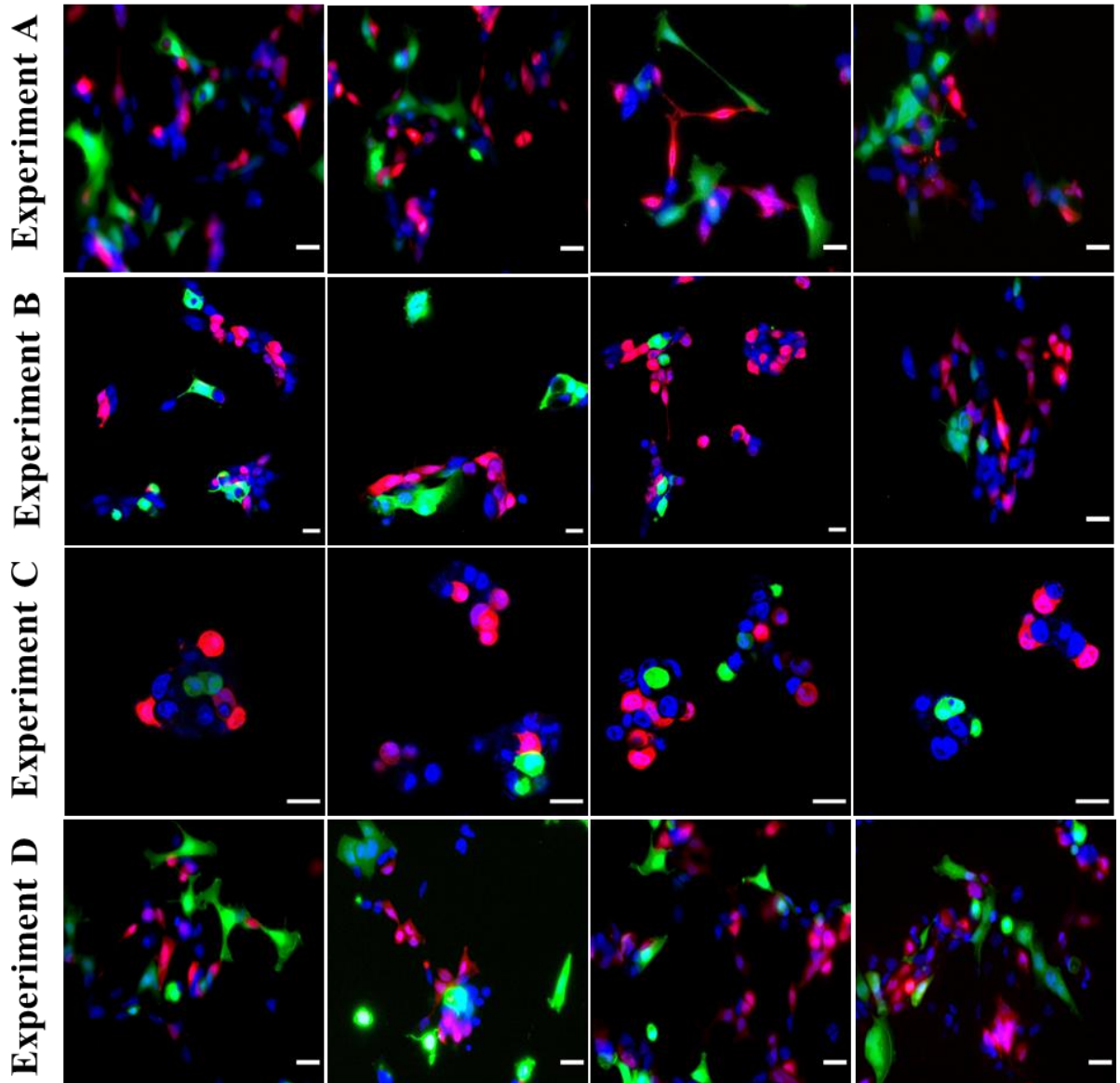


Figure A6: Microscopy images from all four individual experiments (A, B, C, and D) $n=4$, showing cell-cell adhesion in RAGE HEK 293 and WT HEK 293 cells (additional images for figure 3.13 of chapter 3).

The cells were transiently transfected with plasmids encoding the red fluorescent protein (RFP) for RAGE HEK 293 and green fluorescent protein (GFP) for WT HEK 293. Cells were seeded in equal numbers from the two populations on a collagen IV coated surface and imaged after 48hrs. The type of cell contacts was determined by counting the contacts made from RFP and GFP cells. Only the nuclei stained cells were considered nontransfected cells. Scale bar 20 μm .

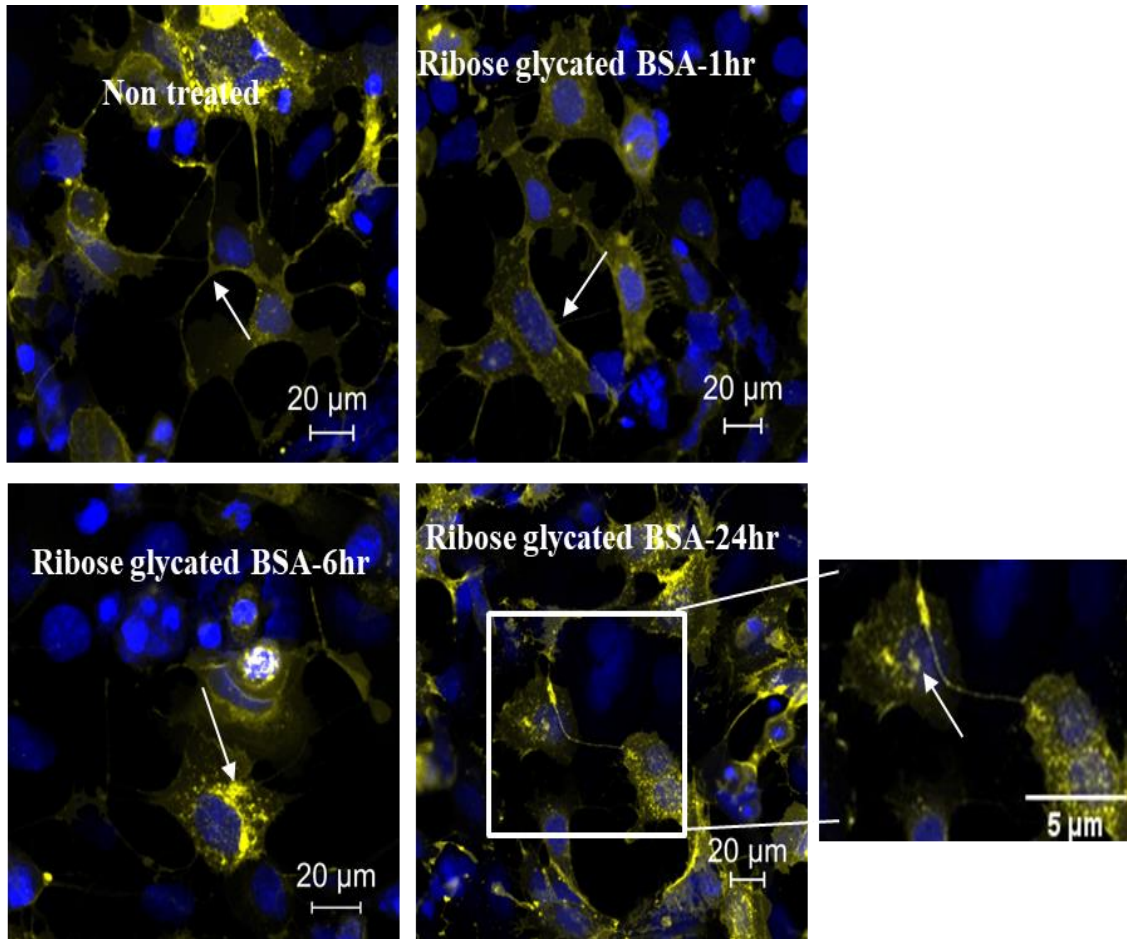


Figure A7: Additional images representing figure 4.2 of chapter 4. Confocal images of HEK 293 cells transfected with FL-RAGE-YFP plasmids and treated with ribose glycated BSA at different time points (1, 6, and 24 hours).

Without AGE treatment, RAGE was localized to the membrane. After 6 hours of AGE treatment (500 μ g/ml), RAGE internalization was observed with increased intracellular RAGE localization. The enlarged image below shows the nuclear localization of RAGE-ICD after 24 hours of ribose glycated BSA treatment (bottom right).

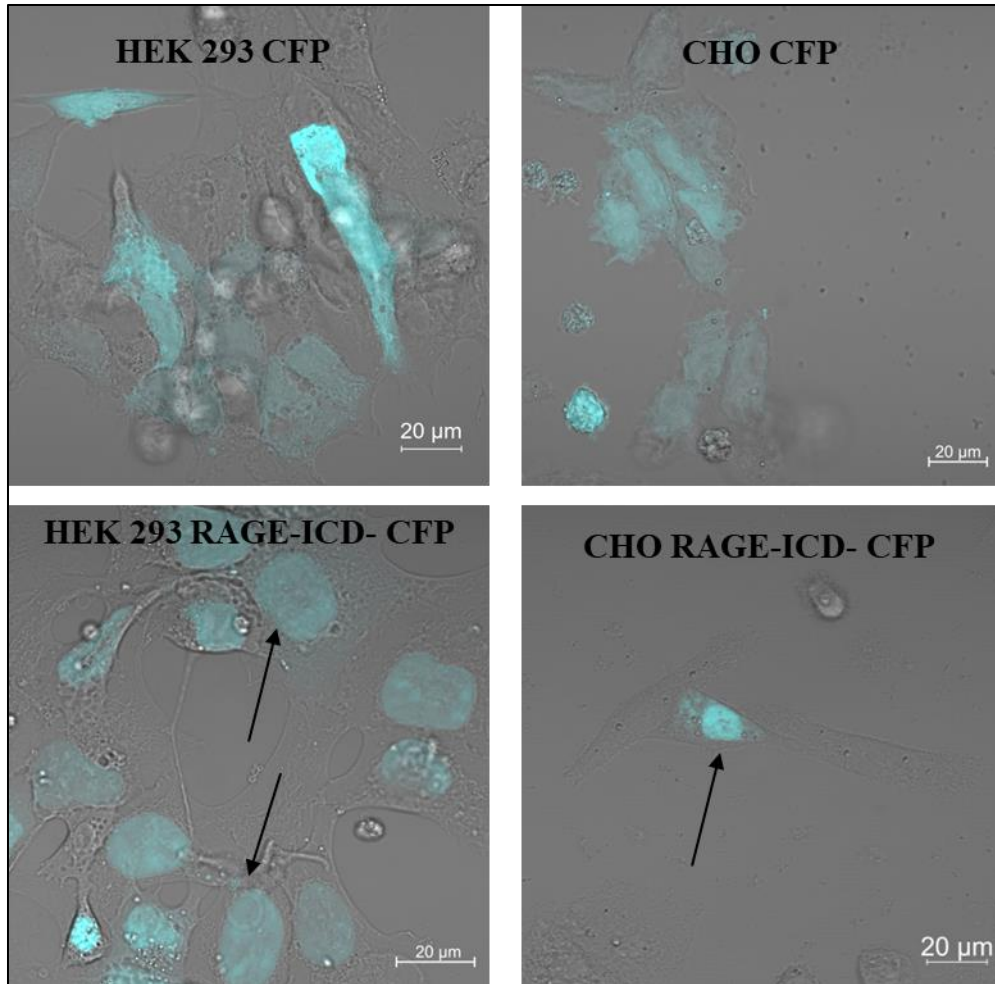


Figure A8: Additional images representing figure 4.3 of chapter 4. Confocal microscopy images of cells transfected with control plasmid containing only cyan fluorescent protein (CFP) tagging and RAGE-ICD CFP in HEK 293 (left) and CHO cells (right). HEK 293 and CHO cells were transfected with CFP and RAGE-ICD CFP plasmids for 24 hours. Image analysis showed distinct nuclear localization of the CFP in cells transfected with RAGE-ICD-CFP. In contrast, the control plasmid transfected cells showed no distinct cellular localization of the fluorescent protein.

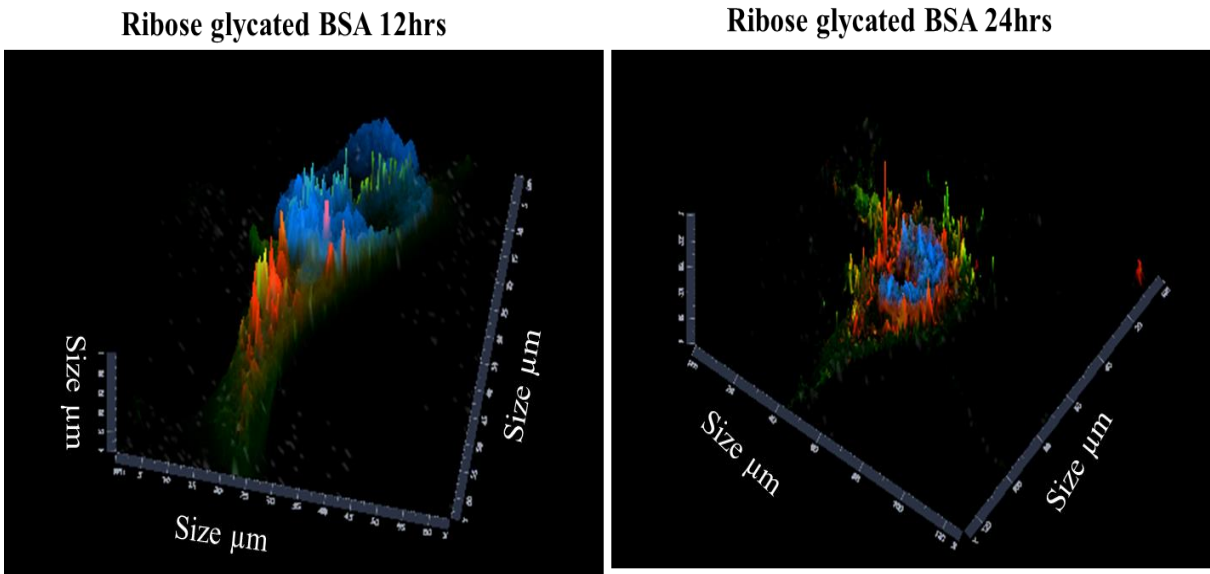
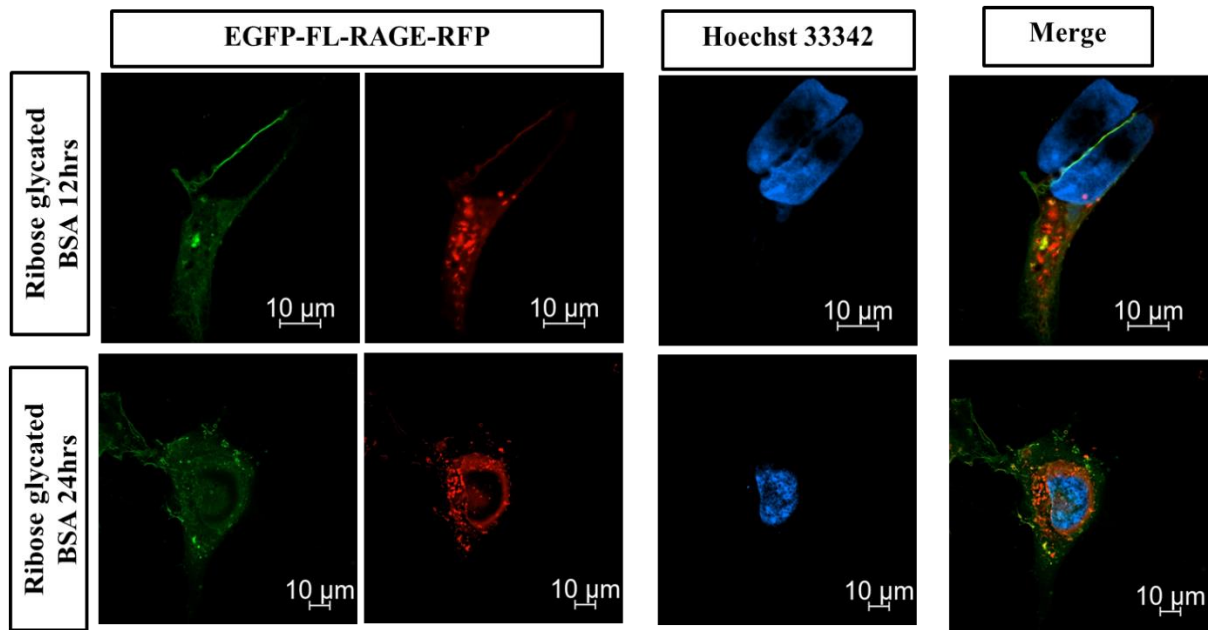


Figure A9: Additional images representing figure 4.5 of chapter 4. Confocal images (2D and 3D view) of WT HEK 293 cells transfected with EGFP-FL- RAGE-RFP plasmid in ribose glycosylated BSA treated conditions.

In non-treated conditions, both EGFP and RFP colocalized to the membrane. The enlarged image beside shows increased colocalization of both fluorescent proteins indicating RAGE clustering at cell-cell contacts. Treatment with ribose glycosylated BSA (500µg/ml) for 12 hours induced cleavage in RAGE, leading to distinct localization of EGFP and RFP. After 24 hours, the RFP tagged to the c-terminus of RAGE showed nuclear localization. The 3D rendering of the corresponding images was shown below the treated conditions.

Enriched biotinylated samples

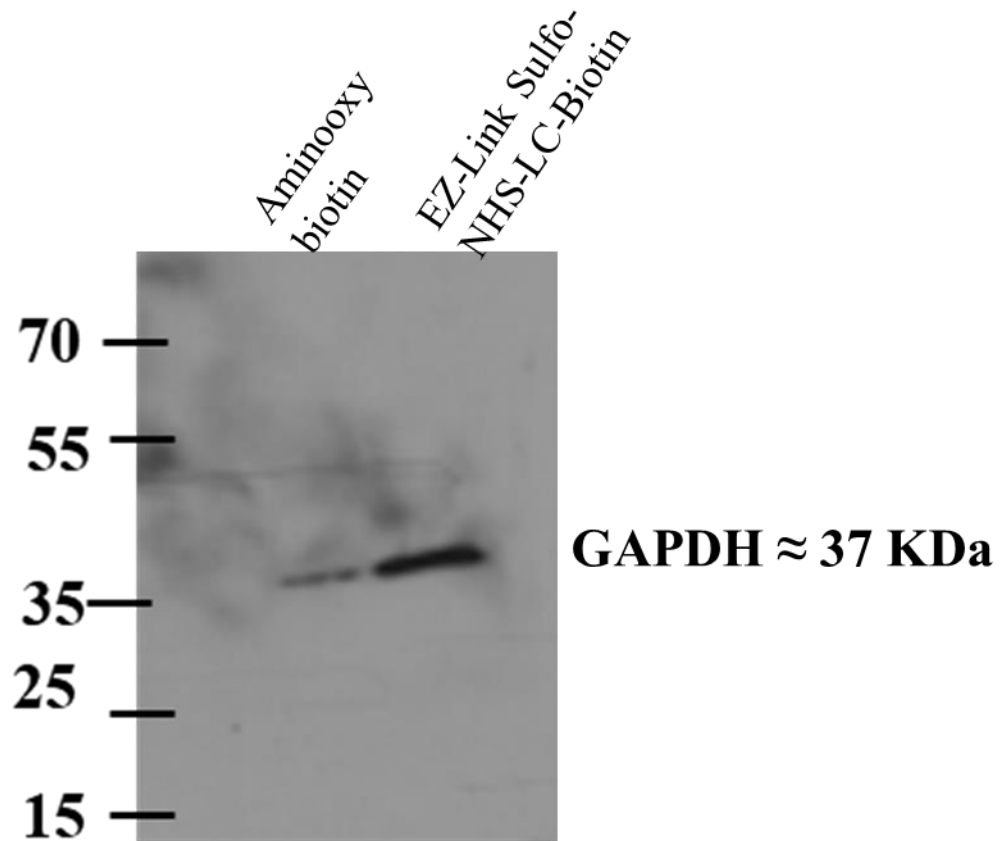


Figure A10: Detection of GAPDH in enriched biotinylated samples labeled with aminoxy biotin and EZ-Link Sulfo-NHS-LC-Biotin.

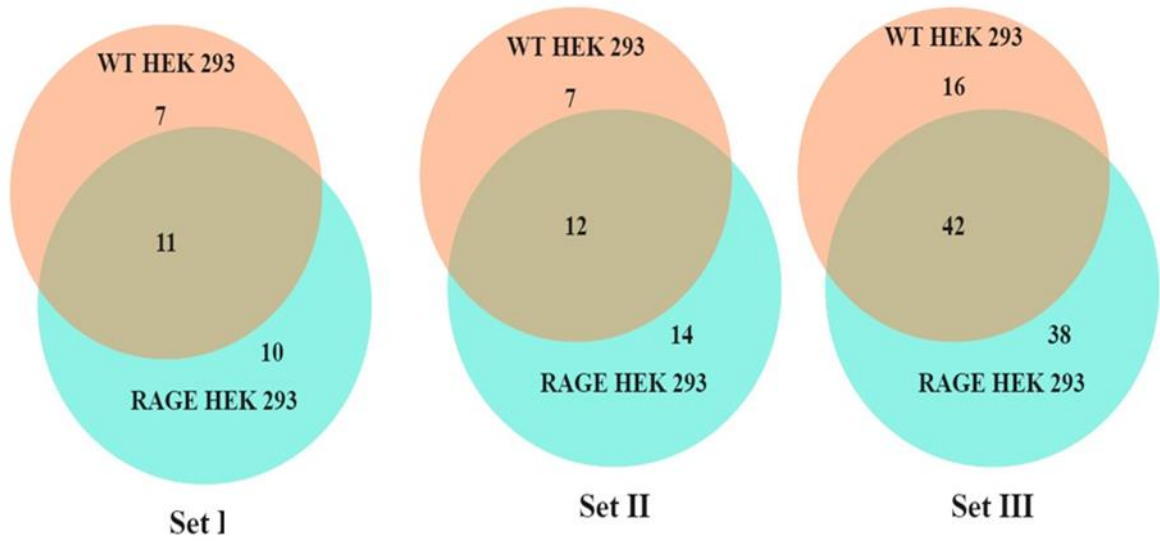
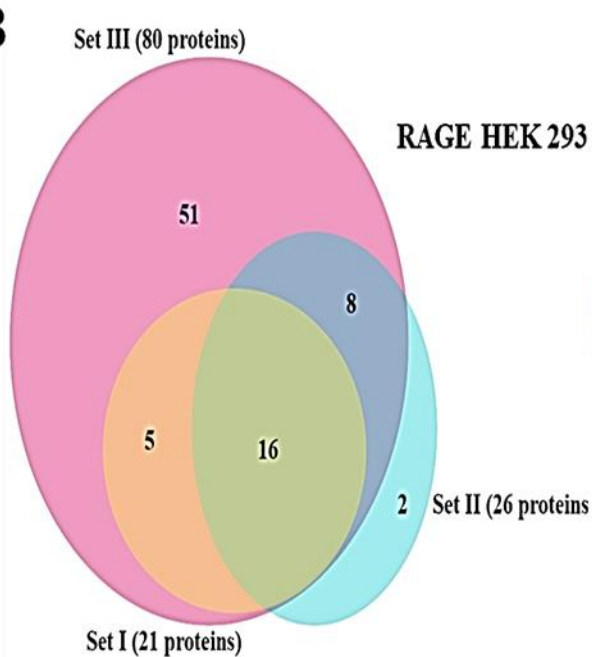
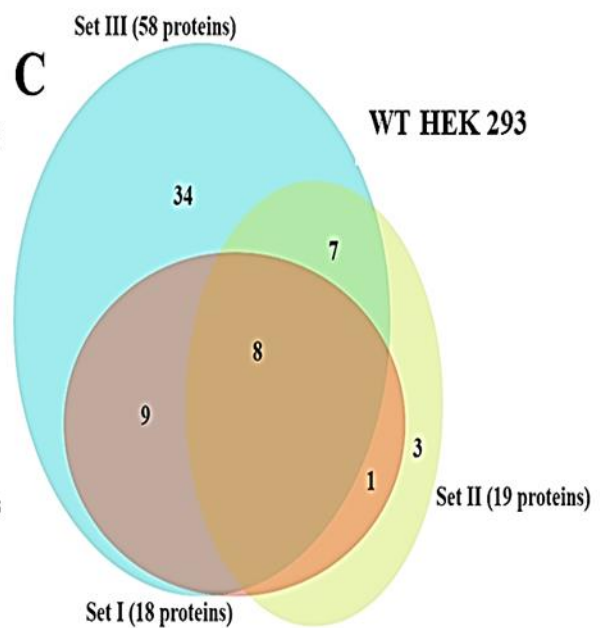
A**B****C**

Figure A11: Venn diagram of adhesion relevant proteins identified from cell surface proteomics. (A) individual experiment sample sets of both WT and RAGE HEK 293 (B) three independent experiments in RAGE HEK 293 and WT HEK 293 samples.

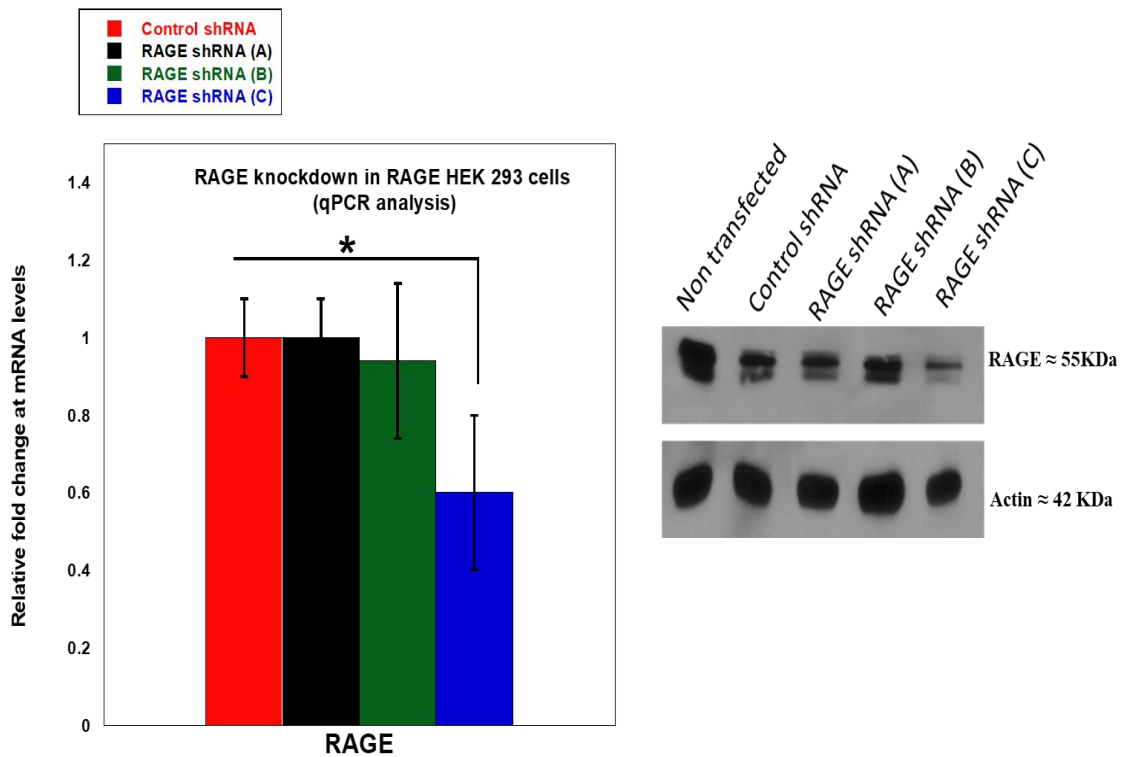


Figure A12: Relative changes in RAGE expression at mRNA and protein levels upon RAGE shRNA transfection in RAGE HEK 293 cells.

RAGE HEK 293 cells are transfected with 3 shRNA plasmids targeting RAGE: RAGE shRNA (A), RAGE shRNA (B), and RAGE shRNA (C) for 72 hrs. Cells were then processed to determine changes in RAGE expression at mRNA and protein levels compared to Control/scrambled shRNA transfected cells. The plot corresponds to a normalized relative fold change of RAGE at the mRNA level by qPCR analysis, and the blot corresponds to RAGE expression at the protein level by western blot analysis.

APPENDIX B. NUCLEOTIDE AND PROTEIN SEQUENCE OF RAGE MUTANTS

(CHAPTER 3 AND 4)

FL-RAGE nucleotide sequence

ATGGCGGGCGGGCACCGCGGTGGGGCGCGTGGGTGCTGGTGCTGAGCCTGTGGGGCGCGGTGGTGGGCG
CGCAGAACATTACCGCGCGCATTGGCGAACCGCTGGTGCTGAAATGCAAAGGCGCGCCGAAAAAACC
GCCGAGCGCCTGGAATGGAACTGAACACCGGCCGCACCGAAGCGTGGAAGTGCTGAGCCCGCAG
GGCGGGCGCCCGTGGGATAGCGTGGCGCGCGTGCTGCCGAACGGCAGCCTGTTTCTGCCGGCGGTGGG
CATTCAAGGATGAAGGCATTTTTTCGCTGCCAGGCGATGAACCGCAACGGCAAAGAAACCAAAGCAAC
TATCGCGTGCGCGTGTATCAGATTCCGGGGCAAACCGGAAATTGTGGATAGCGCGAGCGAACTGACCGC
GGGCGTGCCGAACAAAGTGGGCACCTGCGTGAGCGAAGGCAGCTATCCGGCGGGCACCCCTGAGCTGG
CATCTGGATGGCAAACCGCTGGTGCCGAACGAAAAGGCGTGAGCGTGAAAGAACAGACCCGCGGCC
ATCCGAAACCGGCCTGTTTACCCTGCAGAGCGAACTGATGGTGACCCCGGCGCGCGGGCGGCATCCG
CGCCGACCTTTAGCTGCAGCTTTAGCCCGGGCCTGCCGCGCCATCGCGCGCTGCGCACCCGCGCCGAT
TCAGCCGCGCGTGTGGGAACCGGTGCCGCTGGAAGAAGTGCAGCTGGTGGTGGAAACCGGAAGGCGGC
GCGGTGGCGCCGGGCGGCACCGTGACCCTGACCTGCGAAGTGCCGGCGCAGCCGAGCCCGCAGATTC
ATTGGATGAAAGATGGCGTGCCGCTGCCGCTGCCGCGAGCCCGGTGCTGATTCTGCCGAAATTGGC
CCGAGGATCAGGGCACCTATAGCTGCGTGGCGACCCATAGCAGCCATGGCCCGCAGGAAAGCCGCG
CGGTGAGCATTAGCATTATTGAACCGGGCGAAGAAGGCCCGACCGCGGGCAGCGTGGGCGGCAGCGG
CCTGGGCACCTGGCGCTGGCGCTGGGCATTCTGGGCGGCCCTGGGCACCCGCGCGCTGCTGATTGGCG
TGATTCTGTGGCAGCGCCCGCAGCGCCGCGGCGAAGAACGCAAAGCGCCGAAAACAGGAAGAAGA
AGAAGAACGCGCGGAACTGAACCAGAGCGAAGAACCAGGAAAGCGGGCGAAAGCAGCACCCGGCGGCC
G

ΔV-RAGE nucleotide sequence

ATGGCGGGCGGGCACCGCGGTGGGGCGCGTGGGTGCTGGTGCTGAGCCTGTGGGGCGCGGTGGTGGGCG
CGGTGTATCAGATTCCGGGCAAACCGGAAATTGTGGATAGCGCGAGCGAACTGACCGCGGGCGTGCC
GAACAAAGTGGGCACCTGCGTGAGCGAAGGCAGCTATCCGGCGGGCACCCCTGAGCTGGCATCTGGAT
GGCAAACCGCTGGTGCCGAACGAAAAGGCGTGAGCGTGAAAGAACAGACCCGCGCCATCCGGAAA
CCGCGCTGTTTACCCTGCAGAGCGAACTGATGGTGACCCCGGCGCGCGGGCGGCATCCGCGCCCGACC
TTAGCTGCAGCTTTAGCCCGGGCCTGCCGCGCCATCGCGCGCTGCGCACCCGCGCCGATTCAGCCGCG
CGTGTGGGAACCGGTGCCGCTGGAAGAAGTGCAGCTGGTGGTGGAAACCGGAAGGCGGGCGCGGTGGCG
CCGGGCGGCACCGTGACCCTGACCTGCGAAGTGCCGGCGCAGCCGAGCCCGCAGATTCATTGGATGA
AAGATGGCGTGCCGCTGCCGCTGCCGCCGAGCCCGGTGCTGATTCTGCCGAAATTGGCCCGCAGGAT
CAGGGCACCTATAGCTGCGTGGCGACCCATAGCAGCCATGGCCCGCAGGAAAGCCGCGCGGTGAGCA
TTAGCATTATTGAACCGGGCGAAGAAGGCCCGACCGCGGGCAGCGTGGGCGGCAGCGGCCTGGGCAC
CCTGGCGCTGGCGCTGGGCATTCTGGGCGGCCTGGGCACCCGCGCGCTGCTGATTGGCGTGATTCTGT
GGCAGCGCCCGCAGCGCCGCGGCGAAGAACGCAAAGCGCCGAAAACAGGAAGAAGAAGAAGAAC
GCGCGGAACTGAACCAGAGCGAAGAACCAGGAAAGCGGGCGAAAGCAGCACCCGGCGGCCCG

ΔC1-RAGE nucleotide sequence

ATGGCGGGCGGGCACCGCGGTGGGGCGCGTGGGTGCTGGTGCTGAGCCTGTGGGGCGCGGTGGTGGGCG
CGCAGAACATTACCGCGCGCATTGGCGAACCGCTGGTGCTGAAATGCAAAGGCGCGCCGAAAAAACC
GCCGAGCGCCTGGAATGGAACTGAACACCGGCCGCACCGAAGCGTGGAAGTGCTGAGCCCGCAG
GGCGGGCGCCCGTGGGATAGCGTGGCGCGCGTGCTGCCGAACGGCAGCCTGTTTCTGCCGGCGGTGGG
CATTCAAGGATGAAGGCATTTTTTCGCTGCCAGGCGATGAACCGCAACGGCAAAGAAACCAAAGCAAC
TATCGCGTGCGCGTGTATCAGATTCCGGGGCAAACCGCGCCGATTAGCCGCGCGTGTGGGAACCGGT
GCCGCTGGAAGAAGTGCAGCTGGTGGTGGAAACCGGAAGGCGGGCGCGGTGGCGCCGGGCGGCACCGTG
ACCCTGACCTGCGAAGTGCCGGCGCAGCCGAGCCCGCAGATTCATTGGATGAAAGATGGCGTGCCGCT

GCCGCTGCCGCCGAGCCCGGTGCTGATTCTGCCGAAATTGGCCCGCAGGATCAGGGCACCTATAGCT
GCGTGGCGACCCATAGCAGCCATGGCCCGCAGGAAAGCCGCGCGGTGAGCATTAGCATTATTGAACC
GGGCGAAGAAGGCCCGACCGCGGGCAGCGTGGGCGGCAGCGCCTGGGCACCCTGGCGCTGGCGCTG
GGCATTCTGGGCGGCCTGGGCACCGCGGGCGTCTGATTGGCGTATTCTGTGGCAGCGCCGCCAGCG
CCGCGGCGAAGAACGCAAAGCGCCGAAAACCAGGAAGAAGAAGAACAACGCGCGGAACTGAACCA
GAGCGAAGAACCAGGCGGGCGAAAAGCAGCACCGGCGGCCCG

ΔC2-RAGE nucleotide sequence

ATGGCGGGGGCACCGCGGTGGGCGCGTGGGTGCTGGTGTGAGCCTGTGGGGCGCGGTGGTGGGCG
CGCAGAACATTACCGCGCGCATTGGCGAACCCTGGTGTGAAATGCAAAGGCGCGCCGAAAAAACC
GCCGCAGCGCCTGGAATGGAACTGAACACCGGCCGCACCGAAGCGTGAAAGTGCTGAGCCCGCAG
GGCGGGCGCCCGTGGGATAGCGTGGCGCGCGTGTGCCGAACGGCAGCCTGTTTCTGCCGGCGGTGGG
CATTCAGGATGAAGGCATTTTTTCGCTGCCAGGCGATGAACCGCAACGGCAAAGAAACCAAAGCAAC
TATCGCGTGCAGTGTATCAGATTCCGGGCAAACCGGAAATTGTGGATAGCGCGAGCGAACTGACCGC
GGGCGTGCCGAACAAAGTGGGCACCTGCGTGAGCGAAGGCAGCTATCCGGCGGGCACCCCTGAGCTGG
CATCTGGATGGCAAACCGCTGGTGCCGAACGAAAAAGGCGTGAGCGTGAAAGAACAGACCCCGCCGC
ATCCGGAACCCGCGCTGTTTACCCTGCAGAGCGAACTGATGGTGACCCCGGCGCGGGCGGCGATCCG
CGCCGACCTTTAGCTGCAGCTTTAGCCCGGGCCTGCCGCGCCATCGCGCGTGCACCGCGCCGAT
TCAGCCGATTAGCATTATTGAACCGGGCGAAGAAGGCCCGACCGCGGGCAGCGTGGGCGGCAGCGGC
CTGGGCACCCTGGCGCTGGCGCTGGGCATTCTGGGCGGCTGGGCACCGCGGGCGTCTGATTGGCGT
GATTCTGTGGCAGCGCCGCCAGCGCCGCGGCGAAGAACGCAAAGCGCCGAAAACCAGGAAGAAGA
AGAAGAACGCGCGGAACTGAACCAGAGCGAAGAACCAGGAAAGCGGGCGAAGCAGCACCGGCGGCC
G

DN-RAGE nucleotide sequence

ATGGCGGGGGCACCGCGGTGGGCGCGTGGGTGCTGGTGTGAGCCTGTGGGGCGCGGTGGTGGGCG
CGCAGAACATTACCGCGCGCATTGGCGAACCCTGGTGTGAAATGCAAAGGCGCGCCGAAAAAACC
GCCGCAGCGCCTGGAATGGAACTGAACACCGGCCGCACCGAAGCGTGAAAGTGCTGAGCCCGCAG
GGCGGGCGCCCGTGGGATAGCGTGGCGCGCGTGTGCCGAACGGCAGCCTGTTTCTGCCGGCGGTGGG
CATTCAGGATGAAGGCATTTTTTCGCTGCCAGGCGATGAACCGCAACGGCAAAGAAACCAAAGCAAC
TATCGCGTGCAGTGTATCAGATTCCGGGCAAACCGGAAATTGTGGATAGCGCGAGCGAACTGACCGC
GGGCGTGCCGAACAAAGTGGGCACCTGCGTGAGCGAAGGCAGCTATCCGGCGGGCACCCCTGAGCTGG
CATCTGGATGGCAAACCGCTGGTGCCGAACGAAAAAGGCGTGAGCGTGAAAGAACAGACCCCGCCGC
ATCCGGAACCCGCGCTGTTTACCCTGCAGAGCGAACTGATGGTGACCCCGGCGCGGGCGGCGATCCG
CGCCGACCTTTAGCTGCAGCTTTAGCCCGGGCCTGCCGCGCCATCGCGCGTGCACCGCGCCGAT
TCAGCCGCGCGTGTGGGAACCGGTGCCGCTGGAAGAAGTGAGCTGGTGGTGGAAACCGGAAGGCGGC
GCGGTGGCGCCGGGCGGCACCGTGACCTGCGAAGTGCCGGCGCAGCCGAGCCCGCAGATTC
ATTGGATGAAAGATGGCGTGCCGCTGCCGCTGCCGCCGAGCCCGGTGCTGATTCTGCCGGAATTGGC
CCGCAGGATCAGGGCACCTATAGCTGCGTGCGGACCCATAGCAGCCATGGCCCGCAGGAAAGCCGCG
CGGTGAGCATTAGCATTATTGAACCGGGCGAAGAAGGCCCGACCGCGGGCAGCGTGGGCGGCAGCGG
CCTGGGCACCCTGGCGCTGGCGCTGGGCATTCTGGGCGGCTGGGCACCGCGGGCGTCTGATTGGCG
TGATTCTGTGG

Tm-Cyto nucleotide sequence

ATGGCGGGGGCACCGCGGTGGGCGCGTGGGTGCTGGTGTGAGCCTGTGGGGCGCGGTGGTGGGCA
TTAGCATTATTGAACCGGGCGAAGAAGGCCCGACCGCGGGCAGCGTGGGCGGCAGCGCCTGGGCAC
CCTGGCGCTGGCGCTGGGCATTCTGGGCGGCTGGGCACCGCGGGCGTCTGATTGGCGTATTCTGT
GGCAGCGCCGCCAGCGCCGCGGCGAAGAACGCAAAGCGCCGAAAACCAGGAAGAAGAAGAAGAAC
GCGCGGAACTGAACCAGAGCGAAGAACCAGGAAAGCGGGCGAAAAGCAGCACCGGCGGCCCG

FL-RAGE protein sequence

MAAGTAVGAWVLVLSLWGAVVGAQNITARIGEPLVLKCKGAPKKPPQRLEWKLNTGRTEAWKVLSPQG
GGPWDSVARVLPNGSLFLPAVGIQDEGIFRCQAMNRRNGKETKSNYRVRVYQIPGKPEIVDSASELTAGVPN
KVGTCVSEGSYPAGTLSWHLDGKPLVPNEKGVSVKEQTRRHPEGLFTLQSELMVTPARGGDPRTFSCSF
SPGLPRHRALRTAPIQPRVWEPVPLEEVQLVVEPEGGA VAPGGTVTLTCEVPAQPSQIHWKMDGVPLPLP
PSPVLILPEIGPQDQGTYSVCVATHSSHGPQESRAVSISIIEPGEEGPTAGSVGGSGGLGTLALALGILGGLGTAA
LLIGVILWQRRQRRGEERKAPENQEEEEERAELNQSEEPEAGESSTGGP

Δ V-RAGE protein sequence

MAAGTAVGAWVLVLSLWGAVVGA VYQIPGKPEIVDSASELTAGVPNKVGTVCVSEGSYPAGTLSWHLDGK
PLVPNEKGVSVKEQTRRHPEGLFTLQSELMVTPARGGDPRTFSCSFSPGLPRHRALRTAPIQPRVWEPV
LEEVQLVVEPEGGA VAPGGTVTLTCEVPAQPSQIHWKMDGVPLPLPSPVLILPEIGPQDQGTYSVCVATHS
SHGPQESRAVSISIIEPGEEGPTAGSVGGSGGLGTLALALGILGGLGTAA LLIGVILWQRRQRRGEERKAPENQ
EEEEERAELNQSEEPEAGESSTGGP

Δ C1-RAGE protein sequence

MAAGTAVGAWVLVLSLWGAVVGAQNITARIGEPLVLKCKGAPKKPPQRLEWKLNTGRTEAWKVLSPQG
GGPWDSVARVLPNGSLFLPAVGIQDEGIFRCQAMNRRNGKETKSNYRVRVYQIPGKTAPIQPRVWEPVLEE
VQLVVEPEGGA VAPGGTVTLTCEVPAQPSQIHWKMDGVPLPLPSPVLILPEIGPQDQGTYSVCVATHSSHG
PQESRAVSISIIEPGEEGPTAGSVGGSGGLGTLALALGILGGLGTAA LLIGVILWQRRQRRGEERKAPENQEEE
EERAELNQSEEPEAGESSTGGP

Δ C2-RAGE protein sequence

MAAGTAVGAWVLVLSLWGAVVGAQNITARIGEPLVLKCKGAPKKPPQRLEWKLNTGRTEAWKVLSPQG
GGPWDSVARVLPNGSLFLPAVGIQDEGIFRCQAMNRRNGKETKSNYRVRVYQIPGKPEIVDSASELTAGVPN
KVGTCVSEGSYPAGTLSWHLDGKPLVPNEKGVSVKEQTRRHPEGLFTLQSELMVTPARGGDPRTFSCSF
SPGLPRHRALRTAPIQPISIIEPGEEGPTAGSVGGSGGLGTLALALGILGGLGTAA LLIGVILWQRRQRRGEERK
APENQEEEEERAELNQSEEPEAGESSTGGP

DN-RAGE protein sequence

MAAGTAVGAWVLVLSLWGAVVGAQNITARIGEPLVLKCKGAPKKPPQRLEWKLNTGRTEAWKVLSPQG
GGPWDSVARVLPNGSLFLPAVGIQDEGIFRCQAMNRRNGKETKSNYRVRVYQIPGKPEIVDSASELTAGVPN
KVGTCVSEGSYPAGTLSWHLDGKPLVPNEKGVSVKEQTRRHPEGLFTLQSELMVTPARGGDPRTFSCSF
SPGLPRHRALRTAPIQPRVWEPVPLEEVQLVVEPEGGA VAPGGTVTLTCEVPAQPSQIHWKMDGVPLPLP
PSPVLILPEIGPQDQGTYSVCVATHSSHGPQESRAVSISIIEPGEEGPTAGSVGGSGGLGTLALALGILGGLGTAA
LLIGVILW

Tm-Cyto protein sequence

MAAGTAVGAWVLVLSLWGAVVGISIIEPGEEGPTAGSVGGSGGLGTLALALGILGGLGTAA LLIGVILWQRR
QRRGEERKAPENQEEEEERAELNQSEEPEAGESSTGGP

RAGE-ICD protein sequence

MAQRRQRRGEERKAPE NQEEEEERAELNQSEE PEAGESSTGGP

CFP protein sequence

VSKGEELFTGVVPILVELDGDVNGHKFSVSGEGEGDATYGKLTCLKFICTTGKLPVP
WPTLVTTLTWGVQCFARYPDHMKQHDFFKSAMPEGYVQERTIFFKDDGNYKTRAEVKFEGDTLVNRIEL
KGIDFKEDGNILGHKLEYNAISDNVYITADKQKNGIKANFKIRHNIEDGSVQLADHYQQNTPIGDGPVLLPD
NHYLSTQSKLSKDPNEKRDHMLLEFVTAAGITLGMDELYK

YFP protein sequence:

MVSKGEELFTGVVPILVELDGDVNGHKFSVSGEGEGDATYGKLTCLKFICTTGKLPVPWPTLVTTFGYGLMC
FARYPDHMKQHDFFKSAMPEGYVQERTIFFKDDGNYKTRAEVKFEGDTLVNRIELKGIDFKEDGNILGHKL
EYNYNSHNVYIMADKQKNGIKVNFKIRHNIEDGSVQLADHYQQNTPIGDGPVLLPDNHYLSYQSKLSKDP
NEKRDHMLLEFVTAAGITLGMDELY

EGFP protein sequence

MVSKGEELFTGVVPILVELDGDVNGHKFSVSGEGEGDATYGKLTCLKFICTTGKLPVPWPTLVTTLTYGVC
FSRYPDHMKQHDFFKSAMPEGYVQERTIFFKDDGNYKTRAEVKFEGDTLVNRIELKGIDFKEDGNILGHKL
EYNYNSHNVYIMADKQKNGIKVNFKIRHNIEDGSVQLADHYQQNTPIGDGPVLLPDNHYLSTQSALS
KDPNEKRDHMLLEFVTAAGITLGMDELYK

m-Apple protein sequence

MVSKGEELFTGVVPILVELDGDVNGHKFSVSGEGEGDATYGKLTCLKFICTTGKLPVPWPTLVTTLTYGVC
FSRYPDHMKQHDFFKSAMPEGYVQERTIFFKDDGNYKTRAEVKFEGDTLVNRIELKGIDFKEDGNILGHKL
EYNYNSHNVYIMADKQKNGIKVNFKIRHNIEDGSVQLADHYQQNTPIGDGPVLLPDNHYLSTQSALS
KDPNEKRDHMLLEFVTAAGITLGMDELYK

**APPENDIX C. LIST OF HOUSEKEEPING GENES USED FOR INITIAL SCREENING
IN THE STUDY (CHAPTER 5)**

Gene (Gene ID)	Name	Primers (5' → 3')
ACTB NM_001101	Actin beta	Forward: CATGTACGTTGCTATCCAGGC Reverse: CTCCTTAATGTCACGCACGAT
B2M NM_004048	Beta-2-microglobulin	Forward: GAGGCTATCCAGCGTACTCCA Reverse: CGGCAGGCATACTCATCTTTT
GAPDH NM_008084	Glyceraldehyde 3-phosphate dehydrogenase	Forward: GAAGATGGTGATGGGATTTTC Reverse: GAAGGTGAAGGTCGGAGTC
GUSB NM_000181	Glucuronidase beta	Forward: GTCTGCGGCATTTTGTCCG Reverse: CACACGATGGCATAGGAATGG
HPRT1 NM_000194	Hypoxanthine phosphoribosyl transferase 1	Forward: CCTGGCGTCGTGATTAGTGAT Reverse: AGACGTTCACTCCTGTCCATAA
HSP90AB1 NM_007355	Heat shock protein 90kDa alpha (cytosolic), class B member 1	Forward: AGAAATTGCCCAACTCATGTCC Reverse: ATCAACTCCCGAAGGAAAATCTC
HSP90B1 – V1 NM_003299.3	Human heat shock protein 90kDa beta variant1	Forward: CGGTCAGAGCTGACGATGAA Reverse: TAACTTCGGCTTGAAGGCA
HSP90B1 – V2 NM_003299.3	Human heat shock protein 90kDa beta variant 2	Forward: GGGTGTGGTGGACTCAGATG Reverse: ACGTGTTCGATTTCGAGTGGT
HSP90B1 – V3 NM_003299.3	Human heat shock protein 90kDa beta variant 3	Forward: CAGTACGGATGGTCTGGCAA Reverse: GATACCTGACCGAAGCGTT
LDHA NM_005566	Lactate dehydrogenase A	Forward: CAGCCCGAACTGCAAGTTG Reverse: CCCCATCAGGAACGGAATC
PGK1 NM_000291	Phosphoglycerate kinase	Forward: AGTCGGTAGTCCTTATGAGCC Reverse: TTCCCAGAAGCATCTTTTCCC
PPIA NM_021130	Peptidylprolyl isomerase A	Forward: CCCACCGTGTTCTTCGACATT Reverse: GGACCCGTATGCTTTAGGATGA
RPL13A NM_012423	Ribosomal protein L13a	Forward: GCCATCGTGGCTAAACAGGTA Reverse: GTTGGTGTTCATCCGCTTGC
RPLP0 NM_001002	Ribosomal protein, large, P0	Forward: AGCCCAGAACACTGGTCTC Reverse: ACTCAGGATTTCAATGGTGCC
RPS18 NM_022551	Ribosomal protein S18	Forward: GATGGGCGGCGGAAAATAG Reverse: GCGTGGATTCTGCATAATGGT

**APPENDIX D. LIST OF 67 POTENTIAL GENES CANDIDATES RESPONSIBLE FOR
MEDIATING CELL ADHESION TESTED IN THE STUDY (CHAPTER 5)**

Gene (Gene ID)	Name	Primers (5' → 3')
ADAMTS13 NM_139026	ADAM metallopeptidase with thrombospondin type 1 motif	Forward: GGGTGCCCCAAATATCACAG Reverse: CATCAGGCAACTCCAGGTCA
ALCAM NM_001243281	Activated leukocyte cell adhesion molecule	Forward: ACTTGACGTACCTCAGAATCTCA Reverse: CATCGTCGTA CTGCACACTTT
CD133 NM_001145847	CD133 molecule (PROM1)	Forward: CAGAGTACAACGCCAAACCA Reverse: AAATCACGATGAGGGTCAGC
CD24 NM_013230	CD24 molecule	Forward: CTGCAGTCAACAGCCAGTCT Reverse: ACGTTTCTTGCCCTGAGTCT
CD36 NM_001001548	Platelet glycoprotein 4	Forward: CTTTGGCTTAATGAGACTGGGAC Reverse: GCAACAAACATCACCACACCA
CD44 NM_000610	CD44 Molecule	Forward: TCCCTGCTACCACTTTTGTG Reverse: AGACGTACCAGCCATTTGTG
CDH1 NM_004360	Cadherin 1	Forward: CGAGAGCTACACGTTACCGG Reverse: GGGTGTGAGGGAAAAATAGG
CDH12 NM_004061	Cadherin 12	Forward: TTTGATGGAGGTCTCCTAACACC Reverse: ACGTTTAAACACGTTGGAAATGTG
CDH2 NM_021248	Cadherin 22	Forward: TGTATGTGGGCAAGATCCACT Reverse: CTCGTCGATCAGGAAGATGGT
CNTN1 NM_175038	Contactin 1	Forward: CAGCCCTTCCCGGTTTACAA Reverse: TGCTTCTGACCATCCCGTAGT
Col1a1 NM_005261180	Collagen type XVIII alpha 1 chain	Forward: GTTCCAGAGAATGCCGCTTG Reverse: CCCATCTGAGTCATCGCCTT
CTGF NM_001901	Connective tissue growth factor	Forward: CAGCATGGACGTTCTGCTG Reverse: AACCACGGTTTGGTCCTTGG
CTNNA1 NM_004903	Catenin (cadherin-associated protein), alpha 1	Forward: GGGGATAAAATTGCGAAGGAGA Reverse: GTTGCCTCGCTTCACAGAAGA
CTNNB1 NM_001098209	Catenin beta 1	Forward: CATCTACACAGTTTGATGCTGCT Reverse: GCAGTTTTGTCAGTTCAGGGA
CTNNB1 NM_001098209	Catenin beta 1	Forward: CATCTACACAGTTTGATGCTGCT Reverse: GCAGTTTTGTCAGTTCAGGGA
CTNND1 NM_001085467	Catenin delta 1	Forward: GTGACAACACGGACAGTACAG Reverse: TTCTTGCGGAAATCACGACCC
DDR1 NM_001202523	Discoidin domain receptor tyrosine kinase 1	Forward: AAGGGACATTTTGATCCTGCC Reverse: CCTTGGGAAACACCGACCC
DDR2 NM_001014796	Discoidin domain receptor tyrosine kinase 2	Forward: CCAGTCAGTGGTCAGAGTCCA Reverse: GGGTCCCCACCAGAGTGATAA
DESP/DSP NM_004415	Desmoplakin	Forward: GCAGGATGTACTATTCTCGGC Reverse: CCTGGATGGTGTCTCTGGTTCT
ECAD NM_004360	E-cadherin	Forward: GTCACTGACACCAACGATAATCCT Reverse: TTCAGTGTGGTGATTACGACGTTA
EPCAM NM_002354	Epithelial cell adhesion molecule	Forward: TGATCCTGACTGCGATGAGAG Reverse: CTTGTCTGTTCTTCTGACCCC
EZR NM_003379	Ezrin	Forward: AGCGGCTGATCCCTCAAAG Reverse: GGCATCAACTCCAAGCCAAAG
FN1 NM_212482	Fibronectin	Forward: CGGTGGCTGTCAGTCAAAG Reverse: AAACCTCGGCTTCCCTCCATAA

Gene (Gene ID)	Name	Primers (5' → 3')
HAS3 NM_005329	Hyaluronan synthase 3	Forward: ATTATCAAGGCCACCTACGC Reverse: GGAATGAGGCCAATGAAGTT
ICAM1 NM_000201	Intercellular adhesion molecule 1	Forward: CCAAGTTGTTGGGCATAGAG Reverse: AGTCCAGTACACGGTGAGGA
ITGA1 NM_181501.1	Integrin Subunit Alpha 1	Forward: GTGCTTATTGGTTCTCCGTTAGT Reverse: CACAAGCCAGAAATCCTCCAT
ITGA2 NM_002203	Integrin Subunit Alpha 2	Forward: CCTACAATGTTGGTCTCCCAGA Reverse: AGTAACCAGTTGCCTTTTGATT
ITGA3 NM_005501	Integrin alpha 3	Forward: TGTGGCTTGGAGTGA CTGTG Reverse: TCATTGCCTCGCAGCTAGC
ITGA4 NM_000885	Integrin Subunit Alpha 4	Forward: AGCCCTAATGGAGAACCTTGT Reverse: CCAGTGGGGAGCTTATTTTCAT
INTGA5 NM_002205	Integrin Subunit Alpha 5	Forward: ATCTGTGAGGTCGAAACAGGA Reverse: TGGAGCATACTCAACAGTCTTTG
ITGA7 NM_001144997	Integrin alpha 7	Forward: CTGACTCCATGTTCCGGATCA Reverse: CACCTGTGAAGGTTTGCGC
ITGA8 NM_0032638	Integrin, alpha 8	Forward: GAATGGAGACCTTATTGTGGGA Reverse: GAGCCACTTCCGTCTGCTTT
ITGA10 NM_003637	Integrin alpha 10	Forward: ACTTAGGTGACTACCAACTGGG Reverse: CCACAAGCACGAGACCAGA
ITGA11 NM_001004439	Integrin subunit alpha 11	Forward: GTCACCCTGTCCAACGTGTC Reverse: ACATCCCTGTGGTGTAGTAGG
ITGAL NM_001114380	Integrin, alpha L	Forward: TGCTTATCATCATCACGGATGG Reverse: CTCTCCTTGGTCTGAAAATGCT
ITGAM NM_000632	Integrin alpha M	Forward: CACATGACTTTCGGCGGATGA Reverse: GCTGCGTTATTGGCTTACC
ITGAM NM_001145808	Integrin alpha M	Forward: ACTGGTGAAGCCAATAACGCA Reverse: TCCGTGATGACA ACTAGGATCTT
ITGAV NM_001145000	Integrin alpha V	Forward: ATCTGTGAGGTCGAAACAGGA Reverse: TGGAGCATACTCAACAGTCTTTG
ITGB1 NM_002211	Integrin beta 1	Forward: CCTACTTCTGCACGATGTGATG Reverse: CCTTTGCTACGGTTGGTTACATT
ITGB2 NM_000211	Integrin beta 2 chain	Forward: AGTGTGACACCATCAACTGTG Reverse: GCACTCGCATACGTTGCAGT
ITGB2 NM_000211	Integrin, beta 2	Forward: TGCGTCTCTCTCAGGAGTG Reverse: GGTCCATGATGTCGTCAGCC
ITGB3 NM_000212	Integrin beta 3	Forward: GTGACCTGAAGGAGAATCTGC Reverse: CCGGAGTGCAATCCTCTGG
ITGB4 NM_001005619	Integrin beta 4	Forward: CTCCACCGAGTCAGCCTTC Reverse: CGGGTAGTCCTGTGTCTGTA
ITGB5 NM_002213	Integrin beta 5	Forward: GGAAGTTCGGAAACAGAGGGT Reverse: CTTTCGCCAGCCAATCTTCTC
MCAM NM_006500	Melanoma cell adhesion molecule	Forward: AGCTCCGCGTCTACAAAGC Reverse: CTACACAGGTAGCGACCTCC
MPZL1 NM_001146191	Myelin protein zero like 1	Forward: ACGCCAAAAGAAATCTTTCGTGG Reverse: TCAACCCGCCAGTCGTA CTACTA
MSN NM_002444	Meosin	Forward: ATGCCAAAACGATCAGTGTG Reverse: ACTTGGCACGGA ACTTAAAGAG
MUC18 NM_006500	Melanoma cell adhesion molecule	Forward: AGCTCCGCGTCTACAAAGC Reverse: CTACACAGGTAGCGACCTCC
NCAM1 NM_001076682	Neural cell adhesion molecule	Forward: GGCATTTACAAGTGTGTGGTTAC Reverse: TTGGCGCATTCTTGAACATGA

Gene (Gene ID)	Name	Primers (5' → 3')
NPTN NM_017455	Neuroplastin	Forward: GAGGTCATTATTTCGAGACAGCC Reverse: TTGATCCTGTACTCCATGTTGC
PCDHA3 NM_031497	Protocadherin alpha 3	Forward: GTTTTCGCTAGAGGGCGCAT Reverse: CAACACGAGTCCAAGGGATTTA
PECAM1 NM_000442	Platelette and endothelial cell adhesion molecule	Forward: AACAGTGTTGACATGAAGAGCC Reverse: TGTAACACAGCACGTCATCCTT
PLXB2 NM_012401	Plexin B2	Forward: AGCCTCTTCAAGGGCATCTG Reverse:GCCACGAAAGACTTCTCCCC
PNN NM_002687.3	Desmosome associated protein	Forward: GTCGCCGTGAGAACTTTGC GGTCCTCCTCCACTATCTGAGA
RAGE NM_001136	Receptor for advanced glycation endproducts	Forward: GGGCAGTAGTAGGTGCTCAA Reverse: CGGCCTGTGTTTCAGTTTCCAT
RDX NM_002906	Radixin	Forward: AATTGTGGCTAGGTGTTGATGC Reverse: GGTGCCTTTTTGTGCGATTGGC
SELE NM_000450	Selectin E	Forward: CAGCAAAGGTACACACACCTG Reverse: CAGACCCACACATTGTTGACTT
SELL NM_000655	Selectin L	Forward: ACCCAGAGGGACTTATGGAAC Reverse: GCAGAATCTTCTAGCCCTTTC
SELP NM_003005	Selectin P	Forward: ACTGCCAGAATCGCTACACAG Reverse: CACCCATGTCCATGTCTTATTGT
SGCE NM_001099400	Sarcoglycan epsilon	Forward: GGCGTTTATGTCATGGTTGGT Reverse: AGGTGGACACTTGCTTTGTTT
THBS1 NM_003246	Thrombospondin-1	Forward: AGACTCCGCATCGCAAAGG Reverse: TCACCACGTTGTTGTCAAGGG
THBS2 NM_003247	Thrombospondin-2	Forward: GACACGCTGGATCTCACCTAC Reverse: GAAGCTGTCTATGAGGTCGCA
THBS3 NM_001252607	Thrombospondin 3	Forward: ATGGAGACGCAGGAACCTCG Reverse: AGCTACCATCTGCCGAGACT
VCAM1 NM_001078	Vascular cell adhesion molecule 1	Forward: CAGATAGACAGCCCTCTGAGC Reverse: CTCCACCTGGATTCCCTTT
VCAN NM_004385	Versican core protein	Forward: GTAACCATGCGCTACATAAAGT Reverse: GGCAAAGTAGGCATCGTTGAAA
VIM NM_003380	vimentin	Forward: GGCAGAAGAATGGTACAAATCC Reverse: CTTCCAGCAGCTTCTGTAG
VTN NM_000638	Vitronectin	Forward: CGGGGATGTGTTCACTATGCC Reverse: GTGTCTGCTCAGGATTCCCTT